ADVANCED LECTURES 1982 - GENERAL CIRCULATION OF THE ATMOSPHERE

LECTURE 1 - Introduction and Radiative Heat Balance

1. Introduction

The purpose of this course of lectures is to present and explain the main features of the general circulation of the Earth's atmosphere. Some basic features of the observed circulation will be described first, leading to a consideration of the distribution of radiative heating which drives and maintains the circulation. Zonally-symmetric forcing will be discussed, leading to the simple meridional circulations which were proposed up to about the beginning of this century. This leads to a consideration of the importance of eddies, both standing and transient, and the asymmetric circulations forced by the seasons and the distribution of land, sea and mountains. The observed circulation will then be discussed in more detail, using the results of recent studies, together with the budgets of mass, moisture, heat and momentum. Finally, General Circulation Models (GCM's) will be introduced and their basic structure described. Some of the major GCM results which have led to a greater understanding of the general circulation will be reviewed, and some current areas of research outlined.

2. The observed circulation

In this section some basic facts about the observed general circulation will be reviewed, which will be discussed and explained in the subsequent lectures. More detailed information will be presented in Lectures 5-7.

a. The average climatological distributions of pressure at mean sea level (PMSL) for January and July are shown in Figure 1. These use data from Crutcher and Meserve (1970) and Taljaard et al (1969), as presented by Manabe et al (1979). Note the generally low pressure in equatorial regions and the tendency for the sub-tropical anticyclones to form over the land in winter and over the sea in summer, for both hemispheres. The winter anticyclone over Siberia is replaced by a low surface pressure system in summer, for example. The mid-latitude cyclone tracks show up as regions of low pressure in such time-mean maps; this is especially evident over the northern Atlantic in winter and around Antarctica in both seasons.

b. The zonally-meaned atmospheric temperatures up to 24 km (Figure 2) indicate that there is an equator-ward gradient at all levels up to the tropopause, which slopes from equator to poles. The lowest stratospheric temperatures are found above the tropical tropopause and in the so-called "polar-night" region close to the winter pole. These data are from Newell et al (1972), re-drawn by Washington et al (1979).

c. The corresponding cross-sections of zonal wind (Figure 3), show easterlies in the tropics and at the surface near the poles. In middle and high latitudes the zonal winds are mainly westerly and increase in intensity towards the tropopause. This figure shows that the bulk of the atmosphere is in super-rotation, meaning that it is rotating faster about the earth's axis than the underlying surface.

The temperature and zonal wind cross-sections are linked by the fact that the lower atmosphere is everywhere close to hydrostatic equilibrium, and away from the surface and polewards of latitudes $\pm 10^{\circ}$ or so it is also

in approximate geostrophic balance. The vertical shear of the geostrophic wind $\underline{V}$ is therefore given by the thermal wind equation;

$$\frac{\partial \underline{V}}{\partial z} = -\frac{g}{fT} \nabla_p T \wedge \underline{k} \qquad (1)$$

where g is the acceleration due to gravity, f the coriolis parameter, z and $\underline{k}$ are vertical co-ordinates and T temperature. ∇_p is the gradient on a pressure surface. $\nabla_p T$ is directed towards the equator, so $\partial \underline{V}/\partial z$ is therefore a vector pointing eastwards. This indicates that westerly winds are to be expected in most of the troposphere, increasing with height until the equator-ward temperature gradient weakens in the stratosphere. In the winter stratosphere at high latitudes, however, the temperature decreases with height well above the tropopause, so the tropospheric westerlies link with the "polar-night jet" seen at the top of the figure. In summer, the reverse temperature gradient ensures that the tropospheric westerlies are capped by stratospheric easterlies.

d. The mean meridional mass flux cross-section for March-May (Figure 4) indicates a symmetric, cellular structure in the troposphere, with ascending motion over the equator driving a strong direct cell and weaker cells towards the poles. This example, taken from Newell et al (1969) was deliberately chosen to show a simple symmetric circulation, with "Hadley" and "Ferrel" cells to be discussed in the next lecture. It should be stressed, however, that in general it is only near the equinoxes and in long-term mean fields that such a symmetric circulation is found.

3. Radiative heat balance

The absorption of solar ("shortwave") radiation is the source of energy which drives the circulations of both the atmosphere and oceans. The loss of infrared ("longwave") radiation to space to maintain the radiation balance and internal dissipation represent the sinks of energy. Figure 5, taken from Mason (1976), shows the global radiation balance of the earth-atmosphere system and the way both shortwave and longwave radiation are partitioned. Shortwave radiation is absorbed by H_2O, O_3, CO_2, clouds and the surface, the latter accounting for about half the incoming flux. Shortwave radiation is scattered within the system and back to space, primarily by clouds, so that the globally-averaged cloud cover of about 50% produces a planetary albedo (the ratio of the total reflected shortwave to the incident) of about 30%. The loss of longwave radiation to space, which together with the reflected shortwave equals the incoming shortwave if the system is in equilibrium, is maintained by emission/absorption by the surface, clouds, H_2O, CO_2 and O_3.

It is interesting to consider the temperature structure which would form in the absence of a general circulation. If neither horizontal nor vertical transports were possible, the system would tend to a state of pure radiative equilibrium, with the vertical temperature structure such that the net radiative heating was zero at all levels. Manabe and Strickler (1964) calculated such an equilibrium profile, which is shown in Figure 6 as the solid line. This is close to the observed profile in the stratosphere, indicating that in the mean the stratosphere may be considered to be close to pure radiative equilibrium, but the lapse rate is very steep in the troposphere, the gradients being especially large close to the surface, whose equilibrium temperature is extremely high (335K). The latitudinal variation of the surface temperature would be very large under these conditions.

Figure 6 shows that radiation acting alone would produce a lapse rate which was super-adiabatic throughout the troposphere, so that the earth's atmosphere in pure radiative equilibrium is unstable to convection. Manabe and Strickler (1964), and later authors, therefore considered the so-called radiative/convective equilibrium, in which convection limits the lapse rates and the resulting temperature structure represents a balance between radiation and convection. In their calculation they simply removed any super-adiabatic regions by forcing a maximum lapse rate of 6.5°C/km, and the resulting profile is shown by the dashed line on Figure 6. The surface temperature is closer to the observed mean, being 300 K, although a considerable equator-pole contrast would still be expected. Figure 7 indicates that in these calculations the inclusion of clouds leads to lower equilibrium temperatures. The radiative energy balance is demonstrated in Figure 8, showing that the net radiative cooling of the troposphere of about 1°C/day must be offset by the warming produced by convective mixing. Although such calculations mimic the observed global-mean vertical structure, it is obvious that radiative/convective equilibrium cannot prevail everywhere, because a latitudinal temperature gradient would be produced, with much warmer conditions at the equator than the poles. This would induce pressure gradients and cross-latitude horizontal motions, leading to a circulation acting so as to reduce the latitudinal temperature contrast. Surprisingly, one can learn some important facts about the general circulation by continuing to consider only the distribution of radiative heating.

The components of the Earth's Radiation Budget (ERB) have been measured for several years by instruments on satellites, and these data illustrate the distribution of the radiative forcing on the earth-atmosphere system. Winston et al (1979) have prepared maps of the annual-average absorbed shortwave, outgoing longwave and the resulting net radiation from NOAA satellite data for the period 1974-1978 (Figure 9). These show a maximum in shortwave absorption over the equator, decreasing steadily towards the polar regions. Outgoing longwave radiation is smaller in the tropical regions with a smaller latitudinal gradient, with the result that the net radiation is positive up to about $\pm$ 30° latitude and negative thereafter to the poles. The system is thus radiatively warmed in the tropics and cooled in middle and high latitudes, the imbalance driving meridional circulations. It is interesting to note in passing that these maps illustrate that the forcing is not zonally symmetric, with important anomaly regions over the sub-tropical deserts and stratocumulus regimes, and longitudinal variations along the equator.

The partitioning of the radiative forcing between atmosphere and surface is quite different. Figure 8 showed that in radiative/convective equilibrium the atmosphere is radiatively cooled in the troposphere. This is confirmed by calculations of the mean radiative heating performed by Dopplick (1979), using the observed distributions of temperature, humidity, clouds and principal absorbers (Figure 10). These calculations show that longwave atmospheric cooling dominates shortwave heating almost everywhere in the troposphere, the cooling being largest in the tropical regions. If the system as a whole is radiatively warmed only equatorwards of about $\pm$ 30° (Figure 9) and yet the atmosphere is everywhere cooled (Figure 10), then the surface must be radiatively heated well beyond the tropics. This is illustrated in the zonally-averaged breakdown of the heating rates shown in Figure 11, taken from Sellers (1965) as re-drawn by Perry and Walker (1977). The surface is radiatively heated almost up to the poles in the annual mean. The general circulation of the atmosphere is thus driven from below by surface heating at all latitudes in the mean and from within by net radiative cooling. The circulation removes energy mainly from the tropical surface and transports it polewards and upwards.

The meridional energy transports can be derived from the ERB data by the following simple but powerful argument (Oort and Vonder Haar 1976). Consider

the energy balance for the column shown in Figure 12. The net flux at the top of the atmosphere, F_{TA}, may be stored within the column, but this energy may also be exported by the atmospheric transports T_A and oceanic currents T_o. The balance equation for the change of energy of the system is thus;

$$\frac{\partial E}{\partial t} = F_{TA} - \text{div}\, T_A - \text{div}\, T_o \qquad (2)$$

If in the annual mean there is no net storage of heat in either the atmosphere, land or ocean, which is a good assumption, then $\partial E/\partial t = 0$ and the annual mean net flux gives the combined transports directly. If, in addition, atmospheric data are used to estimate div T_A, then the oceanic transports can be found as a residual. These transports are impossible to measure directly at present, so such indirect estimates are of great value. By integrating Equation (2) away from the pole it is thus possible to plot the mean annual poleward fluxes through each latitude band (Figure 13, from Perry and Walker (1977), using data from Sellers (1965)). The transport of energy polewards is largest at about latitudes $\pm$ 40° and the contribution from ocean currents in maintaining the energy balance is very significant at low latitudes. At high latitudes the transport is almost entirely provided by the atmospheric motions. It must be remembered that the atmospheric energy transport is made up of three components, sensible, latent and potential, as expressed by the moist static energy;

$$h = c_p T + Lq + gz \qquad (3)$$

where c_p is the specific heat at constant pressure and L the latent heat of vaporization. The relative importance of these terms is not constant, the latent heat term, for example, being especially important in the tropics.

References

Crutcher, H L and Meserve, J M (1970) Selected level heights, temperatures and dew points for the Northern Hemisphere. NAVAIR 50-1C-52, US Naval Weather Service, Washington DC.

Dopplick, T G (1979) Radiative heating of the Global Atmosphere: Corrigendum. J Atmos Sci, 36, 1812-1817.

Manabe, S and Strickler, R F (1964) Thermal equilibrium of the atmosphere with a convective adjustment. J Atmos Sci, 21, 361-385.

Manabe, S, Hahn, D G and Holloway, J L (1979) Climate simulations with GFDL spectral models of the atmosphere: Effect of Spectral Truncation, in "Report of the JOC Study Conference on Climate Models: Performance, intercomparison and sensitivity studies", Vol I, pp 41-94, GARP Publications Series No 22.

Mason, B J (1976) Towards the understanding and prediction of climatic variations. Quart J R Met Soc, 102, 473-498.

Newell, R E, Vincent, D G, Dopplick, T G, Ferruza, D and Kidson, J W (1969) The energy balance of the global atmosphere, in "The Global Circulation of the Atmosphere", Royal Met Soc, pp 42-90.

Newell, R E, Kidson, J W, Vincent, D G and Boer, G J (1972) The general circulation of the tropical atmosphere, Vol I MIT press, Cambridge, Mass.

Oort, A H and Vonder Haar, T H (1976) On the observed annual cycle in the Ocean-Atmosphere heat balance over the Northern Hemisphere. J Phys Oceanogr, 6, pp 781-800.

Perry, A H and Walker, J M (1977) The Ocean-Atmosphere System. Longman, London, 160 pp.

Sellers, W D (1965) Physical Climatology, University of Chicago Press, 272 pp.

Taljaard, J J, van Loon, H, Crutcher, H L and Jenne, R L (1969) Climate of the upper air, 1. Southern Hemisphere Vol I. Temperatures, dew points and heights at selected pressure levels. NAVAIR 50-1C-55, US Naval Weather Service, Washington DC.

Washington, W M, Dickinson, R Ramanathan, V, Mayer, T, Williamson, D, Williamson G and Wolski, R (1979) Preliminary atmospheric simulation with the third-generation NCAR general circulation model: January and July. in "Report of the JOC study conference on climate models: performance, intercomparison and sensitivity studies", Vol I, pp 95-138. GARP publications series no. 22.

References continued

Winston, J S, Gruber, A, Gray, T I, Varnadore, M S, Earnest, C L and Mannello, L P (1979) Earth-atmosphere radiation budget analyses derived from NOAA satellite data June 1974-February 1978, NOAA, NESS, Washington DC.

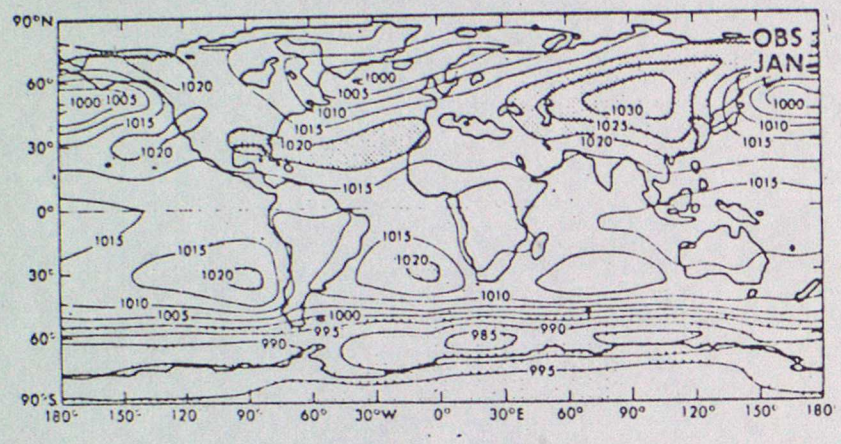

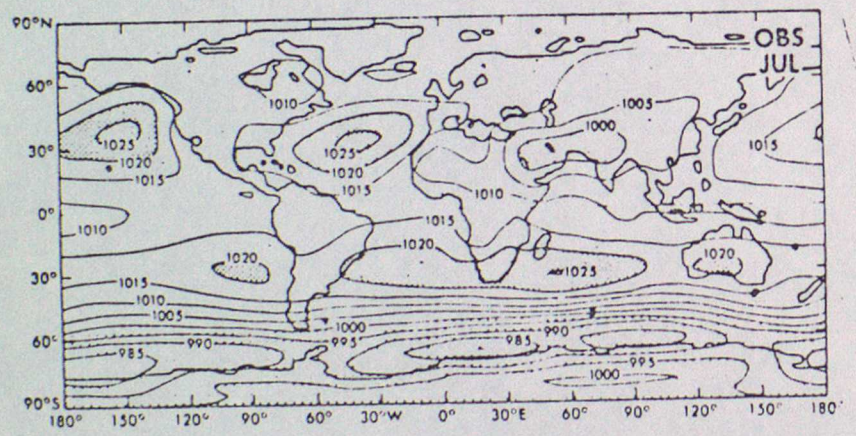

Figure 1. Observed January and July monthly-mean pressure at mean sea level (PMSL- mb)

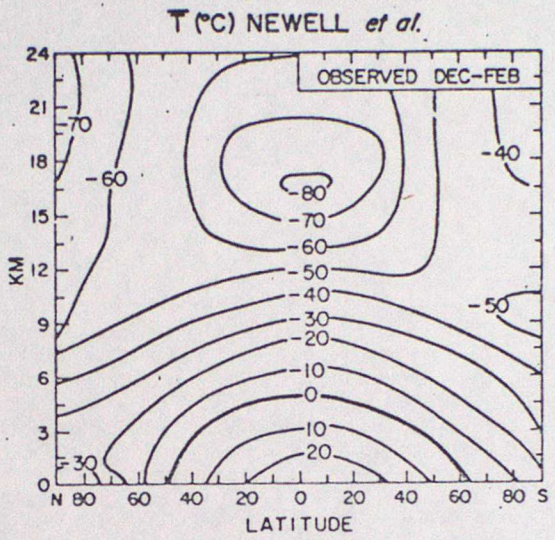

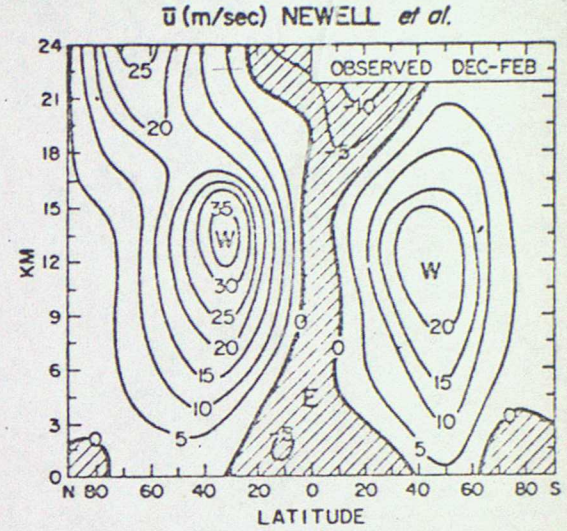

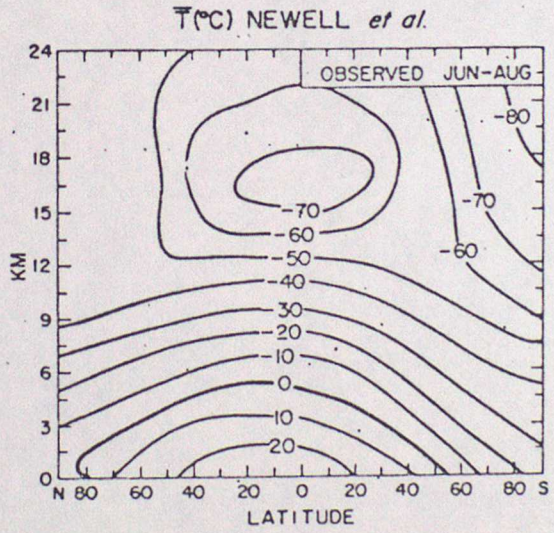

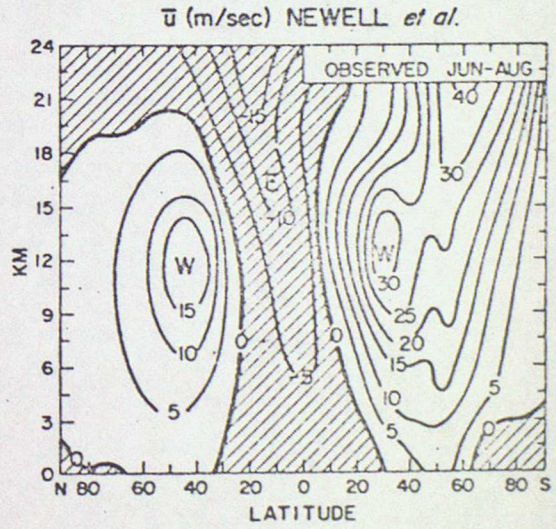

Figures 2/3. Observed December to February and June to August mean latitude-height cross sections of atmospheric temperature (^{o}C) and zonal wind ($m\ s^{-1}$)

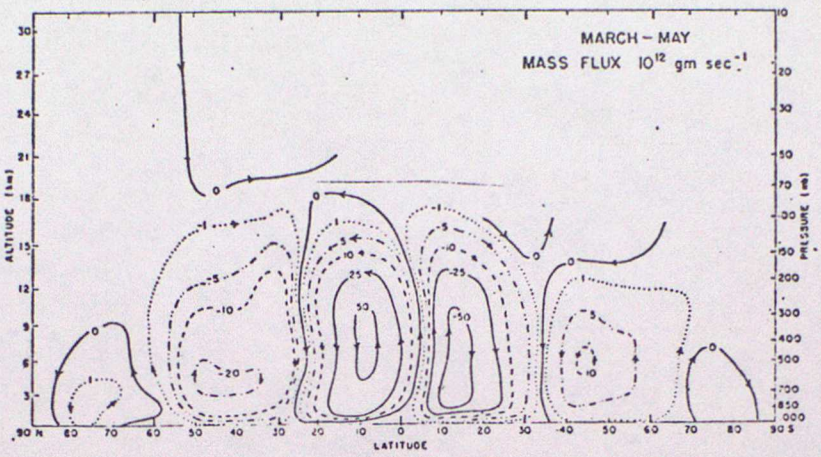

Figure 4. Observed March to May mean meridional mass flux latitude-height cross section (10^{12} g s^{-1})

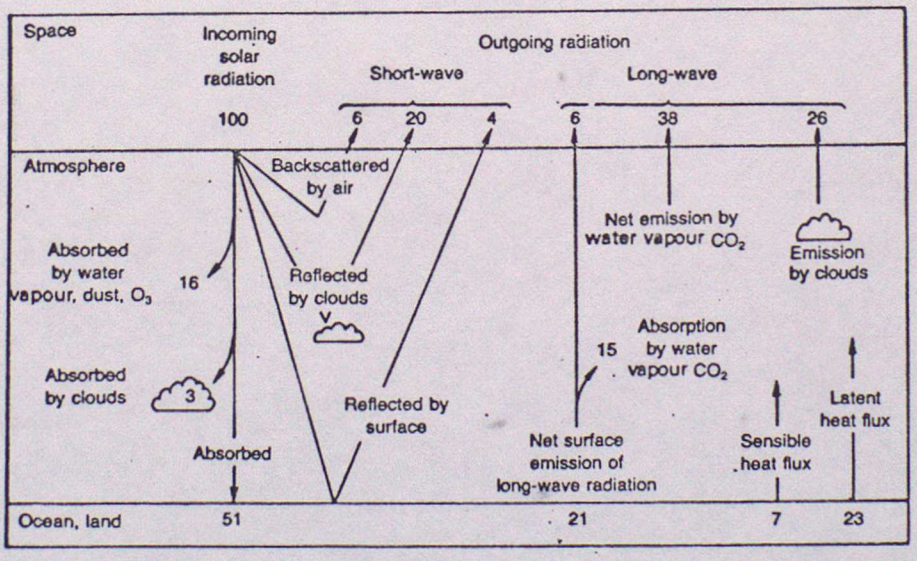

The radiation balance of the atmosphere–earth system showing the redistribution of the incoming solar radiation and the mechanisms by which these are effected. (From the US National Academy Report, 'Understanding Climatic Change', 1975.)

Figure 5.

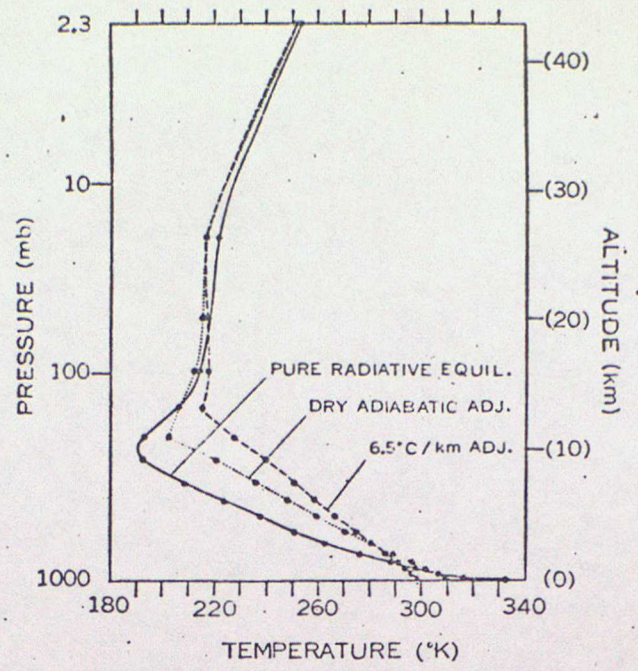

The dashed, dotted, and solid lines show the thermal equilibrium with a critical lapse rate of 6.5 deg km^{-1}, a dry-adiabatic critical lapse rate (10 deg km^{-1}), and pure radiative equilibrium.

Figure 6.

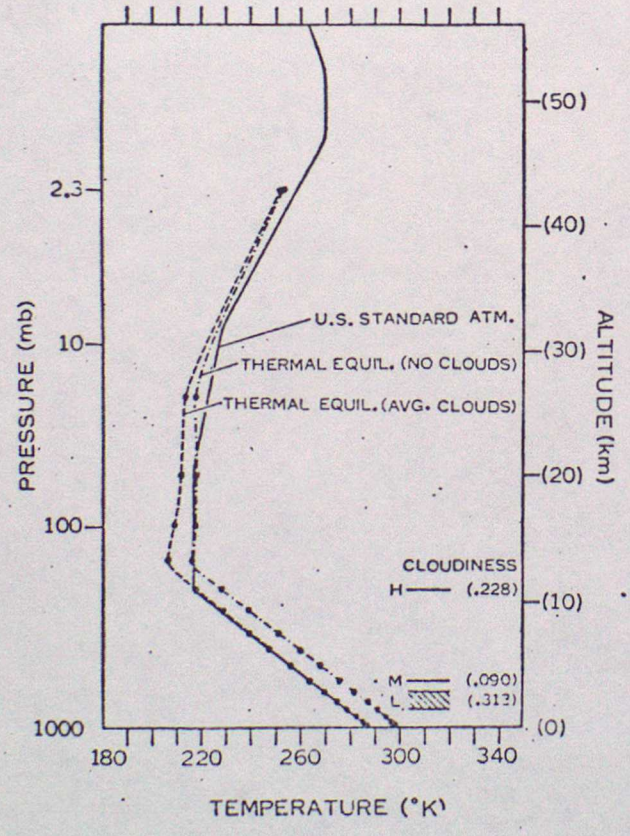

Dash-dotted and dashed lines show the thermal equilibrium of the atmosphere with and without cloudiness. The critical lapse rate for convection is 6.5 deg km^{-1}. The cloud amounts and cloud heights are shown on the right hand side. The solid line shows the U. S. Standard Atmosphere.

Figure 7.

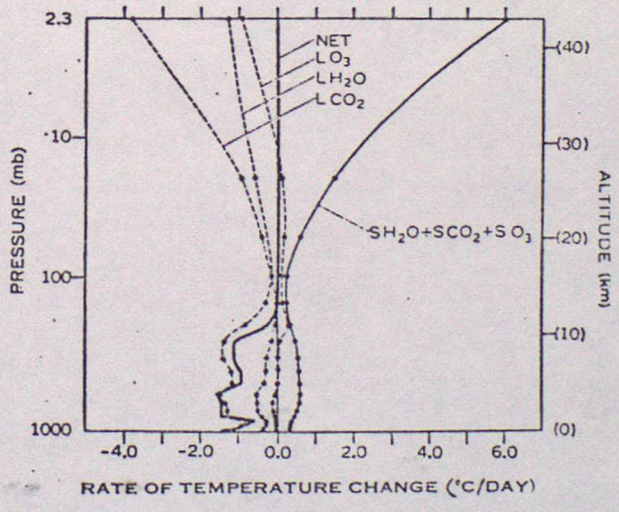

Vertical distributions of radiative balance components for the thermal equilibrium of the atmosphere with the average cloudiness shown in Fig. 7 "Net" means the net rate of temperature change due to all of these components.

Figure 8.

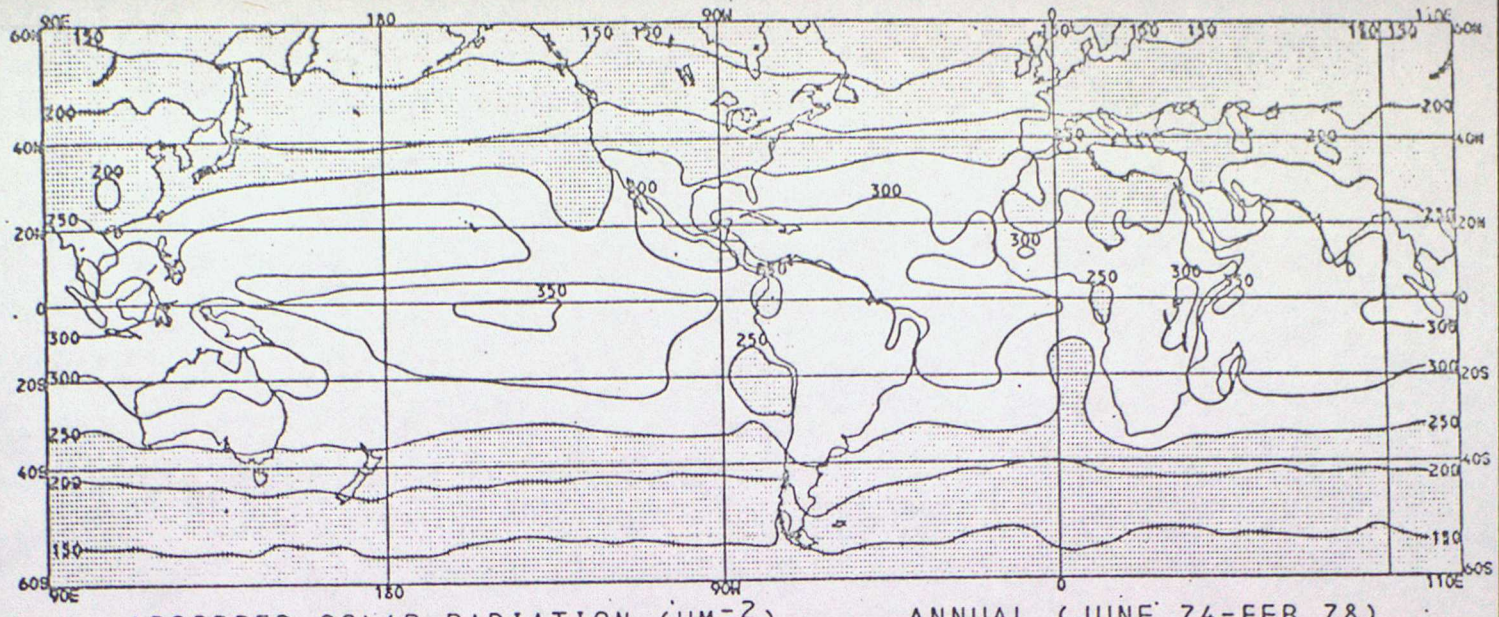

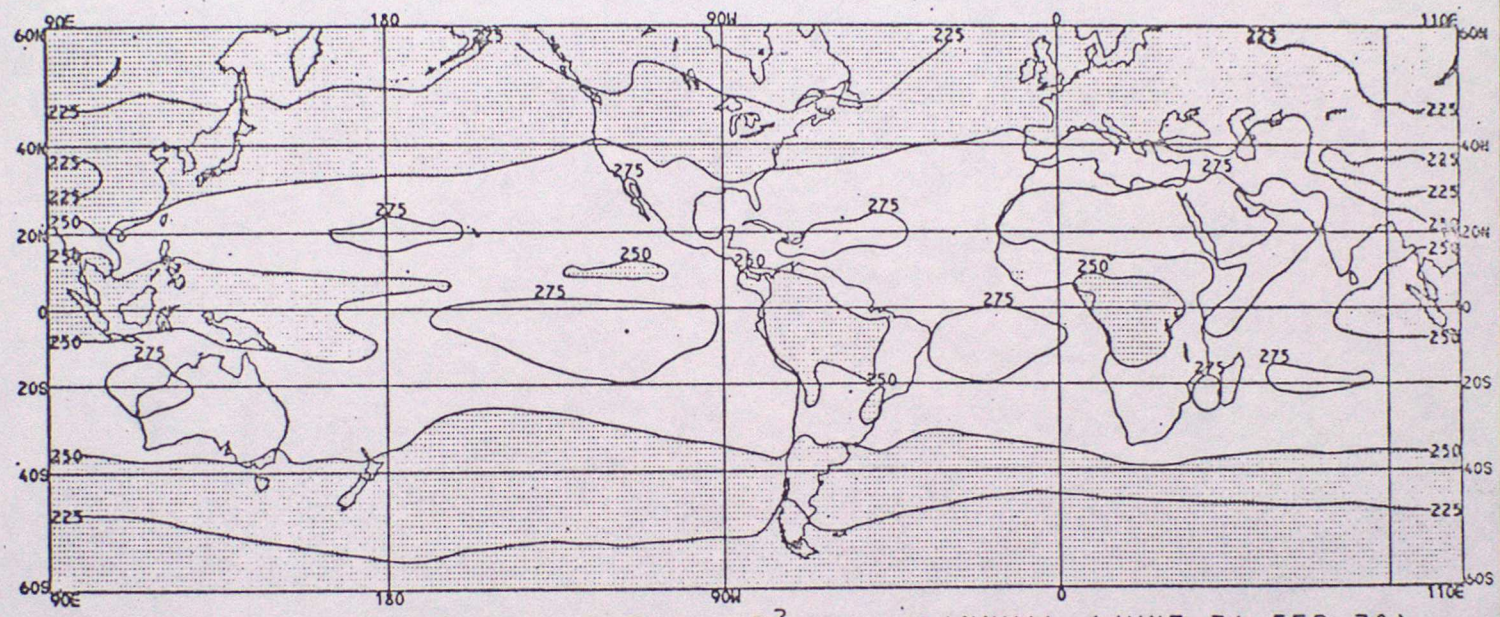

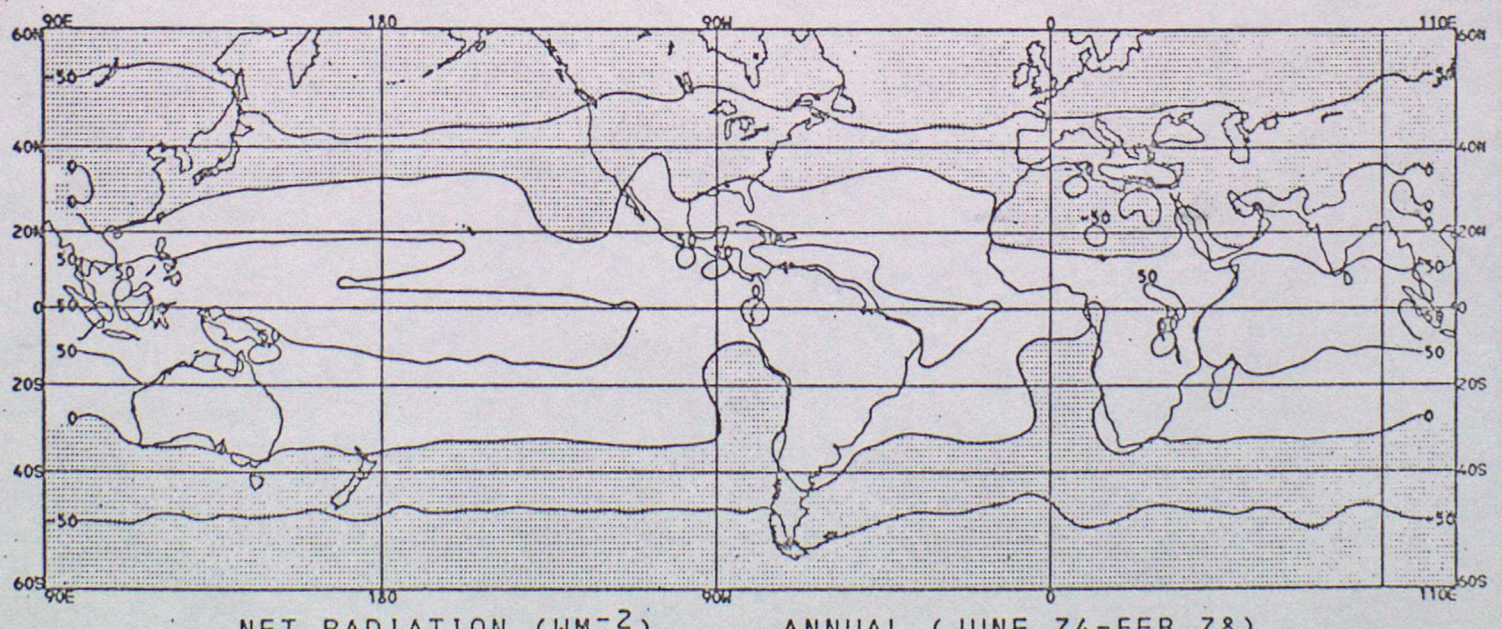

Figure 9. Annual-mean maps of absorbed shortwave, outgoing longwave and net radiation for the Earth-Atmosphere system, as observed from NOAA satellites between 1974 and 1978

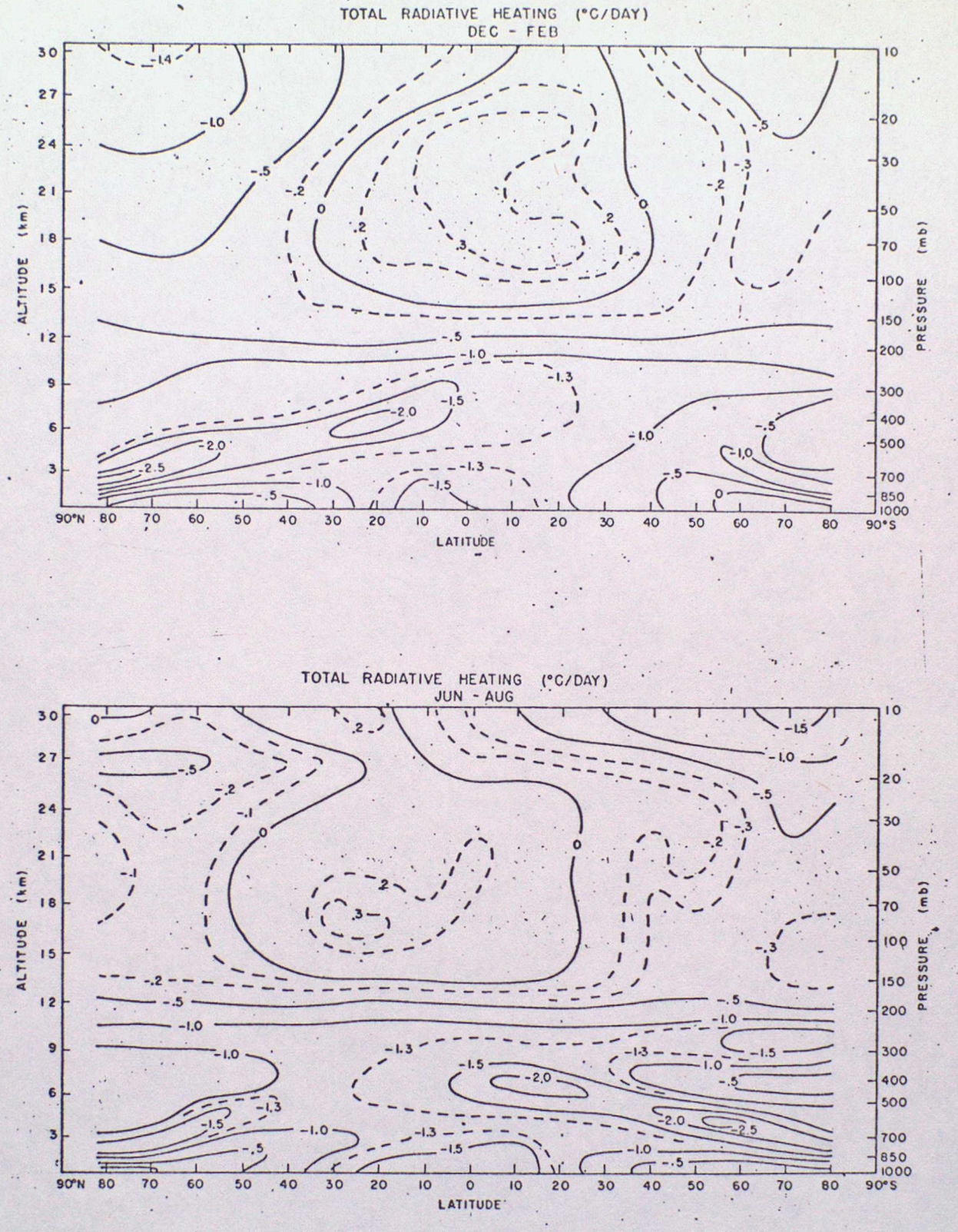

Figure 10. Mean total radiative heating (^{o}C per day) for December to February (top) and June to August (bottom)

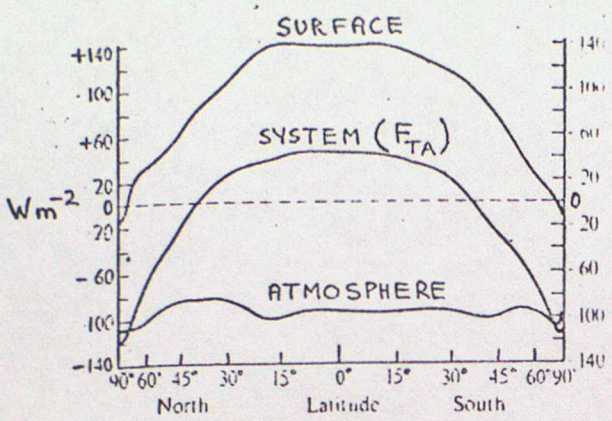

Variation of radiation balance with latitude.

Figure 11.

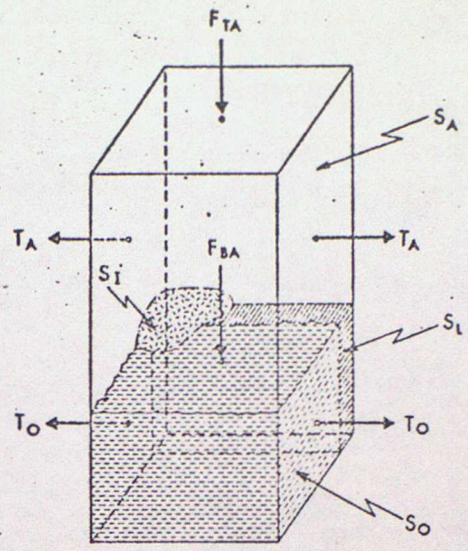

Schematic diagram of the different terms in the earth's energy balance.

Figure 12.

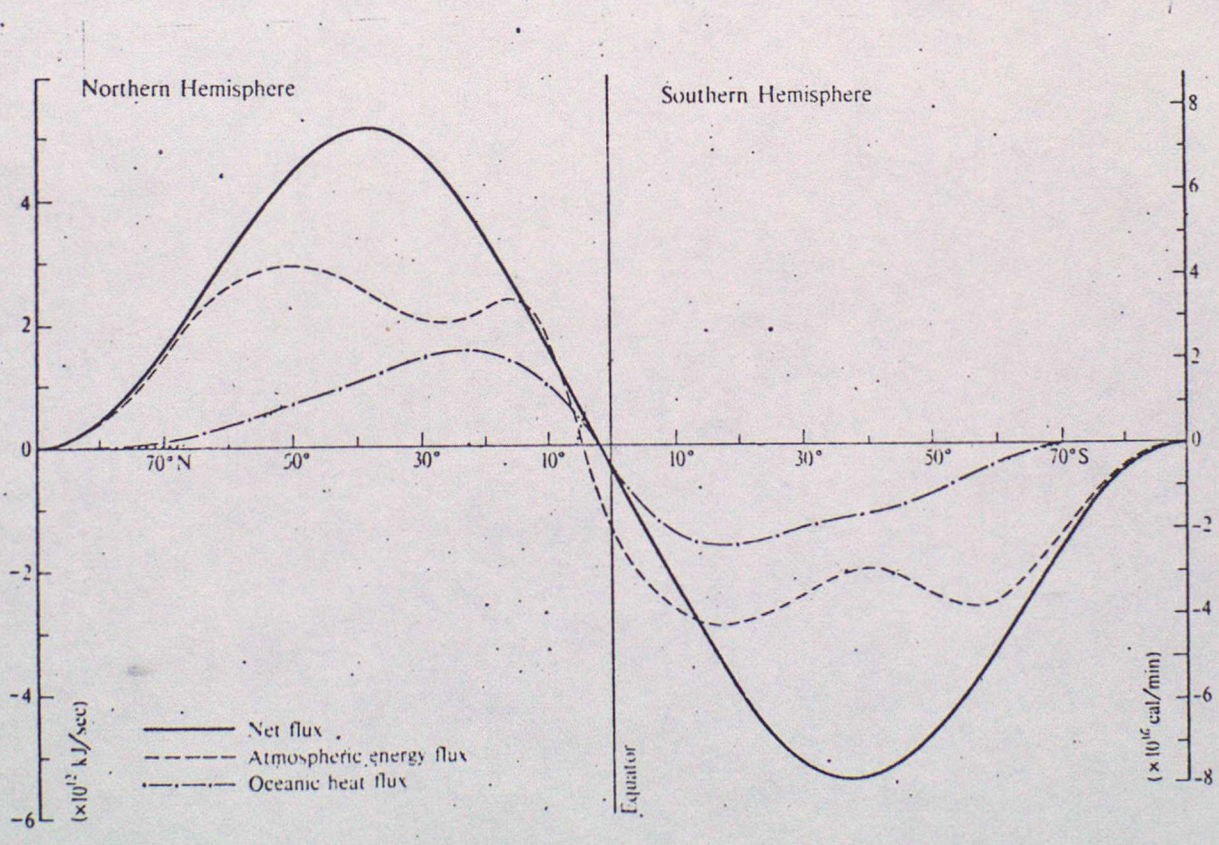

Mean annual fluxes of energy in the ocean–atmosphere system.

Figure 13.

ADVANCED LECTURES 1982 - GENERAL CIRCULATION OF THE ATMOSPHERE

LECTURE 2 - Development of General Circulation Concepts

1. Introduction

In the previous lecture it was established that the radiative forcing drives an atmospheric circulation which transports energy from the tropical surface upwards and polewards. The development of ideas of how the circulation effects this transport will now be discussed. The treatment here follows that of Lorenz (1967), whose monograph is full of careful explanations of difficult concepts and which together with the book by Palmén and Newton (1969) is essential reading.

The first comprehensive source of data was the remarkable paper by Halley (1686), who compiled information on surface winds over the tropical oceans from mariners' reports (Figure 2.1). In some regions the wind direction was known to be roughly constant throughout the year, so that trade links could be established by routeing ships according to these so-called Trade Winds. The monsoonal changes were also known, as well as areas liable to severe storms. Halley identified two important and unexplained features, firstly the generally easterly winds, being north-easterly to the north of the equator and south-easterly to the south of it, and secondly the monsoonal winds. Earlier explanations of the easterly winds included the idea that the air was unable to keep up with the earth's eastward rotation. Halley suggested that the maximum in shortwave heating around local noon would generate low pressure and that as this moved westwards around the equator a net easterly wind would (somehow) be produced. These qualitative arguments were dispensed with by Hadley (1735), who not only provided essentially the correct explanation of the easterlies, but also a zonally-symmetric scheme for the general circulation itself.

2. Symmetric circulations

Hadley (1735) considered the circulation to be expected on a zonally-symmetric earth. He argued that the excess of radiative heating at low latitudes leads to rising motion there and sinking motion at high latitudes. By conservation of mass these motions must be linked by equatorward flow at low levels and poleward flow at high levels. The low level current would approach the equator with a deficit of eastward velocity relative to the surface, because it comes from closer to the earth's axis. It would therefore appear to be deflected to the right, giving the observed north-easterly and south-easterly trade winds. The upper level current would also be deflected to the right, cooled and descend towards the surface to appear as the middle latitude westerlies. The scheme is illustrated in Figure 2.2. Hadley's only major error was to assume conservation of absolute velocity rather than momentum, but the coriolis force was only formally identified a century after his work, so he can perhaps be forgiven.

In devising his circulation Hadley realized that friction at the surface generates a torque between atmosphere and earth. Since the total angular momentum of the system is essentially constant, easterly surface winds at all latitudes would slow the earth down and result in a steady increase in the length of day. Such an increase is not observed, but in any case the surface friction would itself act to reduce the easterly winds and induce a westerly component. Angular momentum balance therefore requires the generally easterly surface winds at low latitudes to be compensated by westerly surface winds at higher latitudes, hence the distribution of surface winds shown in Figure 2.2, and in Figure 1.3. The figures from Lecture 1 will be referred to henceforth in this way. The earth rotates faster about its axis than the atmosphere in

the tropics, which are thus source regions of atmospheric angular momentum. The converse is true in the region of prevailing westerly surface winds. Angular momentum is thus transported from the equatorial regions towards the higher latitudes. The requirement for angular momentum transport is as important as that for energy transport in determining the detailed character of atmospheric motion. Short term exchanges of angular momentum between atmosphere and earth do in fact take place during this transport process. Hide et al (1980) demonstrate this by relating the systematic changes in atmospheric total angular momentum which were observed during FGGE to measurements of the length of day.

It was not until the nineteenth century that deficiencies in Hadley's scheme became apparent. Figure 2.2 indicates north-westerly winds at high latitudes whereas the observed winds are generally south-westerly. During the nineteenth and early twentieth centuries a great many schemes of varying degrees of complexity and plausibility were published as observations and theoretical understanding improved. Only the most important developments will be discussed here; for a review see Lorenz (1967, pp 59-78).

In order to account for the distribution of surface winds while also satisfying the need for energy and angular momentum balance, the single "direct" Hadley cell had to be replaced by more complex circulations. Ferrel first proposed the existence of an indirect cell extending through the full depth of the atmosphere at middle latitudes, which explains the surface wind observations as the westerly winds would drift polewards, but the balance requirements would not be satisfied. Both Thomson (1857) and Ferrel (1859) realized that the indirect cell had to be placed beneath a larger, direct circulation as shown in Figure 2.3 (from Lorenz 1969). It eventually became clear that the high level current, extending throughout the hemisphere from equator to pole, did not exist. It was first argued that, in conserving its absolute angular momentum, such a current would achieve excessive zonal wind speeds by the time it reached middle latitudes. There was also direct evidence from observations of the motion of upper level clouds. These showed that the current extended only about as far as 30° latitude, by which time the direction had become westerly. At higher latitudes no systematic wind towards the poles could be found, and the zonally-symmetric circulations therefore had to be abandoned.

3. The importance of eddies

The existence of cyclones and other departures from zonal symmetry had been known about by Ferrel and Thomson, but they were not considered important in determining the general circulation. Bigelow (1902) asserted that in fact the cyclones were an integral part of the general circulation. For this to be true, the cyclones and anticyclones must transport energy and angular momentum across the middle latitudes, where the cloud observations had shown that there was no symmetric meridional circulation. Defant (1921) considered the first requirement by identifying the cyclones as the elements in large scale turbulence and produced a realistic estimate of the meridional temperature gradient. Jeffreys (1926) subsequently showed that such eddies could also transport the required amounts of angular momentum. This may be accomplished without the need for any net poleward flux of air if the streamlines of the flow are oriented as in Figure 2.4 (from Palmen and Newton 1969). The NE-SW tilting of the eddies transports angular momentum polewards because the air moving northwards has a larger zonal wind component than that moving southwards (Starr 1948).

The question remains as to why the earth's atmosphere is unable to support a symmetric circulation. The accepted explanation is that such a circulation is unstable to asymmetric disturbances so that eddies are an inevitable consequence (Bjerknes 1937). The middle-latitude eddies grow by baroclinic instability, favoured by a high coriolis parameter, gaining their kinetic energy from the

potential energy of the mean zonal flow. The problem of understanding the general circulation of the atmosphere is thus inextricably linked to the growth and behaviour of baroclinic waves and the detailed structure of weather systems. These topics have already been dealt with in detail in previous advanced lectures (Foreman 1980, Dutton 1981). The first comprehensive attempt to quantify the role of the eddies was made by Starr and his co-workers in the MIT Planetary Circulations Project. Some results from this and subsequent work will be presented in Lecture 6.

4. The observed zonally-averaged circulation

Some observed features of the zonally-averaged circulation will now be discussed in relation to the ideas developed in the previous sections. An idealized cross section through such a circulation is shown in Figure 2.5, taken from Palmen and Newton (1969), as re-drawn by Houghton (1977). A direct Hadley circulation is seen in the tropical regions, extending only to about latitudes $\pm 20^{\circ}$. The driving force for this circulation is the strong convection in the Inter-Tropical Convergence Zone (ITCZ), which is fed by the convergence of the trade winds. This convection takes place in deep cumulus and cumulonimbus clouds which may extend from the boundary layer to the tropopause. Although such cloud systems occupy only a fraction of the ITCZ at any one time and there is undoubtedly descent inbetween, they are associated with vertical velocities of several metres per second which produces a net vertical mass flux and drives the Hadley cell. The low pressure trough associated with the ITCZ may be seen on the mean PMSL charts shown in Figure 1.1.

The descending part of the Hadley cell is associated with slow sinking motion on large scales and generally clear skies, the descent being partly assisted by net radiative cooling. The trade wind flow is concentrated mainly in the boundary layer beneath the trade inversion (Figure 2.6, from Augstein (1978)). As this air moves equatorward through the trades it experiences a decreasing large scale divergence. The boundary layer grows in depth and the trade inversion weakens in strength as the ITCZ is approached. The cloudiness also changes in character from the extensive stratocumulus areas over the sub-tropical oceans to the more convective conditions typical of the trades, where the cumulus clouds continually erode the inversion by mixing the boundary layer air upwards. This transition in the cloudiness is often strikingly evident in the Meteosat images on display in the Met Office library.

In the middle and high latitudes the inherent instability of the flow results in the familiar cyclones and anticyclones. Although Figure 2.5 shows the mean position of the polar front, which marks the baroclinic zone separating polar and middle latitude air, it must be appreciated that this shows considerable variation in position. In part this variability is the result of asymmetries in the basic forcing mechanisms, which will be discussed further in Lectures 3 and 4. At these high latitudes the meridional transports are performed mainly by sloping convection associated with frontal zones, as indicated by the arrows crossing the polar front in Figure 2.5. The importance of these transports is emphasized in Figure 2.7, from Houghton (1977), which shows the breakdown of the northern hemisphere heat flux into the eddy and mean circulation components. The Hadley cell dominates the energy transfer up to about 20°N, but thereafter the poleward transfer is accomplished by the eddy fluxes. In fact the mean circulation acts to transfer energy towards the equator in the middle latitudes. This circulation is often referred to as the Ferrel cell and is seen on the mass flux cross section of Figure 1.4 as the indirect cell between latitudes 30° and 60°. This diagram also shows the low-latitude Hadley circulation and weak direct cells in the polar regions. The circulation is rarely as symmetric as in Figure 1.4, however, and in particular the winter branch of the Hadley circulation is considerably stronger than the summer branch, so the circulation often appears as a single cell straddling the equator.

References

Augstein, E (1978) The atmospheric boundary layer over the tropical oceans. In "Meteorology over the tropical oceans", Royal Met Soc, pp 73-103.

Bigelow, F H (1902) Studies of the statics and kinematics of the atmosphere in the United States. Mon Weath Rev, 30, pp 13, 80, 117, 163, 250, 304, 347.

Bjerknes, V (1937) Application of line integral theorems to the hydrodynamics of terrestrial and cosmic vortices. Astrophys Norv, 2, 263-339.

Defant, A (1921) Die Zirkulation der Atmosphäre in den gemässigten Brieten der Erde. Geograf Ann, 3, 209-266.

Dutton, M J (1981) Fronts in the Atmosphere (Advanced Lectures).

Ferrel, W (1859) The motions of fluids and solids relative to the earth's surface. Math Monthly, 1, pp 140, 210, 300, 366, 397.

Foreman, S J (1980) Waves in the atmosphere and oceans. (Advanced Lectures). Met O 11 Technical Note 141.

Hadley, G (1735) Concerning the cause of the general trade winds. Phil Trans, 39, 58-62. Reprinted in "Meteorology over the tropical oceans", Royal Met Soc, pp 3-7.

Halley, E (1686) An historical account of the trade winds, and monsoons, observable in the seas between and near the tropicks, with an attempt to assign the phisical cause of the said winds. Phil Trans, 16, 153-168. (Available in lending pams, Met Office Library).

Hide, R, Birch, N T, Morrison, L V, Shea, D J and White, A A (1980) Atmospheric angular momentum fluctuations and changes in the length of day. Nature, 286, 114-117.

Houghton, J T (1977) The physics of atmospheres. Cambridge University Press.

Jeffreys, H (1926) On the dynamics of geostrophic winds. Quart J R Met Soc, 52, 85-104.

References continued

Lorenz, E N (1967) The nature and theory of the general circulation of the atmosphere. WMO.

(1969) The nature of the global circulation of the atmosphere: a present view. In "The Global Circulation of the Atmosphere", Royal Met Soc, pp 3-23.

Palmén, E and Newton, C W (1969) Atmospheric Circulation Systems. Academic Press.

Starr, V P (1948) An essay on the general circulation of the earth's atmosphere. J Met, 5, 39-43.

Thomson, J (1857) On the grand currents of atmospheric circulation. Lecture, printed in Phil Trans (A), 183, 653-684. (1892)

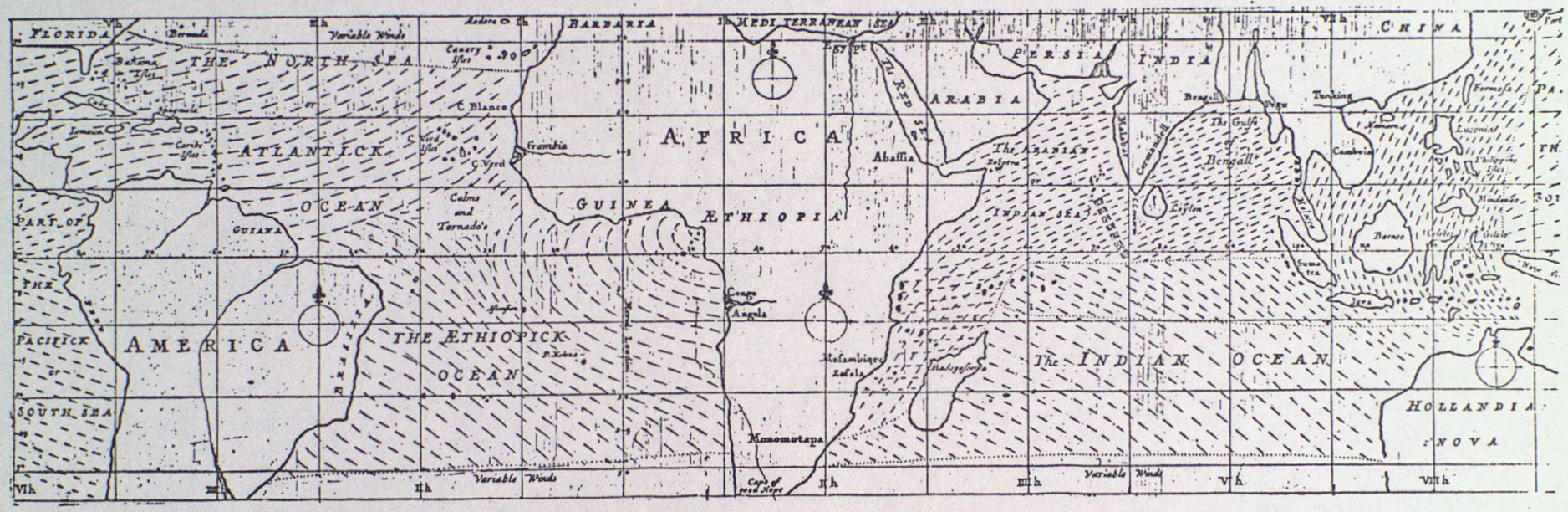

Figure 2.1 Surface winds over the tropical oceans, from Halley(1686)

"I could think of no better way to design the course of the Winds on the Mapp, than by drawing rows of stroaks in the same line that a Ship would move going alwaies before it; the sharp end of each little stroak pointing out that part of the Horizon, from whence the Wind continually comes; and where there are Monsoons the rows of the stroaks run alternately backwards and forwards, by which means they are thicker there than elsewhere"

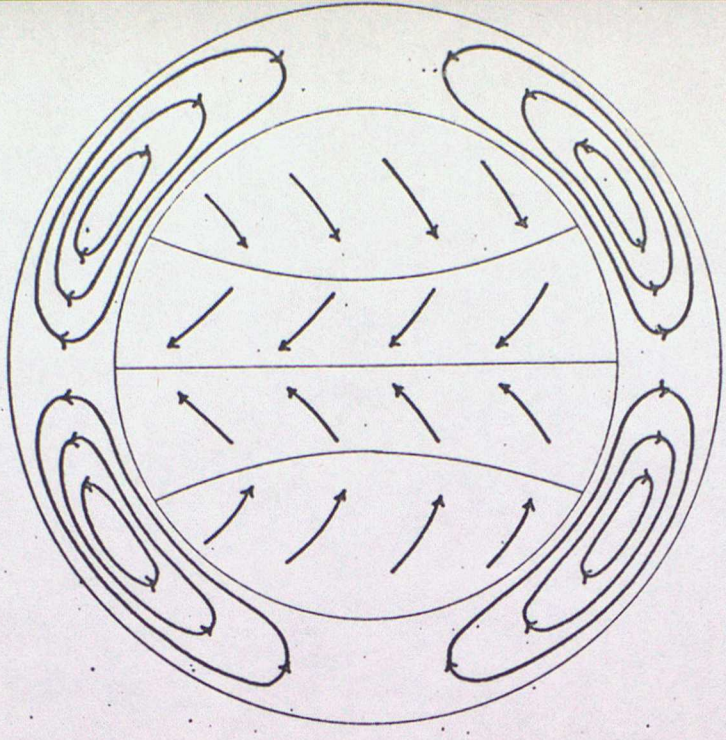

Figure 2.2 A schematic representation of the general circulation of the atmosphere as envisioned by Hadley (1735)

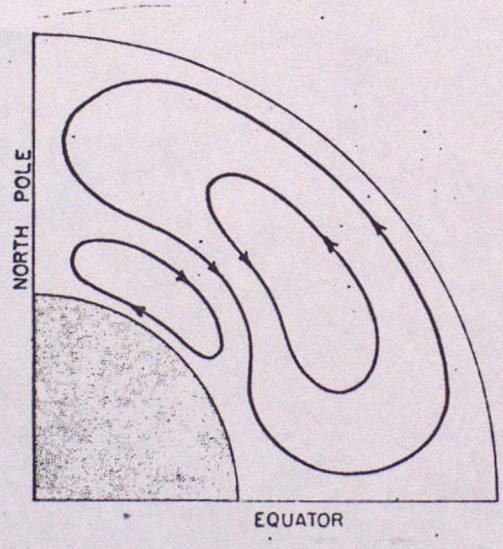

Schematic representation of the mean meridional circulation in one hemisphere, as visualized by Thomson (1857) and Ferrel (1859).

Figure 2.3

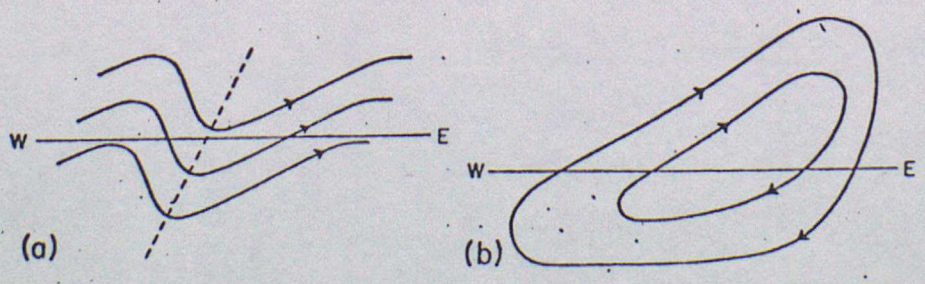

(a) Schematic picture of horizontal streamlines in a typical wave in the upper westerlies; (b) schematic horizontal streamlines in a subtropical anticyclone. (After Starr, 1948.)

Figure 2.4

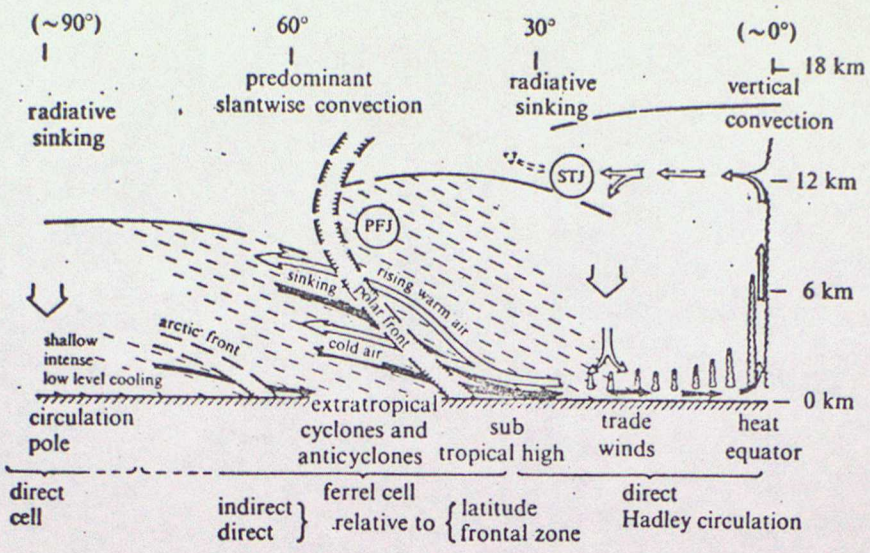

Schematic features of the atmospheric circulation in winter (after Palmén and Newton, 1969) showing Hadley circulation in tropics, sloping convection at mid and high latitudes; showing also polar front associated with which is polar front jet (PFJ) and the sub-tropical jet (STJ) associated with break in tropopause at ~ 30° latitude.

Figure 2.5

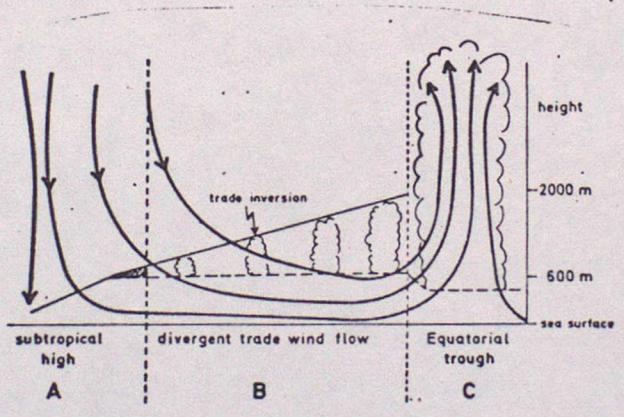

Scheme of the low-level Hadley circulation. Dashed line marks the top of the mixed layer. Stratus cloud in region A indicated by dotted area.

Figure 2.6

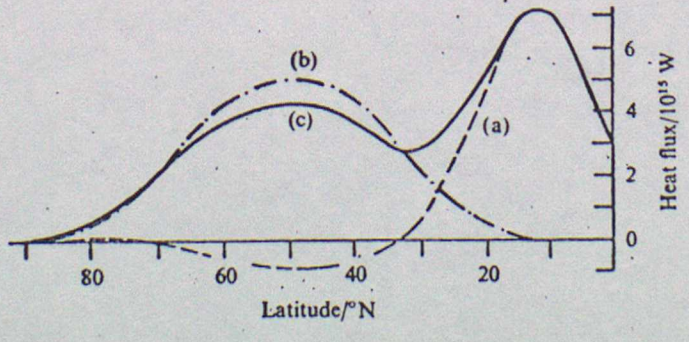

Northward flux of heat in northern hemisphere winter by (a) mean circulations such as the tropical Hadley cell, (b) eddies. Curve (c) is the total flux (after Newton, 1970).

Figure 2.7

ADVANCED LECTURES 1982 - GENERAL CIRCULATION OF THE ATMOSPHERE

LECTURE 3 - Asymmetries (I)

1. Introduction

The schematic cross sections shown in the last lecture represent a useful way of summarising some of the broad features of the circulation. However, zonally-averaged data often obscure important features and can be very misleading. As an example, it is known that the presence of eddies leads to a complex circulation in middle and high latitudes, whereas Figure 1.4 gives the impression of a simple cellular structure. Even in the case of symmetric forcing, such cross sections must therefore be interpreted with care. The atmospheric circulation is not forced symmetrically, however, and three important asymmetries need to be considered;

a. The seasonal variation of incoming shortwave radiation.

b. The distribution of land and sea.

c. The distribution of mountains.

Much of the complexity of the observed circulation and its variation with position and time is due to these effects acting singly or together. The combined effect of the first two is often referred to as Thermal Forcing, because the different surface properties of land and sea produce different surface temperature responses to changes in insolation, and hence variations in the fluxes of sensible and latent heat. The effect of mountains is to change the flow directly and is commonly termed Topographic or Orographic Forcing. This lecture will be mainly concerned with thermal forcing. Mountain influences and the combined effects of forcing mechanisms will be considered in the following lecture.

2. Seasonal changes in insolation

The seasonal changes in the incoming shortwave radiation are the result of the characteristics of the earth's rotation and its orbit around the sun. The orbit is an ellipse, the earth being closest to the sun in January and furthest from it in July. The earth's rotation axis is also inclined at an angle of about $23\frac{1}{2}^{\circ}$ to the axis of the orbit, so that the sun appears to oscillate in declination about the celestial equator, being furthest north or south at the solstices in June and December and crossing the equator at the equinoxes in March and September. This produces large seasonal changes in the amount of shortwave radiation available to the system at any location, as shown in Figure 3.1 (from Perry and Walker 1977). Note that in summer the values actually increase towards the pole, despite the decreasing solar elevation, because of the rapid increase in length of day with latitude. The fact that the earth is closest to the sun in January also means that the southern hemisphere receives more radiation in summer than the northern hemisphere does six months later. Averaged over the year, however, the two hemispheres receive identical amounts.

On a zonally-symmetric earth one might reasonably expect that the effect of such changes would be to shift the main features of the circulation north or south according to the time of year. To a first approximation this also takes place in the real atmosphere, but the effect is modified considerably by the distribution of land and sea.

3. Surface properties of land and sea

In this section the important physical differences between the properties of land and ocean surfaces will be summarised. These differences lead to characteristic surface temperature responses to the seasonal insolation variations, which drive large-scale asymmetries in the atmospheric circulation.

The specific heat of dry land is about half that of water, so one might expect the land surface temperature to be roughly twice as sensitive as that of the sea to changes in heat input. The conductivity of land surfaces is extremely low, however, with the result that changes in the surface energy balance can quickly induce changes in the temperature of the surface layers, the response decaying rapidly with depth. The response is sufficiently fast that the lag between insolation changes and surface temperature is measured in hours or less. This produces a significant diurnal variation of surface temperature, as illustrated by Figure 3.2, from Geiger (1965). The highest surface temperature of 34°C was reached only about 2 hours after noon, while the amplitude of the daily cycle is already halved at a depth of about 2cm. Notice that the cyclic heating of the surface produces temperature waves which slowly penetrate downwards through the soil. A similar behaviour is seen in response to the annual cycle (Figure 3.3, also from Geiger's book), although on this longer timescale the temperature wave penetrates about 2m before it is halved in amplitude. The low conductivity is emphasized by the fact that in the autumn, at depths of a few metres or more, the temperatures are still rising in response to the summer temperature wave from the surface, while the surface itself is cooling towards winter. The resulting reversal of the vertical temperature gradient means that heat is being stored in the land in summer and released in winter, but typical values for the rate of energy storage are only about $5 Wm^{-2}$, which is over an order of magnitude less than the rate of storage in the oceans (e.g. Oort and Vonder Haar 1976).

In the oceans, the energy made available at the surface is distributed through a much greater depth by convective motions and wind-driven mixing. The effective conductivity and hence the thermal capacity of the sea are thus far greater than those of the land. The oceans therefore respond only slowly to changes in insolation so that there is hardly any diurnal variation of sea surface temperature and the annual range of less than about 5°C occurs with a typical phase lag of 2-3 months. The behaviour of the temperature profile at high latitudes is illustrated in figure 3.4 (Perry and Walker 1977). At the end of winter the upper ocean is approximately isothermal following strong mixing by winter storms. As insolation increases a well-mixed layer is formed, whose lower boundary is marked by the so-called seasonal thermocline. In summer the thermocline becomes sufficiently stable to resist erosion by mixing from above, so the upper 100m or so is decoupled from the lower layers and warms rapidly. In autumn and winter this layer cools and the thermocline is progressively eroded by convection and wind-driven mixing.

The albedo, or reflectivity, of the surface to shortwave radiation plays an important part in the surface energy balance. The albedo of water surfaces to direct solar radiation varies from about 5% for an overhead sun to greater than 40% at solar elevations of less than 10°. This means that the oceanic albedo shows a systematic increase from the equator to the poles, the mean value being around 10% (Cogley 1979). Land surfaces show considerable variations in albedo as a result of the geographical distribution of surface type and global maps have been prepared, the most well known of which are those by Posey and Clapp (1964). Land surface albedos range from 10% for tropical rain forests, through about 35% for desert regions, to greater than 80% for fresh snow (Kukla and Robinson 1980).

Apart from the contrasting physical properties of land and sea noted above, there are other important differences. Over the oceans the availability of surface moisture is obviously high, so that evaporation (i.e. a latent heat flux) may be much more important than 'dry' convection (i.e. a sensible heat flux) in the surface energy budget. In contrast, the evaporation from land surfaces is part of a balance with precipitation and runoff, so that the evaporation may be less important and in the case of deserts is negligible.

Finally, it must be remembered that at high latitudes the phase change of water from liquid to solid is important for the heat budget of both land and sea. Sea-ice shows a seasonal variation in extent and strongly influences the surface fluxes. Land surfaces are able to sustain snow cover, which affects the surface heat balance through the latent heat required to melt the snow, as well as by increasing the albedo. This increase in albedo when snow is lying reduces the shortwave energy available to the system, which can lead to a reduction in temperatures and further snow cover. This snow-albedo feedback mechanism can therefore accentuate the tendency of the high-latitude continents to cool in winter.

4. Effect on surface temperature and pressure

The most important result from the previous section is the ability of the oceans to store large quantities of heat in the mixed layer. This ability is enhanced by the low albedo, so that typically 90% of the incident shortwave energy is absorbed. This energy may be advected to other regions by the ocean currents, which accounts for some of the annual-mean poleward transport of heat as shown by Figure 1.13. In general, however, the amount of heat exported by ocean currents from the summer to the winter hemisphere is smaller than the amount stored in each hemisphere separately in summer and subsequently released in winter. The oceans therefore act as efficient reservoirs of heat while the nearby continents show a much stronger seasonal temperature variation in response to the changes in radiation balance. This contrast is illustrated in Figure 3.5, which shows the mean observed surface air temperature for January and July, from Schlesinger and Gates (1979). In winter, the northern hemisphere continents are much colder than the oceans at the same latitude, the differences being 30°C or more at 60°N latitude. In summer, however, the continents are warmer, although the differences are now typically only about 5°C. A similar pattern is seen in the southern hemisphere, although the contrast is less marked due to the smaller land area. In terms of annual means, the continents are generally warmer than the nearby oceans in the tropics and cooler in higher latitudes.

Figure 3.6 shows a simple schematic model for the circulations to be expected from the land/sea surface temperature contrast. During spring and early summer the rise in land surface temperature leads to sensible heating of the air and therefore a reduction in surface pressure relative to the surrounding sea. This pressure difference leads to inflow at low levels and forces ascent of the heated air over the land. The net inflow at low levels must be balanced by outflow in the upper troposphere, leading to the formation of an upper high. The low-level flow is similar to the sea-breeze phenomenon, but this is shallow and transitory, while the continental scale circulations are long lived and may occupy the full depth of the troposphere. In winter, the land cools relative to the ocean, leading to high surface pressure and outflow at low levels. This is balanced by inflow at high levels and hence the formation of an upper low.

Unlike the sea breeze, in such long-lived circulations the wind and pressure fields have time to adjust to geostrophic balance. This means that in summer the low level winds spiral into the surface low with cyclonic vorticity and leave the upper high with anticyclonic vorticity. The sense of rotation is obviously reversed in winter.

5. Anticyclones and Monsoons

The preceeding arguments may be used to explain some of the main features of the PMSL fields shown in Figure 1.1. In doing this it must be appreciated that such thermally-driven circulations are often merely perturbations on some other flow pattern, thus distorting the simple picture of figure 3.6. Nevertheless, the sub-tropical anticyclones do indeed tend to form over the oceans in summer and over the land masses in winter. The different surface characteristics of land and sea thus assist in resolving the sub-tropical high pressure belts into individual cells. As pointed out in lecture 2, this enables absolute angular momentum to be transferred away from the tropics without the need for any large scale symmetric circulation.

The high pressure in the sub-tropics also exerts an important influence on the global moisture budget. Descending motion within the anticyclones leads to low relative humidities and hence small amounts of cloud and precipitation. The clear skies encourage strong shortwave heating of the underlying surface. Over land this can lead to the formation of deserts, where both precipitation and evaporation are small. Over the oceans, however, evaporation may be much greater than precipitation. In general, the sub-tropics are therefore net source regions of atmospheric moisture, whereas the excess of precipitation over evaporation in both the tropics and high latitudes means that these regions are net moisture sinks (see Figure 3.7, from Palmén and Newton (1969)). The general circulation maintains the water balance by transporting moisture between these sources and sinks. The trade winds, for example, remove water from the sub-tropics to enhance the moist convection in the ITCZ.

The most obvious example of the seasonal shift of the anticyclones is the replacement of the so-called Siberian High over central Asia in winter by a low pressure system in summer. The formation of the anticyclone is assisted by the net radiative cooling of both the atmosphere and land in the high latitudes in winter, which is enhanced in this region by the small cloud cover. In contrast, the summer heat low is formed further south due to the strong radiative heating of India and southern Asia. The resulting reversal of the surface winds leads to the familiar Monsoons of southern Asia, which are clearly shown on Halley's map (Figure 2.1). The south-westerly summer monsoon brings moist air from the Indian Ocean over the land, leading to a rainy season. The release of latent heat is an important feature which helps to intensify the circulation. In contrast, the winter monsoon brings north-easterly flow and a dry season.

The tendency for the upper level winds to reverse in direction compared to the low level flow is illustrated in Figure 3.8, taken from Johnson (1969). The outflow from the upper anticyclone over northern India in summer produces easterly winds at 200mb above the low level monsoon inflow. In winter, however, the surface north-easterly flow is compensated by south-westerly flow at 200mb into the intense sub-tropical jet stream at about 30°N latitude.

Although the Asian monsoon is the most well known example of this phenomenon, such wind reversals are also found in Africa, Australia and America. The detailed character of these circulations is determined by the disposition of land and sea, the presence of mountains and other factors. The latitude of the ITCZ thus shows strong variations with both longitude and time, and the simple Hadley cell is at best only a crude approximation to the real circulation. For a basic introduction to Monsoons see the article by Webster (1981) and the advanced lecture by Riddaway (1980), and for a compilation of recent research work see the comprehensive book of Lighthill and Pearce (1981).

References

Cogley, J G (1979) The albedo of water as a function of latitude. Mon. Weath. Rev. 107, 775-781.

Geiger, R (1965) The climate near the ground. Harvard University Press, Cambridge, Mass.

Johnson, D H (1969) The role of the tropics in the global circulation. In "The Global Circulation of the Atmosphere". Royal Met Soc, pp 113-136.

Kukla, G and Robinson, D (1980) Annual cycle of surface albedo. Mon. Weath. Rev., 108, 56-68.

Lighthill, M J and Pearce R P (editors) (1981) Monsoon Dynamics. Cambridge University Press, 735 pp.

Oort, A H and Vonder Haar, T H (1976) On the observed annual cycle in the Ocean-atmosphere heat balance over the northern hemisphere. J. Phys. Oceanogr, 6, 781-800.

Palmén, E and Newton, C W (1969) Atmospheric Circulation Systems. Academic Press, 603 pp.

Perry, A H and Walker, J M (1977) The ocean-atmosphere system. Longman, London, 160 pp.

Posey, J W and Clapp, P F (1964) Global distribution of normal surface albedo. Geofis. Int., 4, 33-48.

Riddaway, R W (1980) Monsoons. From "Some aspects of dynamical meteorology". (Advanced Lectures).

Schlesinger, M E and Gates, W L (1979) Performance of the Oregon state university two-level atmospheric general circulation model. In "Report of the JOC study conference on climate models: Performance, intercomparison and sensitivity studies". Vol.I, pp 139-206, GARP Publications Series no 22.

Webster, P J (1981) Monsoons. Sci. Am., 245, 70-80 (August)

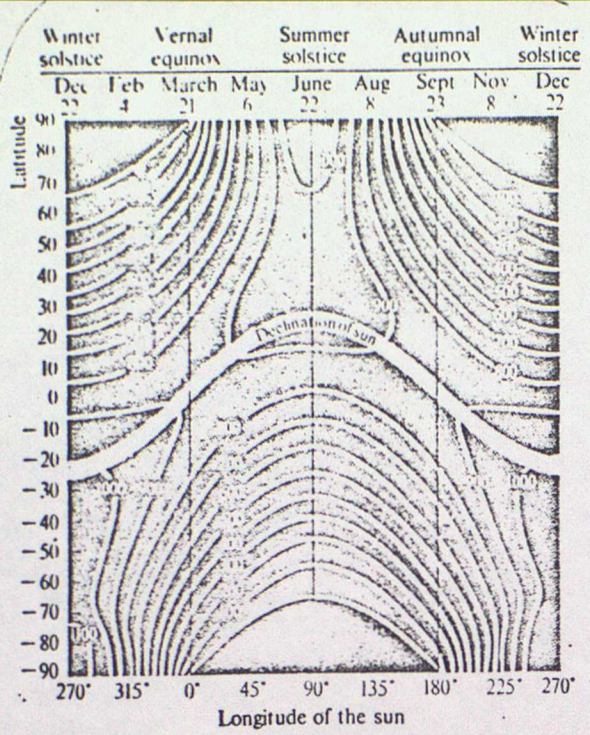

Amount of solar radiation falling daily upon a horizontal surface at the fringe of the atmosphere.

Figure 3.1

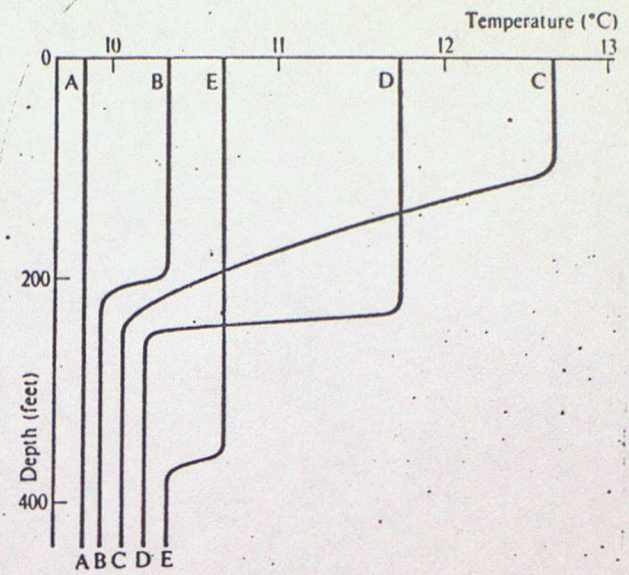

Typical vertical temperature distribution in the North-East Atlantic (a) end of winter, (b) spring, (c) summer, (d) autumn, (e) early winter.

Figure 3.4

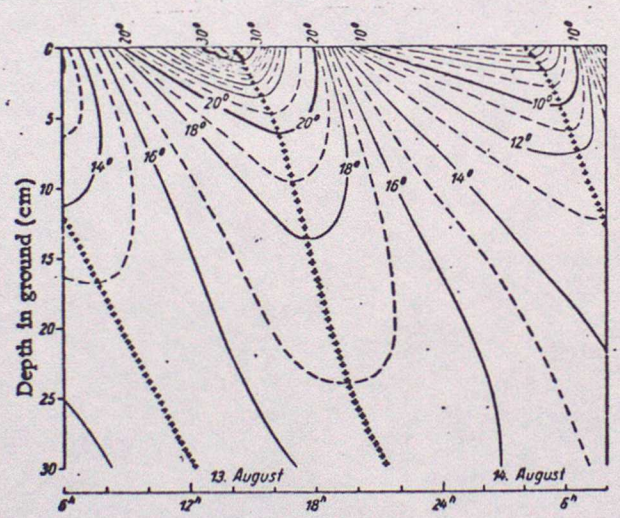

Penetration of the daily heat wave into the ground on an undisturbed summer day. (From observations by T. Homén in Finland)

Figure 3.2

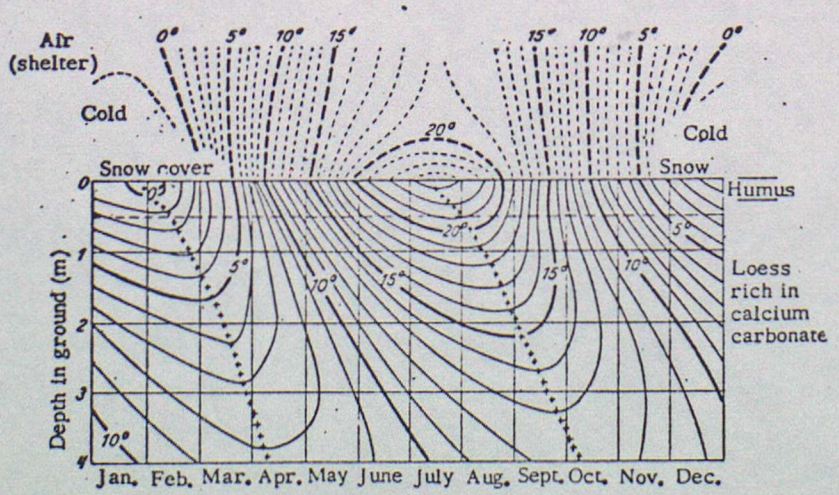

Annual sequence of temperature in the gardens of the Vienna Central Institute. (After M. Toperczer)

Figure 3.3

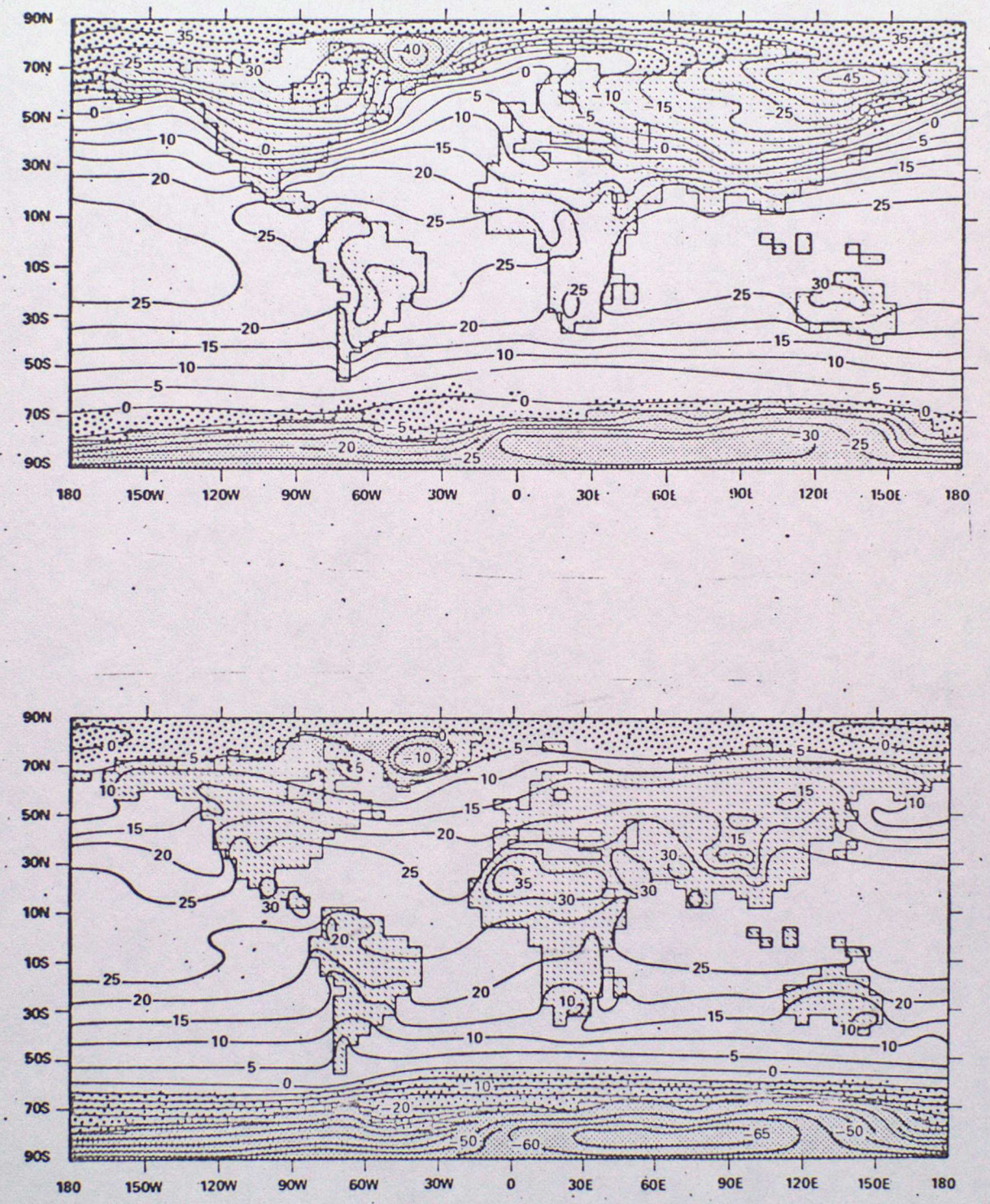

Figure 3.5 Observed surface air temperature (^{o}C) for January (above) and July (below)

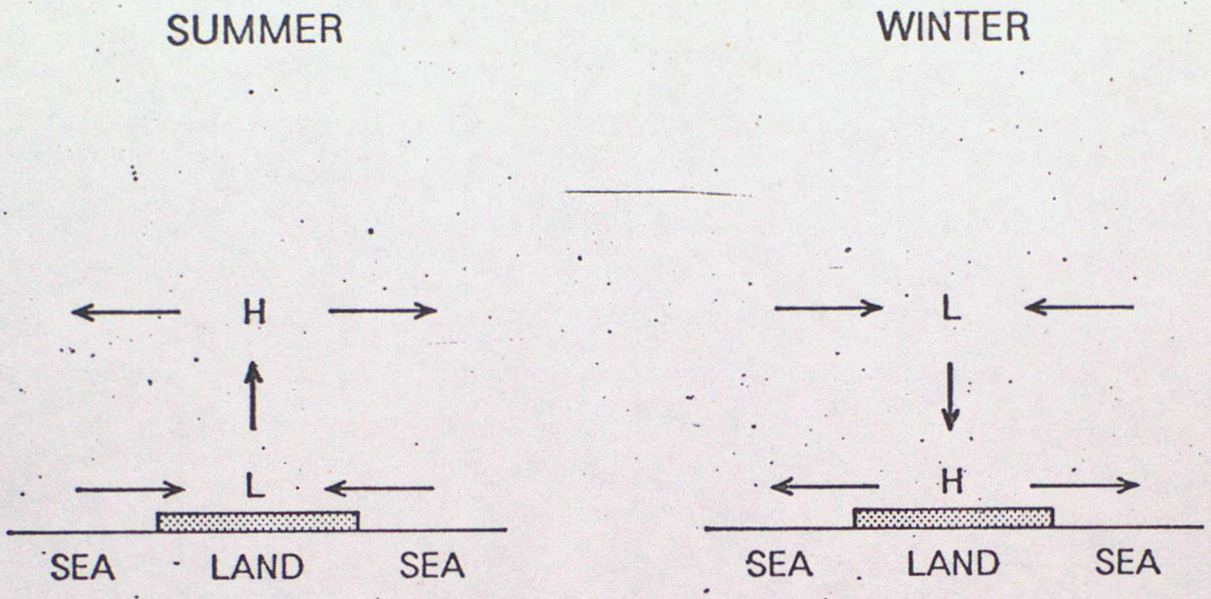

Figure 3.6 Schematic picture of the pressure distribution and circulations to be expected from the differential heating of land and sea

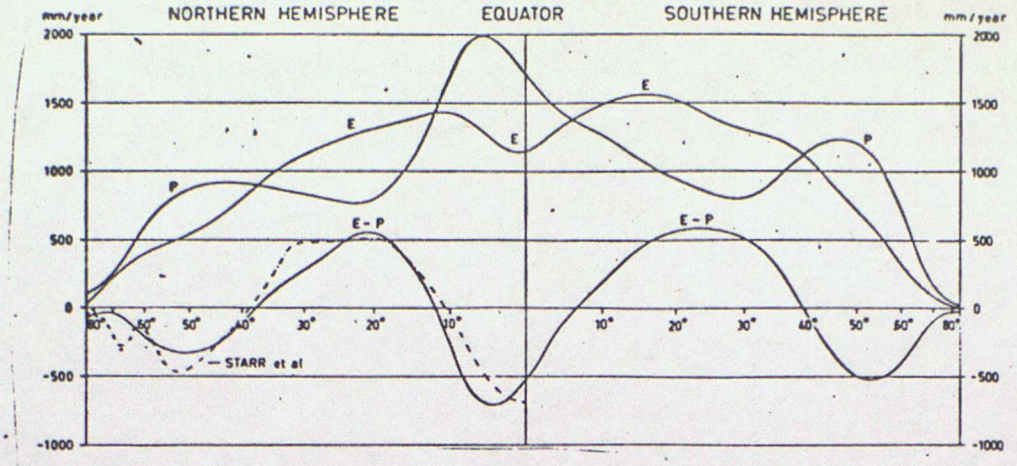

Mean annual distribution of precipitation (P), evaporation (E), and ($E - P$) over the globe, in millimeters per year (after Sellers, 1965). The dash-dotted curve represents ($E - P$) for one year, as computed by Starr *et al.* (1965) from the atmospheric flux of water vapor in the Northern Hemisphere. (Reprinted, redrawn, from W. D. Sellers, *Physical Climatology*, by permission of The University of Chicago Press, copyright 1965 by The University of Chicago.)

Figure 3.7

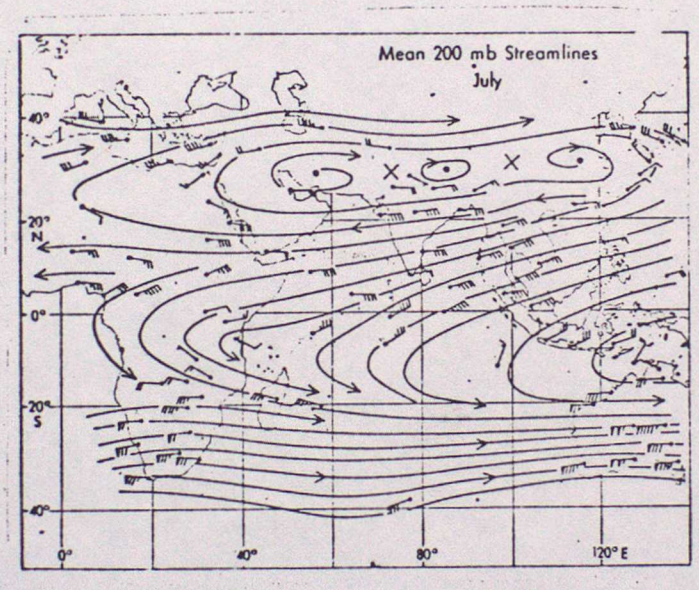

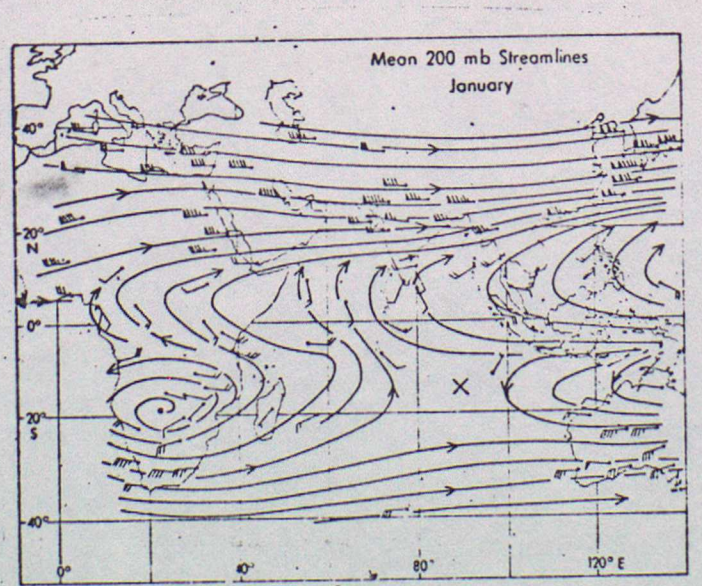

Figure 3.8 Mean 200mb streamlines for the Afro-Asian sector in July and January

ADVANCED LECTURES 1982 - GENERAL CIRCUIATION OF THE ATMOSPHERE

LECTURE 4 - Asymmetries (II)

1. Introduction

The asymmetric distribution of mean sea-level pressure shown in Figure 1.1, which may be accounted for partly by thermal forcing and its seasonal variation, is associated with similar departures from zonal flow at the 500 mb level. At high latitudes such departures can be very obvious on daily charts, where they are often associated with the movement of individual weather systems. When such charts are averaged over long periods these transient features disappear, but a wave-like pattern remains with troughs and ridges in preferred locations. This is illustrated by Figure 4.1, which shows examples of the mean 500 mb height fields for January and July in the northern hemisphere (from Palmén and Newton 1969). In winter there are strong troughs at about 80°W longitude and 140°E, and a weaker one at around 30°E. Although these troughs are less marked in summer, they remain in approximately the same place. The fact that such features appear in fixed geographical locations on time-mean maps indicates that they are forced by characteristics of the earth's surface.

The existence of these wave-like features led Rossby and his collaborators (1939) to examine the stability of a zonal flow to small perturbations. For simplicity, Rossby considered a frictionless, homogeneous, incompressible atmosphere in purely horizontal motion. For such a system the relative vorticity ζ and Coriolis parameter f are linked by the vorticity equation;

$$f + \zeta = \text{constant} \tag{4.1}$$

where $f = 2\Omega \sin\phi$ and $\zeta = \frac{\partial v}{\partial x} - \frac{\partial u}{\partial y}$ (4.2)

Let β be the rate at which the Coriolis parameter increases northward;

$$\beta = \frac{\partial f}{\partial y} = \frac{2\Omega \cos\phi}{R} \tag{4.3}$$

Then from equation 4.1;

$$\frac{\partial \zeta}{\partial t} = -\frac{\partial f}{\partial t} = -\frac{\partial f}{\partial y}\cdot\frac{\partial y}{\partial t} = -\beta v \tag{4.4}$$

By considering perturbations u' and v' to a zonal current of velocity U the following equation is derived;

$$\frac{\partial \zeta}{\partial t} + U\frac{\partial \zeta}{\partial x} = -\beta v' \tag{4.5}$$

which has wave solutions travelling eastward at velocity c;

$$c = U - \frac{\beta L^2}{4\pi^2} \tag{4.6}$$

The presence of the wavelength L in this equation means that Rossby waves are dispersive. There is a critical wavelength L_s for which the wave is stationary, so that the shorter waves propagate eastwards while the longer waves retrogress westwards;

$$L_s = 2\pi\sqrt{\frac{U}{\beta}} \tag{4.7}$$

The variation of the Coriolis parameter with latitude (the "β-effect") thus allows quasi-stationary planetary-scale waves to develop. The restrictive assumptions used here have been relaxed in subsequent work, but the results are essentially the same (eg Holton 1979, 165-168).

Rossby substituted observed values of zonal velocity into equation 4.7 and showed that the number of stationary waves to be expected around the earth was about 3-4, in qualitative agreement with observations. He pointed out, however, that detailed agreement is unlikely, because there is no reason to expect that the zonal velocity will always have such a value that these "free" oscillations will resonate exactly with the distribution of surface forcing around a latitude circle.

At this time it was generally believed that the large-scale features of the flow were forced by thermally driven "solenoidal" circulations arising from the land-sea temperature contrast, as shown by Figure 3.6, and perhaps modified by orographic effects. In the presence of the strong westerly flow aloft such circulations would not be closed, but would appear merely as perturbations superimposed on the flow. The tendency for a cyclonic circulation to be produced in upper levels over a cold land surface, as shown by the right-hand diagram in Figure 3.6, would therefore be expected to lead to a trough in the upper level flow. A ridge would form over regions of surface heating. This seemed to explain the two major winter troughs at 80°W and 140°E which form near the east coasts of North America and Asia, where the land-sea temperature contrast is greatest (eg see the top diagram in Figure 3.5).

2. Orographic Forcing

One obvious objection to thermal forcing as the cause of the asymmetries in the 500 mb flow is that there is no reversal in the phase of the pattern between winter and summer, as would be expected from the changes in surface temperature. This led Charney and Eliassen (1949) to investigate the effect of the forced ascent of the air over the continents. At this time Charney was at the centre of the first steps in numerical weather prediction and this paper is primarily concerned with refinements to the "equivalent-barotropic" model, which was integrated to perform the first numerical forecast (see the fascinating article by Platzmann 1979). In a preliminary forecast without surface forcing, Charney and Eliassen found that the very long waves propagated rapidly towards the west, as might be expected from free oscillations obeying equation (4.6). They included orographic forcing by setting the vertical velocity at the bottom of the atmosphere to be proportional to the slope of the surface, using a smoothed version of the earth's orographic heights. With no frictional dissipation this produced an excessive response, but with a simple treatment of frictional effects in the boundary layer a much improved forecast was obtained. They concluded that orographic forcing was responsible for the quasi-stationary features of the flow.

The profile of topographic height used by Charney and Eliassen at 45°N is shown in Figure 4.2. The main features on this profile are the Rocky mountains at about 110°W and the mountain ranges of central Asia at around 100°E. The great length and consistent elevation of the Rocky mountains in the north-south direction means that they are especially effective as barriers to the zonal flow. For such a barrier it is possible to derive the essential features of the response by considering conservation of potential vorticity. For a homogeneous, incompressible fluid of depth D a more general form of equation (4.1) may be written;

$$\frac{d}{dt}\left(\frac{\zeta+f}{D}\right) = 0 \qquad (4.8)$$

Consider the schematic diagram of the flow over the extensive north-south barrier shown by Figure 4.3 (from Holton 1979). The column of air M is confined between the two potential temperature surfaces θ_0 and $\theta_0 + \delta\theta$. For adiabatic flow the low level air approximately follows the surface contours, whereas the air at upper levels experiences a smaller vertical deflection. As the initially zonal current ($\zeta = 0$) crosses the mountain it therefore shrinks vertically and from equation (4.8) the relative vorticity must therefore become negative. This is equivalent to anticyclonic curvature, as can be seen from equation (4.2), remembering that the second term is assumed to be zero, so the column is deflected southwards. Beyond the mountain the air column returns to its original depth, but because the air is now further south than before, f is smaller and ζ must therefore become positive to satisfy equation (4.8). Cyclonic curvature is produced which remains until the air is back at its original latitude. The air now overshoots northward and experiences an increasing coriolis parameter which returns the air to the south. This oscillatory behaviour continues as the air moves away from the mountain. Such a barrier therefore induces a ridge over the mountain and a lee trough to the east, followed by a train of forced Rossby waves. As Charney and Eliassen found, the effect of surface friction is to reduce the amplitude of these waves progressively as the air moves downstream.

Bolin (1950) extended the work of Charney and Eliassen by considering the effect of an isolated circular mountain and of the finite width of the zonal current. He showed that the perturbations were strongly dependent on the size of the mountain, so that ranges much smaller than the Rockies would not be expected to influence the planetary-scale flow significantly. One would therefore expect to find only two major troughs in the northern hemisphere, downstream of the American and Asian mountain ranges, as is observed. This relationship is emphasized by a comparison of the January mean 500 mb height field (Figure 4.1) with the smoothed topographic heights shown in Figure 4.4. These heights are from a 1° dataset produced at the Scripps Institute of Oceanography, which is here degraded to 2° resolution and plotted using a package developed in Met O 20. Although the smaller mountain ranges do not affect the large-scale flow, the general character of the response shown by Figure 4.3 is still found. The trough which forms to the lee of a range may therefore be a preferred location for cyclogenesis, as described by Riddaway (1980). A case study of cyclogenesis in the lee of the Alps has been carried out by Buzzi and Tibaldi (1978).

It will be noticed from Figure 4.4 that the mountains of central Asia occupy only a narrow latitude band, while their east-west extent is considerable. Their influence on the flow is thus quite different from that of the Rocky mountains. In summer the mean jet at upper levels is found to the north of the Tibetan plateau, where the mountains are considerably lower. This has been taken as the reason for the weakening of the downstream trough at this time of year. In contrast, the winter jet is further south and is split into two, one flowing to the north and one to the south of the plateau, leading to a marked change in the circulation over China (Yeh 1950).

The importance of the torque which surface friction produces between atmosphere and earth was stressed in lecture 2. Mountain ranges contribute an additional torque due to the pressure difference across the range arising from the presence of the lee-side trough (eg see Holton (1979) pp 260-266). The fraction of the earth's surface covered by mountains is small, so the mountain torque can show greater variability than the frictional torque. Until recently, the calculation of these terms has been hampered by inadequate data coverage, but the improved analyses obtained during the First GARP Global Experiment (FGGE) enabled them to be calculated and compared with the observed changes in atmospheric angular momentum. Figure 4.5 shows an example of how the calculated torques compare with that implied by the observed meridional transport of

angular momentum (from Swinbank 1981). It will be seen that the mountain and frictional torques are of similar magnitudes and that there is reasonable agreement between their sum and the torque calculated from the momentum flux. The sense of the torques is such that positive values correspond to a transfer of angular momentum from the atmosphere to the surface, so that as noted in lecture 2 the tropics are in general source regions of atmospheric angular momentum and the mid-latitudes are sinks.

3. Combined effects of forcing mechanisms

The ability of both thermal and orographic forcing to explain major features of the asymmetries in the atmospheric circulation suggests that any general theory must take account of both mechanisms. This has not always been accepted; Sutcliffe (1951), for example, took exception to the work of Charney and Eliassen (1949) and maintained that the observed features were quite consistent with thermal forcing acting alone. Bolin (1950) argued that the effects of the surface temperature contrast between land and sea should diminish upwards, whereas the jet streams would respond strongly to the influence of mountains. He therefore proposed that thermal influences would be most evident in the lower troposphere, while orographic effects would dominate the upper level flow. These conclusions have been borne out by the modelling work of Smagorinsky (1953) and by the GCM studies of Mintz, and later Manabe and his co-workers. The GCM results will be discussed in the final lecture.

The fact that the Rocky mountains are on the west coast of America suggests that the two forcing mechanisms co-operate in maintaining the strong trough near the east coast of the continent in winter. Over Asia, however, the situation is more complicated. The Tibetan plateau, for example, not only affects the flow directly, but it also provides an elevated heat source in summer. Flohn, and later Koteswaram (1958), suggested that this was largely responsible for the upper tropospheric anticyclone in this region, which appears on Figure 3.8 and is more obvious on Figure 4.6 (from Koteswaram 1958, re-drawn by Palmén and Newton 1969). Sutcliffe (1951) pointed out that one important result of the height and east-west extent of the Himalayas is that they act as a barrier between warm air to the south and cold air to the north. This orographic barrier therefore accentuates the meridional temperature contrast and hence the importance of thermal forcing.

References

Bolin, B 1950 On the influence of the earth's orography on the general character of the westerlies. Tellus, 2, 184–195.

Buzzi, A and Tibaldi, S 1978 Cyclogenesis in the lee of the Alps: A case study. Quart J R Met Soc, 104, 271–287.

Charney, J G and Eliassen, A 1949 A numerical method for predicting the perturbations of the middle latitude westerlies. Tellus, 1, 38–54.

Holton, J R 1979 An introduction to dynamic meteorology. (Second Edition), Academic Press, 391 pp.

Koteswaram, P 1958 The easterly jet stream in the tropics. Tellus, 10, 43–57.

Palmén, E and Newton, C W 1969 Atmospheric circulation systems. Academic Press, 603 pp.

Platzmann, G W 1979 The ENIAC computations of 1950 – Gateway to numerical weather prediction. Bull Amer Met Soc, 60, 302–312.

Riddaway, R W 1980 Orographic lows. From "Some aspects of dynamical meteorology". (Advanced Lectures).

Rossby, C–G and Collaborators 1939 Relation between variations in the intensity of the zonal circulation of the atmosphere and the displacements of the semi–permanent centers of action. J Marine Res, 2, 38–55.

Smagorinsky, J 1953 The dynamical influence of large–scale heat sources and sinks on the quasi–stationary mean motions of the atmosphere. Quart J R Met Soc, 79, 342–366.

Sutcliffe, R C 1951 Mean upper contour patterns of the northern hemisphere — the thermal–synoptic view–point. Quart J R Met Soc, 77, 435–440.

Swinbank, R 1981 The global atmospheric angular momentum balance inferred from analyses made during the FGGE and general circulation model experiments. Met O 20 Technical Note II/173.

Yeh, T–C 1950 The circulation of the high troposphere over China in the winter of 1945–46. Tellus, 2, 173–183.

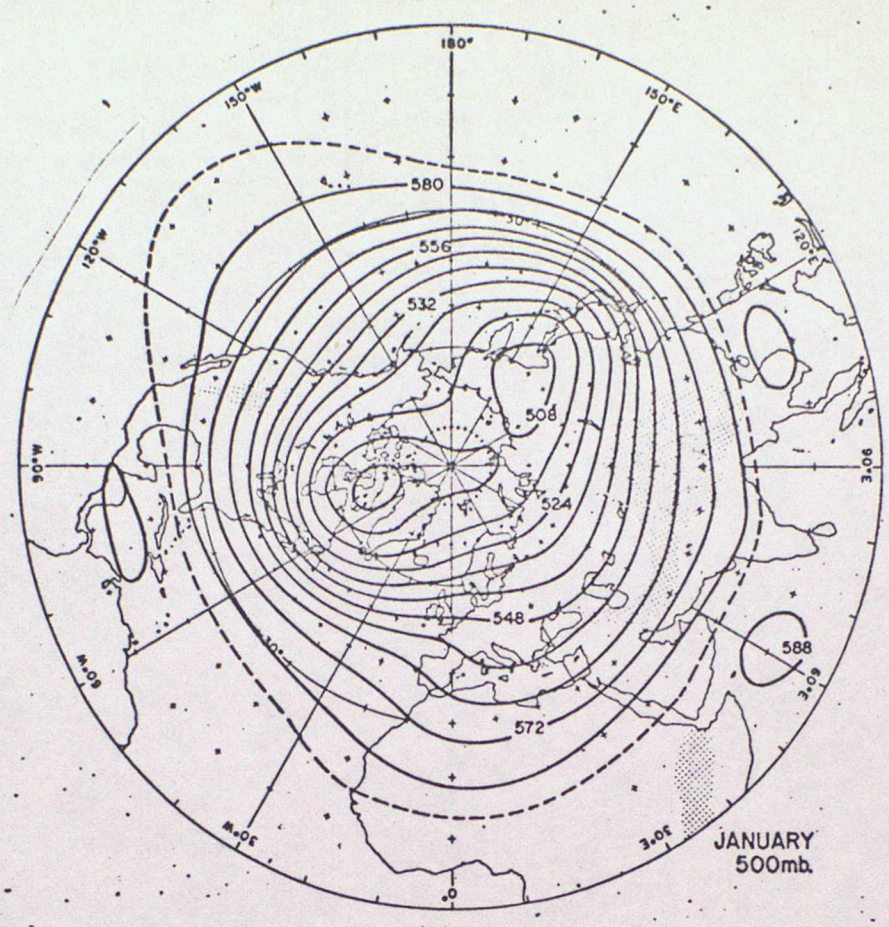

Mean 500-mb contours in January (winter), Northern Hemisphere. Redrawn at 80-m intervals from I. Jacobs (1958). Light and heavier stippling show regions where elevations are above 1.5 km and 5 km (smoothed over 5° latitude-longitude tessera), from Berkofsky and Bertoni (1955).

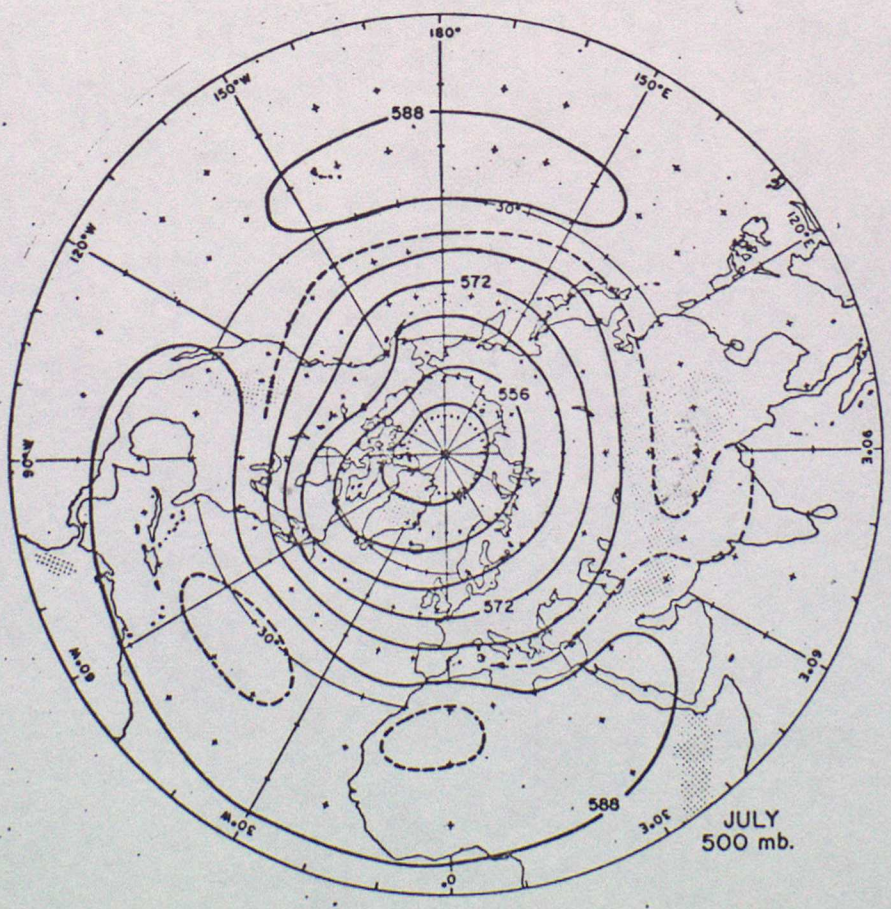

Mean 500-mb contours in July (summer), Northern Hemisphere. (Redrawn, from I. Jacobs, 1958.)

Figure 4.1

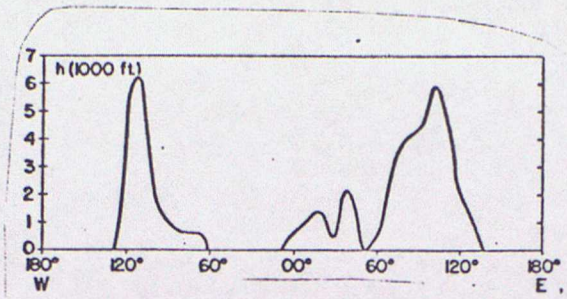

Topographical profile at 45° N. The elevations represent the mean height of the earth's surface, averaged for the interval 40° N to 50° N, as a function of longitude.

Figure 4.2

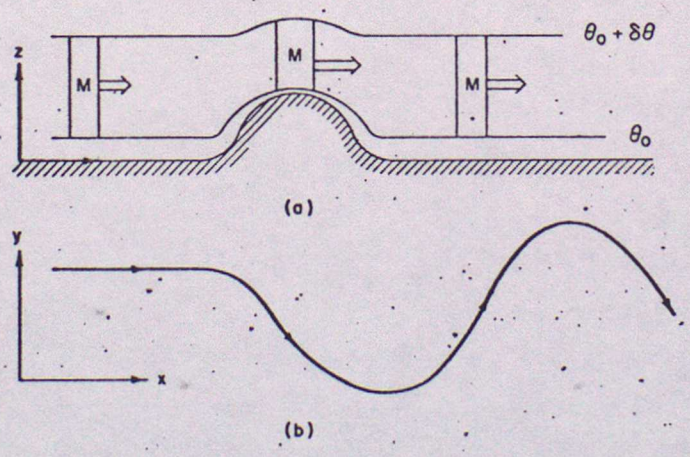

Westerly flow over a topographic barrier: (a) the depth of a column as a function of x, (b) the trajectory of a parcel in the x, y plane.

Figure 4.3

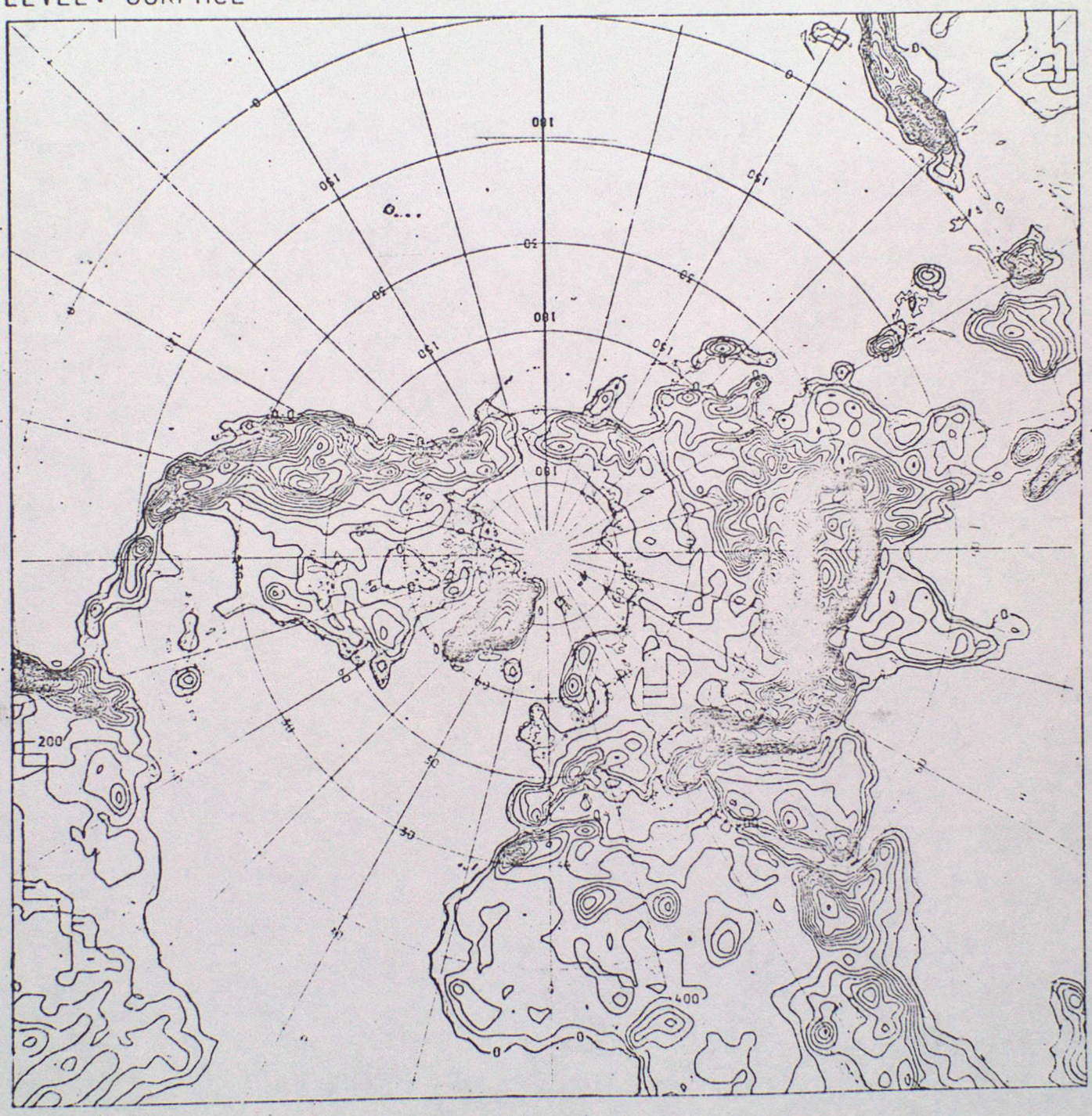

Figure 4.4 Contours of topographic height over the northern hemisphere at 2° resolution. Square contours are artifacts of the plotting program.

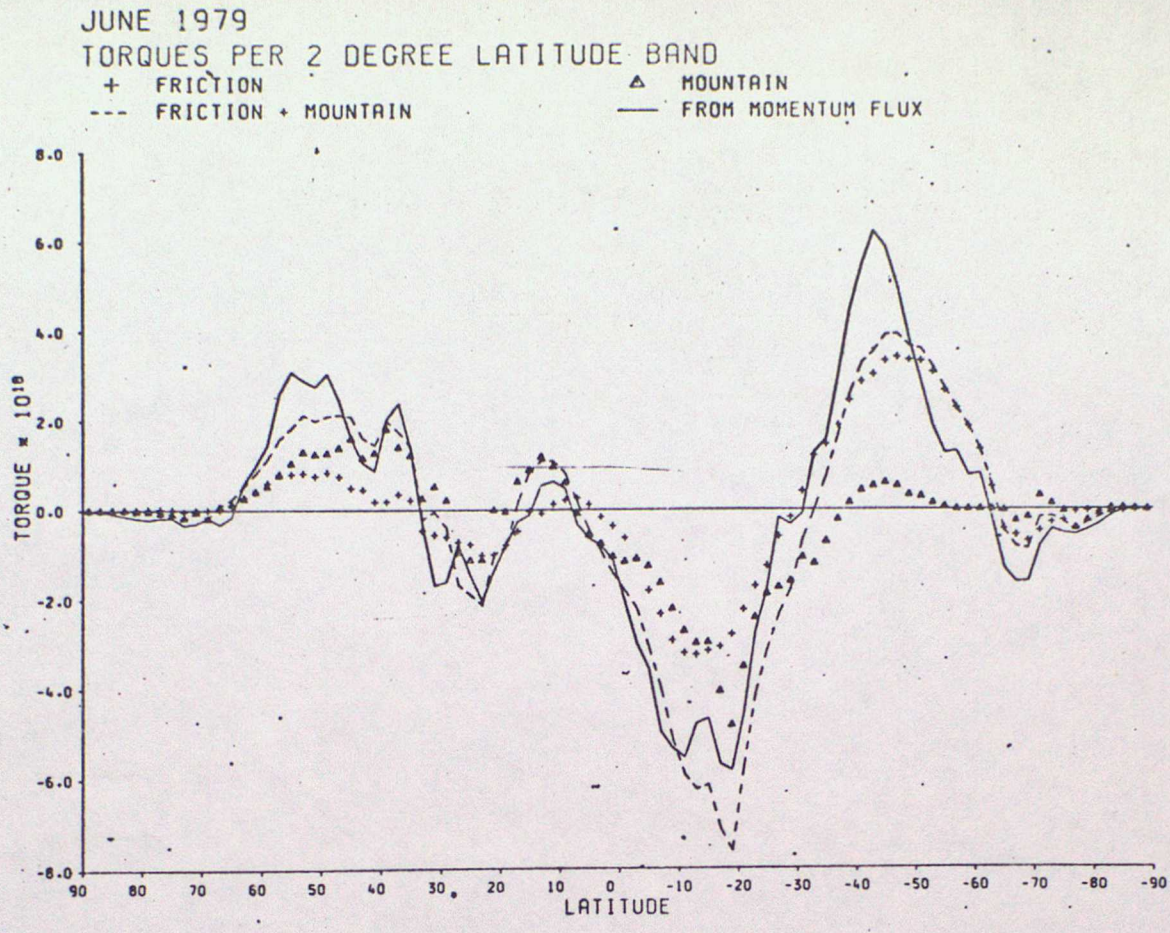

Figure 4.5 Comparison of the Friction and Mountain torques calculated from FGGE data with the torque implied by the observed meridional transport of angular momentum (from Swinbank 1981).

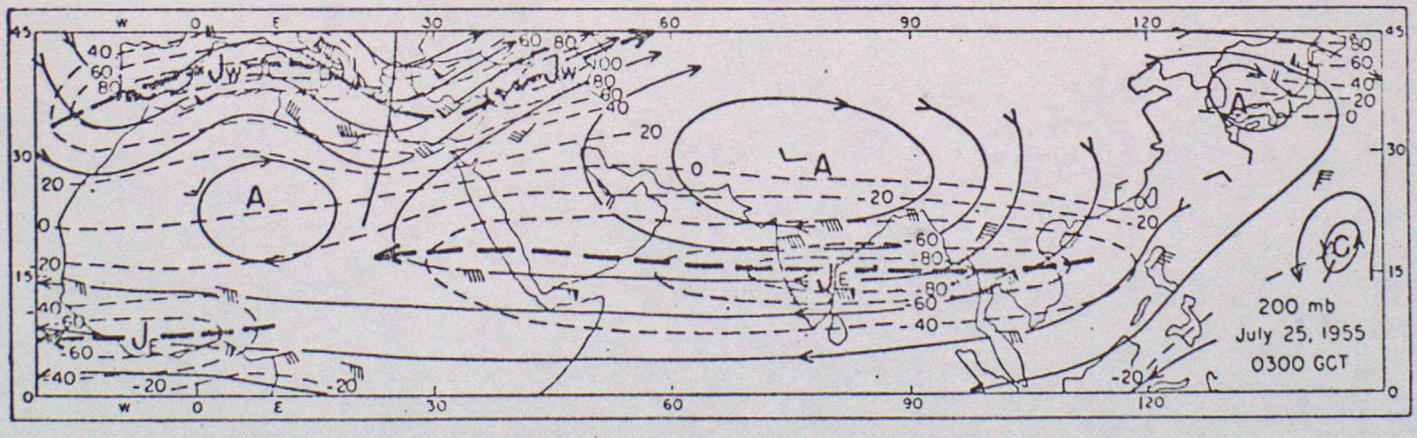

Streamlines and isotachs (knots, negative for easterly component) at 200-mb surface, 03 GCT July 25, 1955. Heavy dashed lines are axes of easterly and westerly jets. (After Koteswaram, 1958.)

Figure 4.6

MD

ADVANCED LECTURES 1982 - GENERAL CIRCULATION OF THE ATMOSPHERE

LECTURE 5 - Observing the General Circulation

1. Why?

a. Description

The first stage in any scientific investigation must be to collect, organise and look at the data. This has been done for the general circulation since at least the 17th century; an example from Halley's 1686 paper was shown in Fig 2.1. Comparison of this with recent data (Fig 5.1) shows that the sea level wind field was well described by Halley. However it should not be assumed from this that nothing significant remains to be discovered. Several interesting phenomena have been noticed this century, and no doubt there will be more.

b. Understanding

Having described a phenomenon, the second stage is to propose hypotheses or models (in the scientific sense of the word) to explain it. These then need to be tested by further observations (or further processing of existing observations). A classic example of this is the work of V Starr and his colleagues of MIT (eg Starr and White 1951, Starr 1953, Starr 1954) showing that eddies enhanced the mean zonal flow, rather than feeding off it, and hence must be a fundamental part of the circulation, rather than just turbulence. Figure 5.2 shows an extract from Starr 1953. Would that all observational studies could be reduced to so simple a graph!

c. Application

Meteorology is an applied science, and having described and understood a phenomenon, it is natural to wish to apply this knowledge in forecasts or other studies. Frequently greater accuracy of measurement is needed for this. Examples are budget studies (described next lecture) where a quantity is measured so as to be able to calculate something else, much work aimed at improving and testing parametrization schemes for numerical models (in the meteorological sense of "model"), and work aimed at establishing methods for medium or long range forecasting. The GARP Atlantic Tropical Experiment (GATE) had improved parametrizations as a main objective:-

> "The main purpose of GATE is to improve our understanding of the relationship between the convective and synoptic-scale motions. This will provide a scientific basis for parametrization of these convective motions and their associated vertical transports in terms of the synoptic-scale wind, temperature and moisture fields. Therefore, it is necessary to monitor the bulk properties and internal structure of the convective ensembles and to relate the features of these ensembles to the synoptic-scale environment." (GARP 1974).

The most expensive scientific experiment ever, the First GARP Global Experiment (FGGE) had both understanding and model development as its first objective:-

> "To obtain a better understanding of atmospheric motion for the development of more realistic models for extending range forecasting, general circulation studies and climate." (GARP 1973).

The Global Atmospheric Research Programme (GARP) itself emphasises model design and testing:-

> "This programme consists of two distinct parts, which are, however, closely interrelated:
>
> (i) The design and testing by computational methods of a series of theoretical models of relevant aspects of the atmosphere's behaviour to permit an increasingly precise description of the significant physical processes and their interactions;
>
> (ii) Observational and experimental studies of the atmosphere to provide the data required for the design of such theoretical models and the testing of their validity."
>
> (Inside cover of any GARP publication).

This emphasis prompted the following remark by Tucker (1981) which I think is worth repeating:-

> "During the decade 1965-75 numerical modelling so dominated meteorology that an impartial observer might have been forgiven for wondering whether the primary concern of research had shifted from the real world, the atmosphere, to the hypothetical world, the model. So much so that many papers describing observational studies began with what was suspiciously like an apology, giving as their rationale the need to develop parametrization schemes or to provide validation data for numerical models. Indeed in many circles the whole concept of FGGE was regarded as being primarily for the benefit of numerical modellers.
>
> More recently, possibly because the limitations of numerical models have become better and more widely understood and something of a plateau in modelling techniques is being approached, there has been a return to a more balanced attitude."

2. How?

In order to derive comprehensible statistics from a large number of scattered observations two processes are necessary; a time averaging and an analysis (ie space averaging and interpolation, transforming to a regular grid or chart). Studies using conventional data can usually be classified according to the order in which these are done, as shown in figure 5.3. A comparison of results using both these schemes has been published by Lau and Oort (1981 and 1982). Much of the next two sections is adapted from their descriptions.

a. Scheme A (station time-averaging, then analysis of mean fields)

The desired statistics are compiled at individual reporting stations for a sufficiently long period such as a month or a season, and the horizontal fields of these statistics are then mapped onto a suitable grid. Prior to the era of automated data processing, the latter step generally involves subjective hand analysis. Since the 1960's, objective analysis techniques utilizing digital computers have been employed.

In this scheme, the quantities to be analyzed are circulation statistics accumulated at the sites of individual stations. Generally, there exists no physical basis for making a priori assumptions on how various patterns should behave in the data-sparse regions. In order to devise an

initial-guess field for the objective analysis step, one often resorts to smoothed quantities such as the zonal or areal average of the available station data. For those long-term averaged statistics with rather smooth patterns, such choices for the first-guess field are probably reasonable. However, the analyzed pattern over the no-data areas would largely reflect the zonal or areal mean conditions, and any actual extremum values there would not be detected.

Examples of observational studies utilizing data compilations based on earlier versions of Scheme A (using subjective analyses) may be found in the voluminous works by V P Starr and his co-workers of the Planetary Circulations Project at the Massachusetts Institute of Technology (MIT). Most of these works are collected in Starr and Saltzmann (1966). These efforts were continued at Environmental Research and Technology, Inc (ERT), for describing the water cycle (see e.g., Peixoto et al, 1978). Various versions of Scheme A were also used by Crutcher (1959) and Crutcher and Meserve (1970) for constructing climatological charts of the Northern Hemisphere, by Oort and Rasmusson (1971) at the Geophysical Fluid Dynamics Laboratory (GFDL) for documenting zonally averaged circulation statistics north of 10°S, and by Newell et al (1972, 1974) at MIT for examining the circulation of the tropical and subtropical atmospheres. These sets of analyzed circulation statistics have laid the groundwork for a variety of observational studies. Such studies include the variability and annual cycle of the atmospheric energetics by Peixoto and Oort (1974) and Oort and Peixoto (1974, 1976), the ocean-atmosphere heat balance by Oort and vonder Haar (1976), the momentum and kinetic energy balances of the tropics by Oort and Chan (1977), the local balances of kinetic energy and vorticity to Holopainen (1978a, b), and the hemispheric distribution of diabatic heating rates by Geller and Avery (1978). More recently, a comprehensive collection of global circulation statistics has been archived at GFDL by processing the radiosonde soundings for the 15-year period from 1958 to 1973. Part of this data set will be published in the form of microfiches (Oort, 1982).

Method A has been, and will continue to be useful for case studies when the dynamical assumptions of Method 3 are undesirable (eg Vincent 1981).

b. Scheme B (synoptic analysis for NWP, then time-averaging)

At regular time intervals, such as every 12 h, synoptic charts are constructed by analyzing the observations of the current atmospheric circulation on a regular grid. The desired statistics are then obtained by processing the gridded data for a long series of these charts. The synoptic analyses are often by-products of the forecast procedures at most operational weather centers, which typically consist of repetitive forecast-analysis-forecast cycles. In these cycles, the numerical prediction model makes use of the gridded synoptic data to generate the forecast for the next synoptic time, which is in turn modified by objectively inserting new observations. The updated version then serves as new initial conditions for the next forecast phase of the cycle.

In this scheme, the initial-guess fields for the objective analysis of synoptic reports are the model-generated forecasts. Through this process new information is continuously fed into the data-sparse regions. The usefulness of such information depends, of course, on the performance of the operational models. This scheme also allows for the routine incorporation of dynamical constraints such as hydrostatic balance and gradient wind balance into the first guess for instantaneous temperature, pressure and motion fields. These constraints are useful for estimating

certain aspects of the circulation in data-sparse regions. For instance, one may infer the wind field in such a region from the pressure gradients prescribed by observations surrounding that region. However, the same constraints also result in systematic bias. For instance, by making use of the gradient wind equation or the balance equation in the first guess, the ageostrophic component of the flow over data-sparse regions would be significantly underestimated. This scheme does make possible direct calculations of vertical transient eddy fluxes in principle although as yet inaccurate in practice because of the constraints just mentioned.

The analyzed products of various versions of Scheme B have been used by Klein (1951) for studying the daily pressure variability, by Clapp (1956) for examining various components of the vorticity balance, by Wiin-Nielsen (1959), Wiin-Nielsen et al (1963, 1964), Brown (1964), and Krueger et al (1965) for studying atmospheric energetics, by Haines and Winston (1963) for analyzing heat transport processes, by van Loon et al (1973) for describing the structure of planetary-scale standing waves, and more recently, by Blackmon (1976), Blackmon et al (1977) and Trenberth (1979, 1980) for examining the local features of the general circulation. Over the years, R L Jenne and his associates at the National Center for Atmospheric Research (NCAR) have made a sustained effort to archive the twice-daily analyses produced by the US National Meteorological Center (NMC), and to consolidate these data grids in a tape library for meteorological research. By making use of these NMC analyses for 11 winter seasons, Lau (1978) has compiled a set of mean, temporal variance and covariance circulation statistics. This data set forms the basis for a series of investigations on the regional characteristics of the Northern Hemisphere wintertime circulation (eg Lau, 1979a, b; Lau and Wallace, 1979; Blackmon and Lau, 1980). G H White of the University of Washington has recently documented a parallel set of the summertime circulation statistics. A selection of the NMC statistics for both seasons is available as an NCAR technical note (Lau et al, 1981).

In the last few years, thanks to the impetus of FGGE, satellite observing systems, and the increase in computing power, objective analyses have become more reliable and generally available. Thus in addition to the above references which used NMC analyses (the longest series available) many other studies are under way and will soon lead to published results. Results from FGGE should be appearing over the next few years (eg Lyne et al 1982, Physick 1981).

A joint Meteorological Office-Reading University project has been calculating diagnostics using ECMWF global analyses since 1980 (James and Raper 1981, White 1982). Because such calculations can now be relatively easily automated, with problems of quality control and objective analysis left to the operational scheme, this method will become much more prevalent than scheme A. Indeed already available results can easily overwhelm one in a mass of indigestable figures, and problems of selection and presentation are large.

c. Unconventional data sources (satellites)

Various useful studies have been performed using data not yet integrated into the "conventional" data used by schemes A and B. First of these data were cloud pictures. Much work has been done on the classification of cloud vortices, and statistics of the frequency of these types, with parametrized transport statistics derived using a model of a cyclone lifecycle, have been presented by Tucker (1979). Animation of

pictures from geostationary satellites have demonstrated clearly some interesting interactions between tropical convection cells and mid-latitudes (Fleming and Bohen 1981) which may lead to an upward revision of earlier estimates of atmospheric heat fluxes.

Satellite data have also been used directly in studies of radiation budget (Winston et al 1979), clouds (Bean and Somerville 1980), the stratosphere (Pick and Brownscombe 1981), rainfall (Rao et al 1976) etc.

d. Studies of quantities difficult to observe directly

Most surface fluxes fall into this category, as do diabatic terms in the heat budget and terms involving ageostrophic or divergent wind and vertical motion.

Two methods are used:-

(i) The direct method

Here parametrized relationships are used to calculate the desired quantity (eg evaporation, radiative heating) from quantities which are known. Examples are Budyko (1973), Newell et al (1974), Dopplick (1979).

(ii) The indirect method

Here the desired quantity is calculated as a residue from a budget study using other observable or parametrizable fluxes. Examples will be given in Lecture 6.

3. How Well?

a. Accuracy

It is well known that the southern hemisphere and tropics are deficient in the conventional radiosonde observations needed for method A. The errors to which this can lead have been studied in a simulation by Oort (1978). Gaps in the northern hemisphere can also be significant since they are biased to the oceans where the wintertime jets are strong, leading to systematic errors. Figure 5.4 shows maps of zonal wind from GFDL (method A) and NMC (method B) analyses, and zonal mean kinetic energies of the zonal mean flow and the standing eddies (from Lau and Oort 1981). Method A's underestimation of the Pacific and Atlantic jets leads to nearly a factor of two difference in the standing eddy kinetic energy. As well as errors due to imperfect data coverage in space, all methods naturally have errors due to estimating long-term averages from limited periods of data. Inter-annual variability can be quite large; some (if viewed from a sufficient distance) essentially random, but some attributable to physical mechanisms having longer timescales than most atmospheric phenomena (eg snowcover, sea surface temperatures). Understanding the latter, or just observing it without understanding, has great importance for long-range forecasting and there have been many studies. This is however beyond the scope of the present lecture series, and I limit myself to giving a few references where data on inter-annual variability may be found (Oort and Peixoto 1976, Oort 1977, Blackmon et al 1977, Carlton 1979, Trenberth 1979, Lau et al 1981).

Method B is highly susceptible to biases in the analysis scheme itself or the numerical weather prediction model used to provide a first-guess. Sometimes these are well understood and the errors can be anticipated, as

in the NMC Hough function analysis which forces non-divergent wind fields and hence zero vertical velocities (Rosen and Salstein 1980). Others are less expected; the Australian analyses were considered about the best available for the southern hemisphere before FGGE, having considerable human interaction and monitoring. However this concentrates on sea level pressure and 1000-500 mb thickness; other fields are not necessarily dynamically consistent. Figure 5.5a (from Van Loon 1980) shows the transient eddy temperature flux from these analyses, the correspondence of peaks with radiosonde stations (without physical justification) indicates that method A would have been more accurate. The zonal mean cross section has an entirely incorrect equatorward stratospheric flow Figure 5.5b) which is not present in NMC analyses (Figure 5.5c). The latter had less data and almost no human intervention in the southern hemisphere and so perhaps were internally more dynamically consistent even if in other ways inferior.

Satellite remote sensing has its own problems; often pushing technology beyond the limits of absolute calibration it generally relies on calibration against conventional data. Thus the coverage obtained gives a qualitatively accurate overall picture, but the absolute accuracy depends on the calibrating conventional data, which are usually insufficient over the oceans. Often the microphysical basis of the conversion from observed radiances to the desired meteorological parameters is not accurately understood, for example microwave scattering-sea surface roughness-surface stress-low level wind, or microwave attenuation-cloud drop distribution-rainfall rate. Lovejoy and Austin (1980) estimate that the latter uncertainty give a limit to potential accuracy in rainfall rate measurements of $\pm$ 70%, with actual accuracy from Nimbus 7 $\pm$ 370%.

Finally, so called direct methods of calculating diabatic heating, vertical motions etc rely entirely on the accuracy of the parametrizations used. Since similar methods are used in general circulation models one must take care when verifying GCM results against these data. Indirect methods, using budget studies are desirable. These are discussed in Lecture 6.

b. Representativeness

"There are three kinds of lies; lies, damned lies, and statistics". (attributed to Mark Twain). As in all science, one should always study how accurate any set of observations is, and as with all statistics, one must be very careful that the impression gained from the results presented is truly justified. For example Figure 1.4 was selected to demonstrate the conventional picture of Hadley, Ferrel and Polar cells. However if, following Krishnamurti (1971), we chose to present the (horizontally) divergent wind using maps of velocity potential as in Figure 5.6, the impression gained is entirely different. (Note that zonal mean v must be divergent). If on the other hand we chose to use potential temperature instead of pressure as vertical co-ordinate we apparently demonstrate that the single thermally direct cell discarded at the beginning of Lecture 2 was correct after all (Figure 5.7 from Townsend and Johnson 1981). Like politicians we can chose our statistics either for or against a Ferrel cell!

4. Some useful data sources

The following, from among the large reference list for this lecture, are useful sources of data.

Budyko	(1963)	Global maps of heat balance, evaporation, radiation etc.
Schutts and Gates	(1971,2,3,4)	Global maps of surface, 800 mb, 400 mb.
Oort and Rasmusson	(1971)	Northern hemisphere zonal mean fields and fluxes (tables and cross-sections). I expect Oort (1982) also to be useful.
Newell et al	(1972,1974)	Tropical and global maps and cross-sections of fields, budget studies.
Lau et al	(1981)	Northern hemisphere maps and cross-sections of fields and fluxes, including time-filtered eddies.
Van Loon et al	(1972)	Southern hemisphere data.

Synoptic Climatology (Met O 13) computer archives. Northern hemisphere daily fields of sea level pressure (since 1881) and 500 mb height (since 1945).

Dynamical Climatology (Met O 20) FGGE computer archives. Global 12 hourly fields 1000 mb–10 mb height, wind, temperature, humidity for the year December 1978–November 1979.

References for Lectures 5 and 6

Alestalo, M. 1981 The energy budget of the earth-atmosphere system in Europe. Tellus 33 360-371.

Bean, S.T. and Somerville, P.N. 1980 Some new worldwide cloud cover models. Statistical Climatology. Developments in Atmospheric Science, 13. S. Ibeda ed. 279-305.

Blackmon, M.L. 1976 A climatological spectral study of the 500 mb geopotential height of the northern hemisphere. J. Atmos. Sci. 33 1607-1623.

Blackmon, M.L. Wallace, J.M., Lau, N-C. and Mullen, S.T. 1977 An observational study of the northern hemisphere wintertime circulation. J. Atmos. Sci. 34 1040-1053.

Blackmon, M.L., and Lau, N-C. 1980 Regional characteristics of the Northern Hemisphere wintertime circulation: a comparison of the simulation of a GFDL general circulation model with observations. J. Atmos. Sci. 37 497-514.

Budyko, M.I. 1963. Atlas of heat balance of the world. Globnaia Geofiz. Observ.

Carlton, A.M. 1979 A synoptic climatology of satellite observed extratropical cyclone activity for the Southern Hemisphere winter. Arch. Met. Geophys. Biobl. B. 27 265-279.

Clapp, P.F. 1956 Some considerations involved in preparing long range weather forecasts by numerical methods. J. Met. 13 341-350.

Crutcher, H.L. 1959 Upper wind statistics charts of the northern hemisphere, Vols 1 & 2. NAVAER 50-IC-535 Office of the Chief of Naval Operations. Washington, D.C.

Crutcher, H.L., and Meserve, J.M. 1970 Selected level heights temperatures and dew points for the northern hemisphere. NAVAIR 50-IC-52 (US Govt Printing Office).

Dopplick, J.G. 1979 Radiative heating of the global atmosphere: Corrigendum. J. Atmos. Sci 36 1812-1817.

ECMWF 1980 Workshop on diagnostics of diabatic processes. European Centre for Medium-range Weather Forecasts Workshop Report 160 pp.

Edmon, H.J., Hoskins, B.J., and McIntyre, M.E. 1980 Eliassen-Palm Cross Sections for the Troposphere. J. Atmos. Sci. 37 2600-2616.

Fleming, R.J. and Bohan, W.H. 1981 An example of large scale eddy forcing of the atmosphere's general circulation. International conference on preliminary FGGE data analysis and results (Bergen 1980). ICSU WMO GARP Geneva 435-449.

GARP 1973 The first GARP Global Experiment Objectives and Plans. Global Atmospheric Research Programme Joint Organizing Committee. GARP Pubs Series No 11. ICSU WMO.

GARP 1974 The Synoptic-Scale Sub-Programme for the GARP Atlantic Tropical Experiment. Global Atmospheric Research Programme GATE Report No 6. ICSU WMO.

Geller, M.A. and Avery, S.K. 1978 Northern Hemisphere distributions of diabatic heating in the troposphere derived from general circulation data. Mon. Wea. Rev. 106 629-636.

Haines, D.A., and Winston, J.S. 1963 Monthly mean values and spatial distribution of meridional transport of sensible heat. Mon. Wea. Rev. 91 319-328.

Halley, E. 1686 An historical account of the trade winds and monsoons, observable in the seas between and near the tropicks, with an attempt to assign the phisical cause of the said winds. Phil Trans, 16 153-168.

Hantel, M, and Hacker, J.M. 1978 On the vertical eddy transports in the Northern Atmosphere: 2. Vertical eddy momentum transport for summer and winter. J. Geophys. Res. 83 1305-1318.

Hide, R., Birch, N.T., Morrison, L.V., Shea, D.J and White, A.A. 1980 Atmospheric angular momentum fluctuations and changes in the length of the day. Nature 286 114-117.

Holopainen, E.O. 1978a A diagnostic study of the kinetic energy balance of the long term mean flow and the associated transient fluctuations in the atmosphere. Geophysica 15 125-145.

Holopainen, E.O. 1978b On the dynamic forcing of the long-term mean flow by the large scale Reynolds' stresses in the atmosphere. J. Atmos. Sci 35 1596-1604.

Holopainen, E.O. 1982 Long-term budget of zonal momentum in the free atmosphere over Europe in winter. Quart. J. Roy. Met. Soc. 108 95-102.

Holopainen, E.O., Lau, N-C. and Oort, A.H. 1980 A diagnostic study of the time-averaged budget of atmospheric zonal momentum over North America. J. Atmos. Sci. 37 2234-2242.

James, I.N. and Raper, S.B.C. 1981 Some diagnostics for January and July 1980. Met O 13/Reading Univ. Joint Project. Tech Note 2.

Kanamitsu, M. 1980 Some climatological and energy budget calculations using the FGGE III-b analysis during January 1979. ECMWF Seminar on Data Assimilation Methods. 399-454.

Klein, W.H. 1951 A hemispheric study of daily pressure variability at sea level and aloft. J. Met. 8 332-346.

Krishmanurti, T.N. 1971 Tropical East-West circulations during the northern summer. J. Atmos. Sci. 28 1342-1347.

Krueger, A.F., Winston, J.S. and Haines, D.A. 1965 Computations of atmospheric energy and its transformations for the Northern Hemisphere for a recent five-year period. Mon. Wea. Rev. 93 227-238.

Lau, N-C. 1978 On the three-dimensional structure of the observed transient eddy statistics of the Northern Hemisphere wintertime circulation. J. Atmos. Sci. 35 1900-1923.

Lau, N-C., 1979a The structure and energetics of transient disturbances in the Northern Hemisphere wintertime circulation. J. Atmos. Sci. 36 982-995.

Lau, N-C, 1979b The observed structure of tropospheric stationary waves and the local balances of vorticity and heat. J. Atmos. Sci. 36 996-1016.

Lau, N-C. and Oort, A.H. 1981 A comparative study of observed northern hemisphere circulation statistics based on GFDL and NMC analyses. Part I: The time-mean fields. Mon. Wea. Rev. 109 1380-1403.

Lau, N-C. and Oort, A.H. 1982 A comparative study of observed northern hemisphere circulation statistics based on GFDL and NMC analyses. Part II: Transient eddy statistics and the energy cycle. Mon. Wea. Rev. (to be published).

Lau, N-C, and Wallace, J.M. 1979 On the distribution of horizontal transports by transient eddies, in the northern hemisphere wintertime circulation. J. Atmos. Sci. 36 1844-1861.

Lau, N-C, White, G.H. and Jenne, R.L. 1981 Circulation statistics for the extra-tropical Northern Hemisphere based on NMC analyses. NCAR Tech Note NCAR/TN/171+STR 138 pp.

Lovejoy, S. and Austin, G.L. 1980 The estimation of rain from satellite-borne radiometers. Quart. J. R. Met. Soc. 106 255-276.

Lyne, W.H., Swinbank, R. and Birch, N.T. 1982 A data assimilation experiment, with results showing the atmospheric circulation during the FGGE special observing periods. Quart. J. R. Met. Soc.

Newell, R.E., Kidson, J.W., Vincent, D.G., and Boer, G.J. 1972 1974 The General circulation of the tropical atmosphere, and interactions with extratropical latitudes. Vol. 1. MIT. Press 258 pp. Vol 2 MIT Press 371 pp.

Oort, A.H. 1964 On estimates of the atmospheric energy cycle. Mon. Wea. Rev. 92 483-493.

Oort, A.H. 1977 The interannual variability of atmospheric circulation statistics. NOAA Professional Paper 8 76pp.

Oort, A.H. 1978 Adequacy of the rawinsonde network for global circulation studies tested through numerical model output. Mon. Wea. Rev. 106 174-195.

Oort, A.H. 1982 Global atmospheric circulation statistics 1958-1973. NOAA Prof Paper.

Oort, A.H. and Chan, P.H. 1977 On the role of the Asian monsoon in the angular momentum and kinetic energy balances of the tropics. Pure Appl. Geoph. 115 1167-1186.

Oort, A.H. and E. M. Razmusson 1971 Atmospheric circulation statistics. NOAA Prof Paper 5, Govt Printing Office, Washington, D.C. 323 pp.

Oort, A.H. and Peixoto, J.P. 1974 The annual cycle of the energetics of the atmosphere on a planetary scale. J. Geophys. Res. 79 2705-2719.

Oort, A.H. and Peixoto, J.P. 1976 On the variability of the atmospheric energy cycle within a 5 year period. J. Geophys. Res. 81 3643-3659.

Oort, A.H. and vonder Haar, T.H. 1976 On the observed annual cycle in the ocean-atmosphere heat balance over the Northern Hemisphere. J. Phys. Oceanog. 6 781-800.

Peixoto, J.P. and Oort, A.H. 1974 The annual distribution of atmospheric energy on a planetary scale. J. Geophys. Res. 79 2149-2159.

Peixoto, J.P. Rosen, R.D. and Salstein, D.A. 1978 Seasonal variability in the pole to pole modes of water vapour transport during the IGY. Arch. Meteor. Geophys. Biodin A27 233-255 .

Physick, W. L. 1981 Winter depression tracks and climatological jet streams in the Southern Hemisphere during the FGGE year. Quart. J. R. Met. Soc. 107 883-898.

Pick, D.R. and Brownscombe, J.L. 1981 Early results based on the stratospheric channels of TOVS on the TIROS-N series of operational satellites. Adv. Space Res. 1 247-260.

Rao, M.S.V., Abbott, W.V. and Theon, J.S. 1976 Satellite-derived global oceanic rainfall atlas (1973 and 1974). NASA SP-410 Washington, D.C.

Razmusson, E.M. 1967 1968 Atmospheric water vapour transport and the water balance of North America: Part I Characteristics of the water vapor flux field. Mon. Wea. Rev. 95 403-426. Part II Large scale water balance investigations. Mon. Wea. Rev. 96 720-734.

Rosen, R.D. and Salstein, D.A. 1980 A comparison between circulation statistics computed from conventional data and NMC Hough Analyses. Mon. Wea. Rev. 108.

Saltzman, B. 1970 Large scale atmospheric energetics in the wavenumber domain. Rev. Geophys. 8 289-302.

Schutz, C. and Gates, W.L. 1971/2/3/4 Global climatic data for surface, 500 mb 400 mb. Santa Monica, Cal., RAND Corp. 4 volumes (January, July, April, October). R-915-ARPA, R-1029-ARPA, R-1317-ARPA, R-1425-ARPA.

Starr, V.P. 1953 Note concerning the nature of the large scale eddies in the atmosphere. Tellus 5 494-498.

Starr, V.P. 1954 Commentaries concerning research on the general circulation. Tellus 6 268-272.

Starr, V.P. and Saltzman, B. (compilers) 1966. Observational studies of the atmospheric general circulation. Scientific Report No 2, Planetary Circulation Project MIT 700 pp.

Starr, V.P. and White, R.M. 1951 A hemispheric study of the atmospheric angular momentum balance. Quart. J. Roy. Met. Soc 77 215-225.

Swinbank, R. 1980 A study of the zonally averaged global circulation during the FGGE. Met O 20 Tech Note II/151 Meteorological Office, London Road, Bracknell, UK. 30 pp.

Swinbank, R. 1981 The global atmospheric angular momentum balance inferred from analyses made during the FGGE and general circulation model experiments. Met O 20 Tech Note II/173.

Thornthwaite, C.W. et al 1964 Average climatic water balance data of the continents. Publications in Climatology, Laboratory of Climatology, Centerton, N.J. (several volumes).

Townsend, R.D. and Johnson, D.R. 1981 The mass and angular momentum balance of the zonally-averaged global circulation. International conference on preliminary FGGE data analysis and results (Bergen 1980). KSU WMO GARP Geneva.

Trenberth, K.E. 1979 Interannual variability of the 500 mb zonal mean flow in the Southern Hemisphere. Mon. Wea. Rev. 107 1515-1524.

Trenberth, K.E. 1980 Planetary waves at 500 mb in the Southern Hemisphere. Mon. Wea. Rev. 108 1378-1389.

Tucker, G.B. 1979 Transient synoptic systems as mechanisms for meridional transport: an observational study in the southern hemisphere. Quart. J. R. Met. Soc. 105 657-672.

Tucker, G.B. 1981 Diagnostic studies of synoptic and planetary scale systems. International Conference on Preliminary FGGE Data Analysis and Results (Bergen 1980). ICSU WMO GARP Geneva 362-376.

Van Loon, H. 1980 Transfer of sensible heat by transient eddies in the atmosphere on the Southern Hemisphere: an appraisal of the data before and during FGGE. Mon. Wea. Rev. 108 1774-1781.

Van Loon, H., Taljaard, J.J., Sazamori, T., London, J., Hoyt, D.V., Labitzke, K. and Newton, C.W. 1972 Meteorology of the Southern Hemisphere edited by Newton, C.W. Met Mon. 13 35 Amer. Met. Soc.

Van Loon, H., Jenne, R.L. and Labitzke, K. 1973 Zonal harmonic standing waves. J. Geophys. Res. 87 319-332.

Vincent, D.G. 1981 Kinematic analysis of the large-scale mean state during phases I, II and III of GATE. Quart. J. Roy. Met. Soc. 107 899-918.

White, A.A. 1978 Topics in dynamical meteorology: 7. Atmospheric energetics (2). Weather 33 446-456.

White, G. 1982 Global circulation statistics for the year December 1980-November 1981 derived from ECMWF analyses.

Wiin-Nielsen, A. 1959 A study of energy conversion and meridional circulation for the large-scale motion in the atmosphere. Mon. Wea. Rev. 87 319-332.

Wiin-Nielsen, A., Brown, J.A. and Drake, M. 1963/4 On atmospheric energy conversions between the zonal flow and the eddies. Tellus 15 261-279.
Further studies of energy exchanges between the zonal flow and the eddies. Tellus 16 168-180.

Winston, J.S., Gruber, A., Gray, T.I., Varnadore, M.S., Earnest, C.L. and Mannello, L.P. 1979 Earth-atmosphere radiation budget analyses derived from NOAA satellites June 1974-February 1978. NOAA NESS Washington D.C.

MET OFFICE FGGE IIIA ANALYSIS
LOW LEVEL JANUARY MEAN WINDS

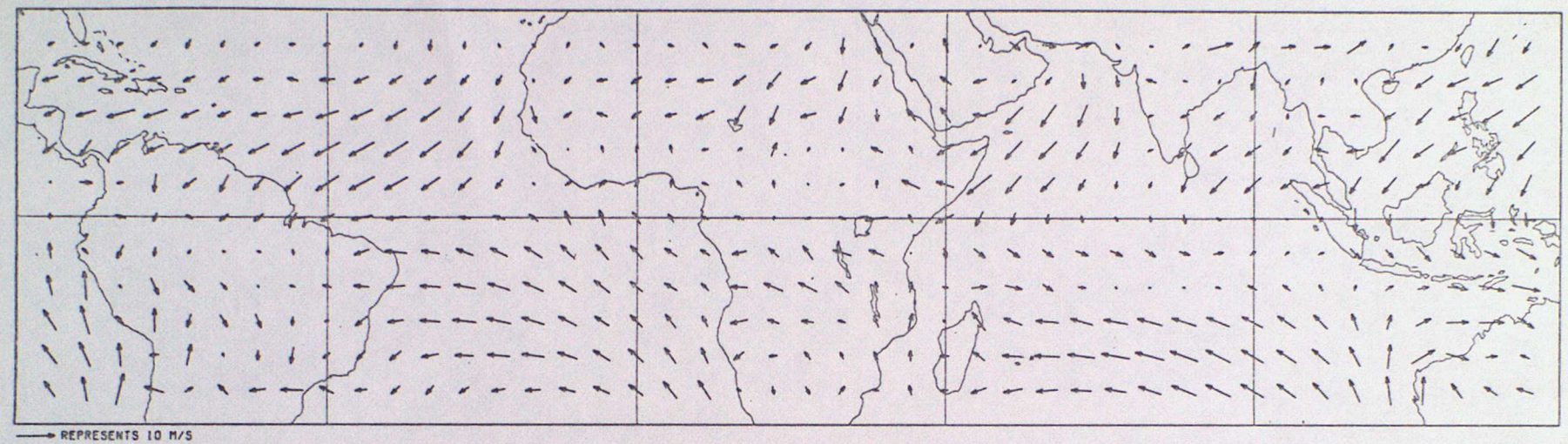

MET OFFICE FGGE IIIA ANALYSIS
LOW LEVEL JULY MEAN WINDS

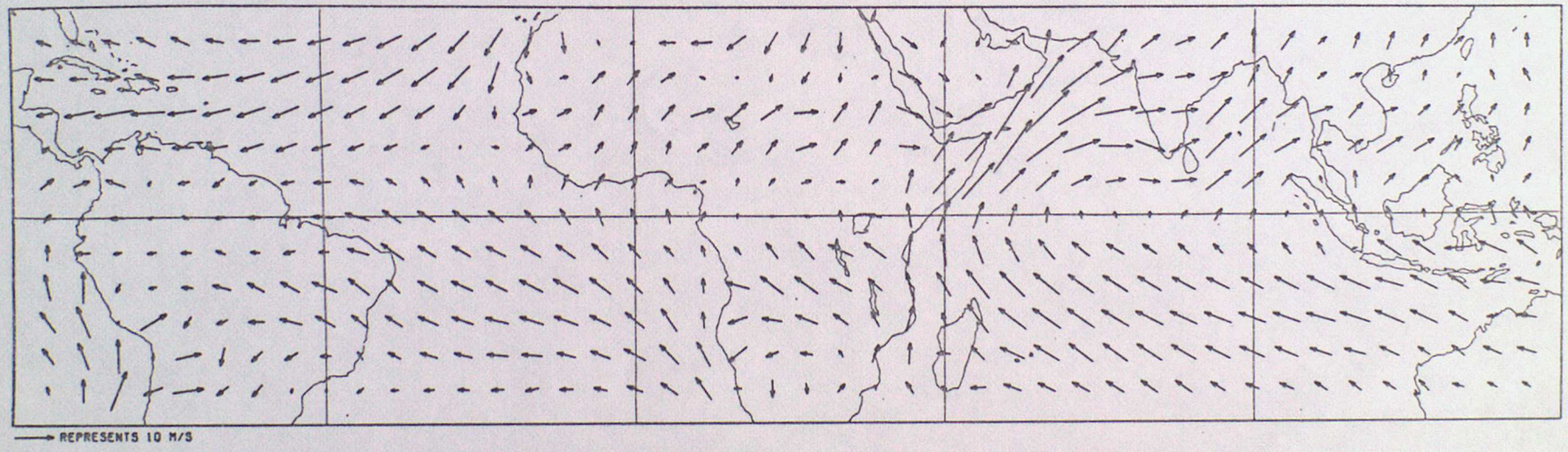

Figure 5.1 Winds at $\sigma = .987$ during 1979 (compare Figure 2.1)

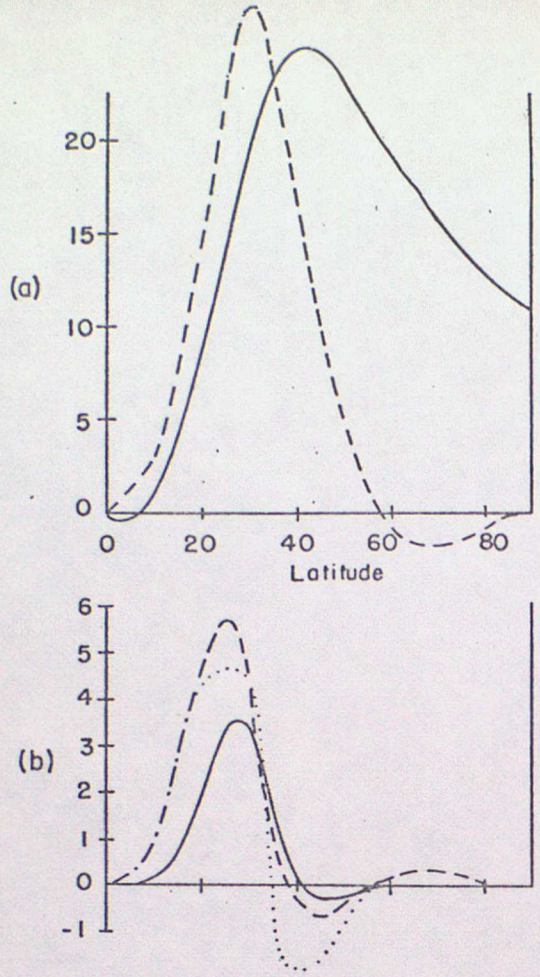

Fig. 1. Relative angular velocity in 10^{-7} sec^{-1} as function of latitude given by full curve in (a). Total angular momentum transport by eddies in 10^{25} c.g.s. units given by dashed curve in (a). Production of zonal kinetic energy using mean wind and total transport (full curve), using 300 mb wind and transport (dashed curve) and using 200 mb wind and transport (dotted curve) shown in (b) in terms of arbitrary units.

Figure 5.2 Extract from Starr (1953)

we may enumerate certain important inferences which may be drawn from the general character of the results, if these latter are correct in main outline, as seems most probable. These are:

1. The large disturbances in the atmosphere produce kinetic energy of mean zonal motions, and not the reverse as has been with few exceptions generally supposed in the past.

2. Since the magnitudes of this generation are of the order of the estimated dissipation, and could regenerate the motions involved in about two weeks, it may be stated that any theory for the general circulation of the atmosphere which omits this effect is crucially deficient, lacking an essential correspondence to reality, however interesting it may otherwise be.

3. Through the years there has been current in meteorology an assortment of general circulation theories which do not presuppose this action of the eddies. The singular sterility and lack of promise which have characterized these can perhaps be ascribed largely to the shortcoming under discussion.

4. It is increasingly clear that a valid formal theory of the general circulation showing how the incoming radiational energy supply results in the observed motions (rather than others) will probably be evolved only slowly because of its inherent complexity.

The problem of the mean zonal motions and the large-scale disturbances is one and inseparable, because of the now demonstrated interdependence of these circulations; hence there exists a natural and direct connection to such other modern developments as those in cyclone theory and similar topics, which latter will first have to be not only better understood but also fitted into the more general picture.

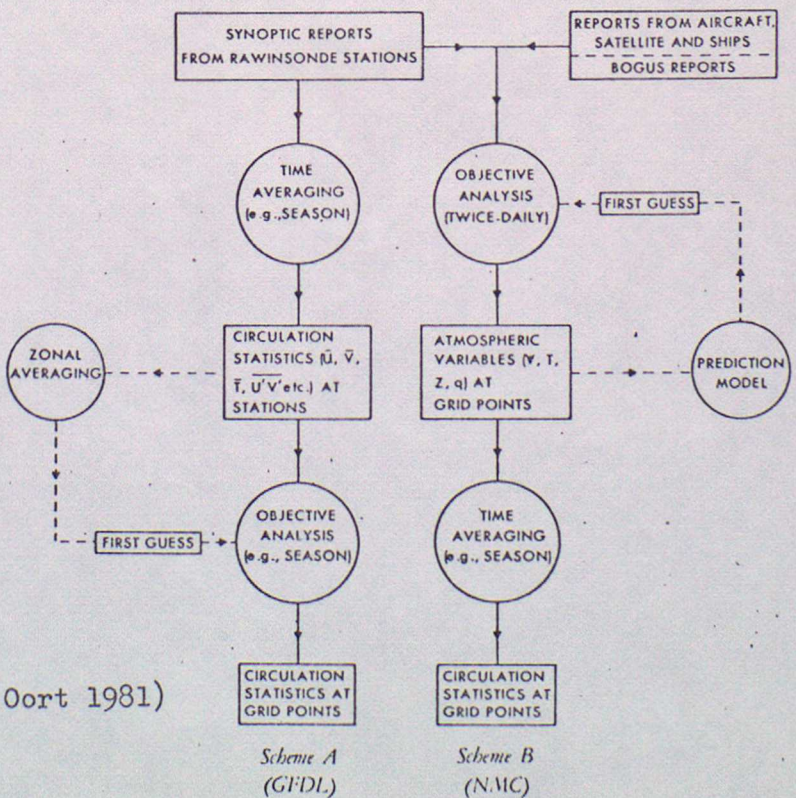

Figure 5.3 (Lau and Oort 1981)

Flow diagram illustrating the two alternative processing schemes for compiling general circulation statistics.

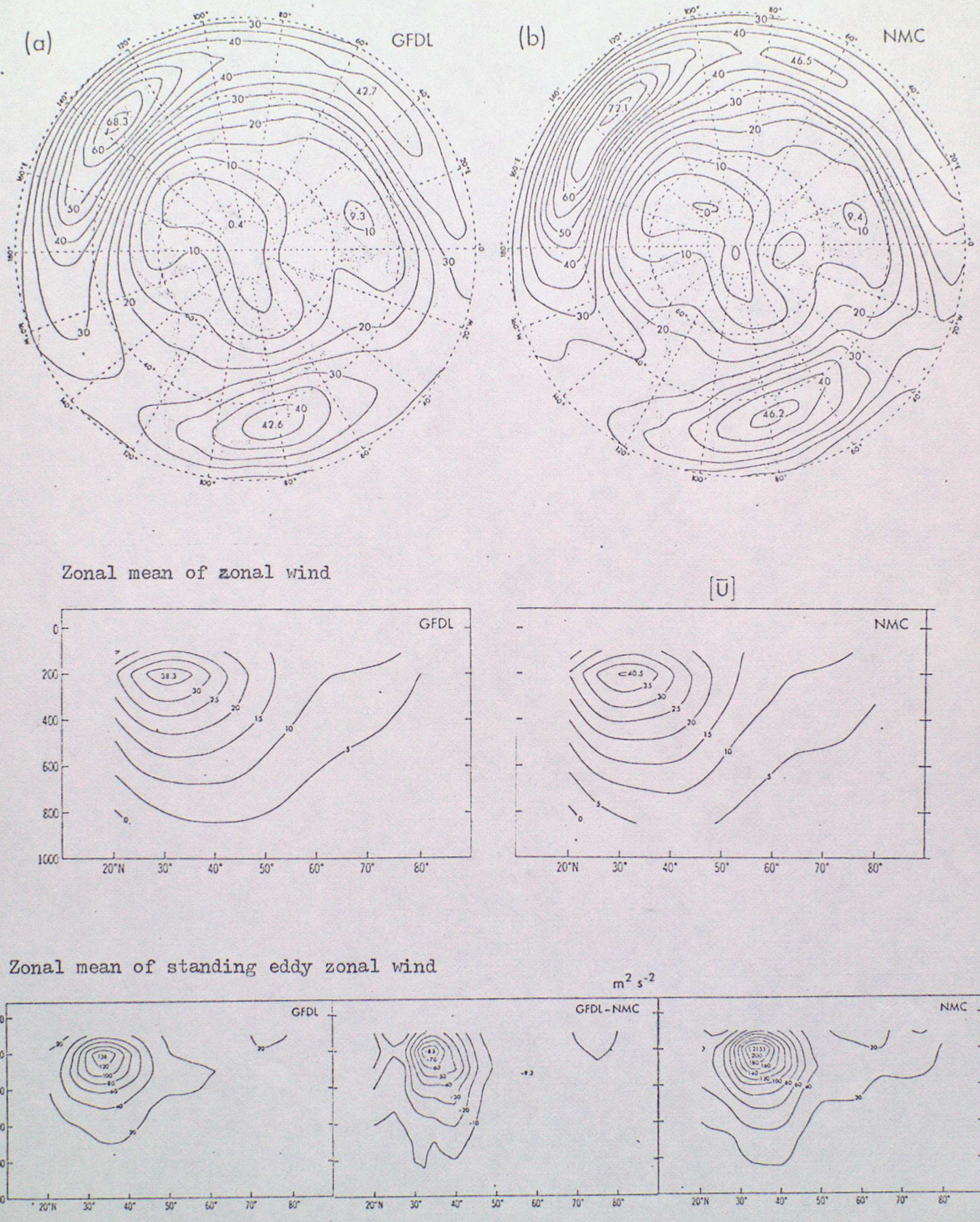

Figure 5.4 (Lau and Oort 1981). Comparison of results from methods A and B.

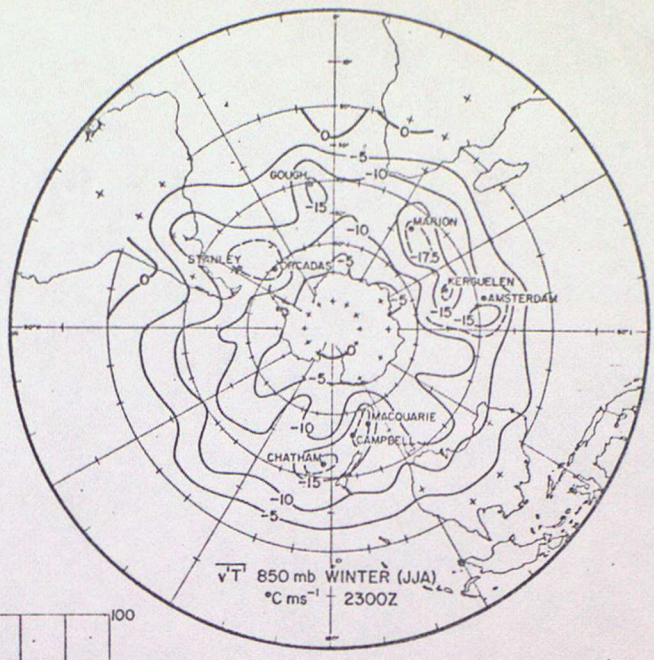

a) Transfer of sensible heat (°C m s^{-1}) in transient eddies in winter (JJA) at 850 mb. Australian 2300 GMT data, 1972–77.

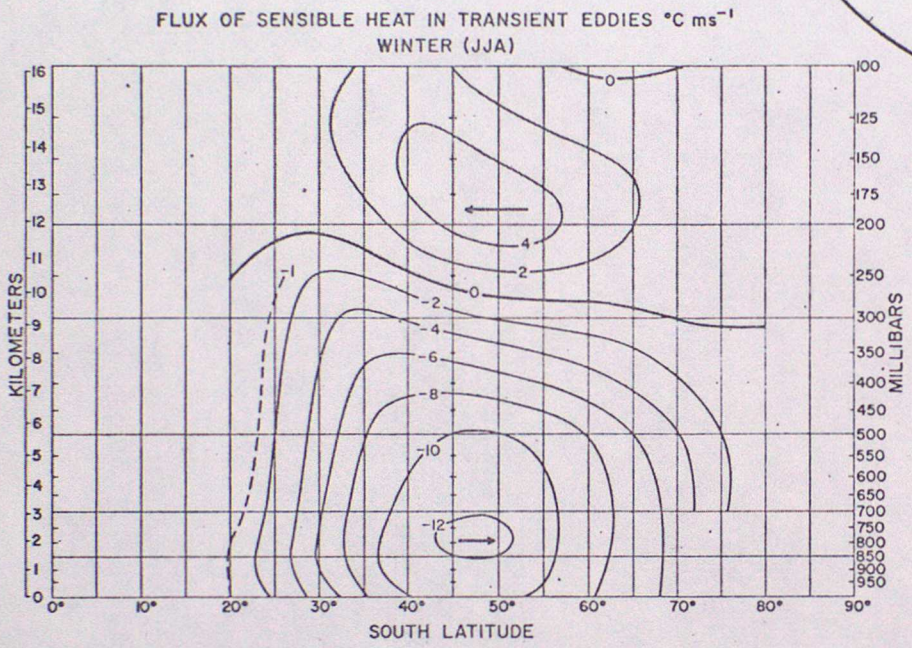

b) Zonally averaged transfer of sensible heat in transient eddies (°C m s^{-1}) on the Southern Hemisphere in winter (JJA). Australian 2300 GMT data, 1972–77.

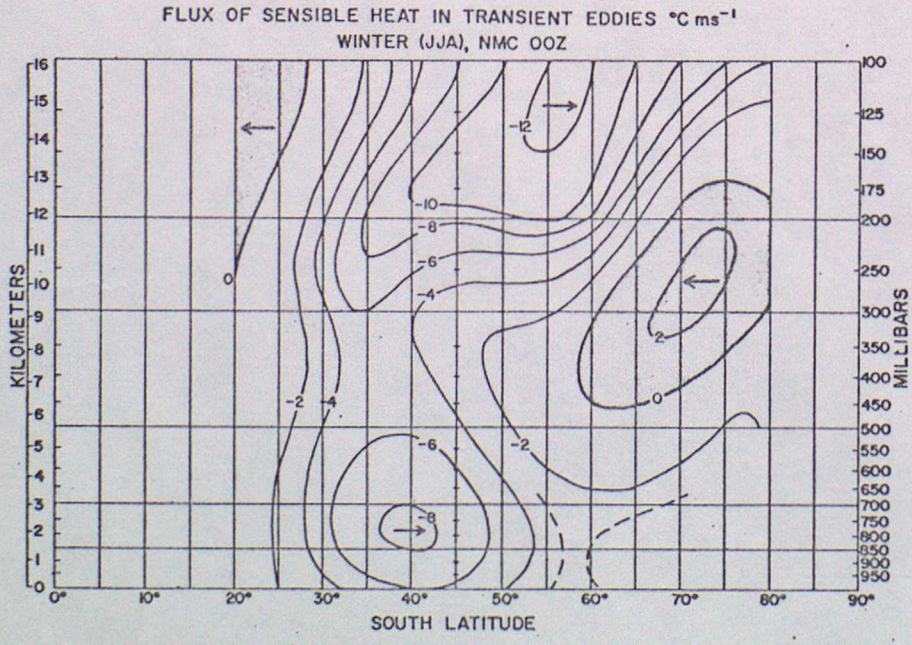

c) Same as b) but with NMC 0000 GMT data for 1976 and 1977.

Figure 5.5 Comparison of method B results (van Loon 1980)

ECMWF FGGE ANALYSIS (T18 SPECTRAL RESOLUTION) JANUARY MEAN.
200MB VELOCITY POTENTIAL (DIVERGENT WIND BLOWS FROM L TO H).

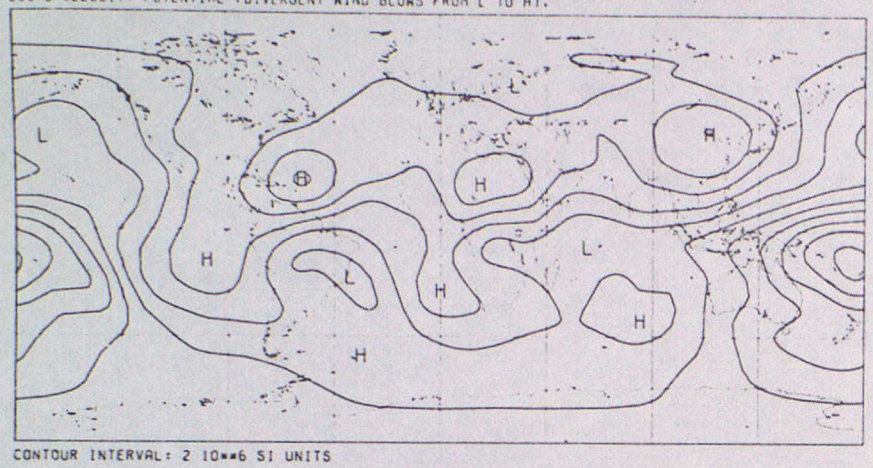

CONTOUR INTERVAL: 2 10**6 SI UNITS

ECMWF FGGE ANALYSIS (T18 SPECTRAL RESOLUTION) APRIL MEAN.
200MB VELOCITY POTENTIAL (DIVERGENT WIND BLOWS FROM L TO H).

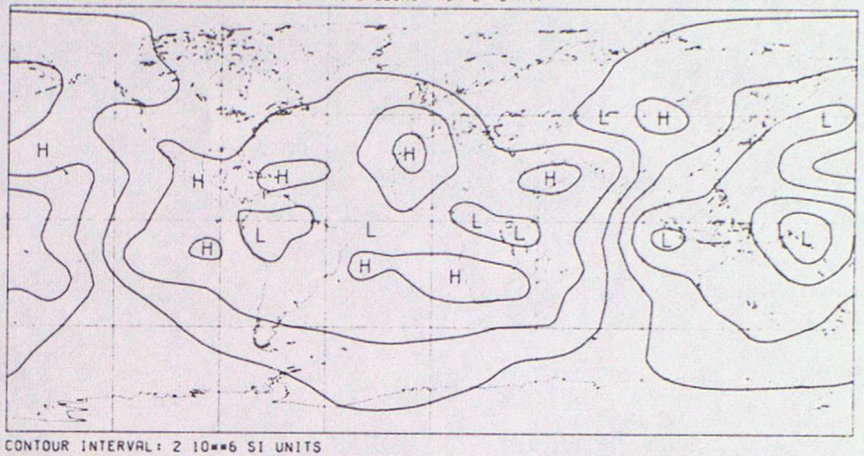

CONTOUR INTERVAL: 2 10**6 SI UNITS

ECMWF FGGE ANALYSIS (T18 SPECTRAL RESOLUTION) JULY MEAN.
200MB VELOCITY POTENTIAL (DIVERGENT WIND BLOWS FROM L TO H).

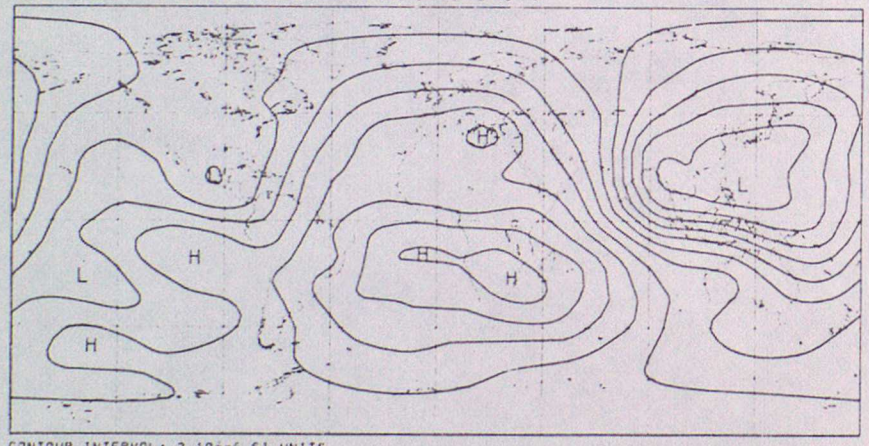

CONTOUR INTERVAL: 2 10**6 SI UNITS

ECMWF FGGE ANALYSIS (T18 SPECTRAL RESOLUTION) OCTOBER MEAN.
200MB VELOCITY POTENTIAL (DIVERGENT WIND BLOWS FROM L TO H).

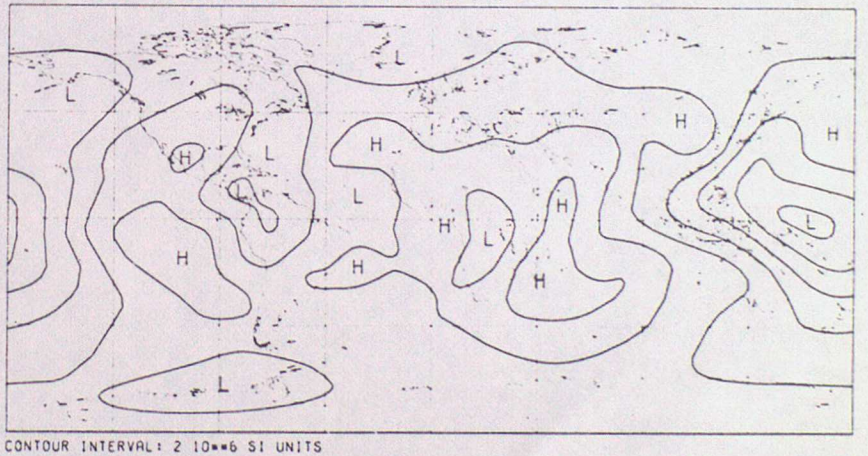

CONTOUR INTERVAL: 2 10**6 SI UNITS

Figure 5.6

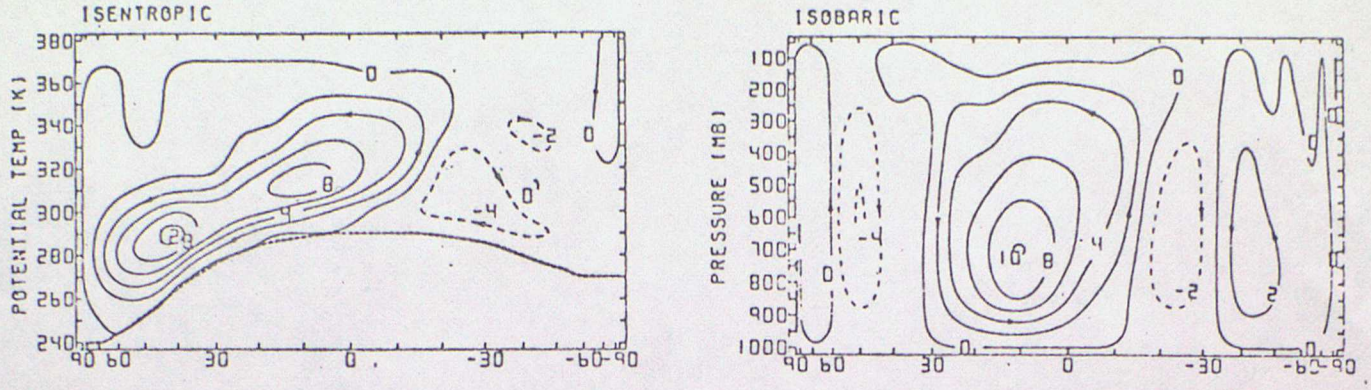

Mass stream function for the isobaric and isentropic mean meridional circulations for January 1979 (units, 10^{10} kg s^{-1}). Arrows indicate the direction of the circulation.

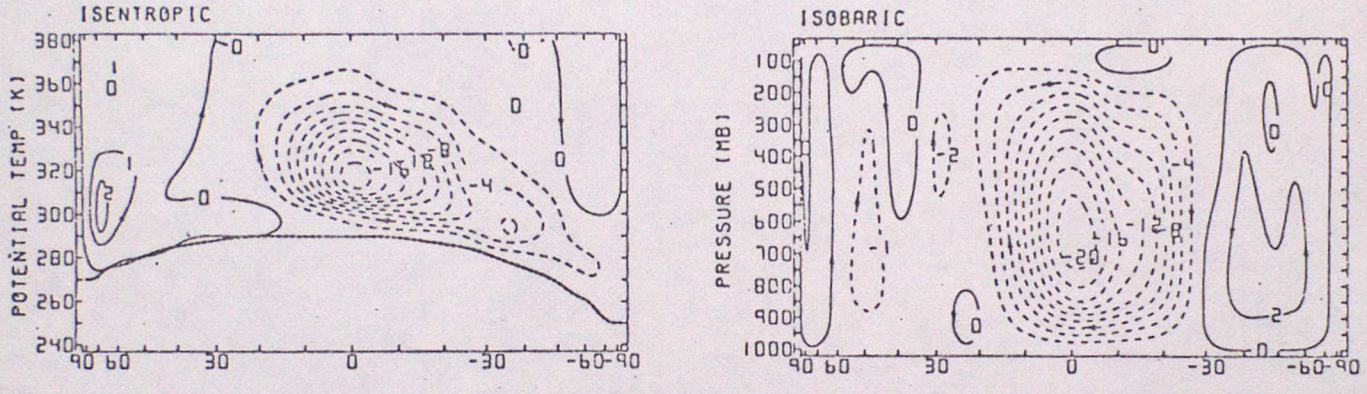

Mass stream function for the isobaric and isentropic mean meridional circulations for July 1979 (units, 10^{10} kg s^{-1}). Arrows indicate the direction of the circulation.

Figure 5.7 (Townsend and Johnson 1981)

PC

ADVANCED LECTURES 1982 - GENERAL CIRCULATION OF THE ATMOSPHERE

LECTURE 6 - Budget Calculations

1. Why?

The term 'General Circulation' is very appropriate; there are many conservative quantities which circulate in the global earth-ocean-atmosphere, and for which flux calculations and budget studies are informative. As well as the basic mass circulation, total energy (heat), moisture, angular momentum, and kinetic and available potential energy, have all been subjected to many budget studies. In this lecture I shall cover neither the detailed mathematical basis of the budget equations and their volume and area integrals, nor the observational method and errors, but rather attempt to present the sorts of conclusion one can draw from such budget studies.

If all significant terms in a budget can be derived from observations then its study might seem scientifically uninteresting. However it is necessary to check and increase confidence in the individual terms and their error estimates. In fact usually some term or terms are not directly observable; a budget study is then the only means of measuring these. Finally the insight obtainedwhile performing such a study frequently leads to an increased understanding not directly due to the budget itself.

2. How?

For a quantity X which is advected by a (three-dimensional) wind $\underset{\sim}{V}$ with a local generation S we have

$$\frac{\partial X}{\partial t} = -\underset{\sim}{\nabla}.(X\underset{\sim}{V}) + S \qquad (6.1)$$

In budget calculations we are interested in time and space integrals of this equation, the space integrals usually performed using Gauss' Theorem to transform the volume integral of a divergence to a surface integral of a flux. Time integrals (or averages) might be for a month, a season, a year, several years, or the same month or season for several years. Space integrals might be for a rather small grid volume, vertical means, area or zonal means, for the atmosphere or the atmosphere earth and ocean. The integrated equation is often expressed in terms of average values of X and V and deviations from these; mean flow and eddies. Depending on which average is used the eddies have different properties, and this nomenclature can thus lead to confusion.

The annual cycle is not usually considered an eddy; it is usually eliminated by averaging individual months, seasons, or seasons with a linear or quadratic trend removed. Inter-annual variation is sometimes included in the eddy terms, sometimes not. For a simple time-average equation 6.1. becomes

$$\underset{\text{storage}}{(X_2 - X_1)/\Delta t} = \underset{\text{mean}}{-\underset{\sim}{\nabla}.(\bar{X}\bar{\underset{\sim}{V}})} \underset{\text{eddies}}{-\underset{\sim}{\nabla}.(\overline{X'\underset{\sim}{V}'})} + \underset{\text{source}}{\bar{S}} \qquad (6.2)$$

These eddies are called transient eddies.

If using method B of Lecture 5, or if analysing GCM results, the smallest space average is for a grid box (typically a few hundred kilometres spacing). Often symbols X and $\underset{\sim}{V}$ are used for averages of this scale without explicit nomenclature, and sub-grid-scale eddy fluxes assigned to a different term. Sub-grid-scale terms can rarely be measured, although they can be parametrized, and particularly in the vertical (convective transport) their estimation is one objective of budget studies.

Traditionally general circulation statistics are presented as zonal-mean cross sections. The commonly (but not universally) used method and nomenclature for this is to do the time-averaging first, giving

$$X = [\bar{X}] + \bar{X}^* + X' \qquad (6.3)$$

$$[X\underset{\sim}{V}] = [\bar{X}][\bar{\underset{\sim}{V}}] + [\bar{X}^*\bar{\underset{\sim}{V}}^*] + [\overline{X'\underset{\sim}{V}'}] \qquad (6.4)$$

mean; standing eddies; transient eddies

Other possibilities are listed by Oort (1964). Note that this definition of transient eddy includes variations in time of the zonal mean flow.

Other subdivisions in time, for instance using band-pass or low-pass filters (Blackmon 1976), or space, for instance into zonal wavenumber (Saltzman 1970), are possible.

3. Mass budget

This is not intrinsically very interesting, since we know that it is conserved, and we can measure the vertical integral very accurately by measuring surface pressu Two budget calculations are important however:

a. To correct inaccurately measured wind fields. A vertically integrated mass budget relates the rate of change of surface pressure, which can be accurately measured, to the vertically integrated horizontal divergence, which cannot. Figure 6.1 shows the vertical profile of the annually averaged horizontal divergence for Europe (Alestalo. 1981). Vertically integrated this implies a loss of 7 atmospheres per year. This can be fatal to the flux divergence of some more sensitive quantity. The flux divergence of equation 6.1 can be expanded

$$\underset{\sim}{\nabla}.(X\ \underset{\sim}{V}) = \underset{\sim}{V}.\underset{\sim}{\nabla}X + X\underset{\sim}{\nabla}.\underset{\sim}{V} \qquad (6.5)$$

The last term is affected by such errors in the vertical integral of $\underset{\sim}{\nabla}.\underset{\sim}{V}$; the error can be reduced by modifying $\underset{\sim}{V}$ so that its vertically integrated divergence corresponds to the change in surface pressure (an awkward procedure to do consistently, involving arbitrary decisions about vertical distribution).

b. Calculation of vertical velocity

The previous example shows the difficulty of observing the horizontal divergent wind. However this can be done reasonably accurately for large scales, particularly near 250 mb where divergences are large and there are usually many observations from aircraft and cloud motions to supplement radiosondes. Some attempt can thus be made to calculate large scale vertical divergences to balance this, and hence vertical motions (assuming appropriate boundary conditions).

4. Moisture Budget

This is much more interesting; it is important for the general circulation and climate on all scales. All the terms are difficult to measure, so budget studies help us judge whether we are estimating them correctly. Consider first an atmospheric column. Vertical fluxes are very difficult to measure; we have just seen the difficulty with large scale vertical motions, sub-grid-scale (cumulus) fluxes are large and unknown, fluxes of liquid water and the vertical distribution

of condensation and evaporation of rain are unknown. For some studies, for example generation of Available Potential Energy (APE) considered later, the vertical distribution is needed and has to be parametrized using cloud and cumulus models. Otherwise we avoid needing to measure these terms except at the ground by integrating vertically. Even horizontal moisture flux divergences are difficult to measure. Being largest at low levels, since q is largest there, they are affected by the inhomogeneity and unrepresentativeness in space and time of observations of both wind and moisture. Figures 6.2 and 6.3 show observations of $\nabla_H \cdot (q \mathbf{v}_H)$ from Rasmusson (1968). The vertical integral is a difference between larger low level convergence and upper level divergence, horizontal integrals will cover regions, at about 1500 km spacing, of convergence and divergence. Rasmusson concludes that the latter are probably spurious systematic errors, appearing most years and seasons (perhaps due to his neglecting to correct for erroneous mass divergences as well as the other difficulties just mentioned). Despite these sources of inaccuracy he goes on to use these data in further budget studies.

By considering the lowest 75 mb or so of the atmosphere, parametrizing surface evapotranspiration, and using the fluxes of figure 6.2, he shows that the flux through 925 mb is largely due to the surface flux, horizontal convergence being a factor of 10 smaller. Since in summer this flux will be closely related to convective rainfall, this is in accordance with current ideas on the importance of land surface evapotranspiration to rainfall and climate.

He goes on to a budget integrated over 5 years for Central and Eastern North America, earth and atmosphere. This involves measuring run-off fluxes on the earth by observing streamflow out of the area, integrating the observed atmospheric convergence, and assuming the change in storage term to be negligible. The imbalance, a net convergence of 21 cm, he attributes to a constant .35 cm/month error in the atmospheric fluxes which he therefore corrects. These corrected values are then used in monthly budgets for the atmosphere alone. The measured storage change in the atmosphere and precipitation are used to calculate indirectly the annual cycle of evapotranspiration, which he compares with direct (ie parametrized) estimates from Budyko's Atlas (1963) and Thornthwaite et al (1964). The comparison is shown in figure 6.4; Rasmusson deduces that Budyko's estimates are better. Using these three different values in monthly budgets for the earth alone enables the annual cycle of storage to be calculated (figure 6.5). The figures are of interest to hydrologists and general circulation modellers. Extended globally and used in a global water budget they are consistent with annual sea level changes of 1 or 2 centimetres. The annual cycle computations are summarized in figure 6.6, which shows observed precipitation and run-off, derived evapotranspiration and storage.

This mean annual cycle for the 5 year period was subtracted from the individual monthly values, and the statistical properties of the residuals examined. Significant correlations were found between moisture convergence and precipitation, and between precipitation and storage. This result at first seems at variance with the conclusion drawn at the beginning of this section and the impression given in figure 6.6 of the importance of evapotranspiration, particularly in summer. This conclusion however referred to the mean climate, which did not change much over the period (standard deviations were near 1 cm/month). The statistics on the other hand refer to deviations from this, and if the evaporation and runoff did not change significantly then changes in moisture convergence would cause changes in precipitation and hence storage.

5. Heat Budget

Understanding the heat or total energy budget is basic to understanding the general circulation, so many aspects have already been covered in these lectures. A comprehensive discussion, with a presentation of the data then available, is given by Newell et al (1974 ch 7 pp 27-94). Some of their values have been superseded (eg Oort and Vonder Haar 1976, Fleming and Bohan 1981, Dopplick 1979), however methods and problems remain the same. More recent references may be found in ECMWF (1980), Alestalo (1981).

As with moisture, budgets may or may not be vertically integrated, for atmosphere or atmosphere earth and ocean. Indeed the moisture budget, via latent heat, is an important component of the total energy budget. Rather than attempt a potted summary of Newell et al's 67 pages, not forgetting the more recent work, I shall present a typical equation then move on. Integrating in time and zonally, dividing by the specific heat, and ignoring terms like the change in kinetic energy, gives an equation for the rate of change of temperature:-

$$\overline{\frac{\partial}{\partial t}[T]} = \underset{(1)}{\frac{[\overline{Q_{\mathrm{RAD}}}]}{C_p}} + \underset{(2)}{\frac{[\overline{Q_{\mathrm{LH}}}]}{C_p}} + \underset{(3)}{\frac{[\overline{Q_{\mathrm{BLH}}}]}{C_p}} + \underset{(4)}{\frac{[\overline{Q_F}]}{C_p}} + \underset{(5)}{\frac{[\overline{Q_{\mathrm{COND}}}]}{C_p}}$$

$$+ \Gamma[\varpi] \underset{(6)}{-} \underset{(7)}{\frac{[\bar{v}]}{a}\frac{\partial[\bar{T}]}{\partial\varphi}} - \underset{(8)}{\frac{1}{a\cos\varphi}\frac{\partial}{\partial\varphi}([\bar{v}^*\bar{T}^*] + [\overline{v'T'}])\cos\varphi} \qquad (6.6)$$

$$- \underset{(9)}{\frac{\partial}{\partial p}[\varpi^*\bar{T}^* + \overline{\omega'T'}]} + \underset{(10)}{\frac{R}{C_p p}[\varpi^*\bar{T}^* + \overline{\omega'T'}]},$$

where $\Gamma = [\bar{T}]\frac{\partial}{\partial p}\ln[\bar{\theta}] = \frac{R}{C_p p}[\bar{T}] - \frac{\partial[\bar{T}]}{\partial p}$.

These terms are:

1. Radiational heating.
2. Latent heating.
3. Boundary layer heating.
4. Frictional heating.
5. Turbulent sub-grid-scale conduction in the free atmosphere.
6. Adiabatic expansion.
7. Horizontal advection.
8, 9. Convergence of horizontal and vertical temperature fluxes by the standing and transient eddies.
10. Adiabatic heating by vertical eddies.

6. Momentum budget

As for the heat budget, the understanding of this is basic to understanding the general circulation. The need for balance between surface easterlies and westerlies has been understood since Hadley, and the importance of eddies in transporting momentum understood since Jeffries and quantified by Starr and others (see Lecture 2 and figure 5.2).

Usually in these studies the quantity considered is the component of the angular momentum vector parallel to the earth's axis (the zonal angular momentum). Budget studies of this can be made on many scales. Global atmospheric budgets for the atmosphere relate changes in storage to the surface torques, from friction and the pressure gradient across mountains. Figure 6.7 shows such a comparison for January-February 1979 (Swinbank 1981). Note that fluctuations on this time-scale are mostly due to the mountain torque. The agreement shown gives confidence in the global mean torques, despite their being calculated as differences of large positive and negative values, and justifies their use in budget studies for the total earth atmosphere ocean system. Angular momentum changes of the earth's mantle can be measured by measuring changes in the length of day, ocean changes estimated, and hence changes in the angular momentum of the earth's core derived (otherwise not easily measured!) (Hide et al 1980).

It is more traditional to examine momentum budgets without the N-S part of the integral; you have already seen in figure 4.5 the zonal mean mountain and frictional torques meaned for June 1979. The N-S fluxes of angular momentum within the atmosphere are of course an essential part of this budget, and an explanation of how the atmosphere achieved these was a major incentive in the derivation of modern theories of the atmospheric circulation (Lecture 2). The solid line in figure 4.5 shows the torque derived from the flux divergence calculated using this theory and FGGE analyses; it agrees well with the observed surface torque. The components of this flux are shown in figure 6.8 (from Swinbank 1980). Points to note are (1) the small contribution of the mean zonal motion except in the wintertime Hadley Cell (which is in fact dominated by the monsoon circulation), (2) the different partition between standing and transient eddies in the two hemispheres, (3) the eddy fluxes being often up-gradient into the jets (figure 5.2).

Coming down to the next stage, and examining the vertical distribution of momentum flux, the equations and concepts become less simple as we need to consider interactions between mean meridional motions, eddy transport, and the maintenance of the zonal flow. Because of the rotating frame of reference, the mean meridional circulation (figure 6.9 top, from Hantel and Hacker 1978) not only transports angular momentum, but also generates it via the Coriolis force. (Note that the vertical integral is zero if the mass distribution is constant.) In the troposphere away from the equator this circulation arranges itself to almost exactly cancel the momentum divergences from other mechanisms, indeed because of the difficulty of observing $[\overline{v}]$ this property has been used to calculate it indirectly. Thus in figure 6.9 (middle) we see eddy flux convergence in winter from 700 mb to 100 mb, 35°N to 65°N. This balances (one might even say drives) the equatorwards branch of the Ferrel Cell. The Coriolis force of the poleward branch is balanced by the friction and mountain torques (figure 6.9 bottom). Because of this near balance, the determination of vertical eddy transports as a residue is difficult; Hantel and Hacker claim an accuracy of 25%. (The approximate relationship just demonstrated between momentum flux convergence and the meridional circulation is further complicated if we consider also the static stability which opposes any vertical circulation. The heating this generates is similarly balanced by temperature flux convergence, their combined effect giving the Eliassen-Palm (EP) flux which is currently fashionable for diagnostic studies (Edmon et al 1980).)

As a final example of momentum budget we come down one further stage, and remove the zonal integral. This adds two further terms to be considered:

1. E-W advection (large because the zonal jets are large) which is included with other horizontal advections in term A of figure 6.10 (from Holopainen et al 1980).

2. Generation by the E-W pressure gradient. This cancels the Coriolis term for the geostrophic part of the meridional wind, leaving term B. Its measurement is only possible with any accuracy in well observed regions without systematic radiosonde errors (Holopainen 1982).

The residue R is probably due to vertical eddies, including frontal circulations, in the plains region, and to mountain effects (lee waves etc) in the mountain region. Confidence in the values obtained is gained by independent calculations using methods A and B of Lecture 5.

7. Kinetic and Available Potential Energy

This is a difficult topic to discuss without getting involved in complicated looking equations, particularly if one is dealing with a limited area and boundary fluxes are involved. I shall ignore these and try to explain the physical principles. You will have to accept that formulae exist for calculating the terms (eg fig 6.11 from Peixoto and Oort 1974), although sometimes these are approximate, and sometimes differences in detail in the definitions lead to different formulations (eg Pearce 1978). A non-mathematical introduction is given by White (1978). I shall give only a quick revision, without any attempt at rigour or completeness.

The Available Potential Energy (APE) of a system is its Total Potential Energy (TPE) minus that of the state with minimum TPE obtainable from it adiabatically. It is thus a measure of the departure of the system from stratified equilibrium, and to generate it we have to make the atmosphere hotter where it is already hot or colder where it is already cold. We can approximate this by integrating the diabatic heating (terms 1-5 of equation 6.6) multiplied by an efficiency factor (figure 6.12). It can be converted to kinetic energy by cellular motion with hot air rising and cold air sinking. Alternatively (and equivalently) this conversion can be viewed as air descending the gradient of geopotential on constant pressure surfaces. The kinetic energy is dissipated by frictional and diffusive processes. If all these terms are evaluated for zonal mean and eddies we get the traditional box diagram (figure 6.13). This includes two further conversions: (1) zonal APE to eddy APE (advection of the equator-pole zonally symmetric temperature contrast by eddy velocity fields). (2) zonal KE to eddy KE (associated with down-gradient, or if negative up-gradient, momentum transport by eddies). The difficulties in performing such a budget study are considerable; the diabatic heating rates needed for C require parametrizations and their net spatial distribution is poorly known, the physical dissipative mechanisms are poorly understood, and the conversion terms require vertical velocities which are difficult to observe. Example results are shown in figure 6.14. The major conclusion from such studies is that the eddies are important, with the direct Hadley type conversion from zonal APE to zonal KE being small. The sort of accuracy achievable is illustrated in figure 6.15, from Lau and Oort (1982). This divides the eddies into standing and transient, and being for $20^{\circ}N$-$90^{\circ}N$ has some boundary fluxes. As discussed in Lecture 5, method A underestimates K_{SE} (figure 5.4), and method B is inaccurate for APE $\rightarrow$ KE conversions because of its geostrophic bias, leading to an unbalanced budget for K_{SE}. Generation, dissipation and transient eddy conversion APE $\rightarrow$ KE were not calculable from the data, although it is clear from the P_{TE} budget that it must be large.

One difficulty in gaining further physical insight from such diagrams is the difference in character of the Hadley and Ferrel circulations, making results dependent on the domain (particularly for the sign of $C(P_M, K_M)$). Limited area studies are complicated by boundary fluxes and the precise definition of APE and eddy. Kanamitsu (1980) has performed limited area budgets for KE in the zonal spectral domain. He calculated the KE, change in KE, and KE to KE conversions for January 1979, the residues giving the sum of conversion from APE, dissipation and boundary fluxes (figures 6.16 and 6.17). The physical conclusions which can be drawn from figure 6.15 are

i. The major KE source outside the tropics is in waves 7–10 (the baroclinic scale).

ii. In the northern hemisphere this maintains the ultralong waves, in the southern hemisphere the zonal flow.

iii. The major KE source in the tropics is the ultralong waves (forced by the large scale convection cells visible in fig 5.6). The energy conversion to medium scale suggests development by barotropic instability.

Further subdivision (figure 6.17) shows differences between polar, mid-latitude and subtropical regions. In mid-latitudes the long waves are all maintained by the baroclinic waves, in the sub-tropics waves 2, 3, 4 are externally forced.

8. On co-ordinate schemes and formulations

In this lecture I have tried to put emphasis on physical conclusions and interpretations, which should be independent of the mathematical methods used. One must be wary of too detailed an interpretation of individual terms in an integrand or sum, these can change beyond recognition with formulation. For instance (1) (figure 5.7) in pressure co-ordinates $[V]$ shows a Ferrel Cell, in isentropic co-ordinates it just shows that warmer air moves polewards. Outside of the tropics the latter is mainly geostrophic; something impossible in pressure co-ordinates (figure 6.18). (2) I dismissed the horizontal mass divergence budget as rather uninteresting in section 3; in isentropic co-ordinates it gives directly the diabatic heating. (3) The torqueby the mountains on the atmosphere appears at the lower boundary in pressure co-ordinates. In sigma co-ordinates it is distributed in the integrand of the vertical integral of the pressure gradient. Because of the roughness of mountains different finite difference formulations can give significant differences in mountain torque (figure 6.19). (4) The equivalent formulations for APE → KE conversion give very different vertical distributions to the integrand (figure 6.20); only the integral is meaningful in the energy budget.

(References for Lecture 6 were included with those for Lecture 5).

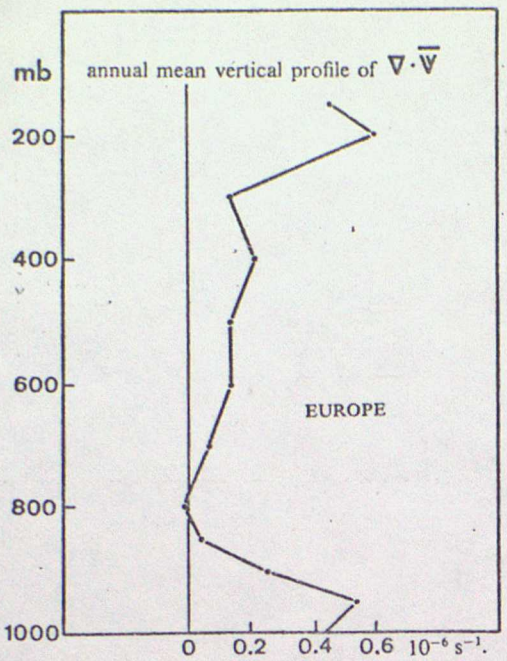

Figure 6.1 Annual mean horizontal divergence for an area over Europe

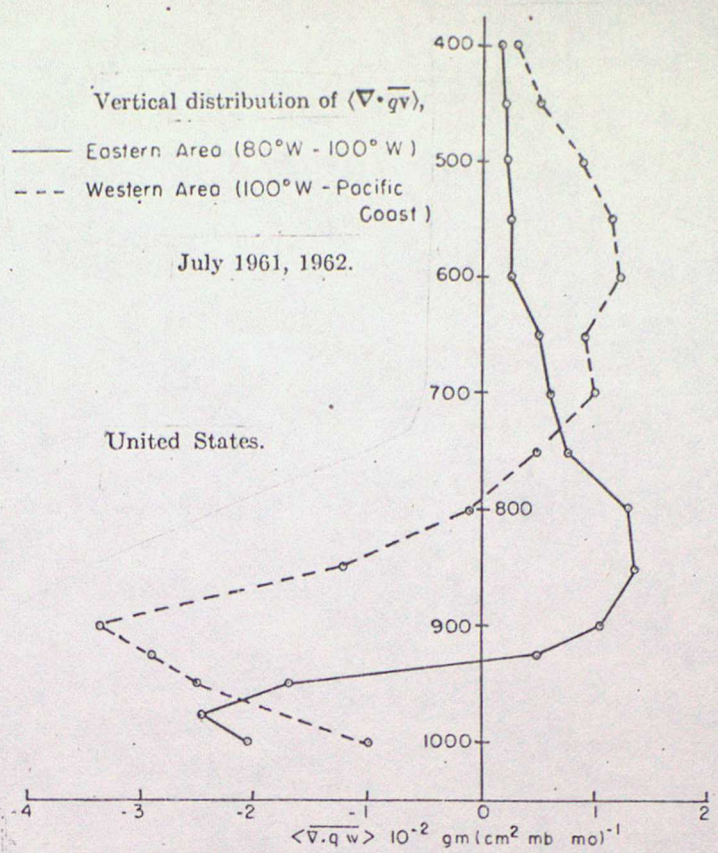

Figure 6.2 July mean water vapour divergence for two areas of America

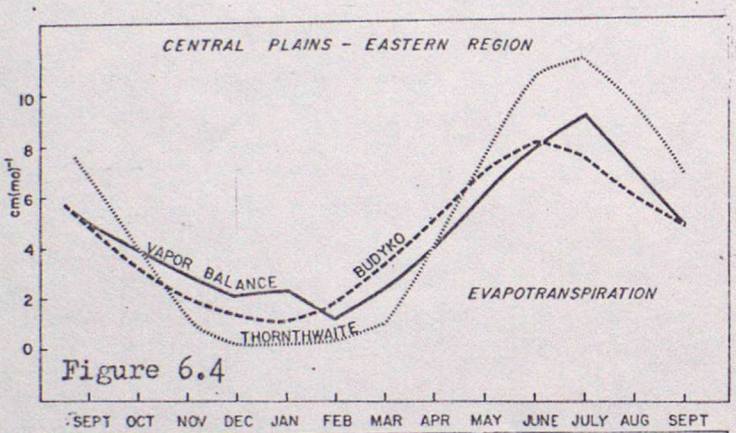

Figure 6.4

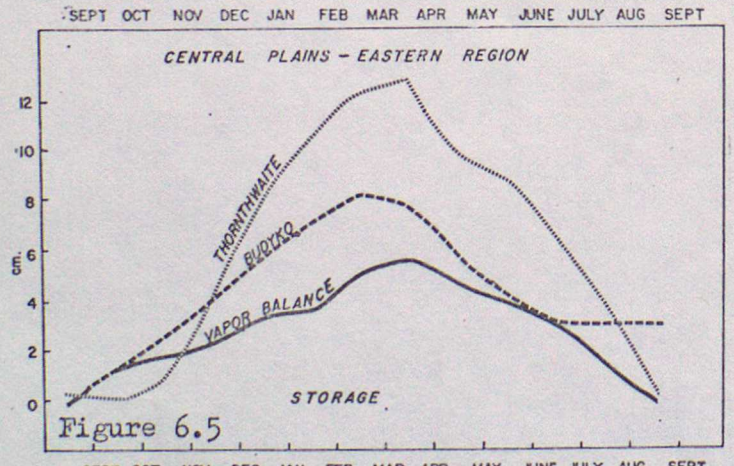

Figure 6.5

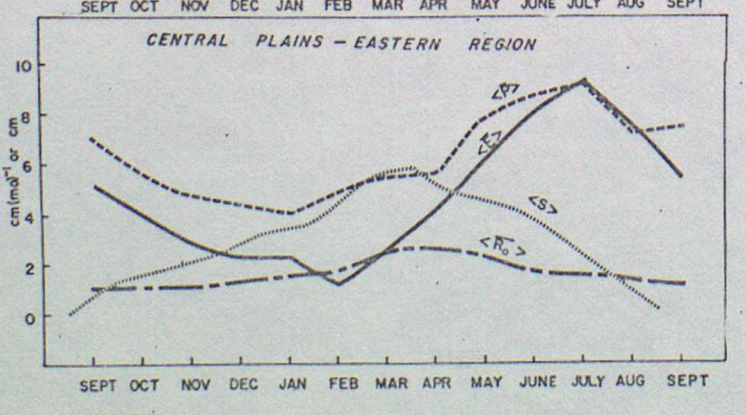

FIGURE 6.6 Water balance: Central Plains and Eastern United States. May 1958–April 1963. Units: cm./mo.

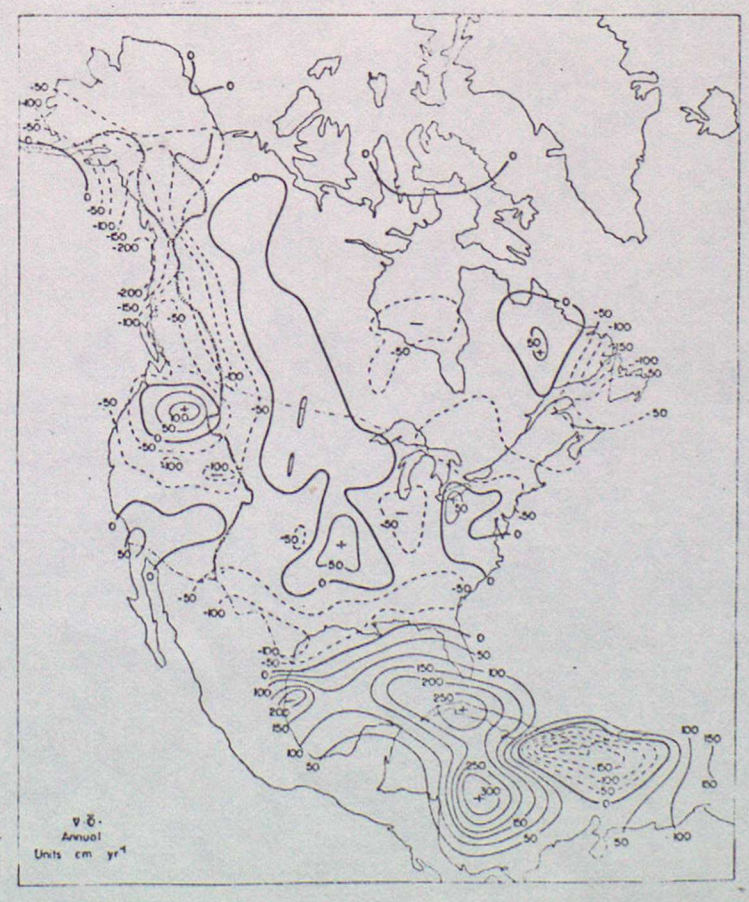

FIGURE 6.3 Computed mean annual divergence of the vertically integrated total water vapor flux. May 1961–April 1963. Units: cm. $yr.^{-1}$ Values are an average of 00 GMT and 12 GMT observations.

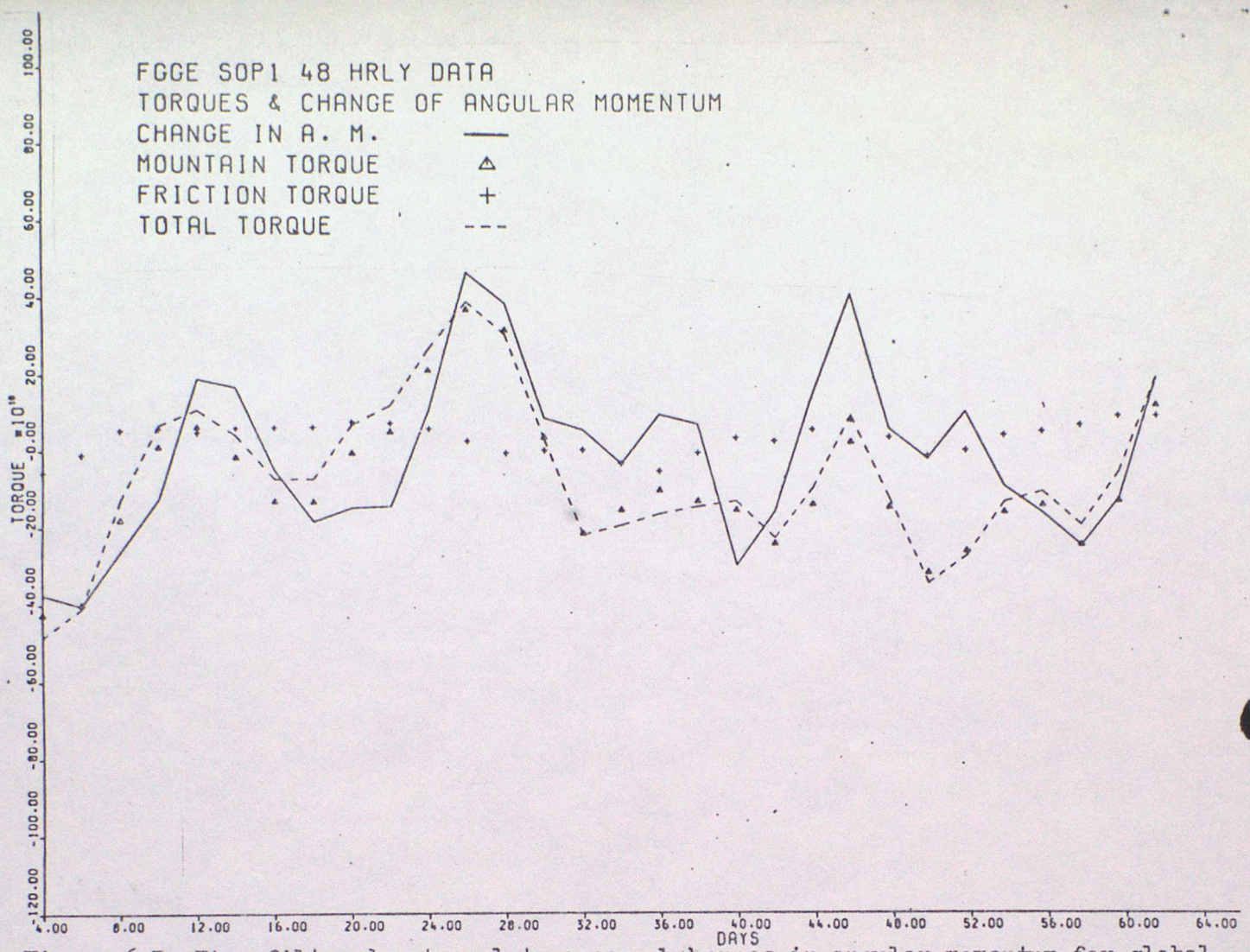

Figure 6.7 Time-filtered external torques and changes in angular momentum for global atmosphere during January and February 1979

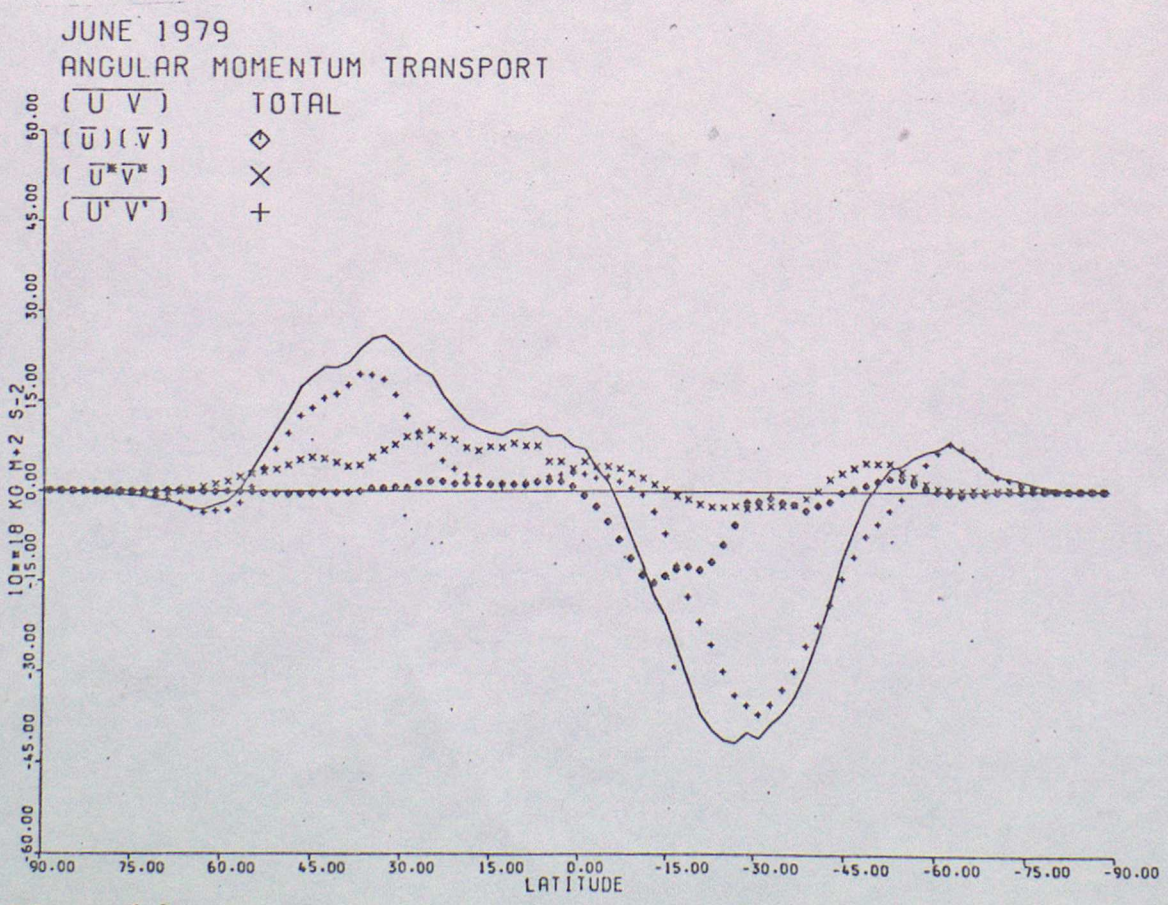

Figure 6.8 Atmospheric angular momentum transport by mean flow and eddies

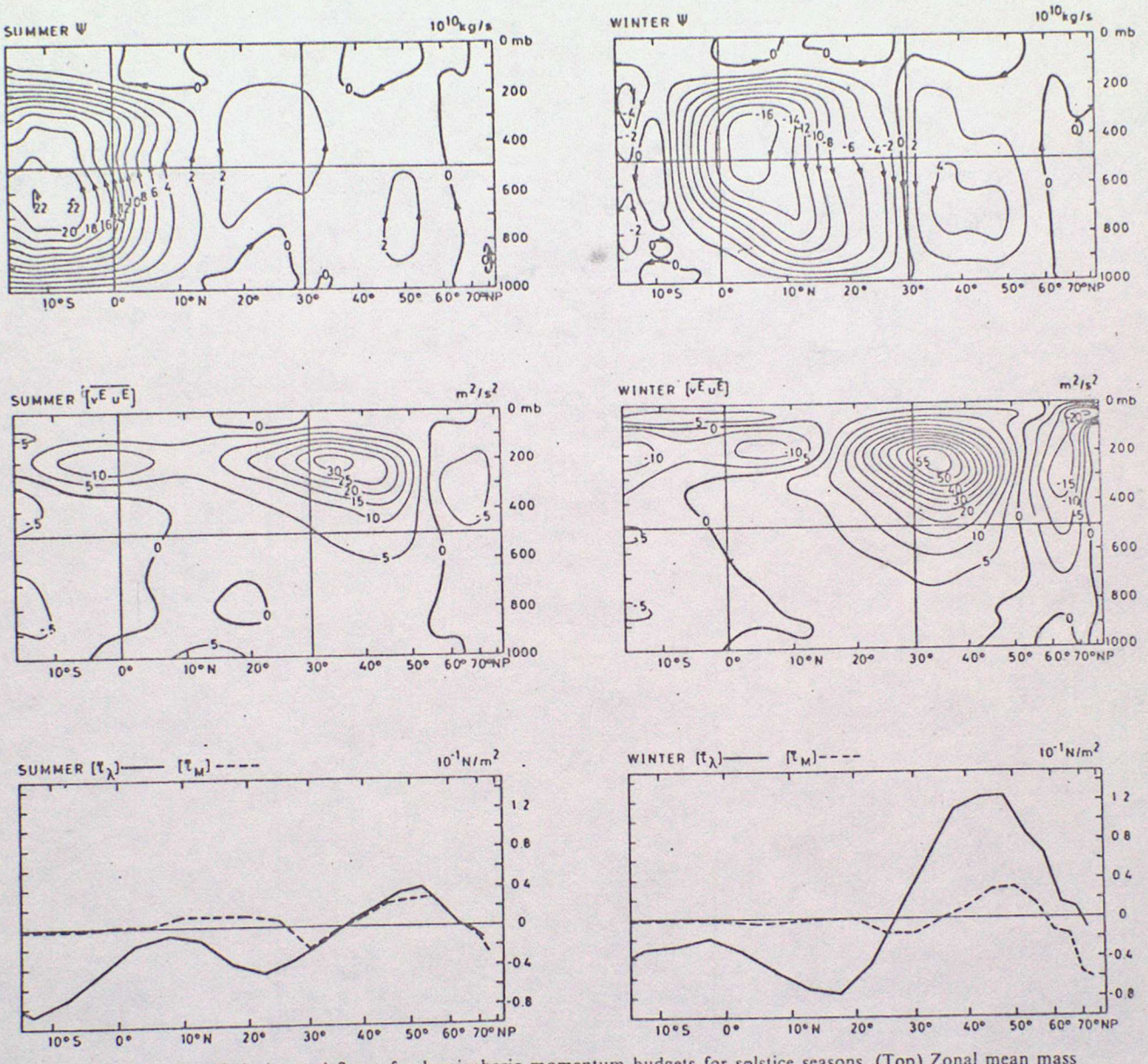

Specified observed fluxes for hemispheric momentum budgets for solstice seasons. (Top) Zonal mean mass transport stream function [*Oort and Rasmusson*, 1970]. (Middle) Net meridional momentum flux due to standing plus transient eddies, from *Oort and Rasmusson* [1971]. (Bottom) Surface wind stress (solid curve) and mountain torque (dashed curve); τ_λ is from *Hellerman* [1967, 1968], parameterized, τ_M is from *Oort and Bowman* [1974], computed from observations.

Figure 6.9

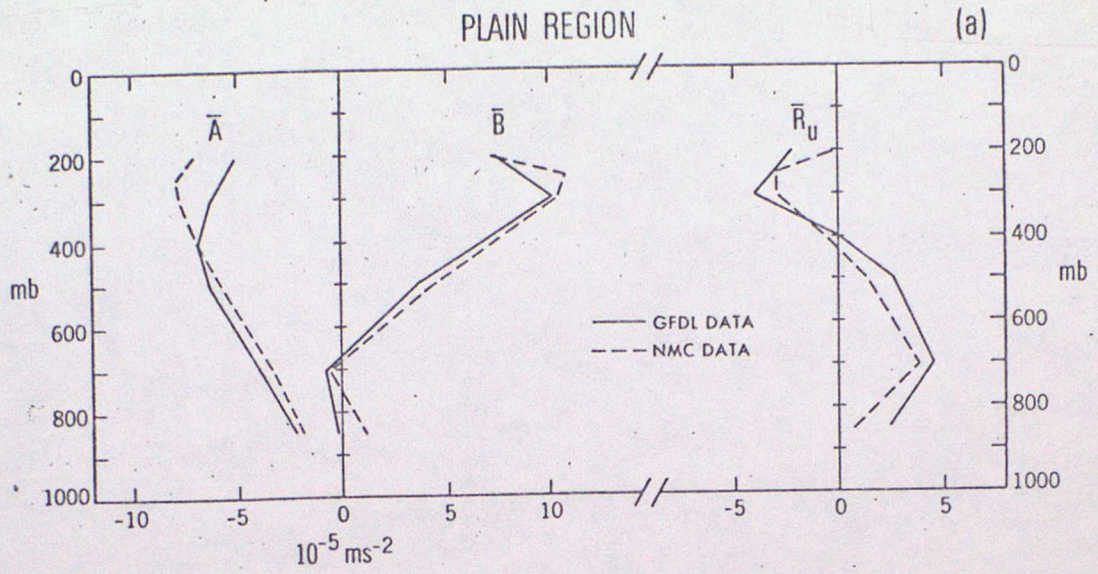

Wintertime budget of zonal momentum over the plain region of North America as obtained from GFDL data (solid line) and from NMC data (dashed line). Units: 10^{-5} m s^{-2}.

$$\bar{A} = -\nabla\cdot\overline{u}\overline{\mathbf{V}} + (\overline{uv}/a)\tan\phi, \qquad \bar{B} = f(\bar{v} - \bar{v}_g), \qquad \bar{R}_u = -\partial(\overline{u\omega})/\partial p + \bar{F}_u.$$

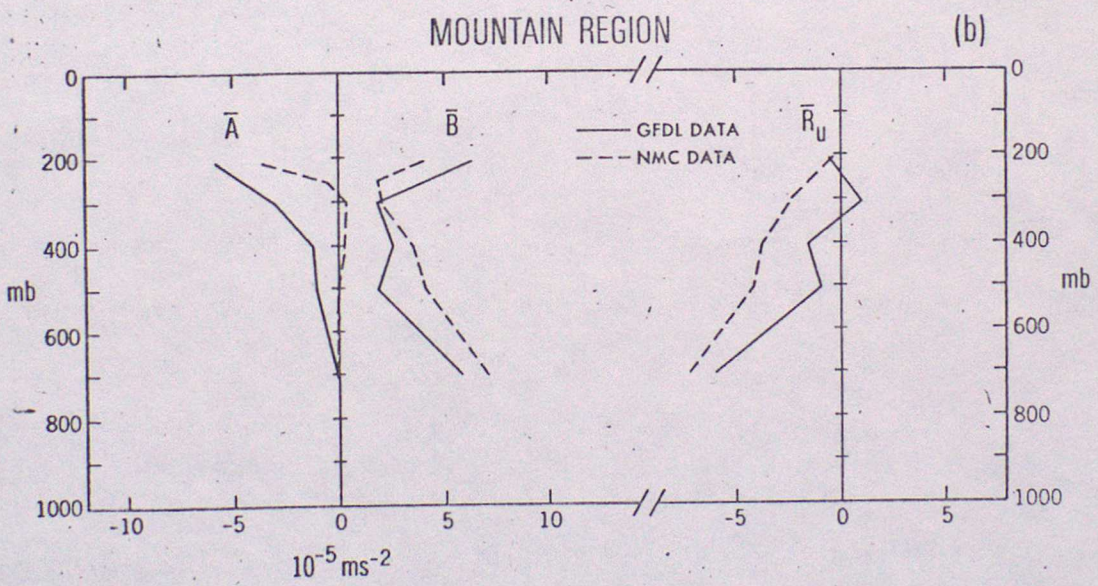

As in (a) except for the mountain region of North America.

Figure 6.10

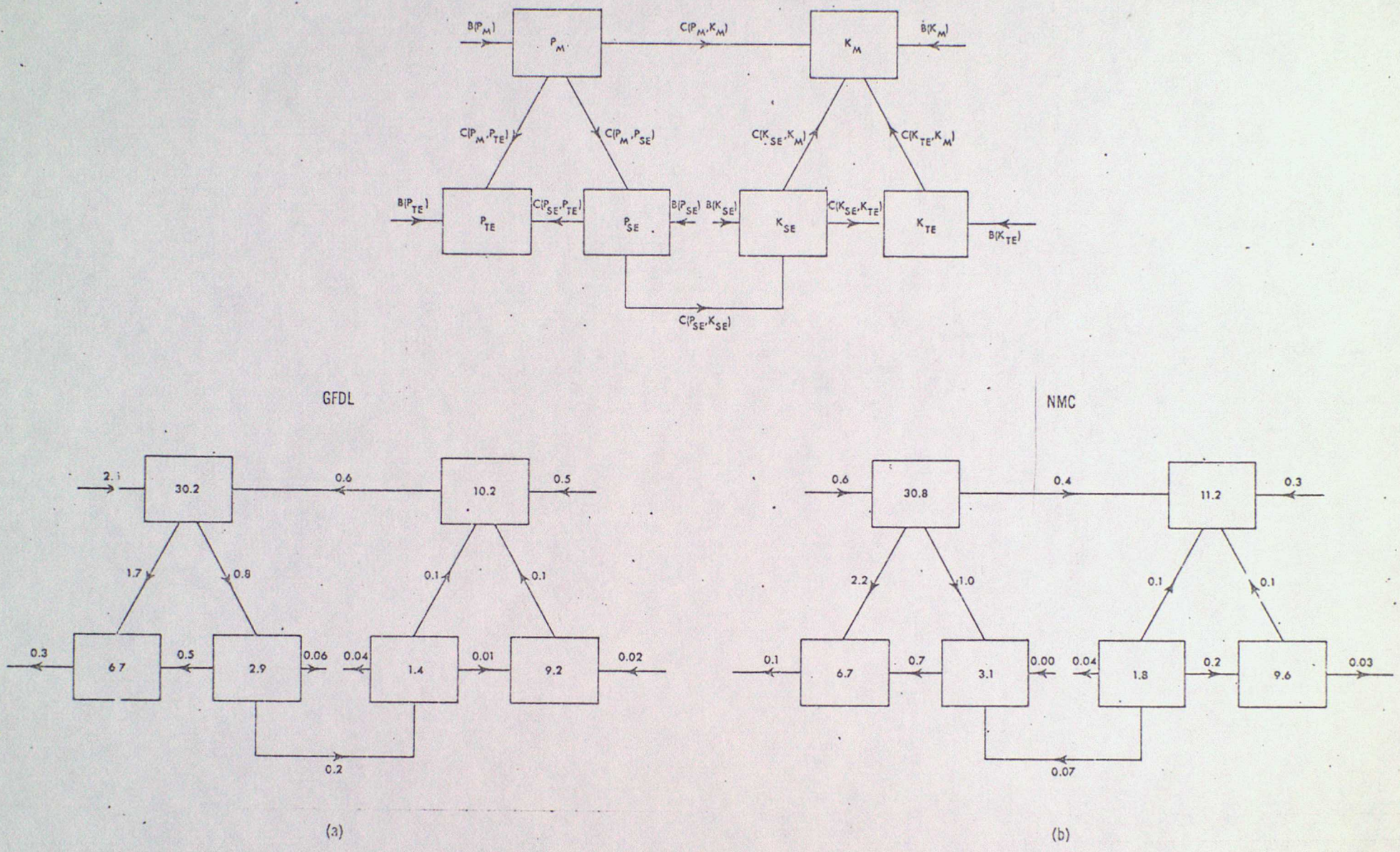

Figure 6.15 Estimates of various components in the atmospheric energy cycle for 20°N-90°N, 850mb-100mb, winter

Figure 6.16

ENERGY DIAGRAM (GLOBAL) JANUARY 1979 250 mb–200 mb

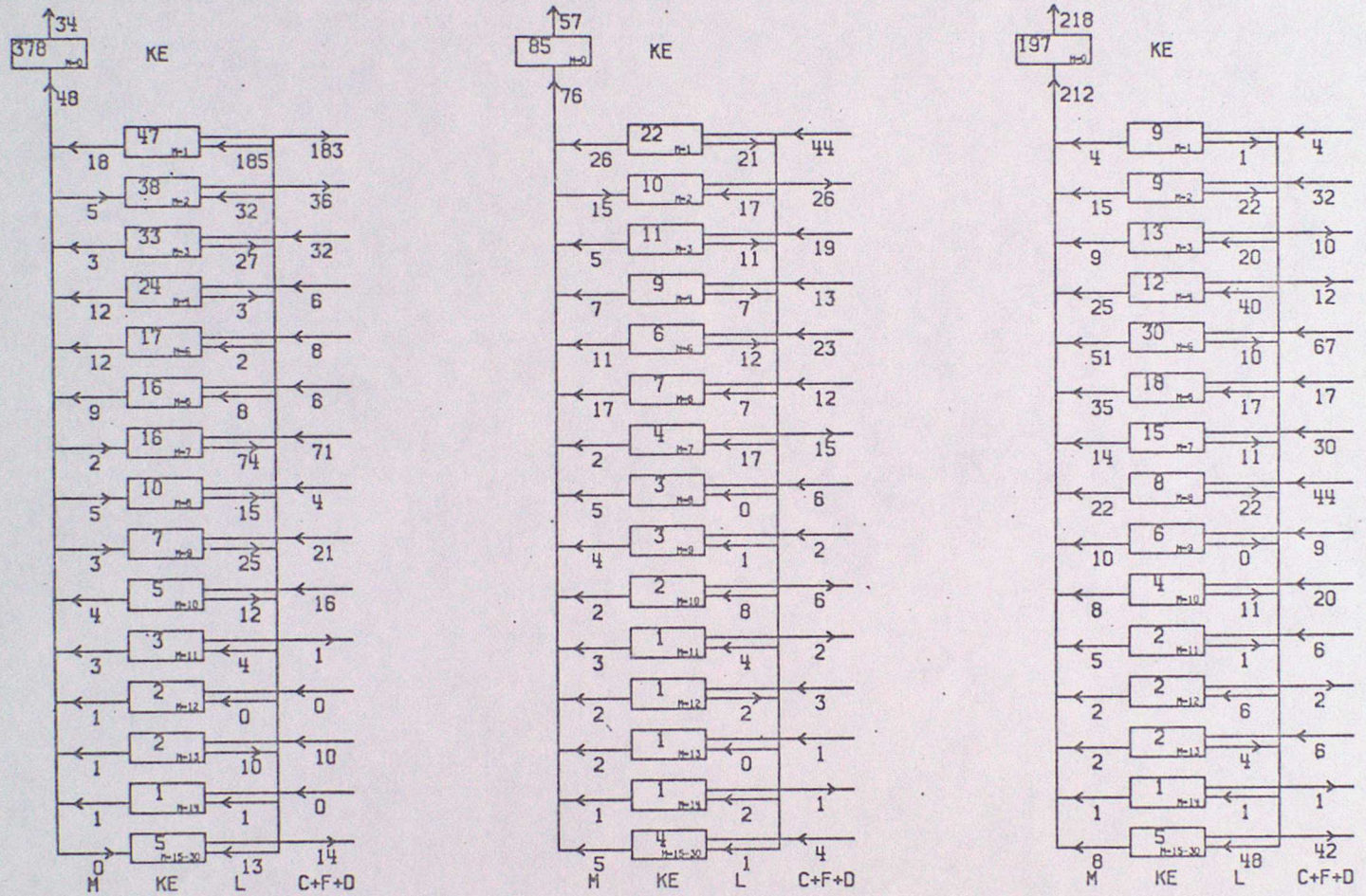

90°-20°N 20°N-20°S 20°-90°S

Energy diagram for the northern hemisphere (left) tropics (centre) and southern hemisphere (right) in the layer between 200 and 250 mb during January 1979 obtained from ECMWF anlyses. The large numbers in the boxes are the area averaged kinetic energies of the zonal Fourier component m indicated by the small number. The box at the top of the diagram is for the zonal mean field (m=o). The arrows and lines at the left side of the diagram connecting the boxes with the one at the top indicate zonal-wave interactions (M) and their directions. Similarly the lines connecting the boxes on the right side of the diagram indicate wave-wave exchanges (L). The other lines on the right and at the top indicate the residuals (the sum of conversion from potential energy, boundary fluxes, dissipations, etc). Units are in $m^2\ sec^{-2}$ for ener[illegible], $m^2\ sec^{-3}$ for the conversions.

Figure 6.17

ENERGY DIAGRAM (NORTHERN HEMISPHERE) JANUARY 1979 250 mb–200 mb

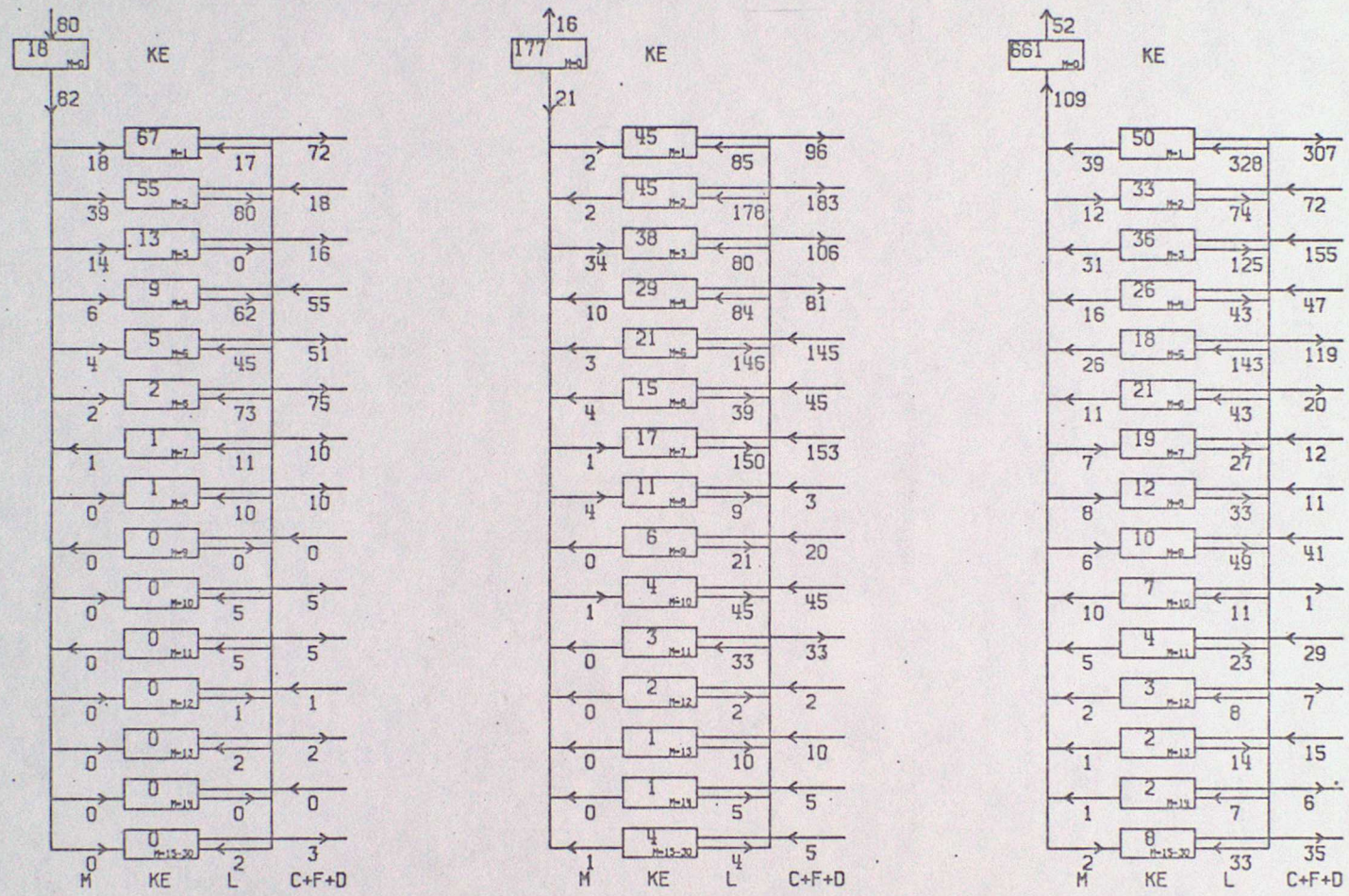

Same as Fig.22 but for the high latitude zones (left) middle latitude zones (centre) and for substropical zones (left)

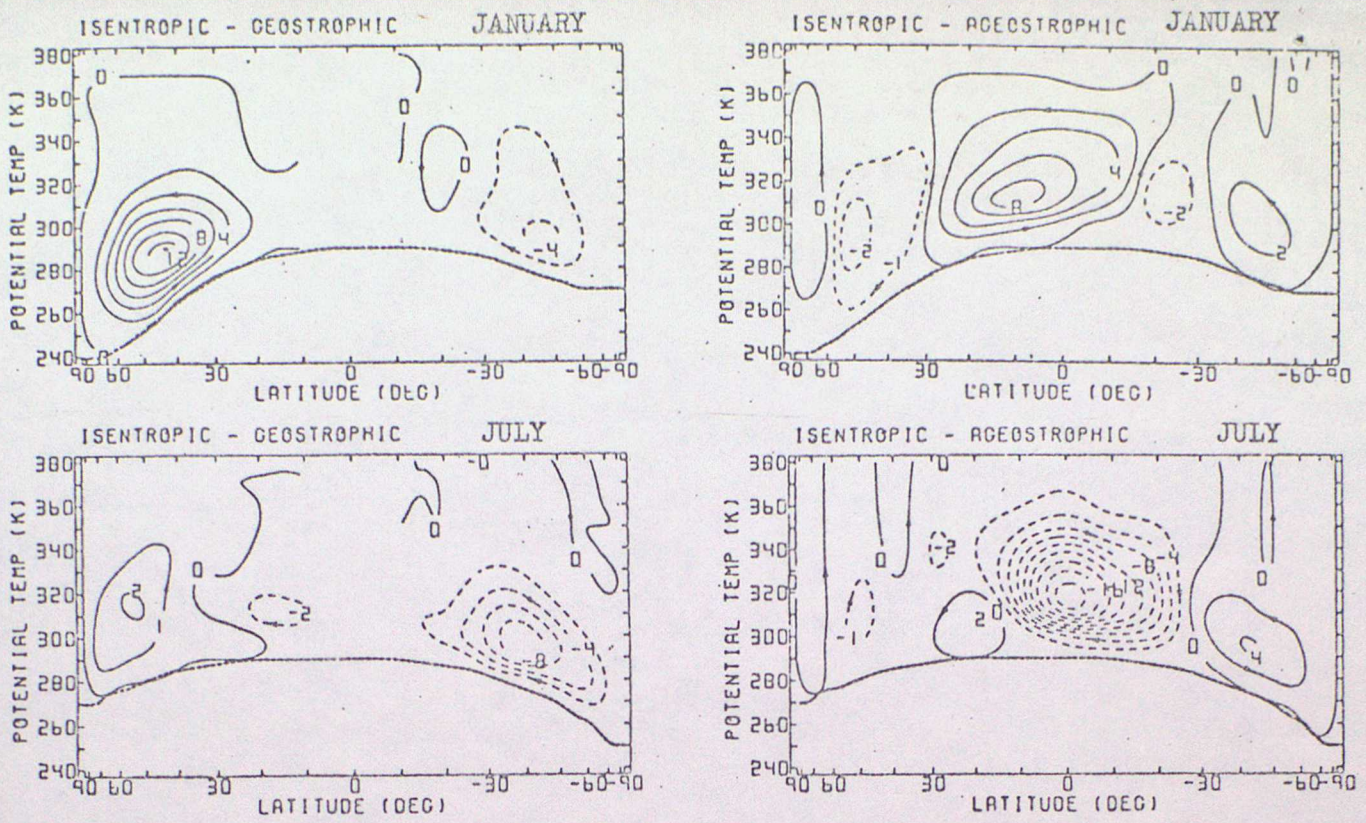

Figure 6.18 Geostrophic and ageostrophic parts of mass stream function in isentropic coordinates zonal mean (compare figure 5.7)

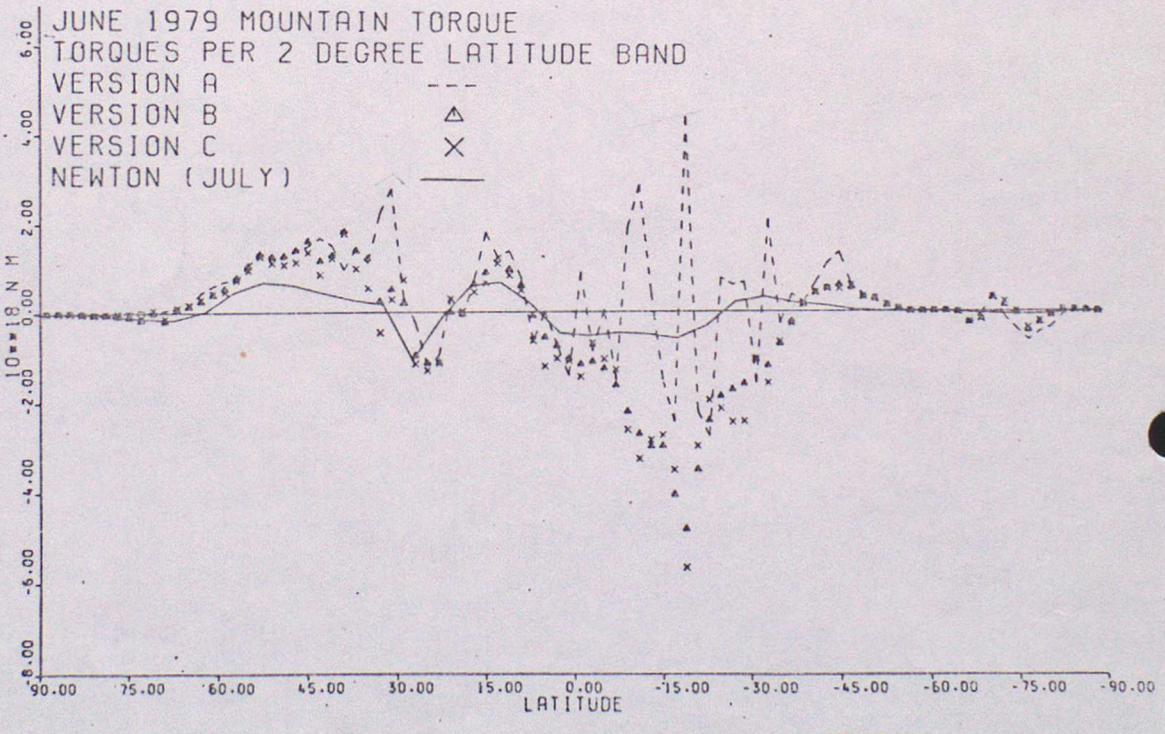

Figure 6.19 Effect of different formulations on mountain torque calculations

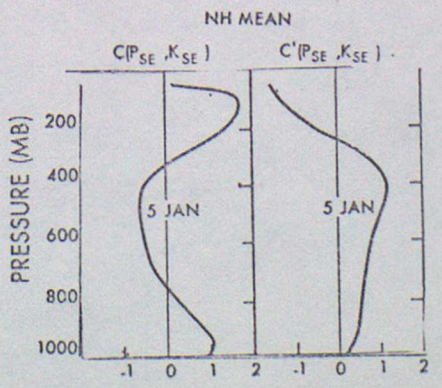

Figure 6.20 Effect of different formulations on the vertical distribution of conversion from APE to KE for standing eddies

Integrand of the conversion rate from eddy potential to eddy kinetic energy for the stationary eddies $C(P_{SE}, K_{SE})$

MD-

ADVANCED LECTURES 1982 - GENERAL CIRCULATION OF THE ATMOSPHERE

LECTURE 7 - Selected examples from recent observational studies

In order to give a flavour of the sort of research currently in progress, in this lecture I present a sample of some recent results. You will see that they fall quite well into the three categories I introduced in Lecture 5: description, understanding and application.

1. FGGE

The mass of data that FGGE produced ($1\frac{1}{2}$ billion numbers filling 35 computer tapes for just one set of analyses) can easily swamp one unless the object of study is predetermined. I have chosen to illustrate the data by presenting some basic maps which I hope will describe the circulation during the FGGE year (December 1978-November 1979) in a reasonable space. During the presentation I shall remark on various aspects for further study. It must be remembered that although the best observed year ever, 1979 was not "the average year"; there is no such thing.

a. Vertical structure during January and July

Figures 1 and 2 show zonal mean cross sections of temperature and horizontal wind components. Note

(i) the thermal wind balance; the vertical gradient of u is related to the horizontal gradient of T.

(ii) the stronger jets in the southern hemisphere, particularly the polar night jet in the stratosphere.

(iii) the marked double jet structure in the southern hemisphere winter. These do not show in the northern hemisphere zonal mean because of the standing eddies.

(iv) regions of both easterly and westerly at the surface.

(v) the marked asymmetry of summer and winter meridional circulation.

Figures 3, 4 and 5 show corresponding maps at selected levels. These maps show the rotational part of the wind as streamfunction contours. The non-divergent flow is parallel to these and its u component proportional to the N-S spacing (NB. the contour interval varies with level). The divergent component of wind is shown as arrows with length proportional to speed. Isotachs of the total wind are shown progressively by dots, light shading, dots, dark shading, dots, no shading (again the contour interval changes with level). Points to note are

(i) at sigma = .987 (about 100 m) the inflow into regions of heating:- summer continents, Indonesia and the western equatorial Pacific in January, India and the Himalayas in July.

(ii) the monsoon flows associated with these last two regions, visible also at 850 mb.

(iii) the strength of the surface westerlies in the southern oceans. The associated Ekman turning of the wind produces the poleward branch of the Ferrel Cell.

(iv) 500 mb has little divergent wind.

(v) the northern hemisphere has two jets at some but not all longitudes.

(vi) the monsoon return flows are clearly visible at 200 mb.

(vii) the asymmetry of the northern winter stratosphere (there was a warming during January 1979).

b. Annual cycle

Figures 6–17 show monthly mean charts of 500 mb heights and sea level pressure, and the rms deviation from these. Figures 18–23 show the corresponding 850 mb and 200 mb winds. Points to note are

(i) variability maxima, shown shaded in figures 6–17, correspond to the storm tracks discussed later in Section 2.

(ii) month to month variability, both in fields and storm tracks, is quite large. For instance January was blocked over the North Atlantic, with unusually low variability and high pressure, a split upper jet, and storms passing to the north and south. This month to month variability is similar in nature to inter-annual variability, and is the basis of the teleconnection patterns discussed in Section 2 later.

(iii) the preferred location of anticyclones over summer oceans.

(iv) the depth of the southern ocean low pressure belt.

(v) the disruption of the zonal mean meridional circulation by the summer monsoon during June, July, August.

c. Transient activity

Figures 24–30 show daily 200 mb wind fields during June. Points to note are

(i) the sporadic nature of the Hadley type circulation in time and with longitude.

(ii) the transport of momentum by the eddies from the sub-tropical jet towards the pole.

(iii) the interrelation between these two; the divergent wind feeds energy and momentum into the sub-tropical jet, this is then carried on by the rotational wind of the eddies.

June was chosen because of the onset of the summer monsoon. Points specifically related to this which occur similarly in many years are

(iv) a region of ascent (ie 200 mb divergence) moves westward to the Arabian Sea (often associated with a low level onset vortex), strengthens, then moves eastward to the Bay of Bengal and the Himalayas.

(v) the northern hemisphere jet establishes itself north of the Himalayas.

(vi) a region of descent (with associated surface high pressure) moves from South Africa eastward and strengthens.

(vii) associated with this is a strong southern hemisphere jet.

(viii) an equatorial easterly jet is established.

2. Separation of time scales

The baroclinic eddies which are so important for mid-latitude energy conversions have a characteristic lifetime of about a week. Their properties are significantly different from those of longer or shorter period variations, so a separation is worthwhile. One way of achieving this is via time filters. An example is shown in Figure 31 (Blackmon 1976). A simpler method is to look at deviations from a short-term mean for the shorter period variations, and at variability of the means for longer periods. Results using both methods exhibit similar patterns. Northern hemisphere variabilities using these bands and low pass filters are also shown in Figure 31 (from Lau et al 1981).

a. Long periods, teleconnections, blocking

These periods explain a large part of the total variability, so any predictability would be a useful forecasting took. The variability is associated with standing rather than progressive waves. In the northern hemisphere these standing waves have preferred locations, which can be studied using spatial correlations of the interannual variability of monthly means (Wallace and Gutzler 1981). The spatial correlation for three such locations are shown in Figure 32 a,b,c. The difference between December 1978 and January 1979 fits this pattern quite well (Figures 6 and 7). If for every point we find the most negative value of this correlation (eg -.73 for 25°N 25°W in Figure 32a) and plot it, we get Figure 32d. This is called the teleconnectivity. It is clear from figures 6, 7, 8 etc that the state of these patterns affects the position of the storm tracks; with positive sign this phenomenon is called blocking. Various hypotheses exist for the dynamical cause of these patterns - eddy transport by the higher frequency eddies, resonant interaction of long waves with orography, standing wave response to tropical heating etc. Further observational studies to test these are needed.

b. Medium periods, storm tracks

Periods of about 2 days to a week are associated with moving baroclinic waves with zonal wave number of about 4 to 7. It is in this scale that the major baroclinic energy conversion takes place (see Figure 6.16). These waves also give us our "weather", so their detailed understanding is important. For instance many forecast models and GCMs have systematic errors which seem to be related to over-deep depressions at the end of storm-tracks. Are they not filling old storms fast enough (incorrect parametrization of drag coefficient), or are they not going through the lifecycle fast enough (inefficient baroclinic conversion), or is the external long-wave stearing wrong (bad boundary conditions)? Again further comparison of models with detailed and precise observational studies are needed.

c. Short periods, parametrization

High frequency waves are associated with short wavelengths, neither of which are resolved by the standard observational network or by current large

scale models. In the models their effect is parametrized. To test these parametrization schemes we can either use indirect budget methods (eg Figure 6.10), or else special observational studies are necessary. There have been several of these:- GATE (for convection), AMTEX (air mass transformation), JASIN (air-sea interaction), and ALPEX (mountains), are examples.

3. Spatial variations

Throughout these lectures the importance of variations from the zonal mean state has been emphasized. As a final example I show some results from Blackmon et al (1977) and Lau (1978). Figure 33a shows the winter northern hemisphere jets and storm tracks. The jets are initiated by thermally direct Hadley type cells, as shown in Figure 33b. Baroclinic waves travel along the jets, amplifying by eddy APE $\rightarrow$ KE conversion. This is shown in Figure 33d. (Assuming geostrophy the term plotted equals $\chi \cdot \nabla \phi$). These waves become significant amplitude storms towards the end of the jet, and take over the transport of heat and momentum, driving a Ferrel type cell (Figure 33c). The process is summarized in Figure 33e. Comparison with Figure 1 shows that these sector mean meridional circulations are an order of magnitude larger than the zonal mean Ferrel cell.

Obviously this is a simplified summary of the picture, I recommend reading the references given.

(References were given with Lecture 5).

Figure 1

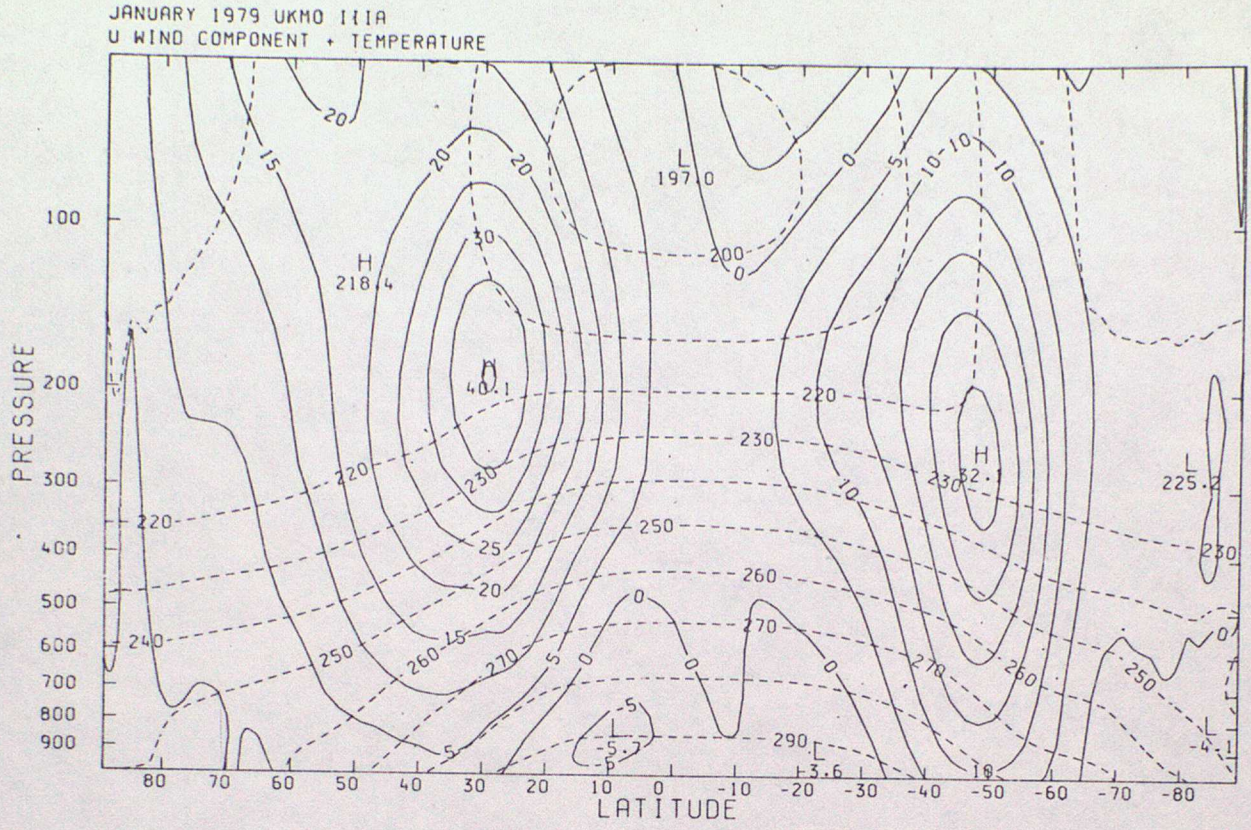
JANUARY 1979 UKMO IIIA
U WIND COMPONENT + TEMPERATURE
PRESSURE
LATITUDE
100
200
300
400
500
600
700
800
900
80 70 60 50 40 30 20 10 0 -10 -20 -30 -40 -50 -60 -70 -80
H 218.4
L 197.0
H 40.1
H 32.1
L 225.2
L -5.7
L +3.6
L -4.1

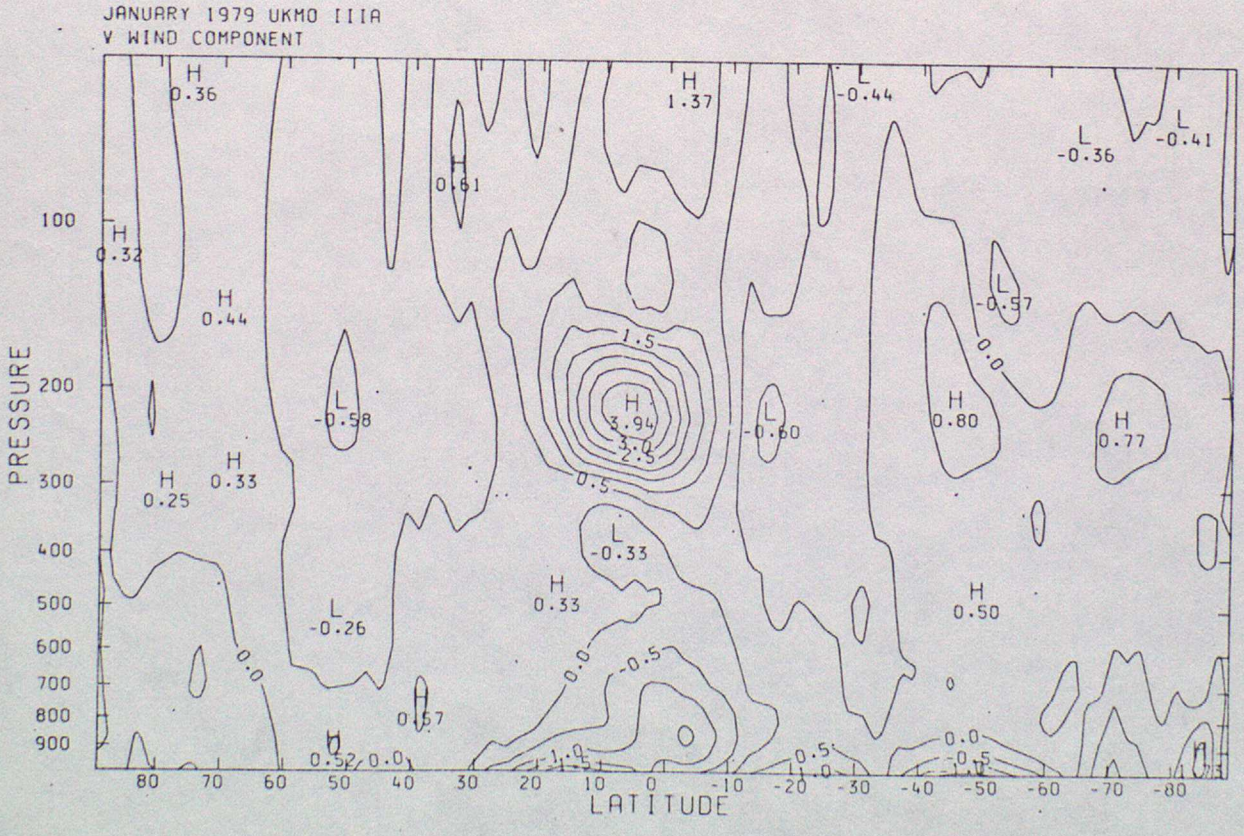
JANUARY 1979 UKMO IIIA
V WIND COMPONENT
PRESSURE
LATITUDE
100
200
300
400
500
600
700
800
900
80 70 60 50 40 30 20 10 0 -10 -20 -30 -40 -50 -60 -70 -80
H 0.36
H 1.37
L -0.44
L -0.36
L -0.41
H 0.61
H 0.32
H 0.44
L -0.57
H 3.94
L -0.58
L -0.60
H 0.80
H 0.77
H 0.25
H 0.33
L -0.33
H 0.33
H 0.50
L -0.26
H 0.57
H 0.52
0.0
1.5
3.0
2.5
0.5
-0.5
-1.0
-1.5

Figure 2

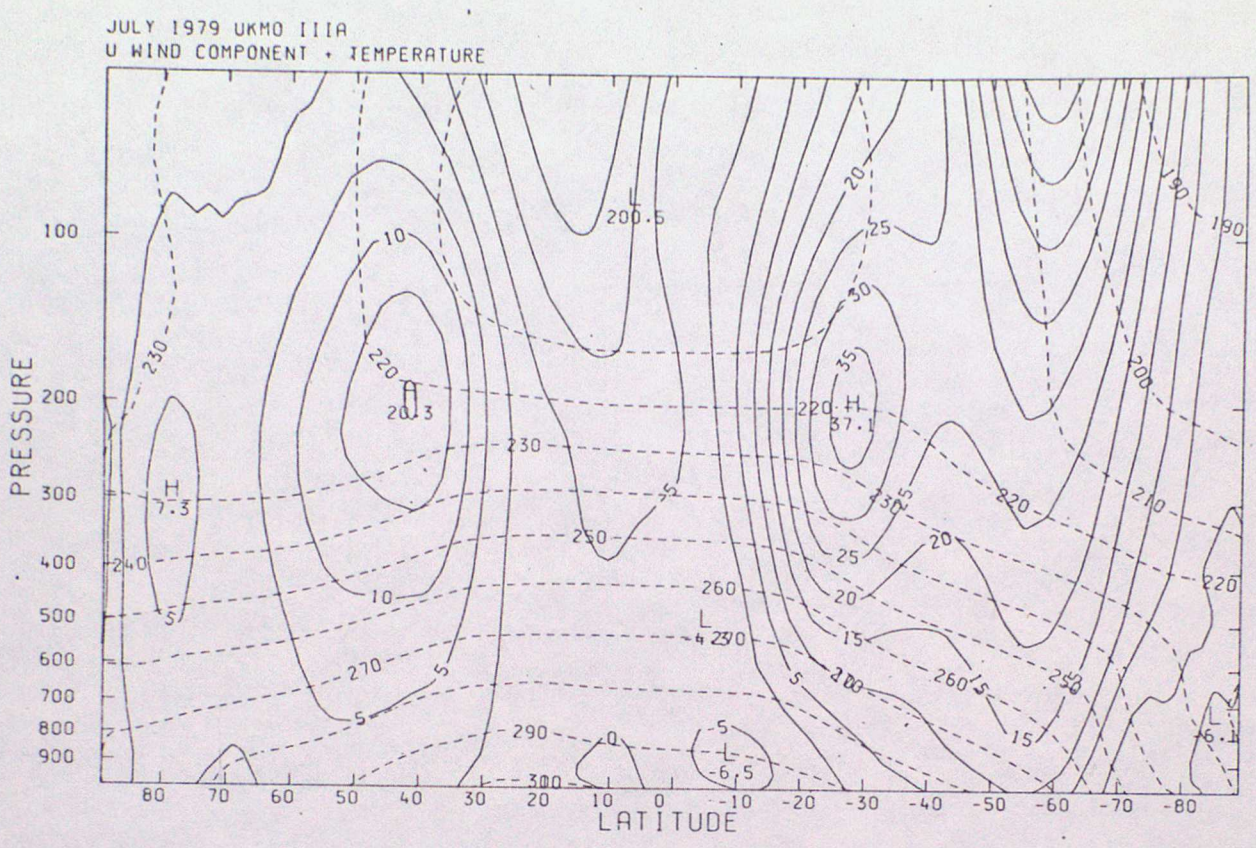
JULY 1979 UKMO IIIA
U WIND COMPONENT + TEMPERATURE
PRESSURE
LATITUDE

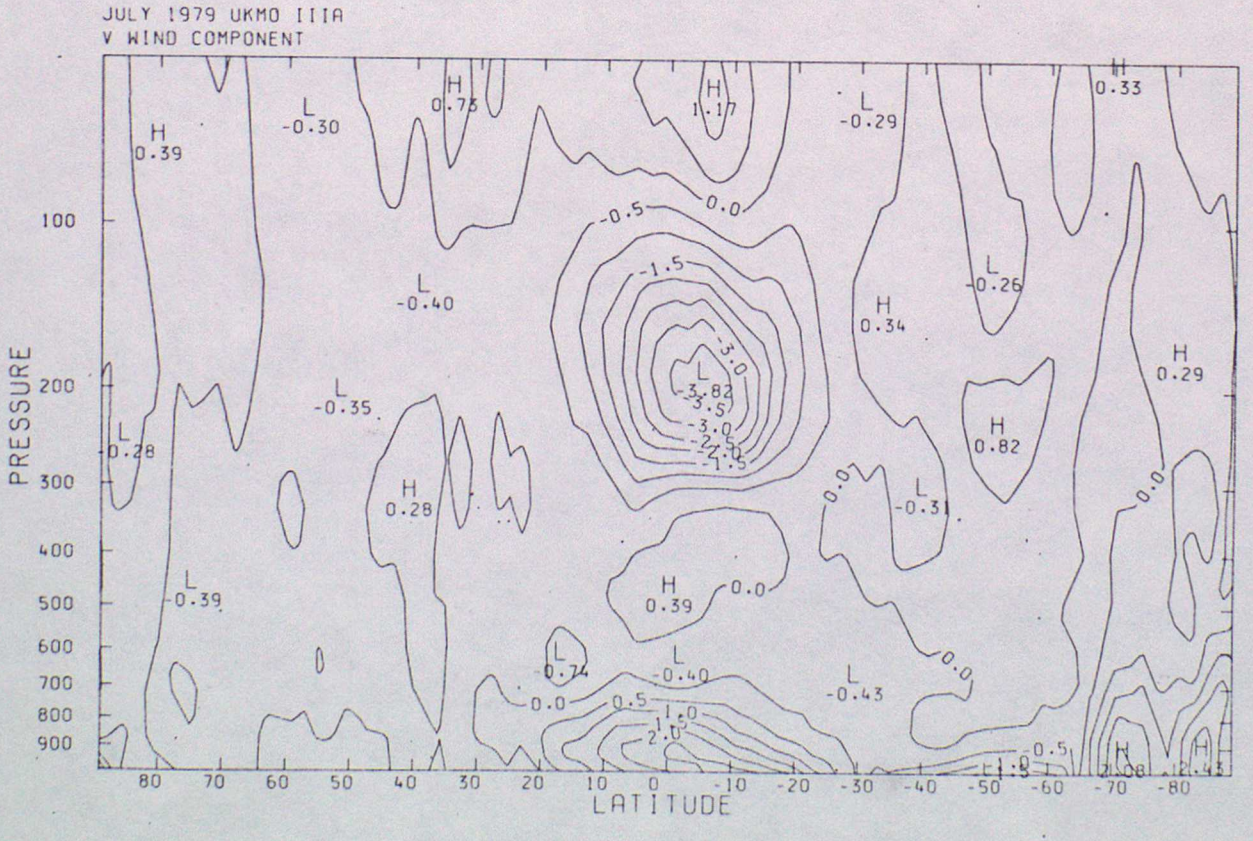
JULY 1979 UKMO IIIA
V WIND COMPONENT
PRESSURE
LATITUDE

Figure 3

MET. OFFICE FGGE IIIA ANALYSIS MONTHLY MEAN WIND (JANUARY 1979).
STREAMFUNCTION + DIVERGENT WIND ARROWS + TOTAL ISOTACHS (DOTS & SHADING).
VALID AT 12Z ON 31/1/79 MODEL TIME: DAY 31 HR 12
LEVEL: SIGMA=0.987 EXPERIMENT NO.: 2

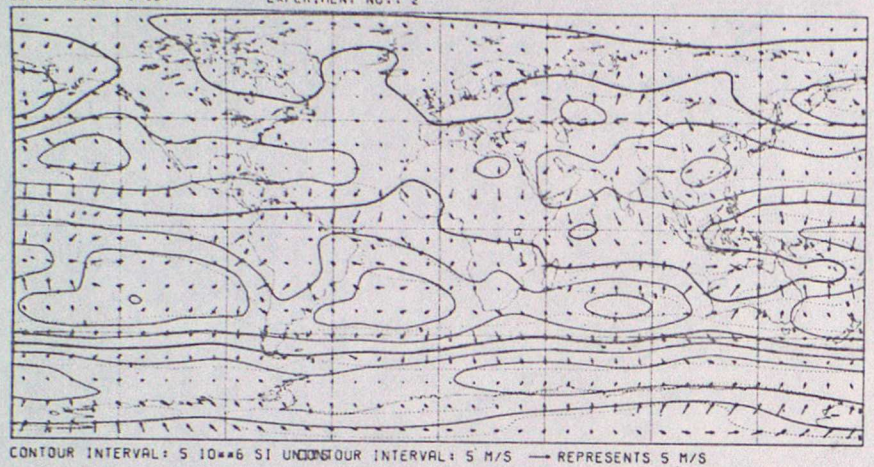

CONTOUR INTERVAL: 5 10**6 SI UNITS CONTOUR INTERVAL: 5 M/S → REPRESENTS 5 M/S

MET. OFFICE FGGE IIIA ANALYSIS MONTHLY MEAN WIND (JULY 1979).
STREAMFUNCTION + DIVERGENT WIND ARROWS + TOTAL ISOTACHS (DOTS & SHADING).
VALID AT 12Z ON 31/7/79 MODEL TIME: DAY 212 HR 12
LEVEL: SIGMA=0.987 EXPERIMENT NO.: 3

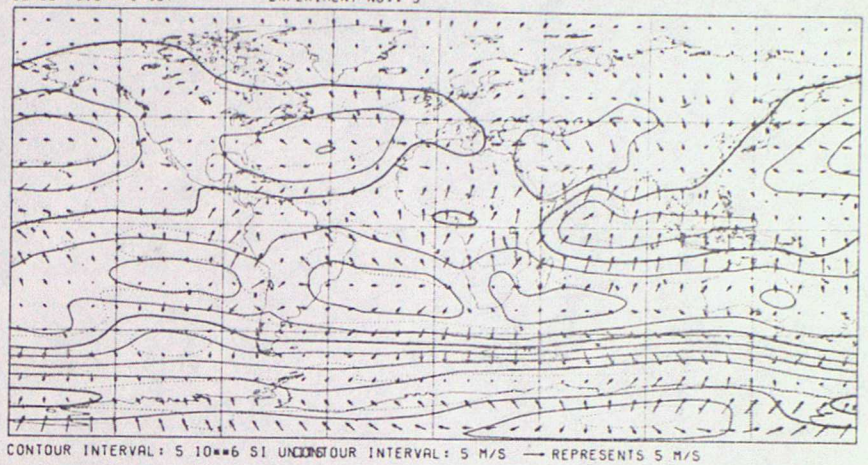

CONTOUR INTERVAL: 5 10**6 SI UNITS CONTOUR INTERVAL: 5 M/S → REPRESENTS 5 M/S

MET. OFFICE FGGE IIIA ANALYSIS MONTHLY MEAN WIND (JANUARY 1979).
STREAMFUNCTION + DIVERGENT WIND ARROWS + TOTAL ISOTACHS (DOTS & SHADING).
VALID AT 12Z ON 31/1/79 MODEL TIME: DAY 31 HR 12
LEVEL: 850 MB EXPERIMENT NO.: 2

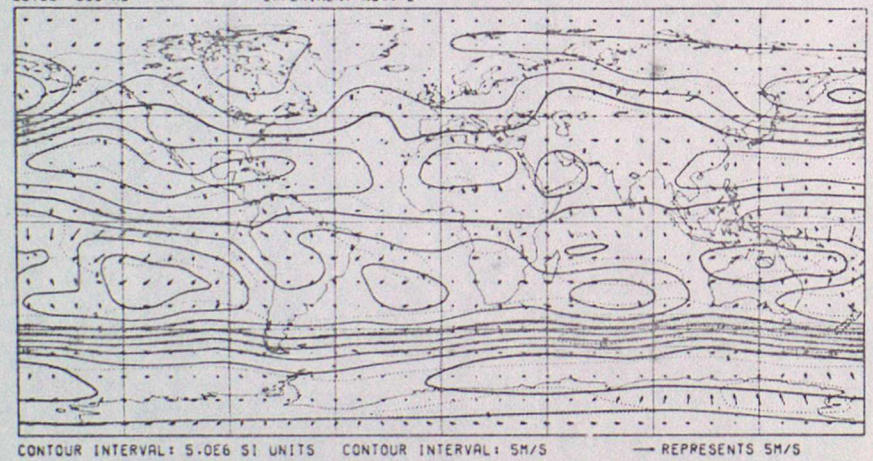

CONTOUR INTERVAL: 5.0E6 SI UNITS CONTOUR INTERVAL: 5M/S → REPRESENTS 5M/S

MET. OFFICE FGGE IIIA ANALYSIS MONTHLY MEAN WIND (JULY 1979).
STREAMFUNCTION + DIVERGENT WIND ARROWS + TOTAL ISOTACHS (DOTS & SHADING).
VALID AT 12Z ON 31/7/79 MODEL TIME: DAY 212 HR 12
LEVEL: 850 MB EXPERIMENT NO.: 3

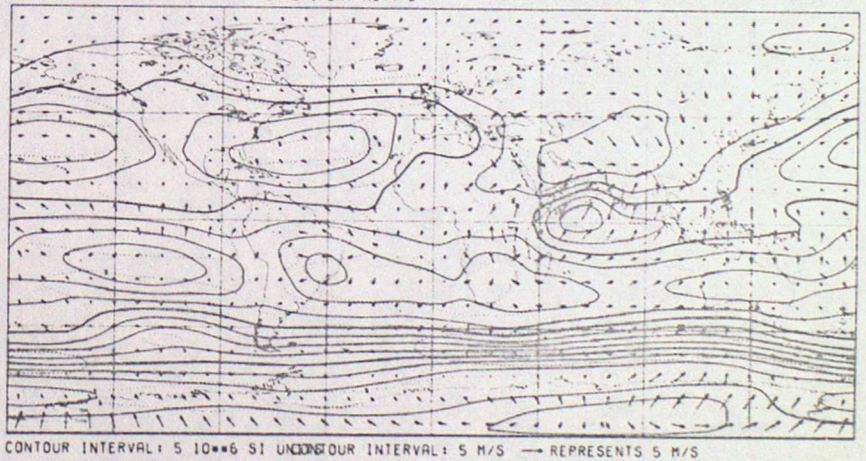

CONTOUR INTERVAL: 5 10**6 SI UNITS CONTOUR INTERVAL: 5 M/S → REPRESENTS 5 M/S

Figure 4

MET. OFFICE FGGE IIIA ANALYSIS MONTHLY MEAN WIND (JANUARY 1979).
STREAMFUNCTION + DIVERGENT WIND ARROWS + TOTAL ISOTACHS (DOTS & SHADING).
VALID AT 12Z ON 31/1/79 MODEL TIME: DAY 31 HR 12
LEVEL: 500 MB EXPERIMENT NO.: 2

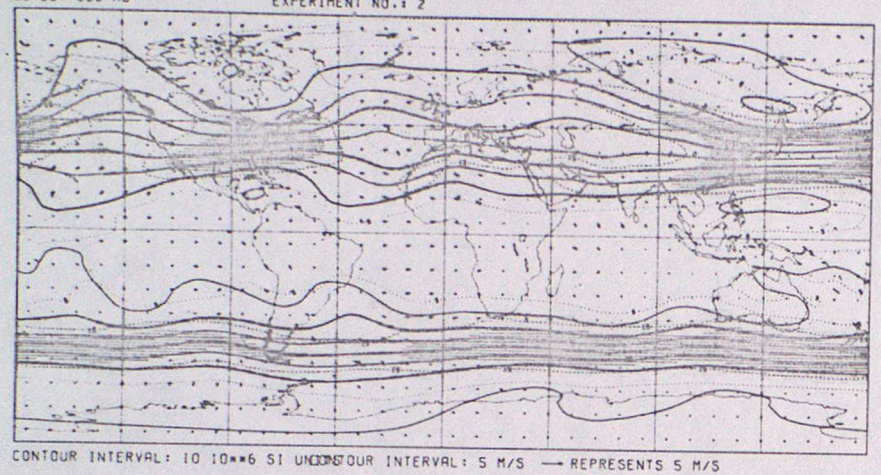

CONTOUR INTERVAL: 10 10**6 SI UNITS CONTOUR INTERVAL: 5 M/S ⟶ REPRESENTS 5 M/S

MET. OFFICE FGGE IIIA ANALYSIS MONTHLY MEAN WIND (JULY 1979).
STREAMFUNCTION + DIVERGENT WIND ARROWS + TOTAL ISOTACHS (DOTS & SHADING).
VALID AT 12Z ON 31/7/79 MODEL TIME: DAY 212 HR 12
LEVEL: 500 MB EXPERIMENT NO.: 3

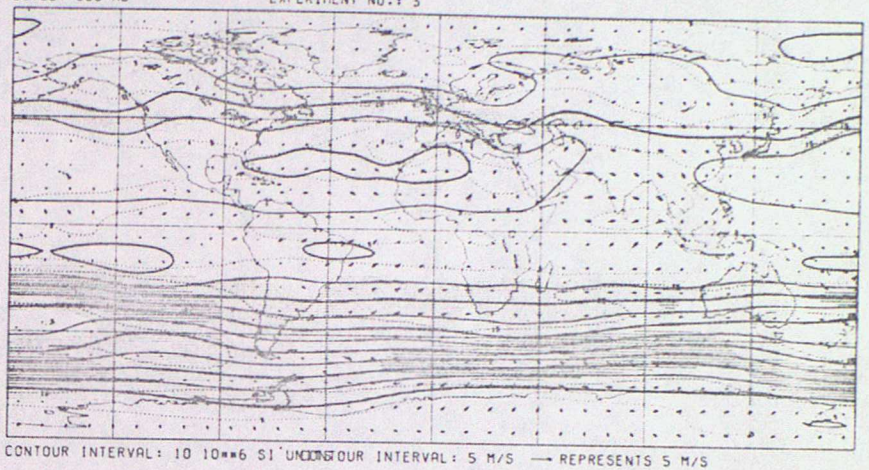

CONTOUR INTERVAL: 10 10**6 SI UNITS CONTOUR INTERVAL: 5 M/S ⟶ REPRESENTS 5 M/S

MET. OFFICE FGGE IIIA ANALYSIS MONTHLY MEAN WIND (JANUARY 1979).
STREAMFUNCTION + DIVERGENT WIND ARROWS + TOTAL ISOTACHS (DOTS & SHADING).
VALID AT 12Z ON 31/1/79 MODEL TIME: DAY 31 HR 12
LEVEL: 200 MB EXPERIMENT NO.: 2

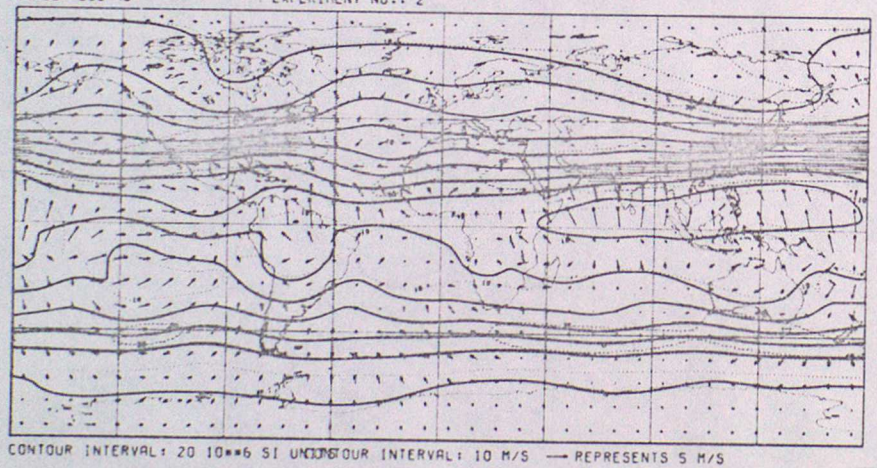

CONTOUR INTERVAL: 20 10**6 SI UNITS CONTOUR INTERVAL: 10 M/S ⟶ REPRESENTS 5 M/S

MET. OFFICE FGGE IIIA ANALYSIS MONTHLY MEAN WIND (JULY 1979).
STREAMFUNCTION + DIVERGENT WIND ARROWS + TOTAL ISOTACHS (DOTS & SHADING).
VALID AT 12Z ON 31/7/79 MODEL TIME: DAY 212 HR 12
LEVEL: 200 MB EXPERIMENT NO.: 3

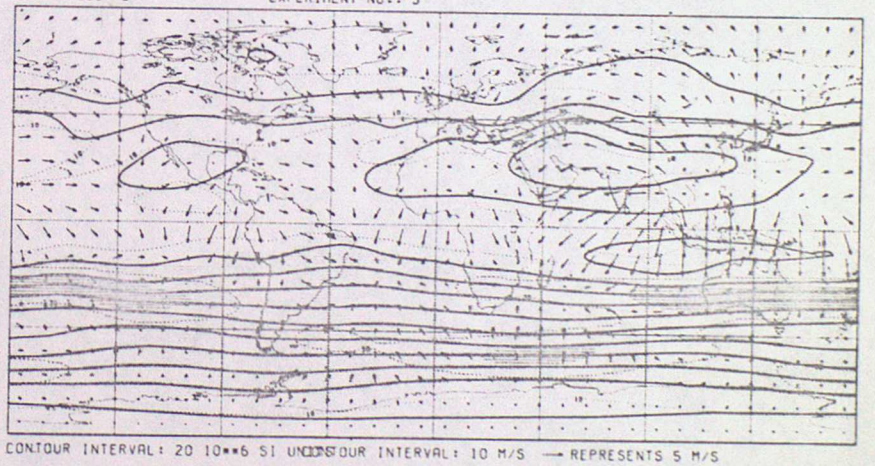

CONTOUR INTERVAL: 20 10**6 SI UNITS CONTOUR INTERVAL: 10 M/S ⟶ REPRESENTS 5 M/S

Figure 5

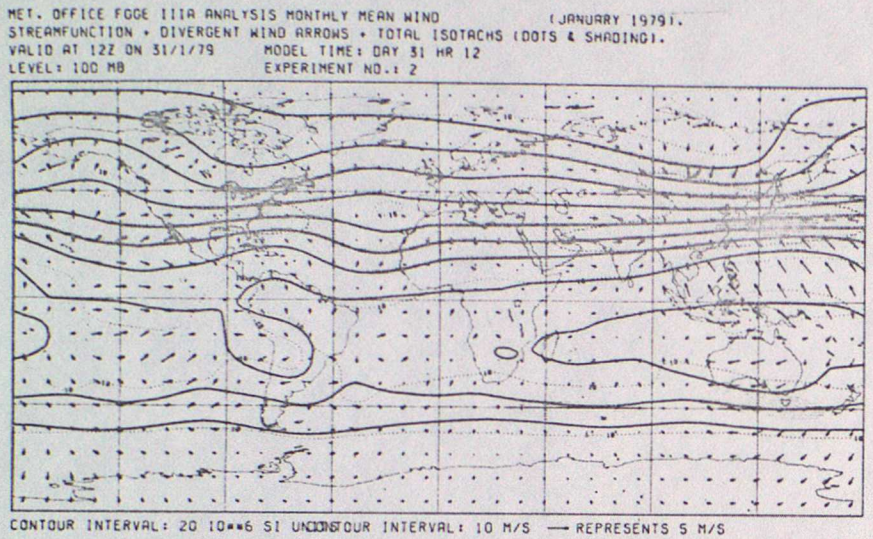
MET. OFFICE FGGE IIIA ANALYSIS MONTHLY MEAN WIND (JANUARY 1979).
STREAMFUNCTION + DIVERGENT WIND ARROWS + TOTAL ISOTACHS (DOTS & SHADING).
VALID AT 12Z ON 31/1/79 MODEL TIME: DAY 31 HR 12
LEVEL: 100 MB EXPERIMENT NO.: 2
CONTOUR INTERVAL: 20 10**6 SI UNITS CONTOUR INTERVAL: 10 M/S — REPRESENTS 5 M/S

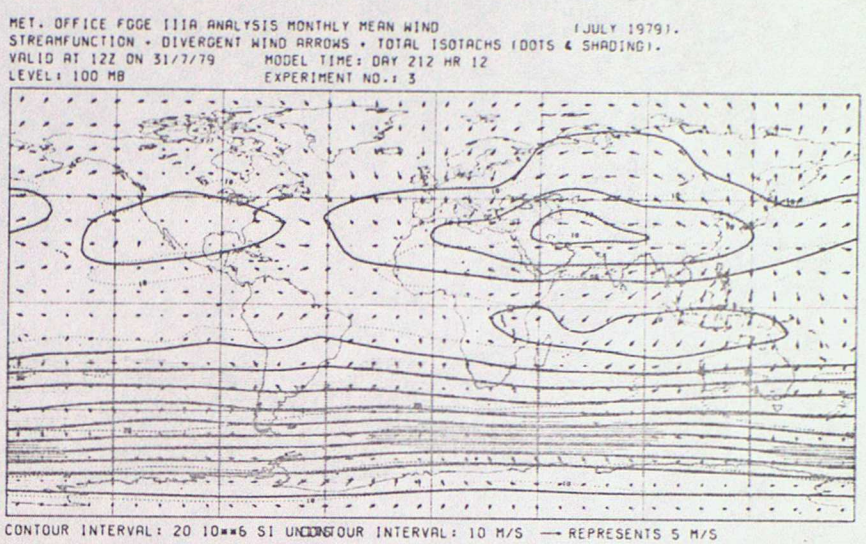
MET. OFFICE FGGE IIIA ANALYSIS MONTHLY MEAN WIND (JULY 1979).
STREAMFUNCTION + DIVERGENT WIND ARROWS + TOTAL ISOTACHS (DOTS & SHADING).
VALID AT 12Z ON 31/7/79 MODEL TIME: DAY 212 HR 12
LEVEL: 100 MB EXPERIMENT NO.: 3
CONTOUR INTERVAL: 20 10**6 SI UNITS CONTOUR INTERVAL: 10 M/S — REPRESENTS 5 M/S

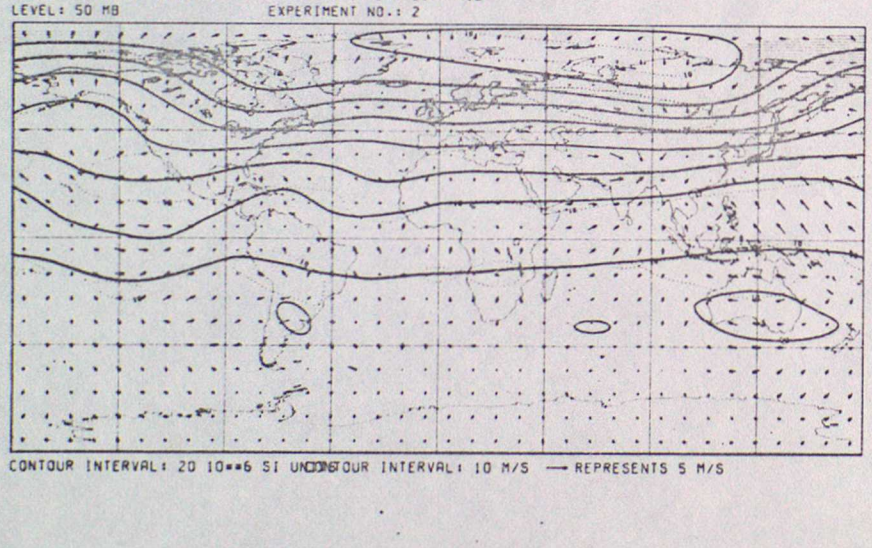
MET. OFFICE FGGE IIIA ANALYSIS MONTHLY MEAN WIND (JANUARY 1979).
STREAMFUNCTION + DIVERGENT WIND ARROWS + TOTAL ISOTACHS (DOTS & SHADING).
VALID AT 12Z ON 31/1/79 MODEL TIME: DAY 31 HR 12
LEVEL: 50 MB EXPERIMENT NO.: 2
CONTOUR INTERVAL: 20 10**6 SI UNITS CONTOUR INTERVAL: 10 M/S — REPRESENTS 5 M/S

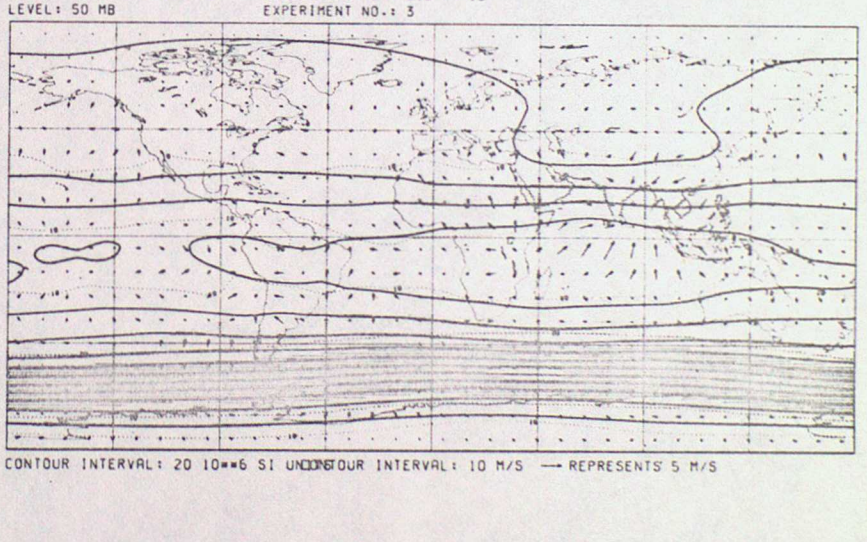
MET. OFFICE FGGE IIIA ANALYSIS MONTHLY MEAN WIND (JULY 1979).
STREAMFUNCTION + DIVERGENT WIND ARROWS + TOTAL ISOTACHS (DOTS & SHADING).
VALID AT 12Z ON 31/7/79 MODEL TIME: DAY 212 HR 12
LEVEL: 50 MB EXPERIMENT NO.: 3
CONTOUR INTERVAL: 20 10**6 SI UNITS CONTOUR INTERVAL: 10 M/S — REPRESENTS 5 M/S

Figure 6

ECMWF FGGE IIIB ANALYSES. TIME-MEAN & S.D. (DECEMBER 1978)
HEIGHT: MEAN (THICKER AT 32DAM INTERVALS) & SD (DOTTED. WITH SHADING >15DAM)
START TIME: 0Z ON 1/12/78 MODEL TIME: DAY 335 HR 0
LEVEL: 500 MB AVERAGED OVER 31 DAYS

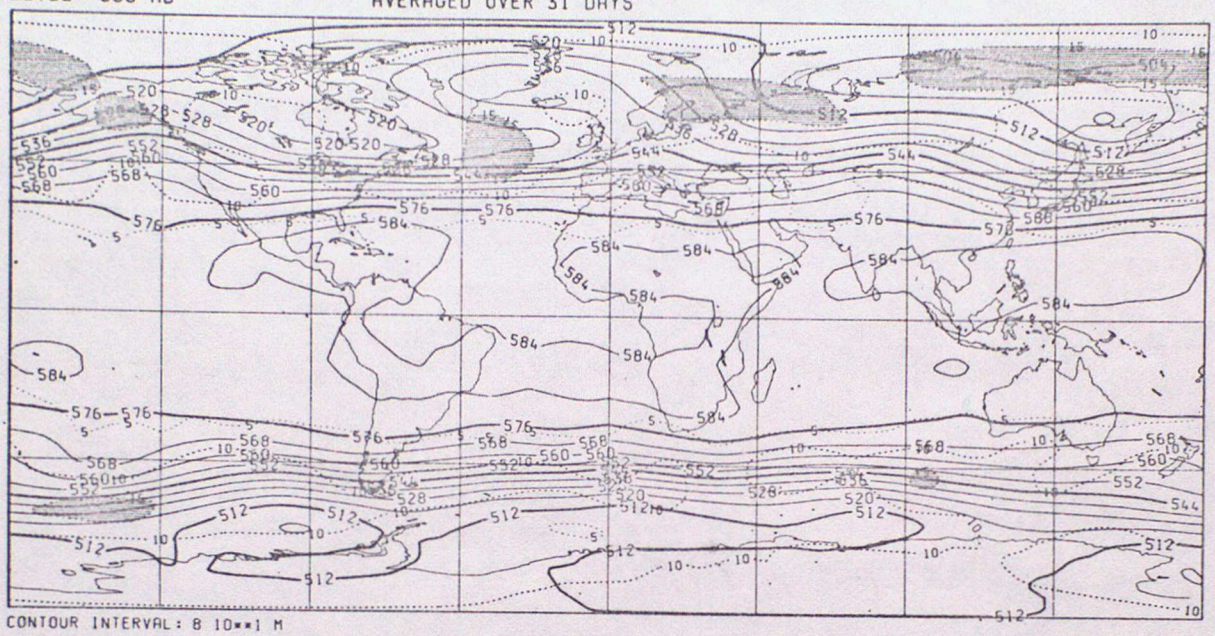

CONTOUR INTERVAL: 8 10**1 M

ECMWF FGGE IIIB ANALYSES. TIME-MEAN & S.D. (DECEMBER 1978)
PMSL: MEAN (980.1000.1020MB THICKER) & SD (DOTTED. WITH SHADING >15MB)
START TIME: 0Z ON 1/12/78 MODEL TIME: DAY 335 HR 0
LEVEL: SEA LEVEL AVERAGED OVER 31 DAYS

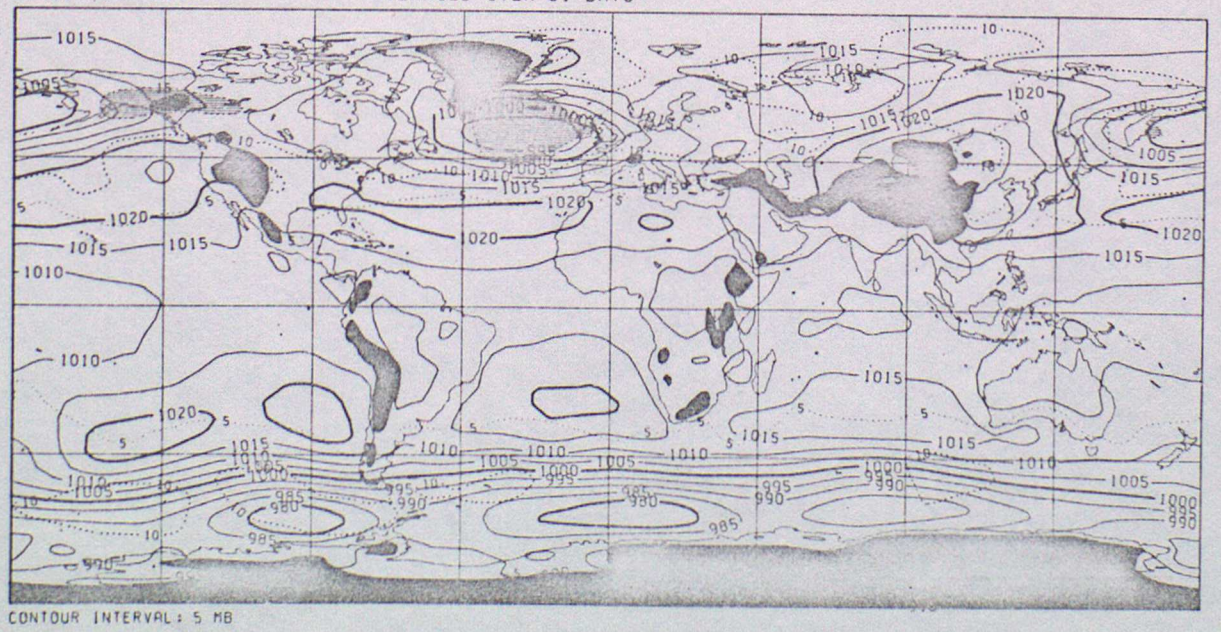

CONTOUR INTERVAL: 5 MB

Figure 7

ECMWF FGGE IIIB ANALYSES. TIME-MEAN & S.D. (JANUARY 1979)
HEIGHT: MEAN (THICKER AT 320AM INTERVALS) & SD (DOTTED. WITH SHADING >150AM)
START TIME: 0Z ON 1/1/79 MODEL TIME: DAY 1 HR 0
LEVEL: 500 MB AVERAGED OVER 31 DAYS

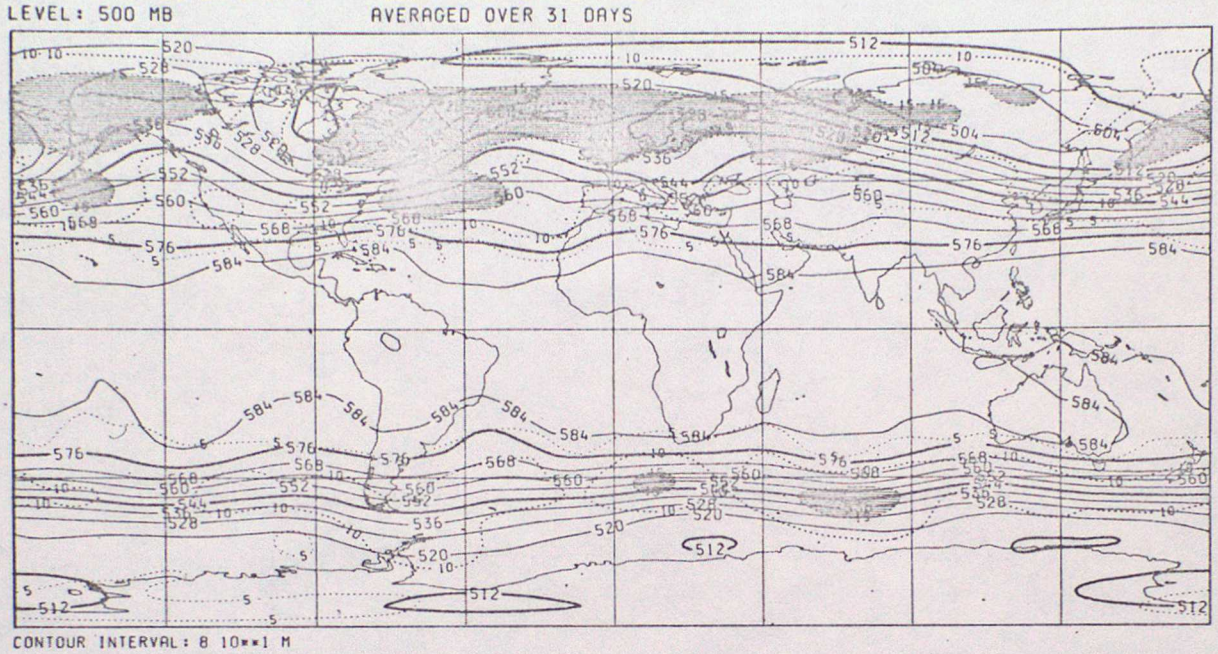

CONTOUR INTERVAL: 8 10**1 M

ECMWF FGGE IIIB ANALYSES. TIME-MEAN & S.D. (JANUARY 1979)
PMSL: MEAN (980,1000,1020MB THICKER) & SD (DOTTED. WITH SHADING >15MB)
START TIME: 0Z ON 1/1/79 MODEL TIME: DAY 1 HR 0
LEVEL: SEA LEVEL AVERAGED OVER 31 DAYS

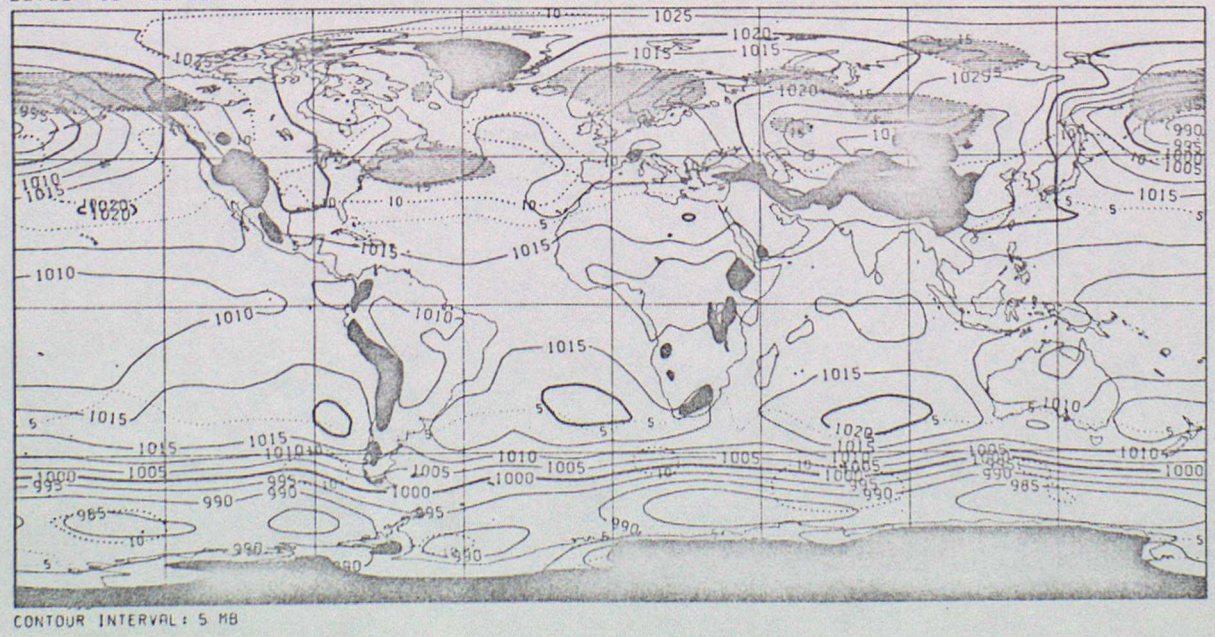

CONTOUR INTERVAL: 5 MB

Figure 8

ECMWF FGGE IIIB ANALYSES. TIME-MEAN & S.D. (FEBRUARY 1979)
HEIGHT: MEAN (THICKER AT 32DAM INTERVALS) & SD (DOTTED. WITH SHADING >15DAM)
START TIME: 0Z ON 1/2/79 MODEL TIME: DAY 32 HR 0
LEVEL: 500 MB AVERAGED OVER 28 DAYS

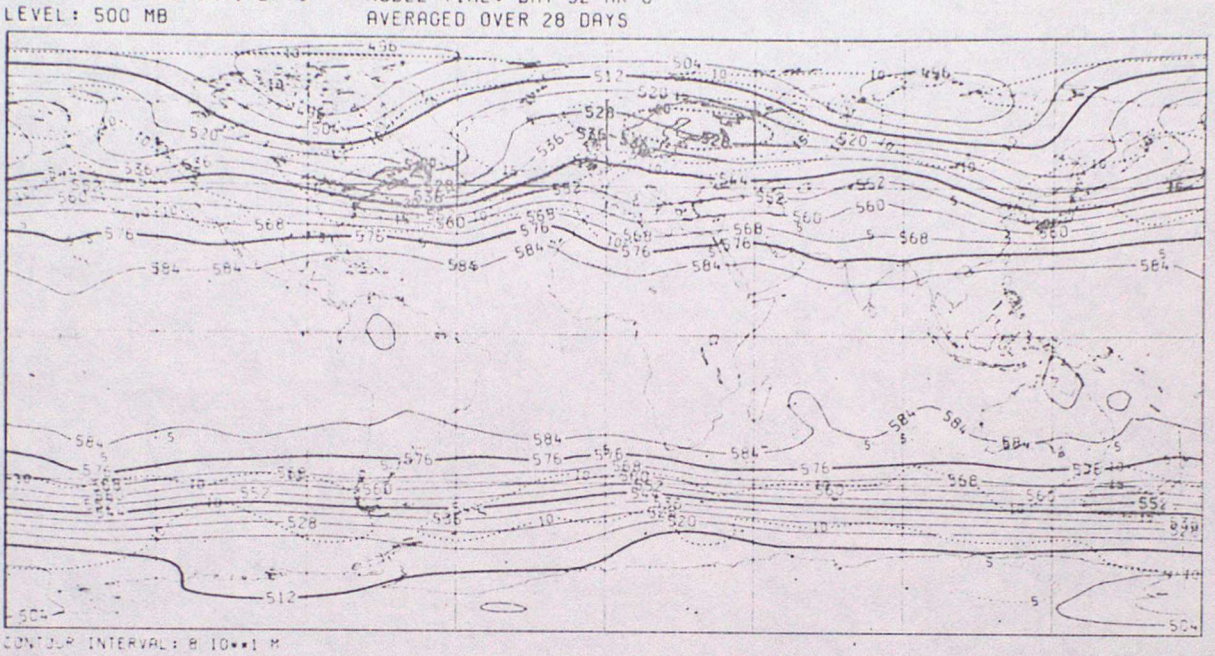

CONTOUR INTERVAL: 8 10**1 M

ECMWF FGGE IIIB ANALYSES. TIME-MEAN & S.D. (FEBRUARY 1979)
PMSL: MEAN (980.1000.1020MB THICKER) & SD (DOTTED. WITH SHADING >15MB)
START TIME: 0Z ON 1/2/79 MODEL TIME: DAY 32 HR 0
LEVEL: SEA LEVEL AVERAGED OVER 28 DAYS

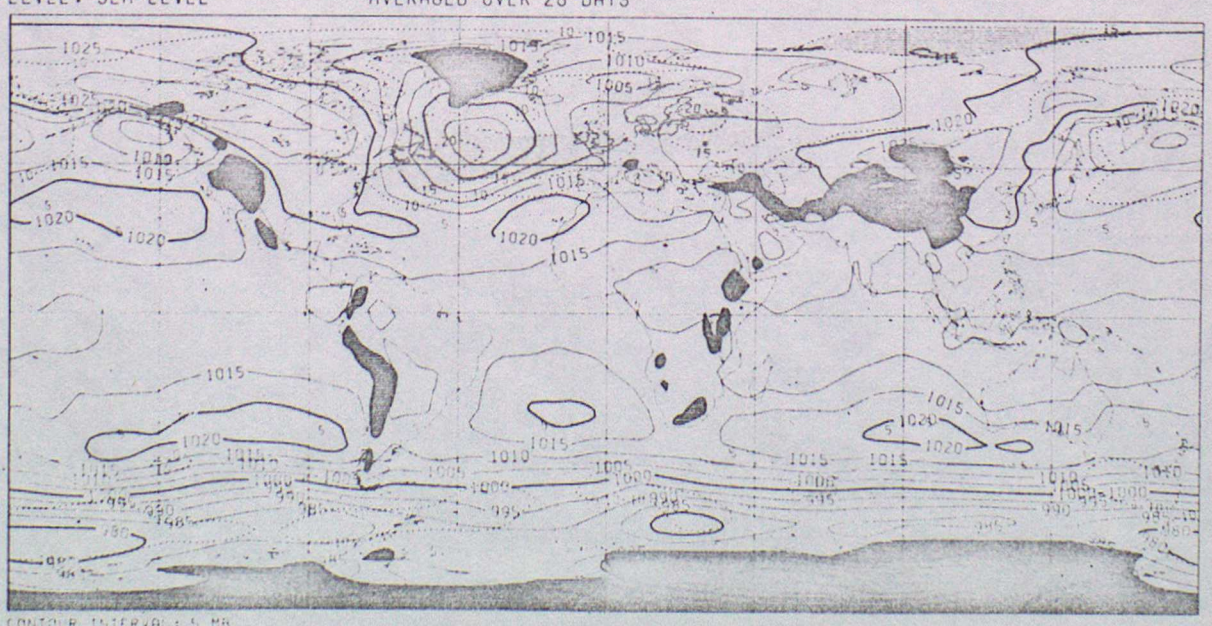

CONTOUR INTERVAL: 5 MB

Figure 9

ECMWF FGGE IIIB ANALYSES. TIME-MEAN & S.D. (MARCH 1979)
HEIGHT: MEAN (THICKER AT 32DAM INTERVALS) & SD (DOTTED. WITH SHADING >15DAM)
START TIME: 0Z ON 1/3/79 MODEL TIME: DAY 60 HR 0
LEVEL: 500 MB AVERAGED OVER 31 DAYS

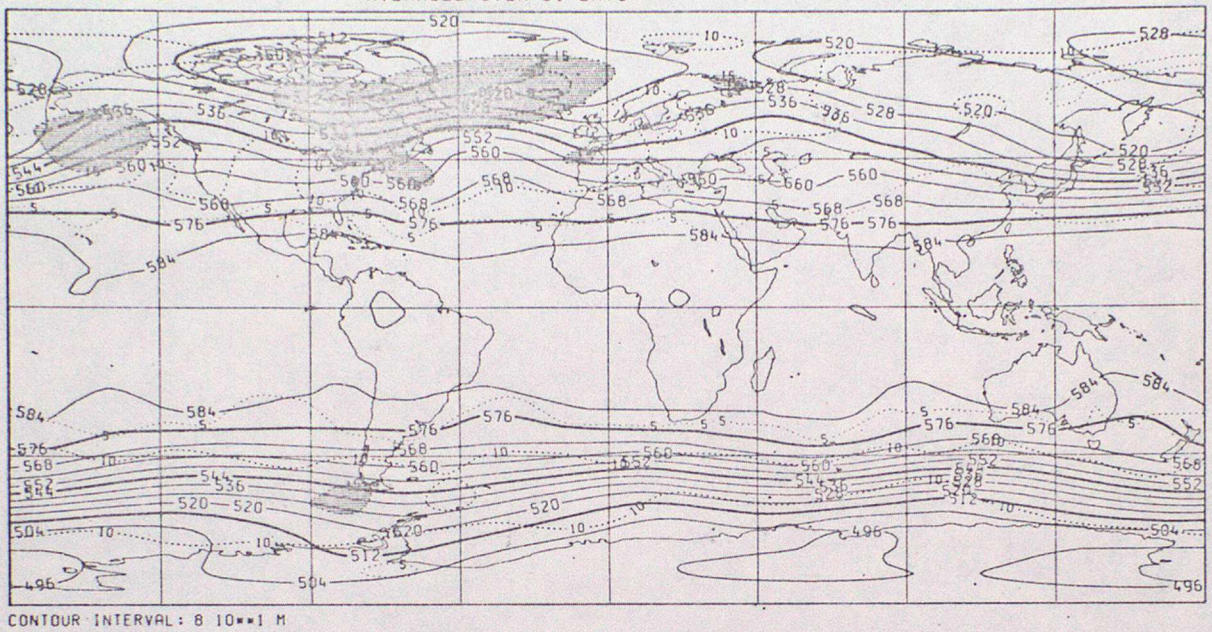

CONTOUR INTERVAL: 8 10**1 M

ECMWF FGGE IIIB ANALYSES. TIME-MEAN & S.D. (MARCH 1979)
PMSL: MEAN (980,1000,1020MB THICKER) & SD (DOTTED. WITH SHADING >15MB)
START TIME: 0Z ON 1/3/79 MODEL TIME: DAY 60 HR 0
LEVEL: SEA LEVEL AVERAGED OVER 31 DAYS

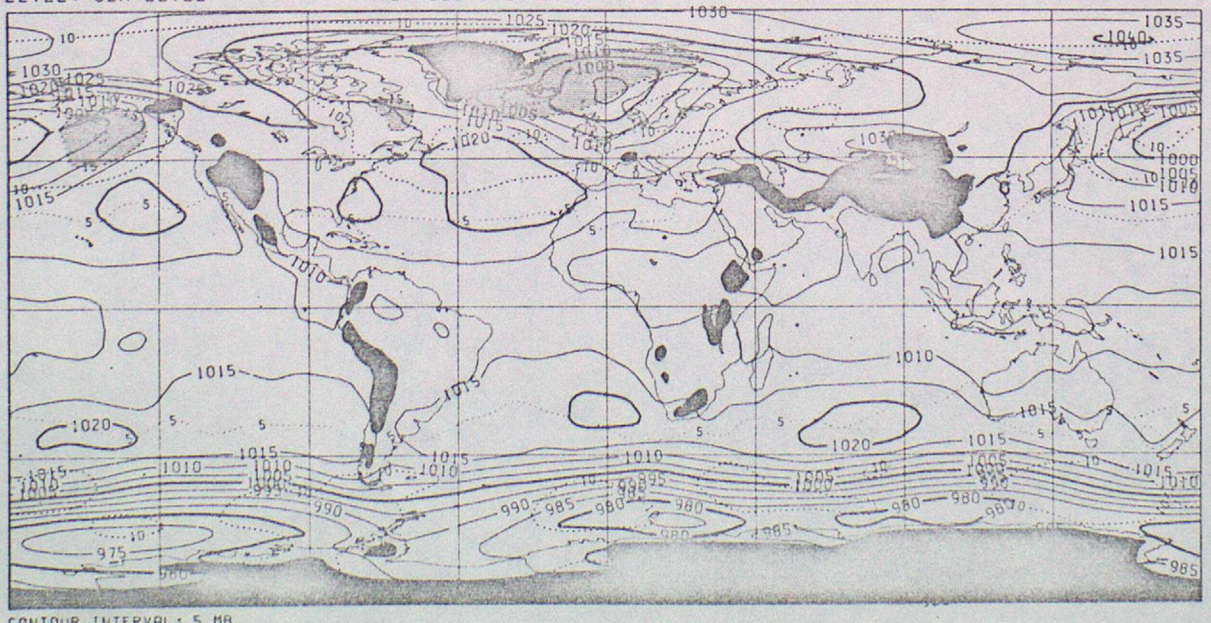

CONTOUR INTERVAL: 5 MB

Figure 10

ECMWF FGGE IIIB ANALYSES. TIME-MEAN & S.D. (APRIL 1979)
HEIGHT: MEAN (THICKER AT 32DAM INTERVALS) & SD (DOTTED, WITH SHADING >15DAM)
START TIME: 0Z ON 1/4/79 MODEL TIME: DAY 91 HR 0
LEVEL: 500 MB AVERAGED OVER 30 DAYS

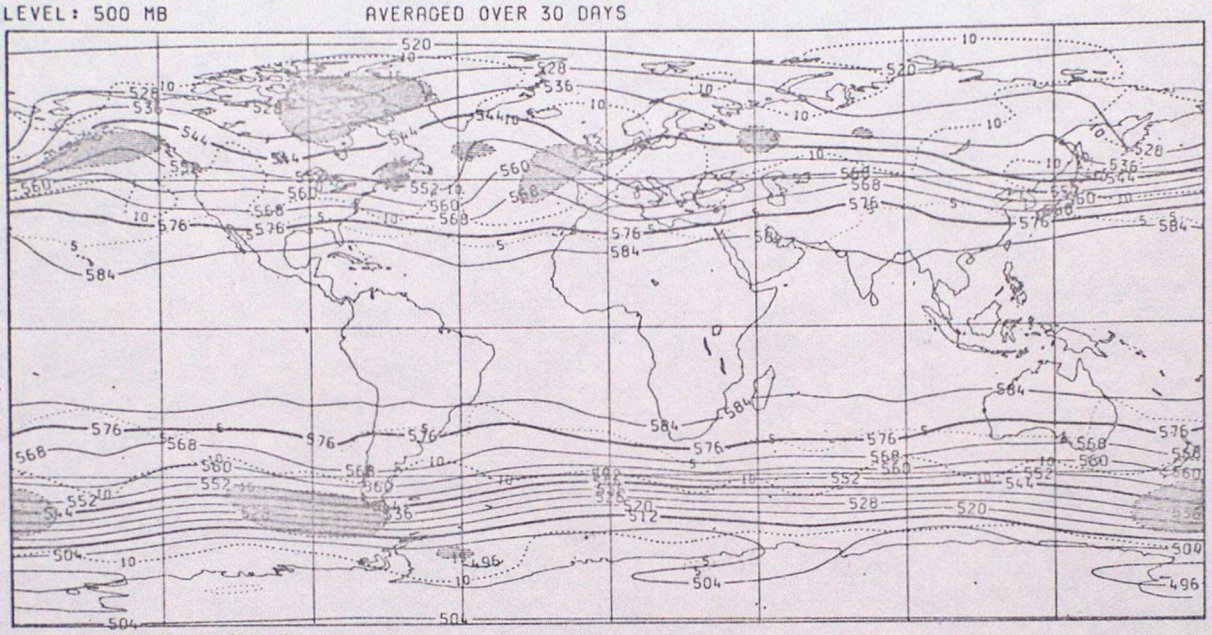

CONTOUR INTERVAL: 8 10**1 M

ECMWF FGGE IIIB ANALYSES. TIME-MEAN & S.D. (APRIL 1979)
PMSL: MEAN (980,1000,1020MB THICKER) & SD (DOTTED, WITH SHADING >15MB)
START TIME: 0Z ON 1/4/79 MODEL TIME: DAY 91 HR 0
LEVEL: SEA LEVEL AVERAGED OVER 30 DAYS

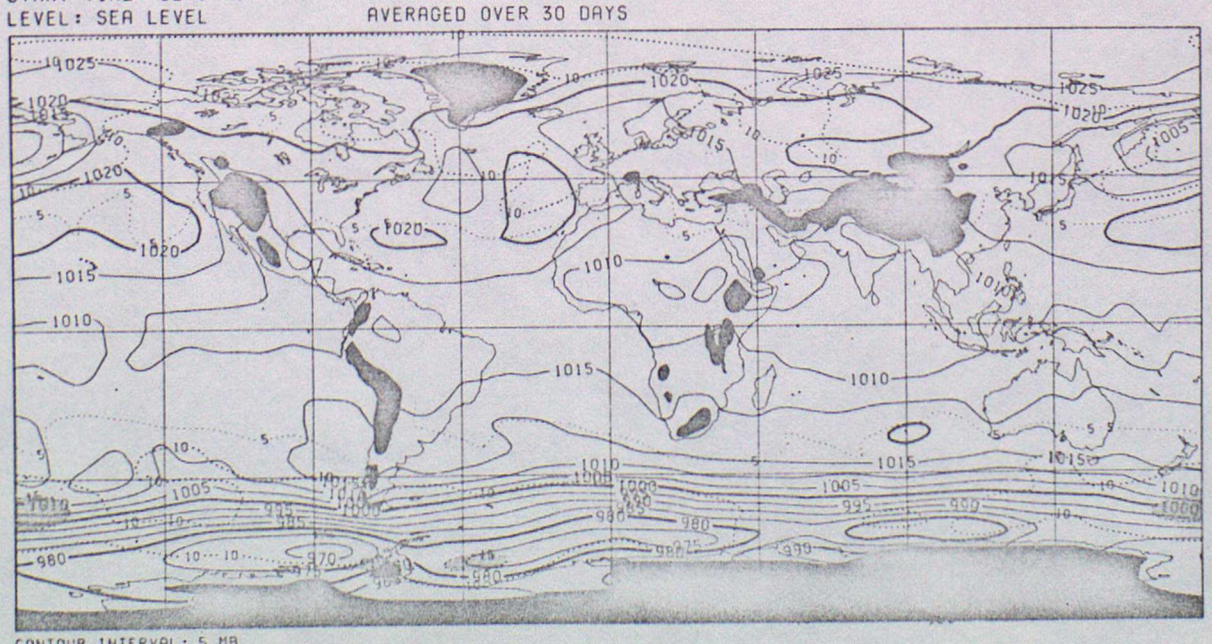

CONTOUR INTERVAL: 5 MB

Figure 11

ECMWF FGGE IIIB ANALYSES. TIME-MEAN & S.D. (MAY 1979)
HEIGHT: MEAN (THICKER AT 320AM INTERVALS) & SD (DOTTED, WITH SHADING >150AM)
START TIME: 0Z ON 1/5/79 MODEL TIME: DAY 121 HR 0
LEVEL: 500 MB AVERAGED OVER 31 DAYS

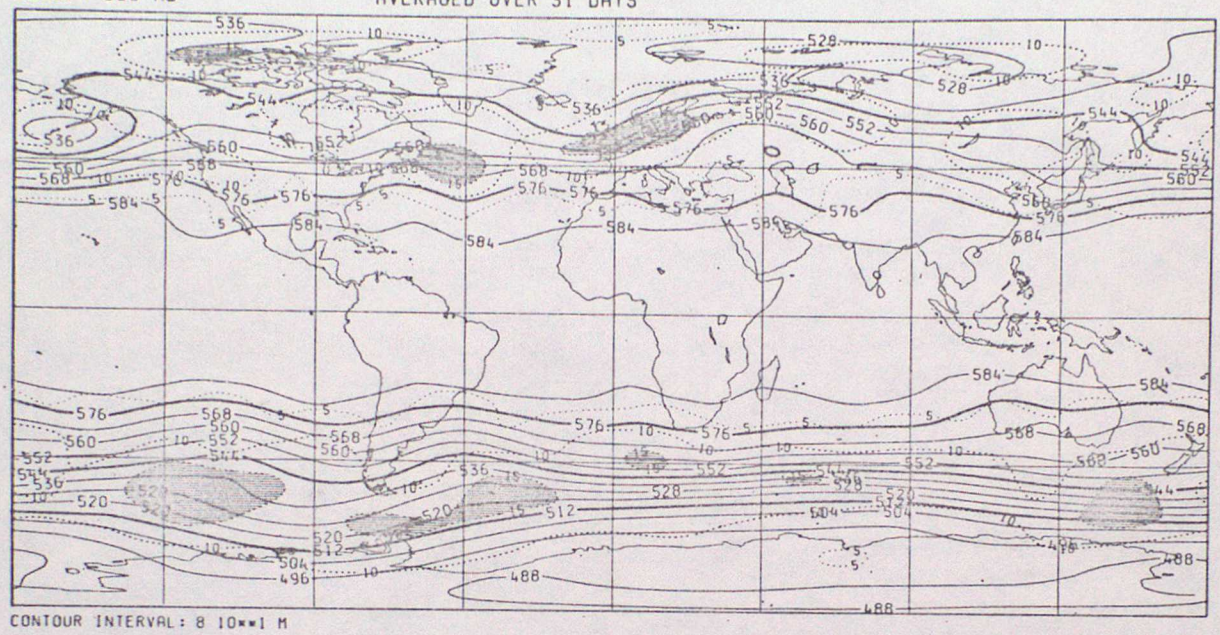

CONTOUR INTERVAL: 8 10**1 M

ECMWF FGGE IIIB ANALYSES. TIME-MEAN & S.D. (MAY 1979)
PMSL: MEAN (980,1000,1020MB THICKER) & SD (DOTTED, WITH SHADING >15MB)
START TIME: 0Z ON 1/5/79 MODEL TIME: DAY 121 HR 0
LEVEL: SEA LEVEL AVERAGED OVER 31 DAYS

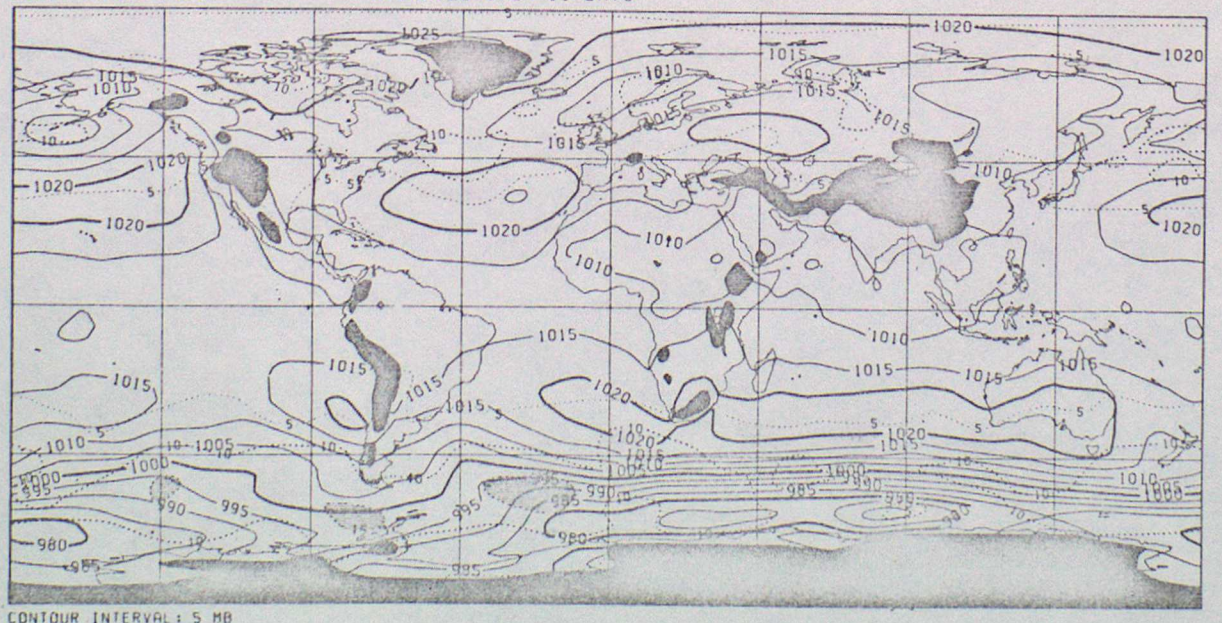

CONTOUR INTERVAL: 5 MB

Figure 12

ECMWF FGGE IIIB ANALYSES. TIME-MEAN & S.D. (JUNE 1979)
HEIGHT: MEAN (THICKER AT 320AM INTERVALS) & SD (DOTTED. WITH SHADING >150AM)
START TIME: 0Z ON 1/6/79 MODEL TIME: DAY 152 HR 0
LEVEL: 500 MB AVERAGED OVER 30 DAYS

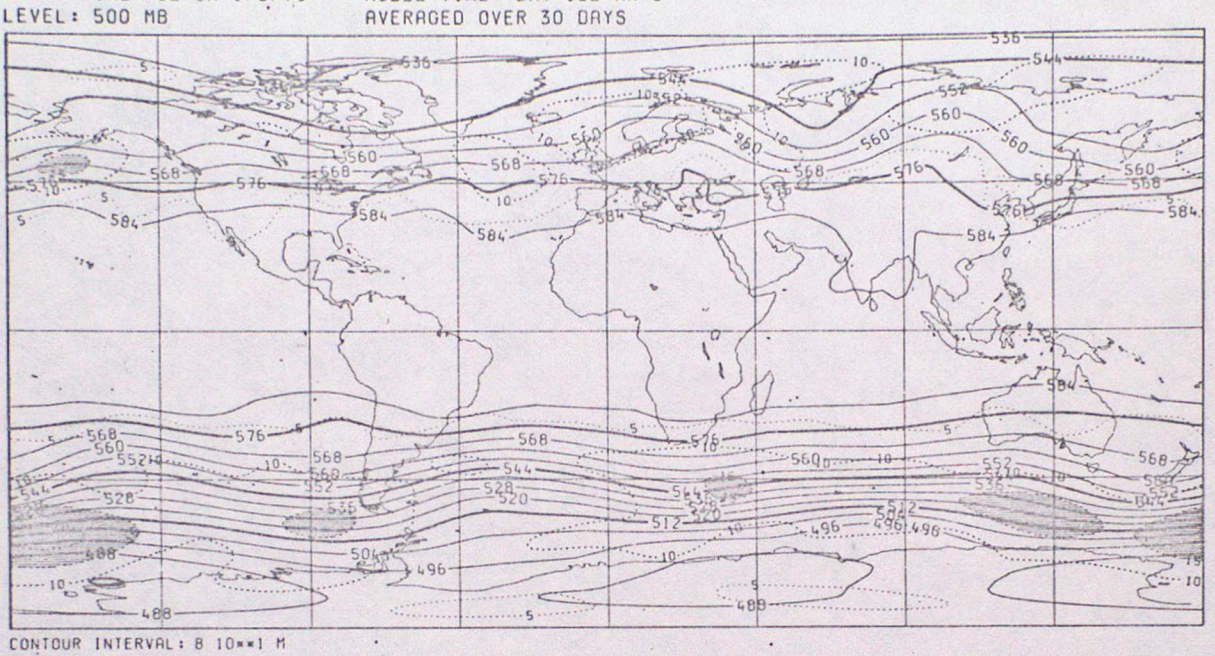

CONTOUR INTERVAL: 8 10**1 M

ECMWF FGGE IIIB ANALYSES. TIME-MEAN & S.D. (JUNE 1979)
PMSL: MEAN (980.1000.1020MB THICKER) & SD (DOTTED. WITH SHADING >15MB)
START TIME: 0Z ON 1/6/79 MODEL TIME: DAY 152 HR 0
LEVEL: SEA LEVEL AVERAGED OVER 30 DAYS

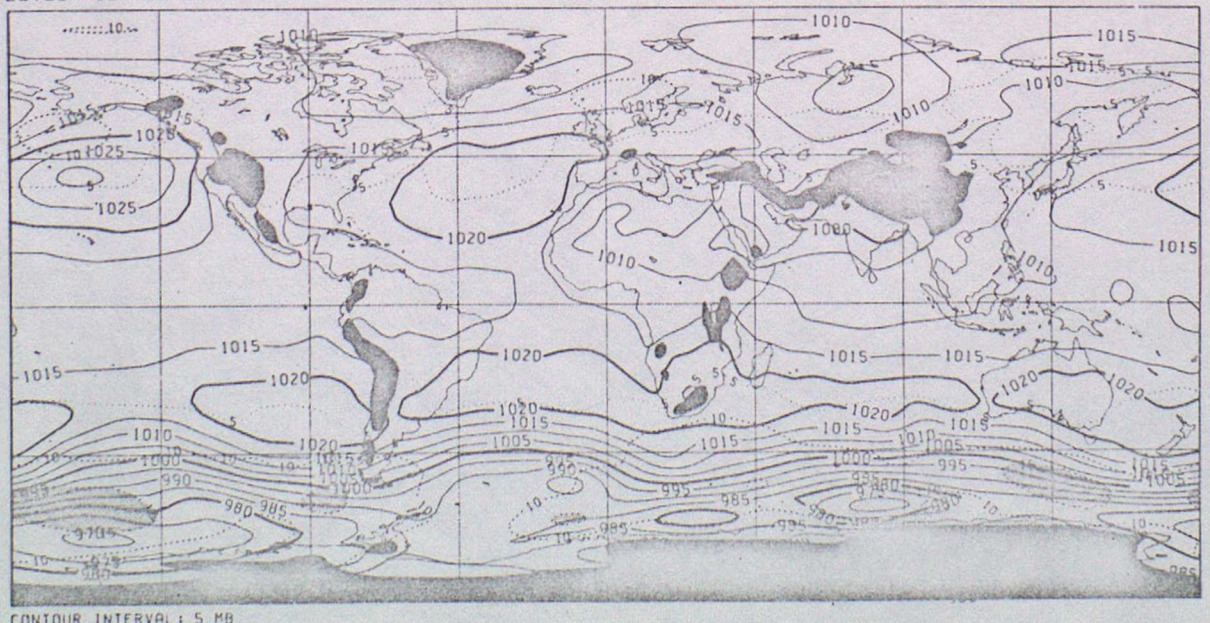

CONTOUR INTERVAL: 5 MB

Figure 13

ECMWF FGGE IIIB ANALYSES. TIME-MEAN & S.D. (JULY 1979)
HEIGHT: MEAN (THICKER AT 320AM INTERVALS) & SD (DOTTED. WITH SHADING >150AM)
START TIME: 0Z ON 1/7/79 MODEL TIME: DAY 182 HR 0
LEVEL: 500 MB AVERAGED OVER 31 DAYS

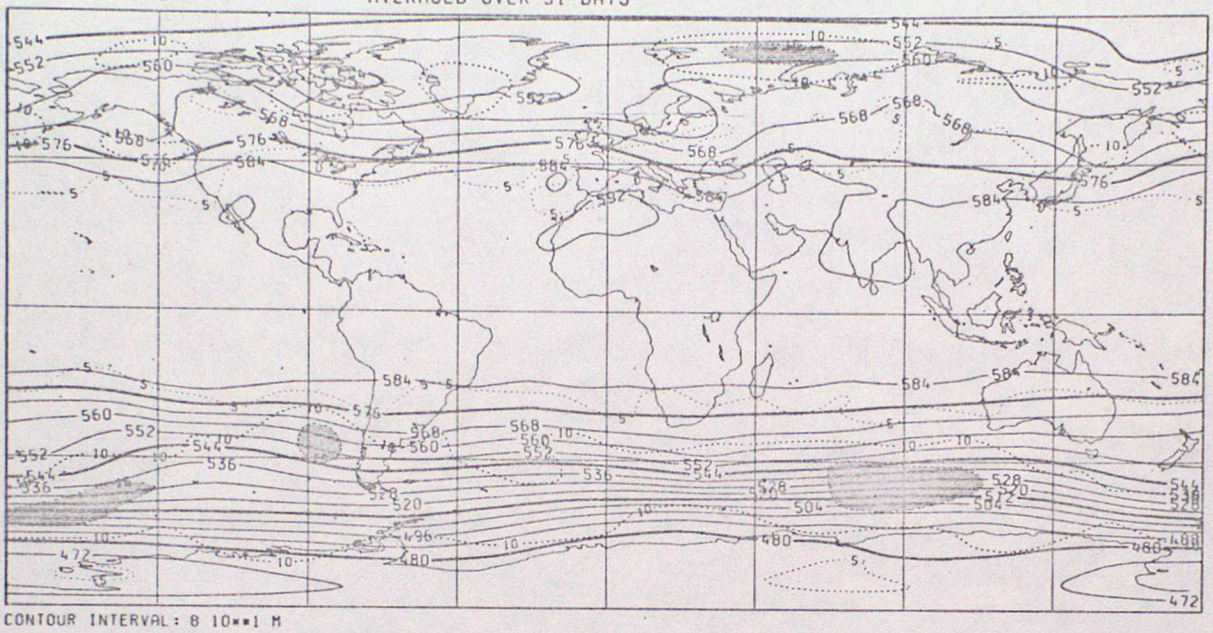

CONTOUR INTERVAL: 8 10**1 M

ECMWF FGGE IIIB ANALYSES. TIME-MEAN & S.D. (JULY 1979)
PMSL: MEAN (980.1000.1020MB THICKER) & SD (DOTTED. WITH SHADING >15MB)
START TIME: 0Z ON 1/7/79 MODEL TIME: DAY 182 HR 0
LEVEL: SEA LEVEL AVERAGED OVER 31 DAYS

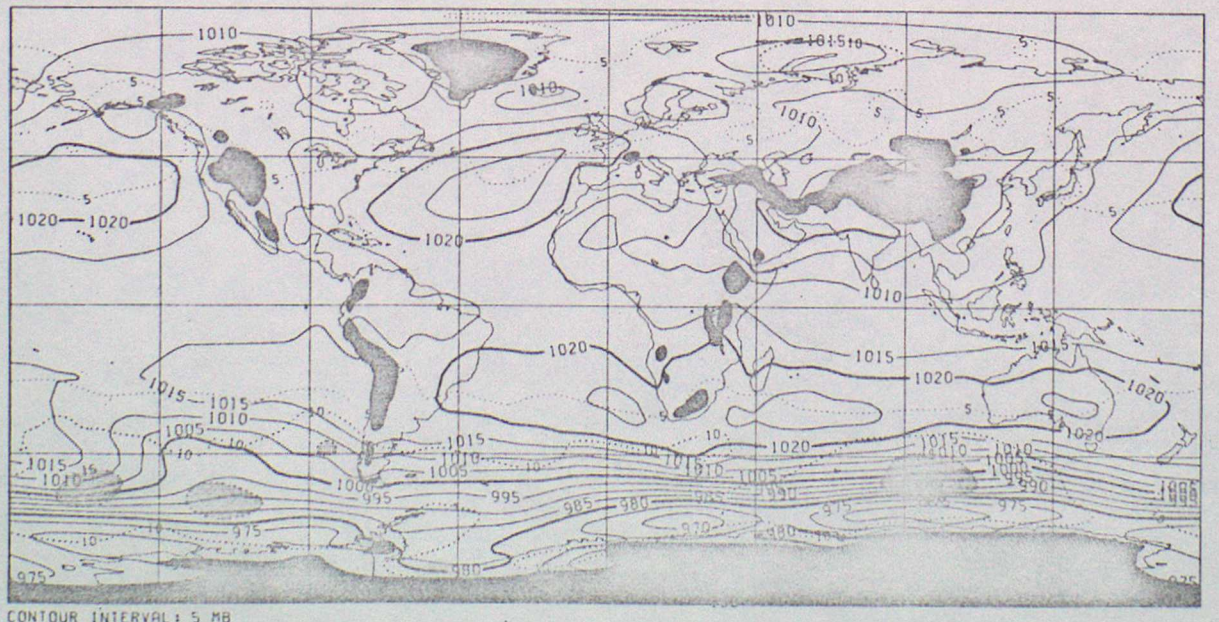

CONTOUR INTERVAL: 5 MB

Figure 14

ECMWF FGGE IIIB ANALYSES. TIME-MEAN & S.D. (AUGUST 1979)
HEIGHT: MEAN (THICKER AT 32DAM INTERVALS) & SD (DOTTED, WITH SHADING >15DAM)
START TIME: 0Z ON 1/8/79 MODEL TIME: DAY 213 HR 0
LEVEL: 500 MB AVERAGED OVER 31 DAYS

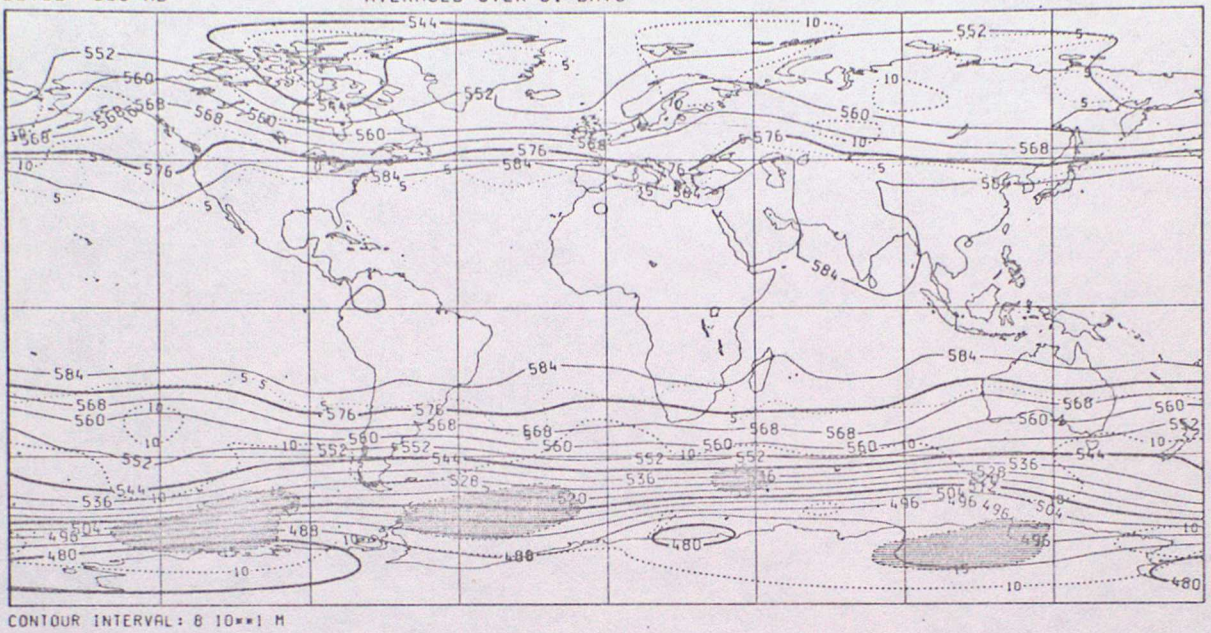

CONTOUR INTERVAL: 8 10**1 M

ECMWF FGGE IIIB ANALYSES. TIME-MEAN & S.D. (AUGUST 1979)
PMSL: MEAN (980.1000.1020MB THICKER) & SD (DOTTED, WITH SHADING >15MB)
START TIME: 0Z ON 1/8/79 MODEL TIME: DAY 213 HR 0
LEVEL: SEA LEVEL AVERAGED OVER 31 DAYS

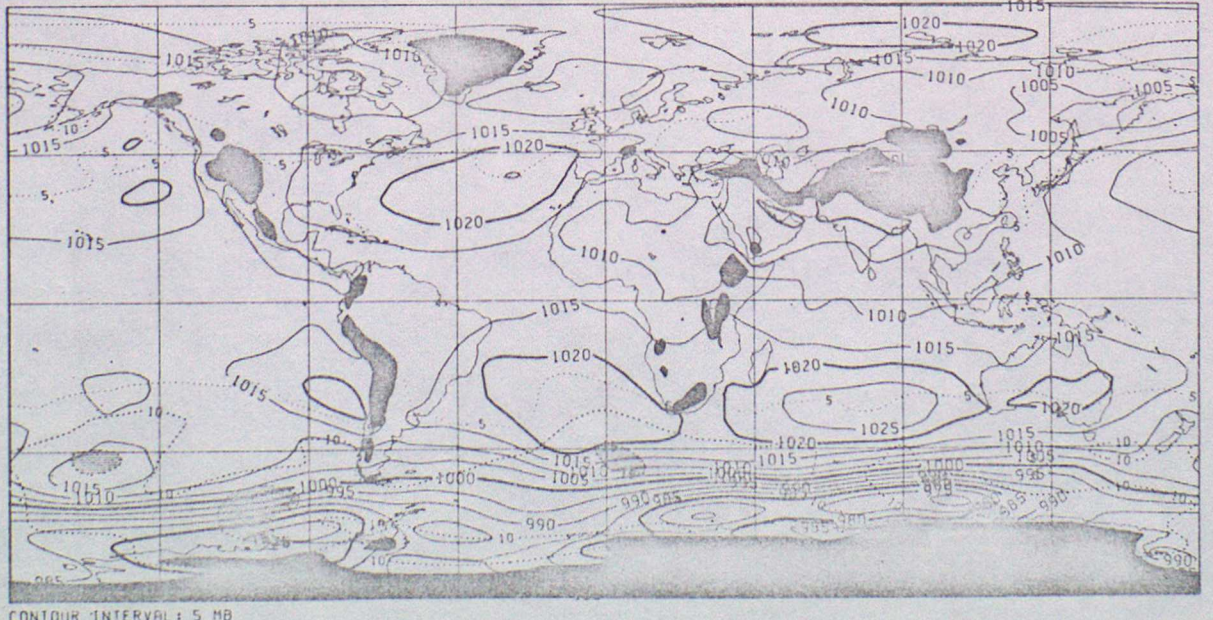

CONTOUR INTERVAL: 5 MB

Figure 15

ECMWF FGGE IIIB ANALYSES. TIME-MEAN & S.D. (SEPTEMBER 1979)
HEIGHT: MEAN (THICKER AT 320AM INTERVALS) & SD (DOTTED, WITH SHADING >150AM)
START TIME: 0Z ON 1/9/79 MODEL TIME: DAY 244 HR 0
LEVEL: 500 MB AVERAGED OVER 30 DAYS

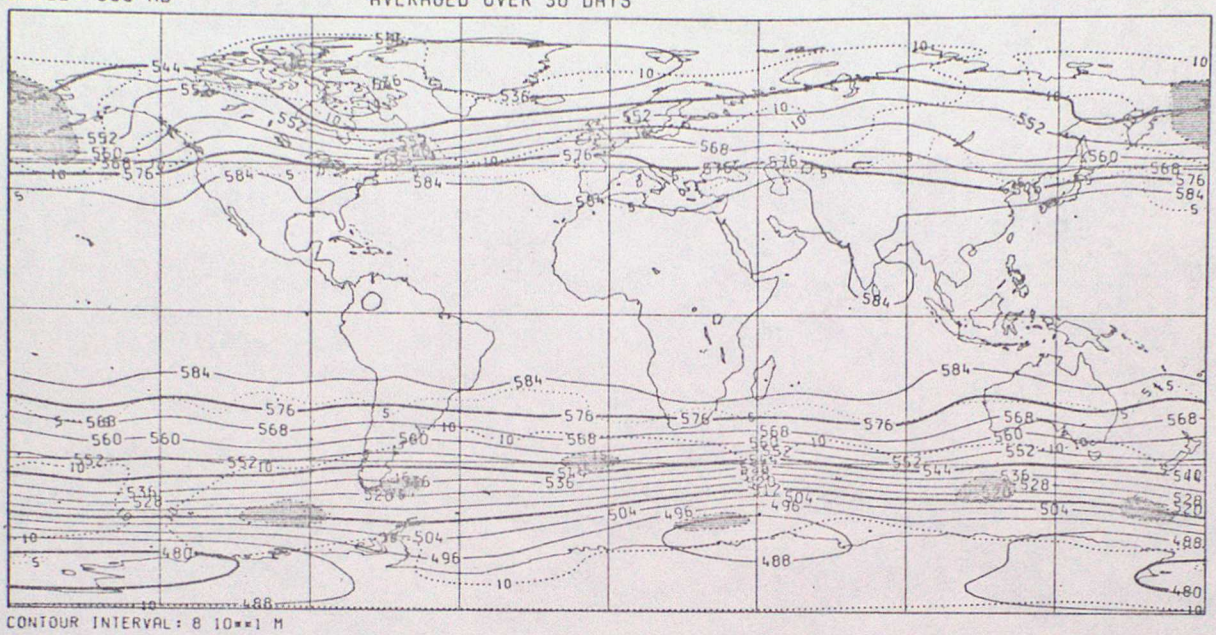

CONTOUR INTERVAL: 8 10=1 M

ECMWF FGGE IIIB ANALYSES. TIME-MEAN & S.D. (SEPTEMBER 1979)
PMSL: MEAN (980,1000,1020MB THICKER) & SD (DOTTED, WITH SHADING >15MB)
START TIME: 0Z ON 1/9/79 MODEL TIME: DAY 244 HR 0
LEVEL: SEA LEVEL AVERAGED OVER 30 DAYS

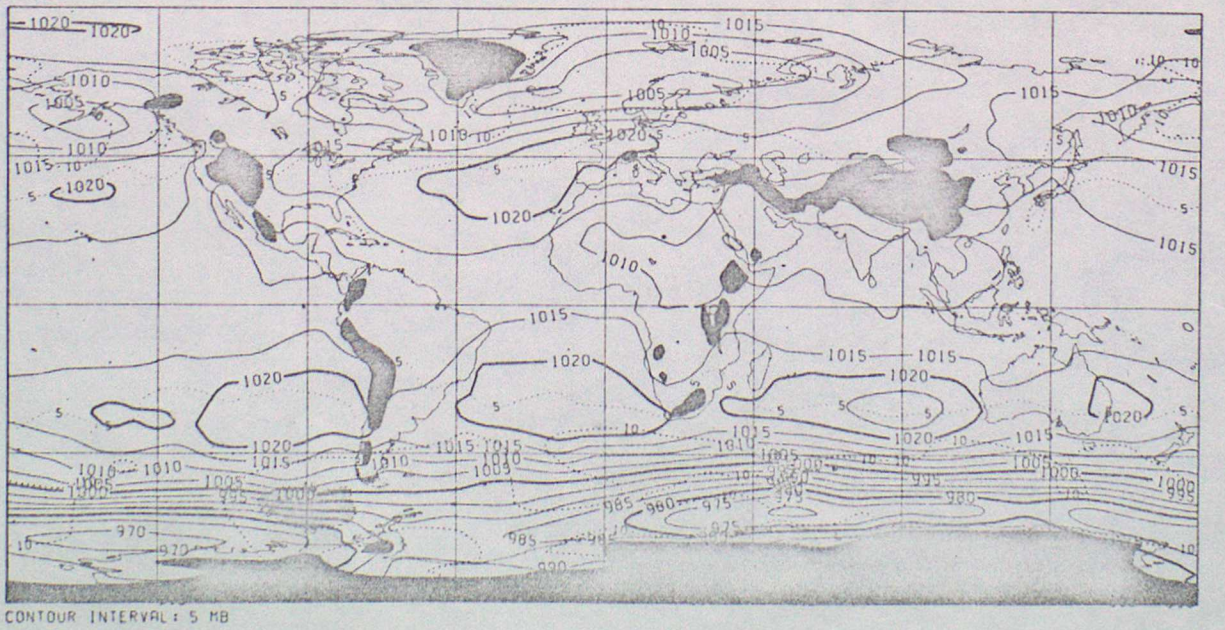

CONTOUR INTERVAL: 5 MB

Figure 16

ECMWF FGGE IIIB ANALYSES. TIME-MEAN & S.D. (OCTOBER 1979)
HEIGHT: MEAN (THICKER AT 32DAM INTERVALS) & SD (DOTTED, WITH SHADING >15DAM)
START TIME: 0Z ON 1/10/79 MODEL TIME: DAY 274 HR 0
LEVEL: 500 MB AVERAGED OVER 31 DAYS

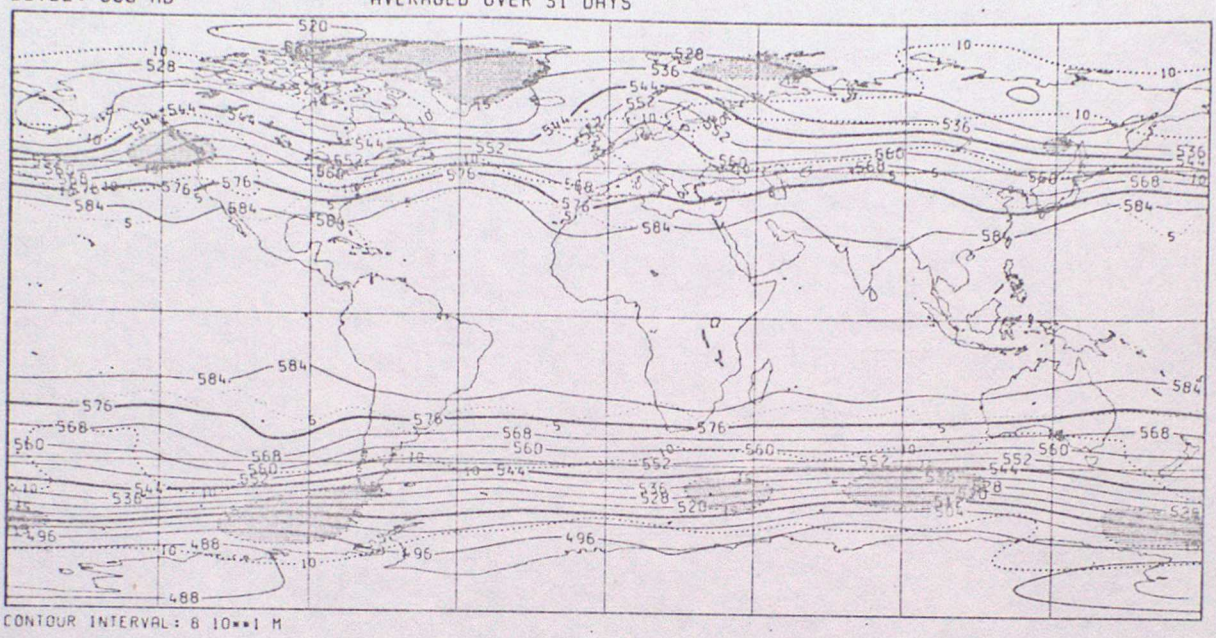

CONTOUR INTERVAL: 8 10**1 M

ECMWF FGGE IIIB ANALYSES. TIME-MEAN & S.D. (OCTOBER 1979)
PMSL: MEAN (980,1000,1020MB THICKER) & SD (DOTTED, WITH SHADING >15MB)
START TIME: 0Z ON 1/10/79 MODEL TIME: DAY 274 HR 0
LEVEL: SEA LEVEL AVERAGED OVER 31 DAYS

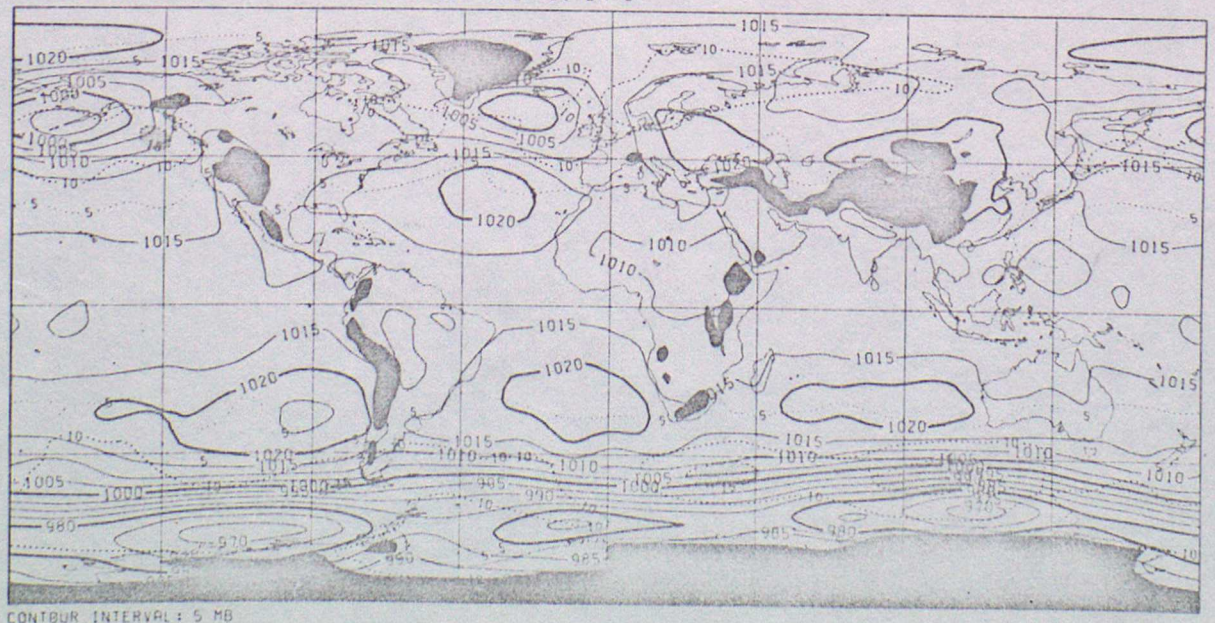

CONTOUR INTERVAL: 5 MB

Figure 17

ECMWF FGGE IIIB ANALYSES. TIME-MEAN & S.D. (NOVEMBER 1979)
HEIGHT: MEAN (THICKER AT 320AM INTERVALS) & SD (DOTTED. WITH SHADING >150AM)
START TIME: 0Z ON 1/11/79 MODEL TIME: DAY 305 HR 0
LEVEL: 500 MB AVERAGED OVER 30 DAYS

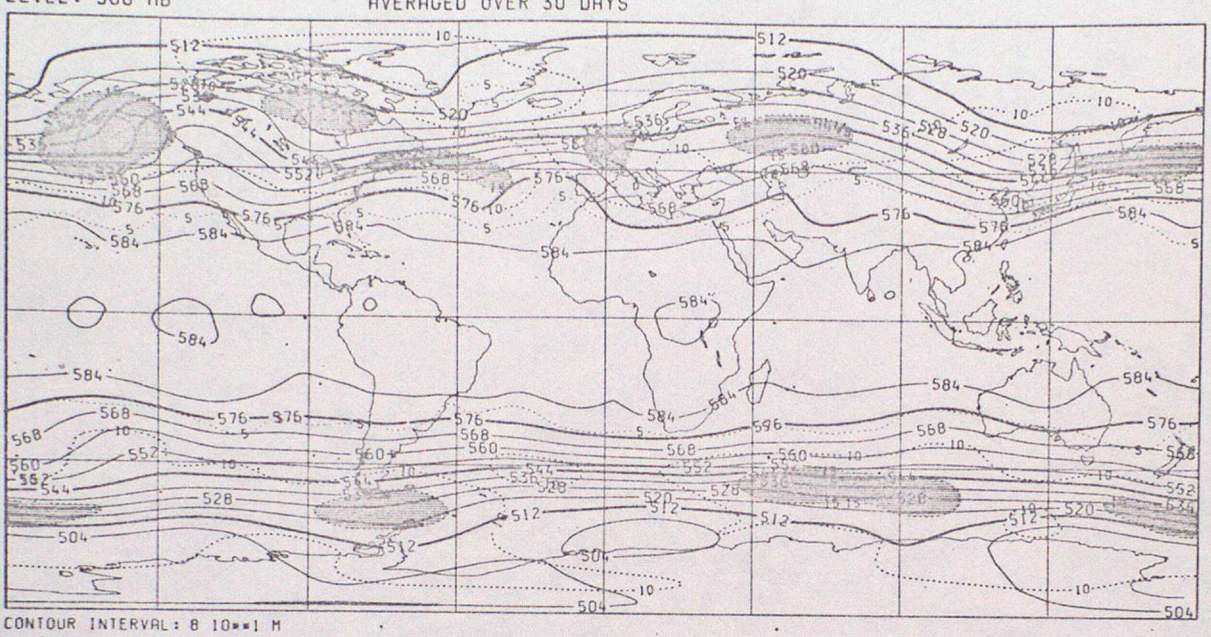

CONTOUR INTERVAL: 8 10=1 M

ECMWF FGGE IIIB ANALYSES. TIME-MEAN & S.D. (NOVEMBER 1979)
PMSL: MEAN (980,1000,1020MB THICKER) & SD (DOTTED. WITH SHADING >15MB)
START TIME: 0Z ON 1/11/79 MODEL TIME: DAY 305 HR 0
LEVEL: SEA LEVEL AVERAGED OVER 30 DAYS

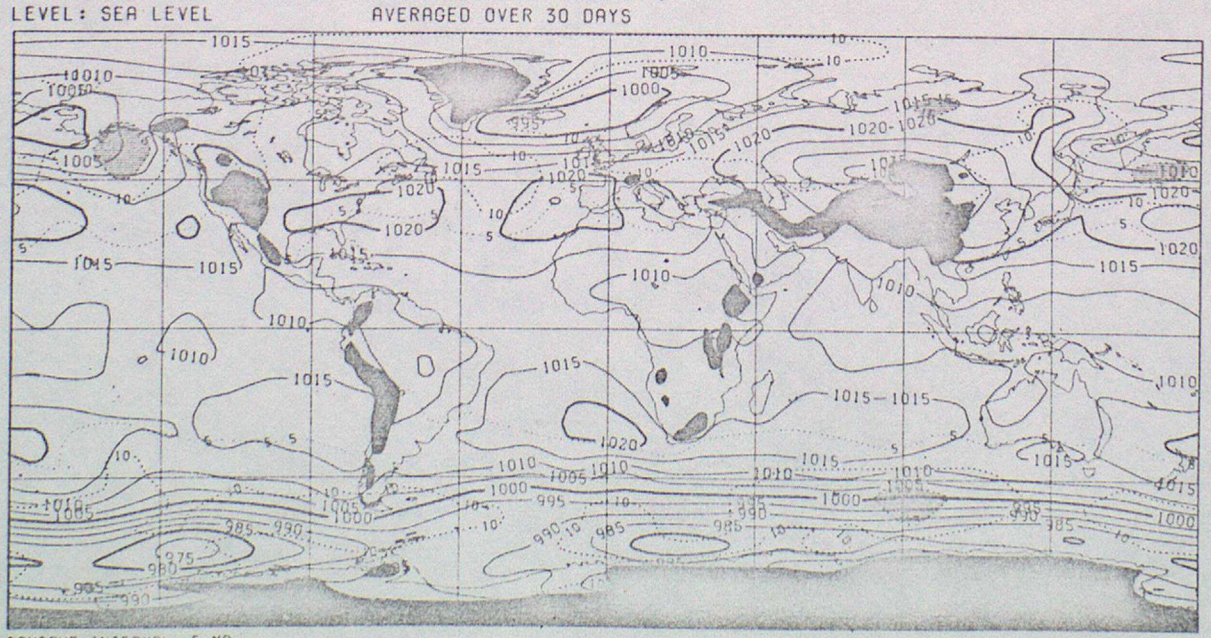

CONTOUR INTERVAL: 5 MB

Figure 18

ECMWF FGGE IIIB ANALYSIS MONTHLY MEAN WIND (DECEMBER 1978).
STREAMFUNCTION + DIVERGENT WIND ARROWS + TOTAL ISOTACHS (DOTS & SHADING).
START TIME: 0Z ON 1/12/78 MODEL TIME: DAY 335 HR 0
LEVEL: 200 MB AVERAGED OVER 31 DAYS

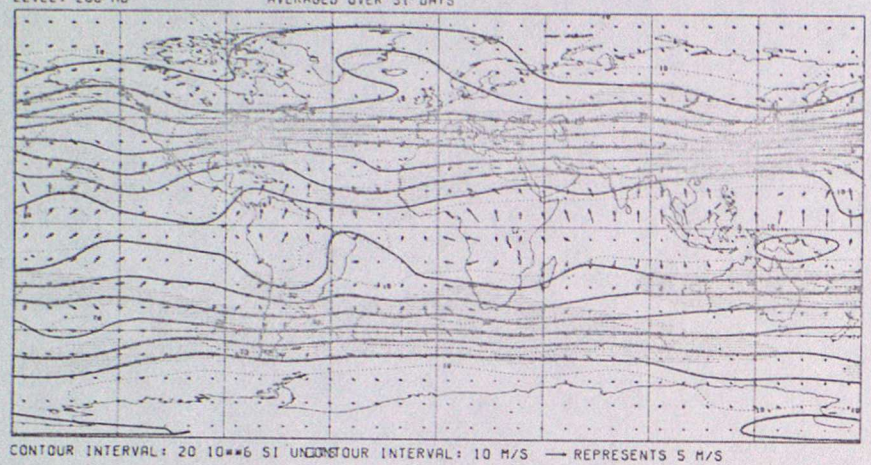

CONTOUR INTERVAL: 20 10**6 SI UNITS CONTOUR INTERVAL: 10 M/S ⟶ REPRESENTS 5 M/S

ECMWF FGGE IIIB ANALYSIS MONTHLY MEAN WIND (JUNE 1979).
STREAMFUNCTION + DIVERGENT WIND ARROWS + TOTAL ISOTACHS (DOTS & SHADING).
START TIME: 0Z ON 1/6/79 MODEL TIME: DAY 152 HR 0
LEVEL: 200 MB AVERAGED OVER 30 DAYS

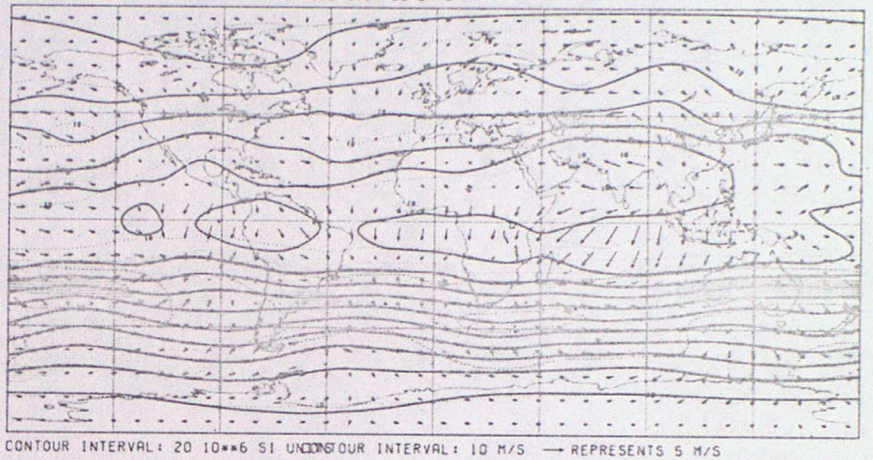

CONTOUR INTERVAL: 20 10**6 SI UNITS CONTOUR INTERVAL: 10 M/S ⟶ REPRESENTS 5 M/S

ECMWF FGGE IIIB ANALYSIS MONTHLY MEAN WIND (DECEMBER 1978).
STREAMFUNCTION + DIVERGENT WIND ARROWS + TOTAL ISOTACHS (DOTS & SHADING).
START TIME: 0Z ON 1/12/78 MODEL TIME: DAY 335 HR 0
LEVEL: 850 MB AVERAGED OVER 31 DAYS

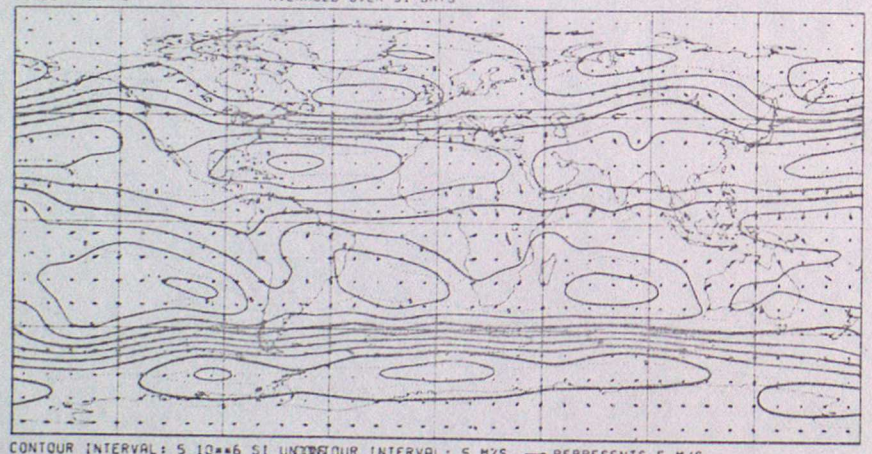

CONTOUR INTERVAL: 5 10**6 SI UNITS CONTOUR INTERVAL: 5 M/S ⟶ REPRESENTS 5 M/S

ECMWF FGGE IIIB ANALYSIS MONTHLY MEAN WIND (JUNE 1979).
STREAMFUNCTION + DIVERGENT WIND ARROWS + TOTAL ISOTACHS (DOTS & SHADING).
START TIME: 0Z ON 1/6/79 MODEL TIME: DAY 152 HR 0
LEVEL: 850 MB AVERAGED OVER 30 DAYS

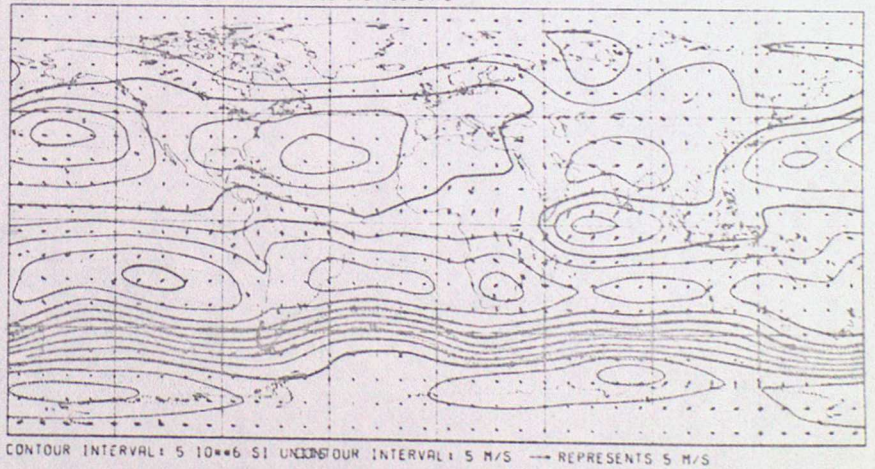

CONTOUR INTERVAL: 5 10**6 SI UNITS CONTOUR INTERVAL: 5 M/S ⟶ REPRESENTS 5 M/S

Figure 19

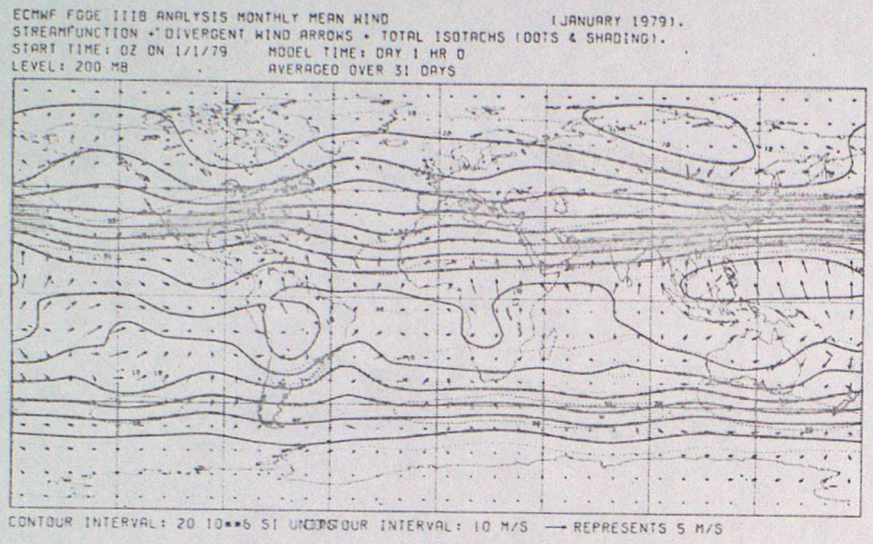
ECMWF FGGE IIIB ANALYSIS MONTHLY MEAN WIND (JANUARY 1979).
STREAMFUNCTION + DIVERGENT WIND ARROWS + TOTAL ISOTACHS (DOTS & SHADING).
START TIME: 0Z ON 1/1/79 MODEL TIME: DAY 1 HR 0
LEVEL: 200 MB AVERAGED OVER 31 DAYS
CONTOUR INTERVAL: 20 10**6 SI UNITS CONTOUR INTERVAL: 10 M/S — REPRESENTS 5 M/S

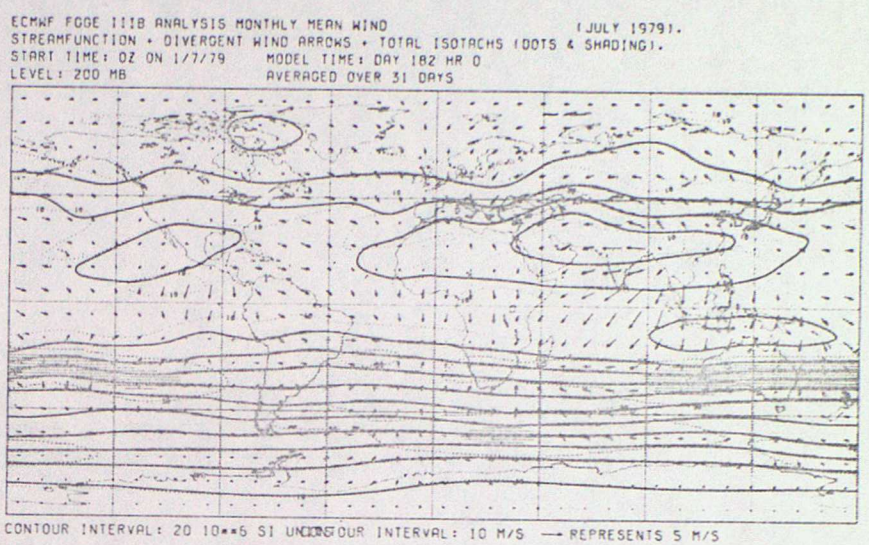
ECMWF FGGE IIIB ANALYSIS MONTHLY MEAN WIND (JULY 1979).
STREAMFUNCTION + DIVERGENT WIND ARROWS + TOTAL ISOTACHS (DOTS & SHADING).
START TIME: 0Z ON 1/7/79 MODEL TIME: DAY 182 HR 0
LEVEL: 200 MB AVERAGED OVER 31 DAYS
CONTOUR INTERVAL: 20 10**6 SI UNITS CONTOUR INTERVAL: 10 M/S — REPRESENTS 5 M/S

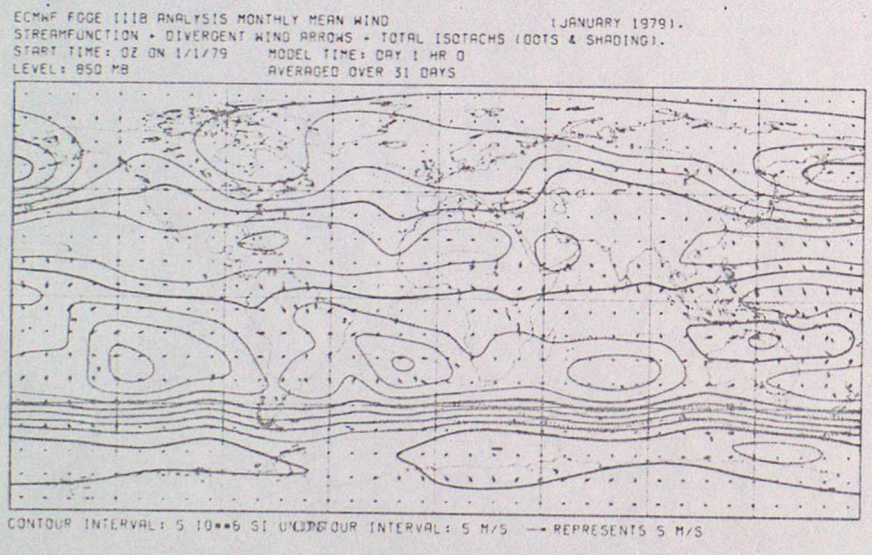
ECMWF FGGE IIIB ANALYSIS MONTHLY MEAN WIND (JANUARY 1979).
STREAMFUNCTION + DIVERGENT WIND ARROWS + TOTAL ISOTACHS (DOTS & SHADING).
START TIME: 0Z ON 1/1/79 MODEL TIME: DAY 1 HR 0
LEVEL: 850 MB AVERAGED OVER 31 DAYS
CONTOUR INTERVAL: 5 10**6 SI UNITS CONTOUR INTERVAL: 5 M/S — REPRESENTS 5 M/S

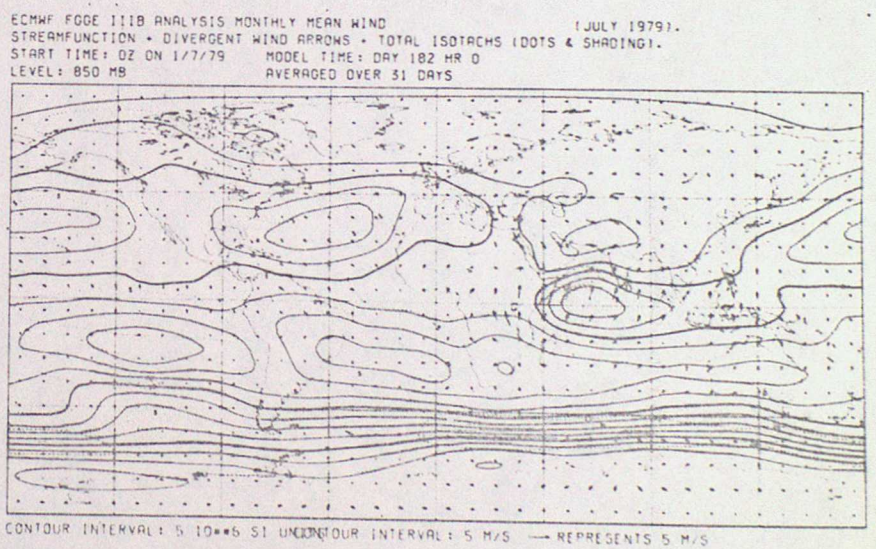
ECMWF FGGE IIIB ANALYSIS MONTHLY MEAN WIND (JULY 1979).
STREAMFUNCTION + DIVERGENT WIND ARROWS + TOTAL ISOTACHS (DOTS & SHADING).
START TIME: 0Z ON 1/7/79 MODEL TIME: DAY 182 HR 0
LEVEL: 850 MB AVERAGED OVER 31 DAYS
CONTOUR INTERVAL: 5 10**6 SI UNITS CONTOUR INTERVAL: 5 M/S — REPRESENTS 5 M/S

Figure 20

ECMWF FGGE IIIB ANALYSIS MONTHLY MEAN WIND (FEBRUARY 1979).
STREAMFUNCTION + DIVERGENT WIND ARROWS + TOTAL ISOTACHS (DOTS & SHADING).
START TIME: 0Z ON 1/2/79 MODEL TIME: DAY 32 HR 0
LEVEL: 200 MB AVERAGED OVER 28 DAYS

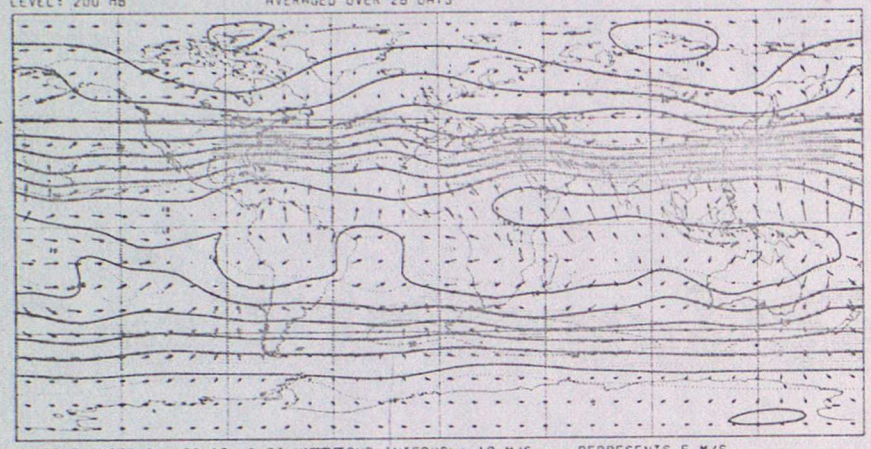

CONTOUR INTERVAL: 20 10**6 SI UNITS CONTOUR INTERVAL: 10 M/S ⟶ REPRESENTS 5 M/S

ECMWF FGGE IIIB ANALYSIS MONTHLY MEAN WIND (AUGUST 1979).
STREAMFUNCTION + DIVERGENT WIND ARROWS + TOTAL ISOTACHS (DOTS & SHADING).
START TIME: 0Z ON 1/8/79 MODEL TIME: DAY 213 HR 0
LEVEL: 200 MB AVERAGED OVER 31 DAYS

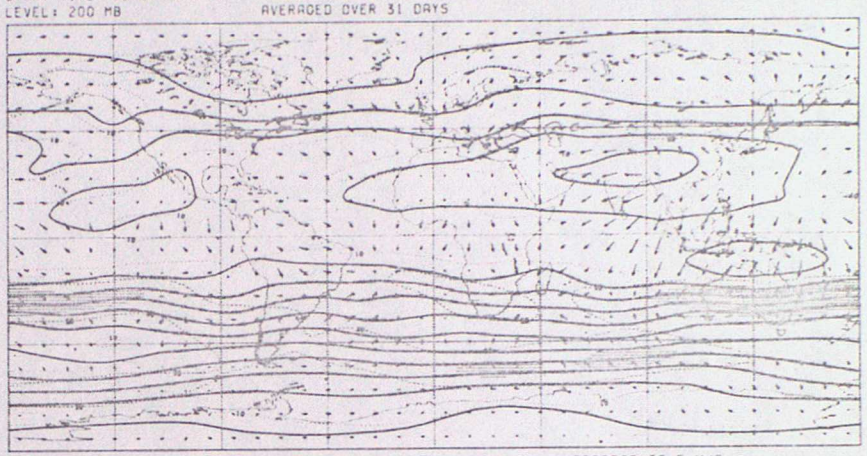

CONTOUR INTERVAL: 20 10**6 SI UNITS CONTOUR INTERVAL: 10 M/S ⟶ REPRESENTS 5 M/S

ECMWF FGGE IIIB ANALYSIS MONTHLY MEAN WIND (FEBRUARY 1979).
STREAMFUNCTION + DIVERGENT WIND ARROWS + TOTAL ISOTACHS (DOTS & SHADING).
START TIME: 0Z ON 1/2/79 MODEL TIME: DAY 32 HR 0
LEVEL: 850 MB AVERAGED OVER 28 DAYS

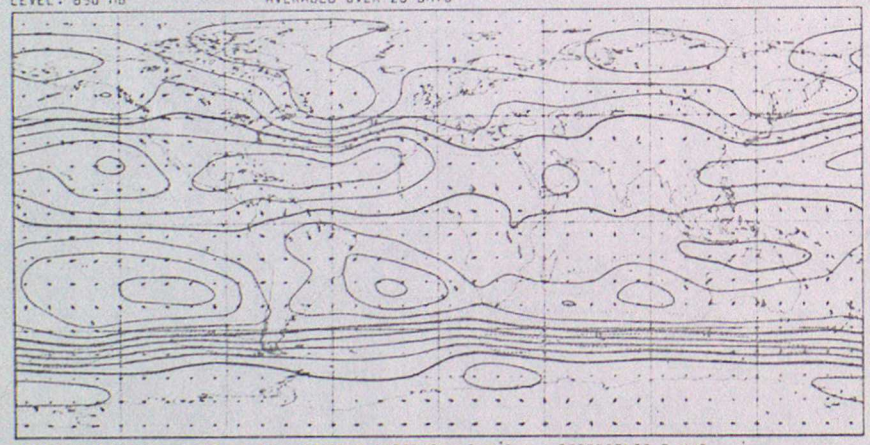

CONTOUR INTERVAL: 5 10**6 SI UNITS CONTOUR INTERVAL: 5 M/S ⟶ REPRESENTS 5 M/S

ECMWF FGGE IIIB ANALYSIS MONTHLY MEAN WIND (AUGUST 1979).
STREAMFUNCTION + DIVERGENT WIND ARROWS + TOTAL ISOTACHS (DOTS & SHADING).
START TIME: 0Z ON 1/8/79 MODEL TIME: DAY 213 HR 0
LEVEL: 850 MB AVERAGED OVER 31 DAYS

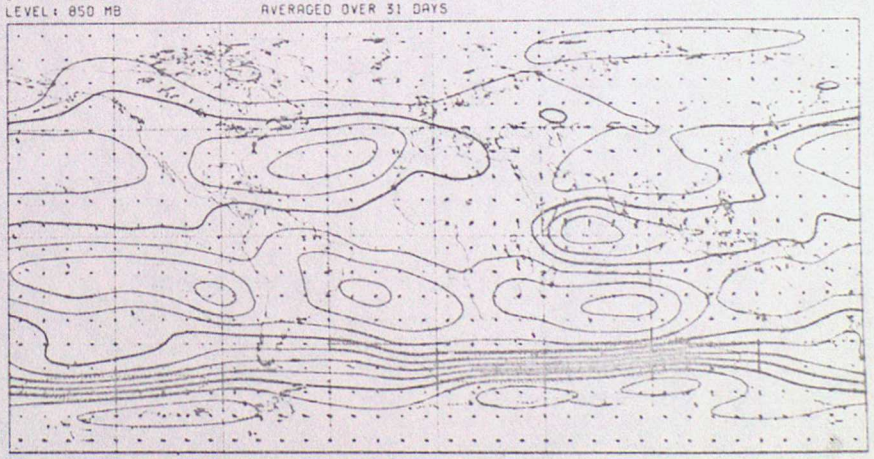

CONTOUR INTERVAL: 5 10**6 SI UNITS CONTOUR INTERVAL: 5 M/S ⟶ REPRESENTS 5 M/S

Figure 21

ECMWF FGGE IIIB ANALYSIS MONTHLY MEAN WIND (MARCH 1979).
STREAMFUNCTION + DIVERGENT WIND ARROWS + TOTAL ISOTACHS (DOTS & SHADING).
START TIME: 0Z ON 1/3/79 MODEL TIME: DAY 60 HR 0
LEVEL: 200 MB AVERAGED OVER 31 DAYS

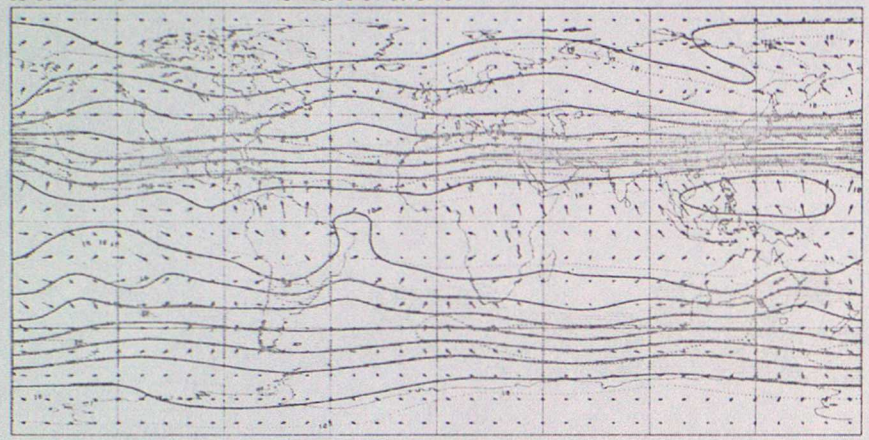

CONTOUR INTERVAL: 20 10**6 SI UNITS CONTOUR INTERVAL: 10 M/S — REPRESENTS 5 M/S

ECMWF FGGE IIIB ANALYSIS MONTHLY MEAN WIND (SEPTEMBER 1979).
STREAMFUNCTION + DIVERGENT WIND ARROWS + TOTAL ISOTACHS (DOTS & SHADING).
START TIME: 0Z ON 1/9/79 MODEL TIME: DAY 244 HR 0
LEVEL: 200 MB AVERAGED OVER 30 DAYS

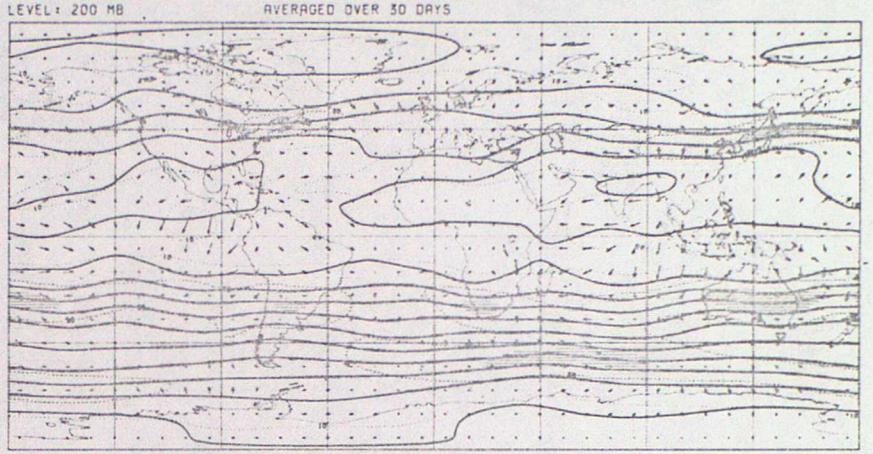

CONTOUR INTERVAL: 20 10**6 SI UNITS CONTOUR INTERVAL: 10 M/S — REPRESENTS 5 M/S

ECMWF FGGE IIIB ANALYSIS MONTHLY MEAN WIND (MARCH 1979).
STREAMFUNCTION + DIVERGENT WIND ARROWS + TOTAL ISOTACHS (DOTS & SHADING).
START TIME: 0Z ON 1/3/79 MODEL TIME: DAY 60 HR 0
LEVEL: 850 MB AVERAGED OVER 31 DAYS

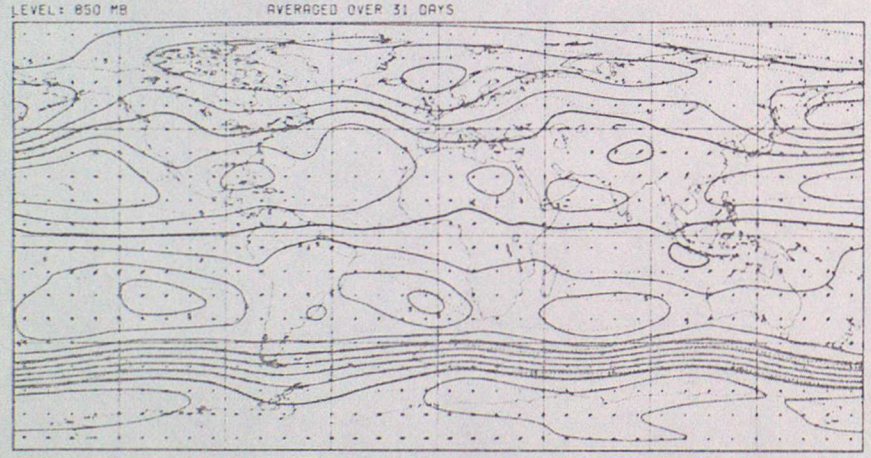

CONTOUR INTERVAL: 5 10**6 SI UNITS CONTOUR INTERVAL: 5 M/S — REPRESENTS 5 M/S

ECMWF FGGE IIIB ANALYSIS MONTHLY MEAN WIND (SEPTEMBER 1979).
STREAMFUNCTION + DIVERGENT WIND ARROWS + TOTAL ISOTACHS (DOTS & SHADING).
START TIME: 0Z ON 1/9/79 MODEL TIME: DAY 244 HR 0
LEVEL: 850 MB AVERAGED OVER 30 DAYS

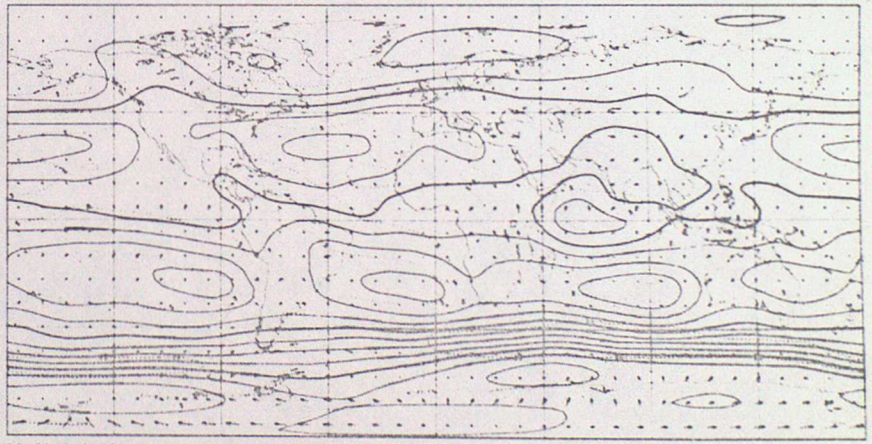

CONTOUR INTERVAL: 5 10**6 SI UNITS CONTOUR INTERVAL: 5 M/S — REPRESENTS 5 M/S

Figure 22

ECMWF FGGE IIIB ANALYSIS MONTHLY MEAN WIND (APRIL 1979).
STREAMFUNCTION + DIVERGENT WIND ARROWS + TOTAL ISOTACHS (DOTS & SHADING).
START TIME: 0Z ON 1/4/79 MODEL TIME: DAY 91 HR 0
LEVEL: 200 MB AVERAGED OVER 30 DAYS

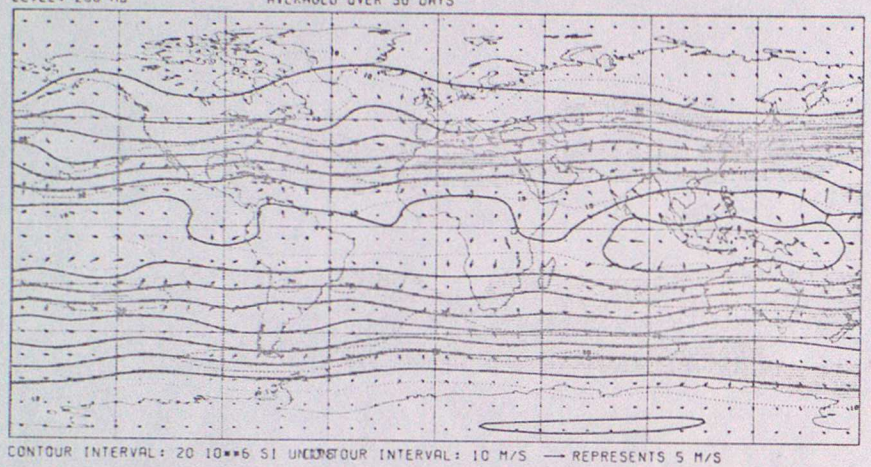

CONTOUR INTERVAL: 20 10**6 SI UNITS CONTOUR INTERVAL: 10 M/S —→ REPRESENTS 5 M/S

ECMWF FGGE IIIB ANALYSIS MONTHLY MEAN WIND (OCTOBER 1979).
STREAMFUNCTION + DIVERGENT WIND ARROWS + TOTAL ISOTACHS (DOTS & SHADING).
START TIME: 0Z ON 1/10/79 MODEL TIME: DAY 274 HR 0
LEVEL: 200 MB AVERAGED OVER 31 DAYS

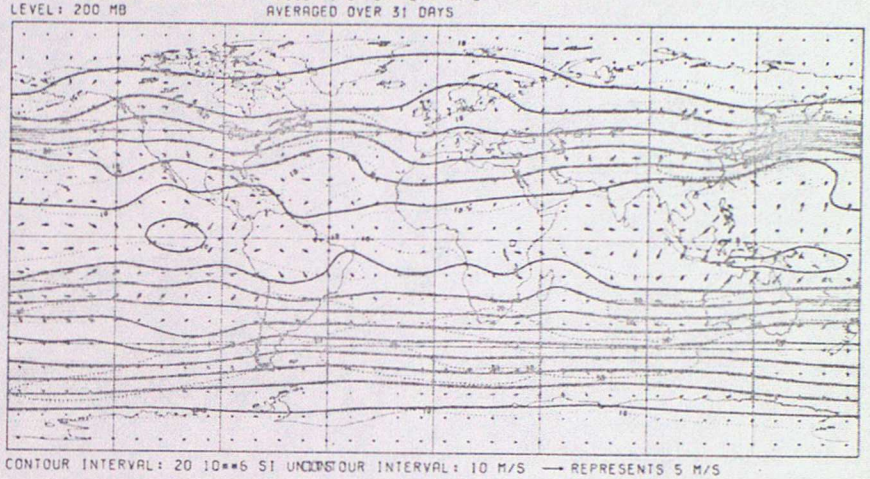

CONTOUR INTERVAL: 20 10**6 SI UNITS CONTOUR INTERVAL: 10 M/S —→ REPRESENTS 5 M/S

ECMWF FGGE IIIB ANALYSIS MONTHLY MEAN WIND (APRIL 1979).
STREAMFUNCTION + DIVERGENT WIND ARROWS + TOTAL ISOTACHS (DOTS & SHADING).
START TIME: 0Z ON 1/4/79 MODEL TIME: DAY 91 HR 0
LEVEL: 850 MB AVERAGED OVER 30 DAYS

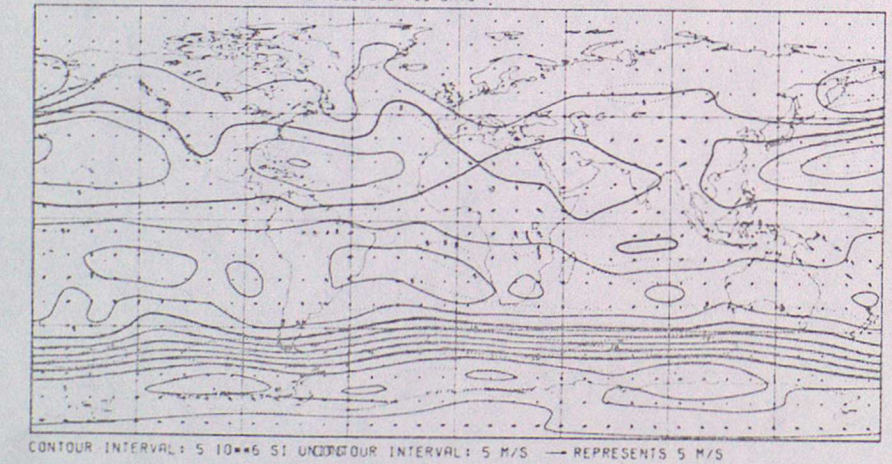

CONTOUR INTERVAL: 5 10**6 SI UNITS CONTOUR INTERVAL: 5 M/S —→ REPRESENTS 5 M/S

ECMWF FGGE IIIB ANALYSIS MONTHLY MEAN WIND (OCTOBER 1979).
STREAMFUNCTION + DIVERGENT WIND ARROWS + TOTAL ISOTACHS (DOTS & SHADING).
START TIME: 0Z ON 1/10/79 MODEL TIME: DAY 274 HR 0
LEVEL: 850 MB AVERAGED OVER 31 DAYS

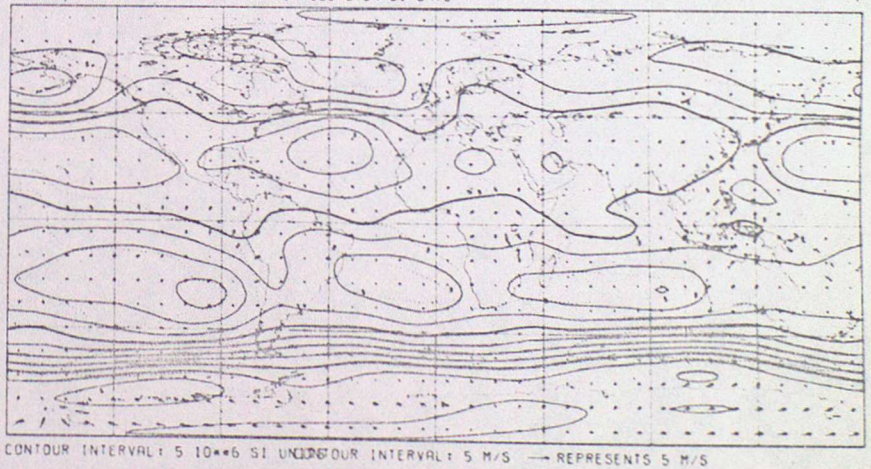

CONTOUR INTERVAL: 5 10**6 SI UNITS CONTOUR INTERVAL: 5 M/S —→ REPRESENTS 5 M/S

Figure 23

ECMWF FGGE IIIB ANALYSIS MONTHLY MEAN WIND (MAY 1979).
STREAMFUNCTION + DIVERGENT WIND ARROWS + TOTAL ISOTACHS (DOTS & SHADING).
START TIME: 0Z ON 1/5/79 MODEL TIME: DAY 121 HR 0
LEVEL: 200 MB AVERAGED OVER 31 DAYS

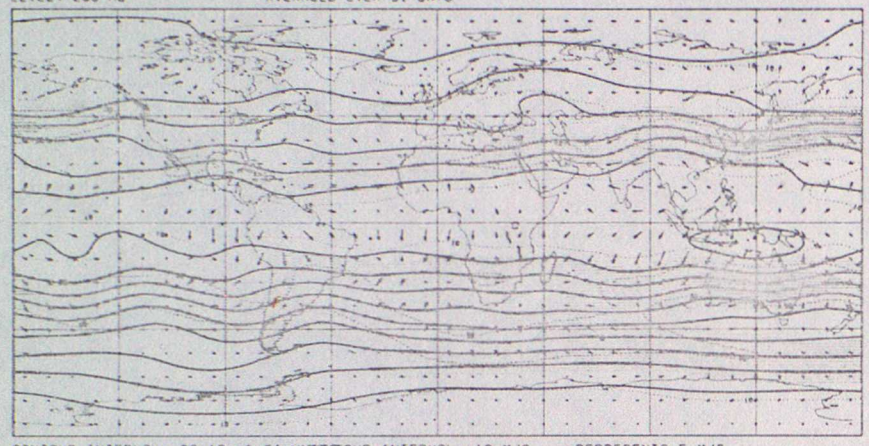

CONTOUR INTERVAL: 20 10**6 SI UNITS CONTOUR INTERVAL: 10 M/S —→ REPRESENTS 5 M/S

ECMWF FGGE IIIB ANALYSIS MONTHLY MEAN WIND (NOVEMBER 1979).
STREAMFUNCTION + DIVERGENT WIND ARROWS + TOTAL ISOTACHS (DOTS & SHADING).
START TIME: 0Z ON 1/11/79 MODEL TIME: DAY 305 HR 0
LEVEL: 200 MB AVERAGED OVER 30 DAYS

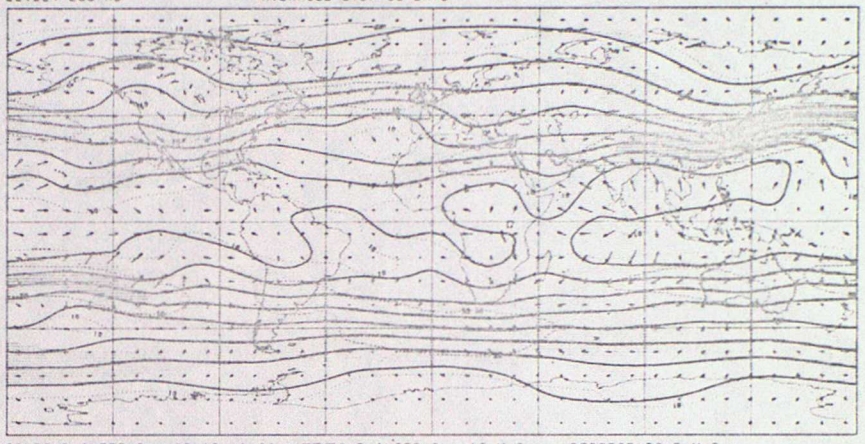

CONTOUR INTERVAL: 20 10**6 SI UNITS CONTOUR INTERVAL: 10 M/S —→ REPRESENTS 5 M/S

ECMWF FGGE IIIB ANALYSIS MONTHLY MEAN WIND (MAY 1979).
STREAMFUNCTION + DIVERGENT WIND ARROWS + TOTAL ISOTACHS (DOTS & SHADING).
START TIME: 0Z ON 1/5/79 MODEL TIME: DAY 121 HR 0
LEVEL: 850 MB AVERAGED OVER 31 DAYS

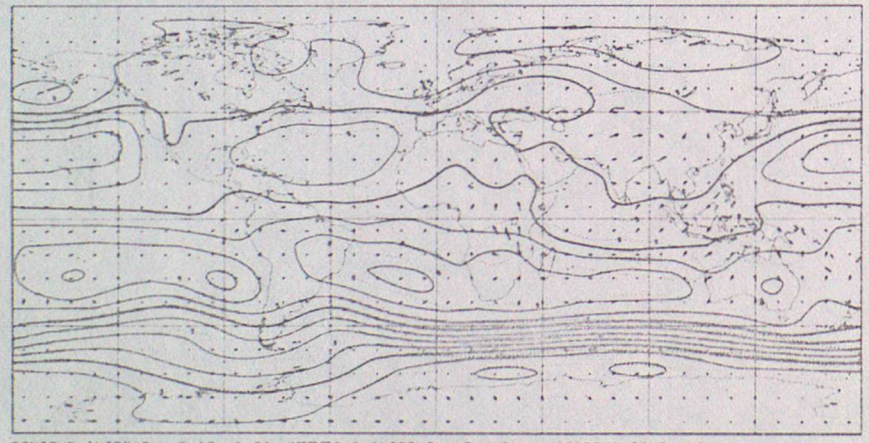

CONTOUR INTERVAL: 5 10**6 SI UNITS CONTOUR INTERVAL: 5 M/S —→ REPRESENTS 5 M/S

ECMWF FGGE IIIB ANALYSIS MONTHLY MEAN WIND (NOVEMBER 1979).
STREAMFUNCTION + DIVERGENT WIND ARROWS + TOTAL ISOTACHS (DOTS & SHADING).
START TIME: 0Z ON 1/11/79 MODEL TIME: DAY 305 HR 0
LEVEL: 850 MB AVERAGED OVER 30 DAYS

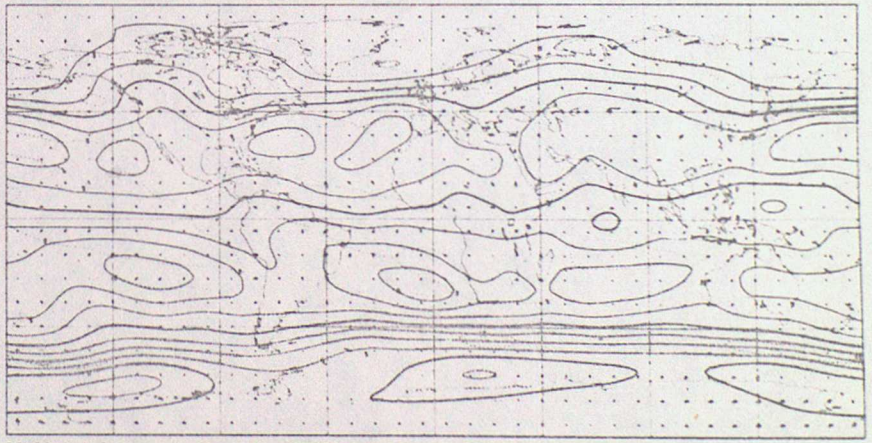

CONTOUR INTERVAL: 5 10**6 SI UNITS CONTOUR INTERVAL: 5 M/S —→ REPRESENTS 5 M/S

Figure 24

MET OFFICE FGGE IIIA ANALYSIS. SMOOTHED IN SPACE (T18) & TIME (24HRS).
STREAMFUNCTION + DIVERGENT WIND ARROWS + TOTAL ISOTACHS (>20M/S & >40M/S SHADED)
VALID AT 12Z ON 1/6/79 MODEL TIME: DAY 152 HR 12
LEVEL: 200 MB EXPERIMENT NO.: 3

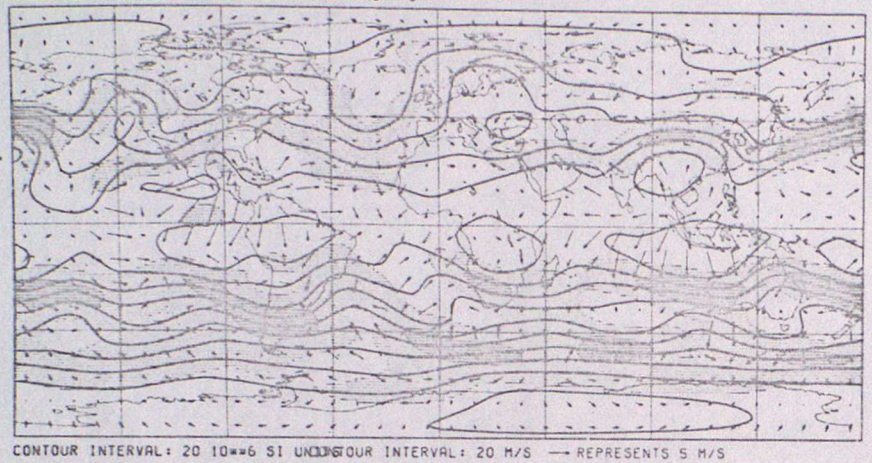

CONTOUR INTERVAL: 20 10**6 SI UNITS CONTOUR INTERVAL: 20 M/S → REPRESENTS 5 M/S

MET OFFICE FGGE IIIA ANALYSIS. SMOOTHED IN SPACE (T18) & TIME (24HRS).
STREAMFUNCTION + DIVERGENT WIND ARROWS + TOTAL ISOTACHS (>20M/S & >40M/S SHADED)
VALID AT 12Z ON 2/6/79 MODEL TIME: DAY 153 HR 12
LEVEL: 200 MB EXPERIMENT NO.: 3

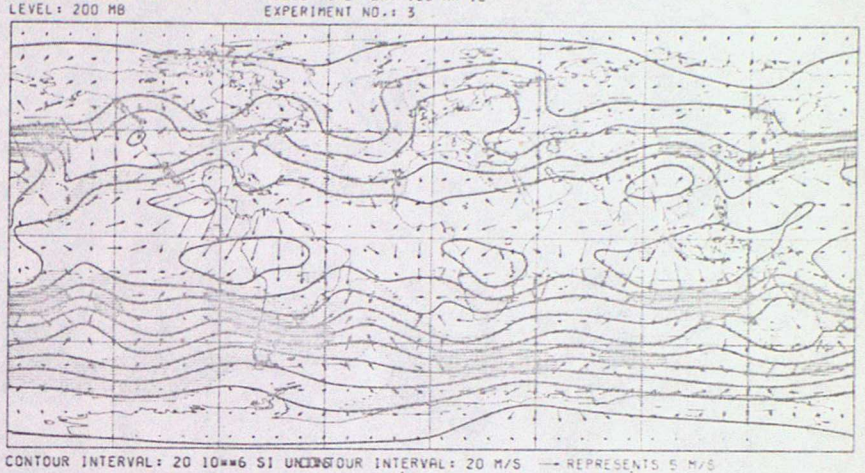

CONTOUR INTERVAL: 20 10**6 SI UNITS CONTOUR INTERVAL: 20 M/S → REPRESENTS 5 M/S

MET OFFICE FGGE IIIA ANALYSIS. SMOOTHED IN SPACE (T18) & TIME (24HRS).
STREAMFUNCTION + DIVERGENT WIND ARROWS + TOTAL ISOTACHS (>20M/S & >40M/S SHADED)
VALID AT 12Z ON 3/6/79 MODEL TIME: DAY 154 HR 12
LEVEL: 200 MB EXPERIMENT NO.: 3

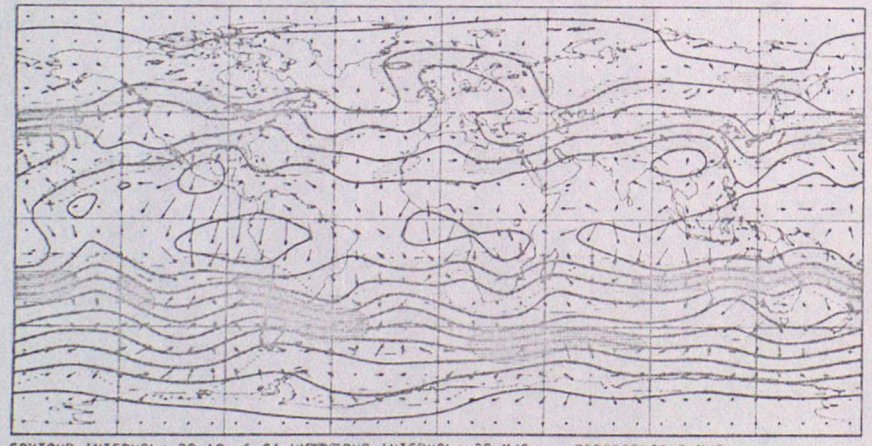

CONTOUR INTERVAL: 20 10**6 SI UNITS CONTOUR INTERVAL: 20 M/S → REPRESENTS 5 M/S

MET OFFICE FGGE IIIA ANALYSIS. SMOOTHED IN SPACE (T18) & TIME (24HRS).
STREAMFUNCTION + DIVERGENT WIND ARROWS + TOTAL ISOTACHS (>20M/S & >40M/S SHADED)
VALID AT 12Z ON 4/6/79 MODEL TIME: DAY 155 HR 12
LEVEL: 200 MB EXPERIMENT NO.: 3

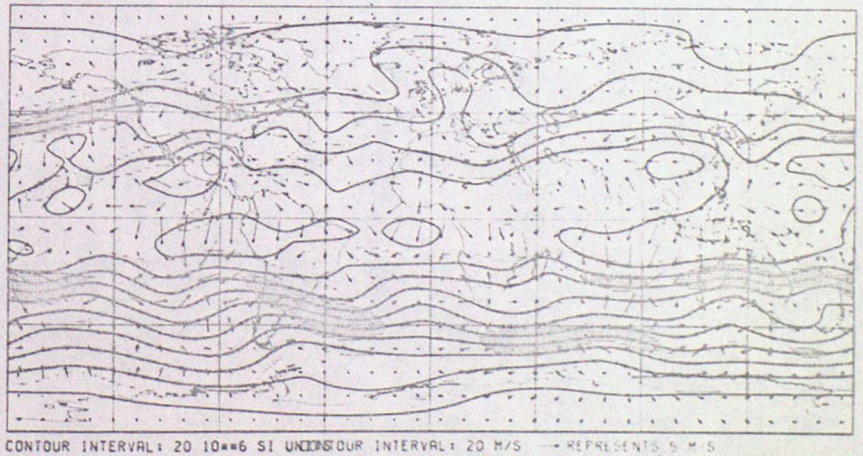

CONTOUR INTERVAL: 20 10**6 SI UNITS CONTOUR INTERVAL: 20 M/S → REPRESENTS 5 M/S

Figure 25

MET OFFICE FGGE IIIA ANALYSIS. SMOOTHED IN SPACE (T18) & TIME (24HRS).
STREAMFUNCTION + DIVERGENT WIND ARROWS + TOTAL ISOTACHS (>20M/S & >40M/S SHADED)
VALID AT 12Z ON 5/6/79 MODEL TIME: DAY 156 HR 12
LEVEL: 200 MB EXPERIMENT NO.: 3

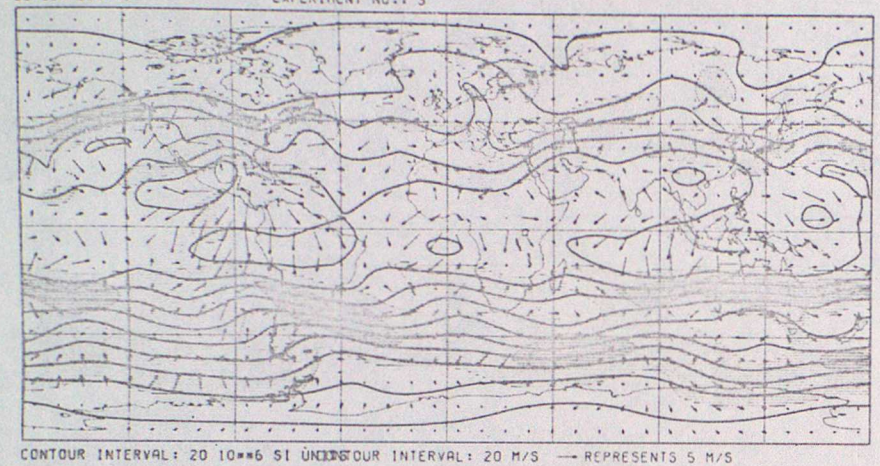

CONTOUR INTERVAL: 20 10**6 SI UNITS CONTOUR INTERVAL: 20 M/S —→ REPRESENTS 5 M/S

MET OFFICE FGGE IIIA ANALYSIS. SMOOTHED IN SPACE (T18) & TIME (24HRS).
STREAMFUNCTION + DIVERGENT WIND ARROWS + TOTAL ISOTACHS (>20M/S & >40M/S SHADED)
VALID AT 12Z ON 6/6/79 MODEL TIME: DAY 157 HR 12
LEVEL: 200 MB EXPERIMENT NO.: 3

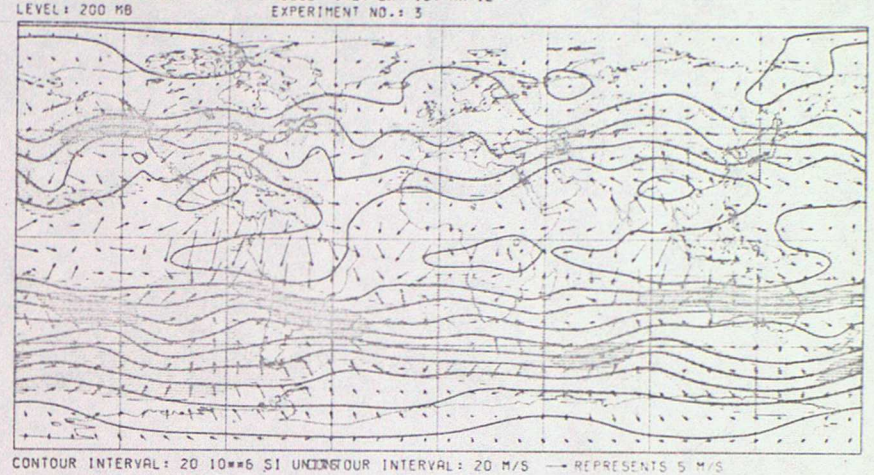

CONTOUR INTERVAL: 20 10**6 SI UNITS CONTOUR INTERVAL: 20 M/S —→ REPRESENTS 5 M/S

MET OFFICE FGGE IIIA ANALYSIS. SMOOTHED IN SPACE (T18) & TIME (24HRS).
STREAMFUNCTION + DIVERGENT WIND ARROWS + TOTAL ISOTACHS (>20M/S & >40M/S SHADED)
VALID AT 12Z ON 7/6/79 MODEL TIME: DAY 158 HR 12
LEVEL: 200 MB EXPERIMENT NO.: 3

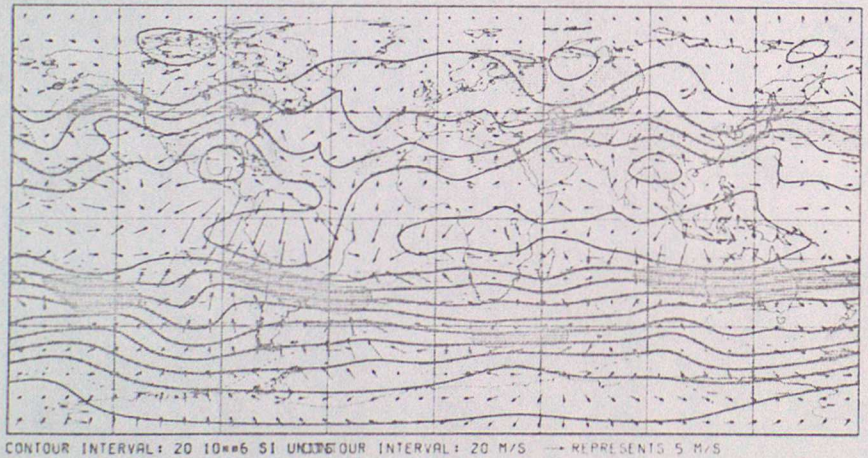

CONTOUR INTERVAL: 20 10**6 SI UNITS CONTOUR INTERVAL: 20 M/S —→ REPRESENTS 5 M/S

MET OFFICE FGGE IIIA ANALYSIS. SMOOTHED IN SPACE (T18) & TIME (24HRS).
STREAMFUNCTION + DIVERGENT WIND ARROWS + TOTAL ISOTACHS (>20M/S & >40M/S SHADED)
VALID AT 12Z ON 8/6/79 MODEL TIME: DAY 159 HR 12
LEVEL: 200 MB EXPERIMENT NO.: 3

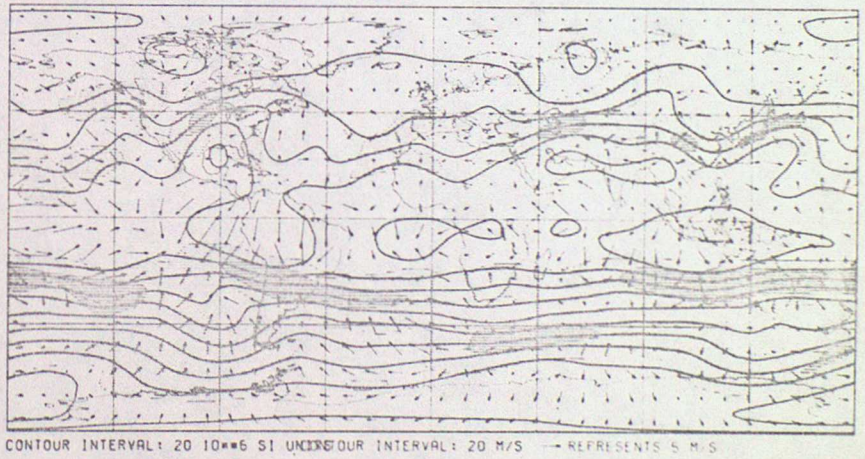

CONTOUR INTERVAL: 20 10**6 SI UNITS CONTOUR INTERVAL: 20 M/S —→ REPRESENTS 5 M/S

Figure 26

MET OFFICE FGGE IIIA ANALYSIS. SMOOTHED IN SPACE (T18) & TIME (24HRS).
STREAMFUNCTION + DIVERGENT WIND ARROWS + TOTAL ISOTACHS (>20M/S & >40M/S SHADED)
VALID AT 12Z ON 9/6/79 MODEL TIME: DAY 160 HR 12
LEVEL: 200 MB EXPERIMENT NO.: 3

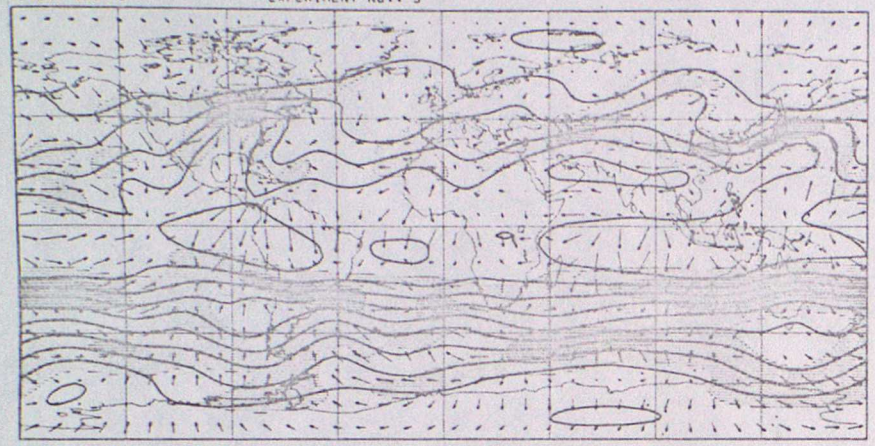

CONTOUR INTERVAL: 20 10**6 SI UNITS CONTOUR INTERVAL: 20 M/S → REPRESENTS 5 M/S

MET OFFICE FGGE IIIA ANALYSIS. SMOOTHED IN SPACE (T18) & TIME (24HRS).
STREAMFUNCTION + DIVERGENT WIND ARROWS + TOTAL ISOTACHS (>20M/S & >40M/S SHADED)
VALID AT 12Z ON 10/6/79 MODEL TIME: DAY 161 HR 12
LEVEL: 200 MB EXPERIMENT NO.: 3

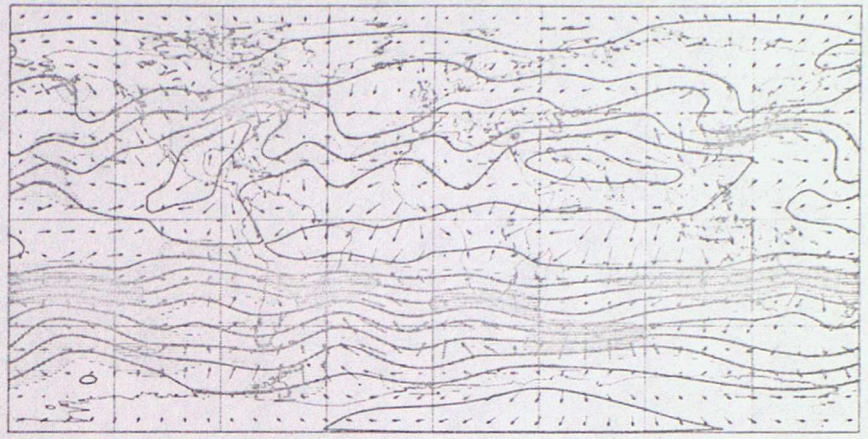

CONTOUR INTERVAL: 20 10**6 SI UNITS CONTOUR INTERVAL: 20 M/S → REPRESENTS 5 M/S

MET OFFICE FGGE IIIA ANALYSIS. SMOOTHED IN SPACE (T18) & TIME (24HRS).
STREAMFUNCTION + DIVERGENT WIND ARROWS + TOTAL ISOTACHS (>20M/S & >40M/S SHADED)
VALID AT 12Z ON 11/6/79 MODEL TIME: DAY 162 HR 12
LEVEL: 200 MB EXPERIMENT NO.: 3

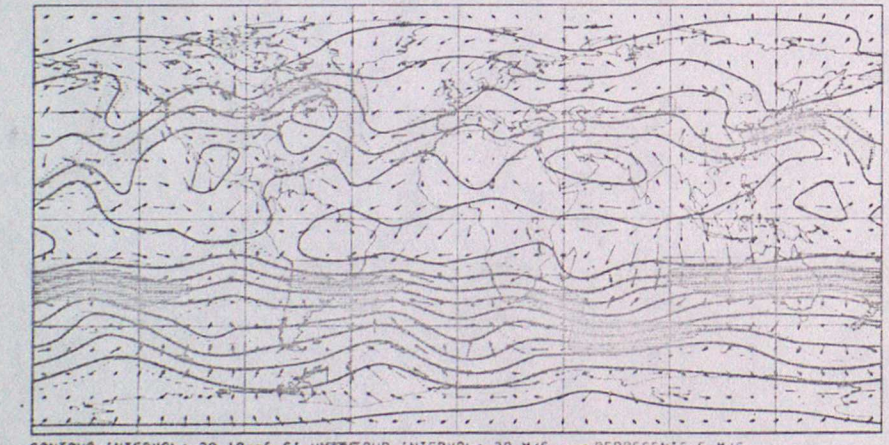

CONTOUR INTERVAL: 20 10**6 SI UNITS CONTOUR INTERVAL: 20 M/S → REPRESENTS 5 M/S

MET OFFICE FGGE IIIA ANALYSIS. SMOOTHED IN SPACE (T18) & TIME (24HRS).
STREAMFUNCTION + DIVERGENT WIND ARROWS + TOTAL ISOTACHS (>20M/S & >40M/S SHADED)
VALID AT 12Z ON 12/6/79 MODEL TIME: DAY 163 HR 12
LEVEL: 200 MB EXPERIMENT NO.: 3

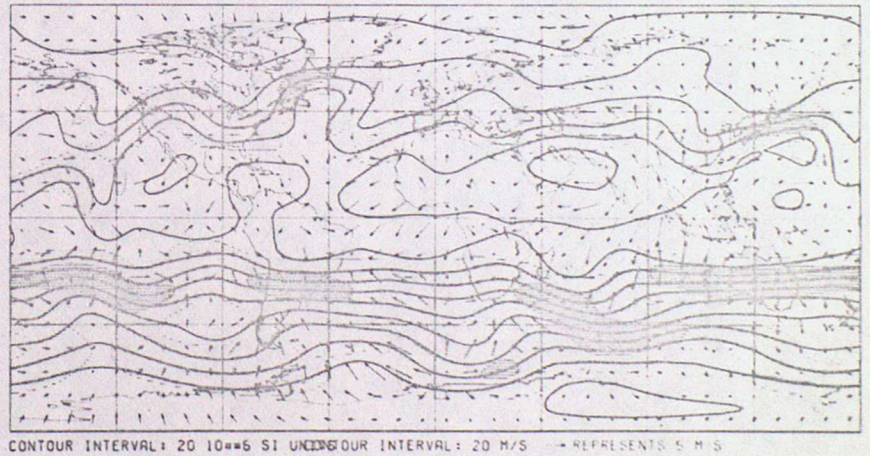

CONTOUR INTERVAL: 20 10**6 SI UNITS CONTOUR INTERVAL: 20 M/S → REPRESENTS 5 M/S

Figure 27

MET OFFICE FGGE IIIA ANALYSIS. SMOOTHED IN SPACE (T18) & TIME (24HRS).
STREAMFUNCTION + DIVERGENT WIND ARROWS + TOTAL ISOTACHS (>20M/S & >40M/S SHADED)
VALID AT 12Z ON 13/6/79 MODEL TIME: DAY 164 HR 12
LEVEL: 200 MB EXPERIMENT NO.: 3

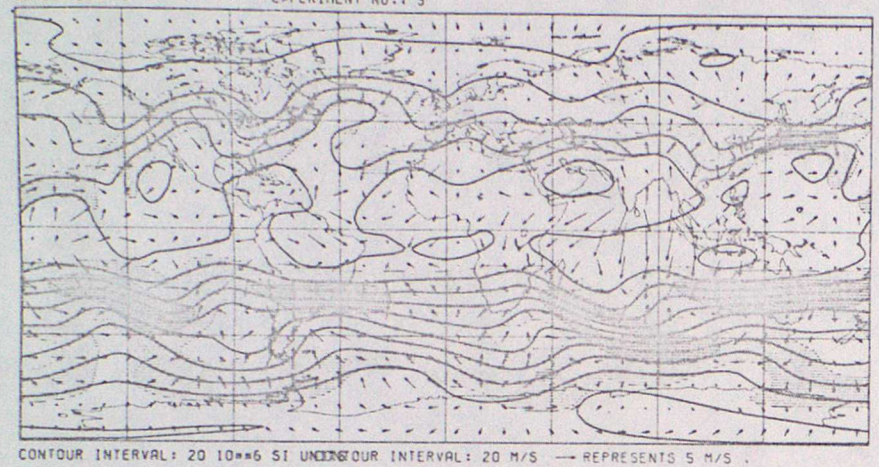

CONTOUR INTERVAL: 20 10**6 SI UNITS CONTOUR INTERVAL: 20 M/S → REPRESENTS 5 M/S

MET OFFICE FGGE IIIA ANALYSIS. SMOOTHED IN SPACE (T18) & TIME (24HRS).
STREAMFUNCTION + DIVERGENT WIND ARROWS + TOTAL ISOTACHS (>20M/S & >40M/S SHADED)
VALID AT 12Z ON 14/6/79 MODEL TIME: DAY 165 HR 12
LEVEL: 200 MB EXPERIMENT NO.: 3

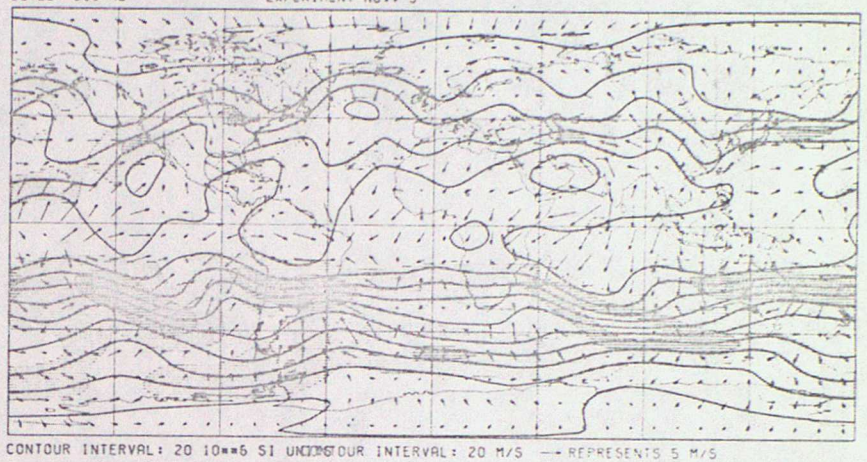

CONTOUR INTERVAL: 20 10**6 SI UNITS CONTOUR INTERVAL: 20 M/S → REPRESENTS 5 M/S

MET OFFICE FGGE IIIA ANALYSIS. SMOOTHED IN SPACE (T18) & TIME (24HRS).
STREAMFUNCTION + DIVERGENT WIND ARROWS + TOTAL ISOTACHS (>20M/S & >40M/S SHADED)
VALID AT 12Z ON 15/6/79 MODEL TIME: DAY 166 HR 12
LEVEL: 200 MB EXPERIMENT NO.: 3

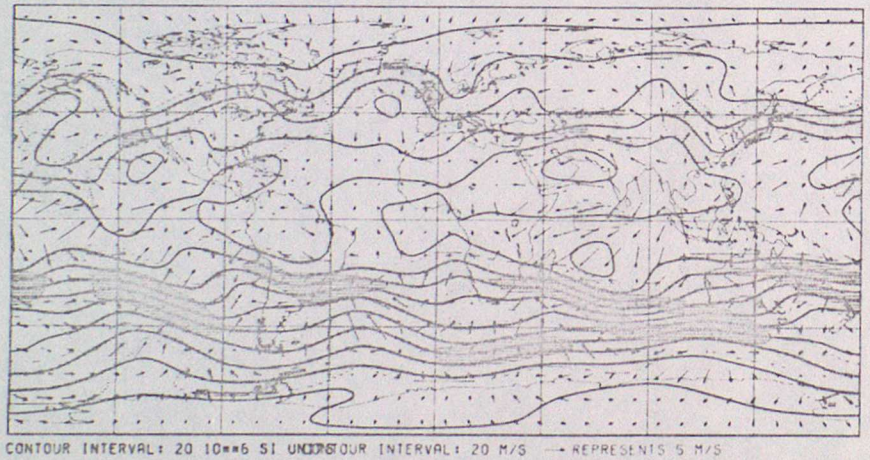

CONTOUR INTERVAL: 20 10**6 SI UNITS CONTOUR INTERVAL: 20 M/S → REPRESENTS 5 M/S

MET OFFICE FGGE IIIA ANALYSIS. SMOOTHED IN SPACE (T18) & TIME (24HRS).
STREAMFUNCTION + DIVERGENT WIND ARROWS + TOTAL ISOTACHS (>20M/S & >40M/S SHADED)
VALID AT 12Z ON 16/6/79 MODEL TIME: DAY 167 HR 12
LEVEL: 200 MB EXPERIMENT NO.: 3

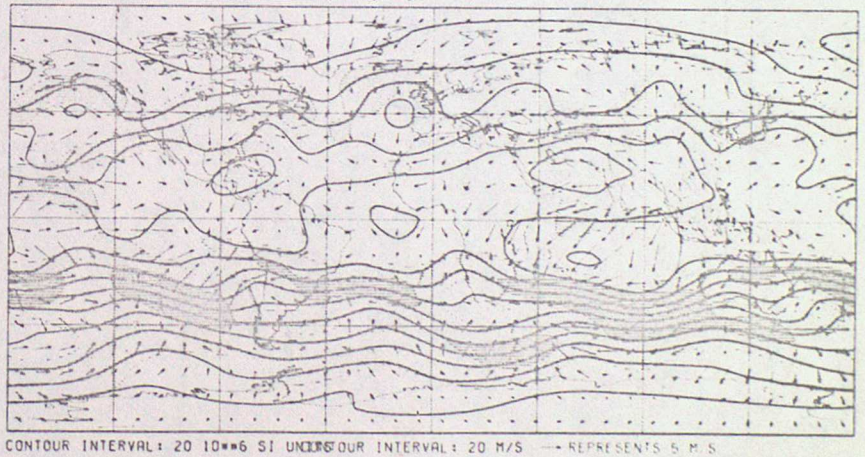

CONTOUR INTERVAL: 20 10**6 SI UNITS CONTOUR INTERVAL: 20 M/S → REPRESENTS 5 M/S

Figure 28

MET OFFICE FGGE IIIA ANALYSIS. SMOOTHED IN SPACE (T18) & TIME (24HRS).
STREAMFUNCTION + DIVERGENT WIND ARROWS + TOTAL ISOTACHS (>20M/S & >40M/S SHADED)
VALID AT 12Z ON 17/6/79 MODEL TIME: DAY 168 HR 12
LEVEL: 200 MB EXPERIMENT NO.: 3

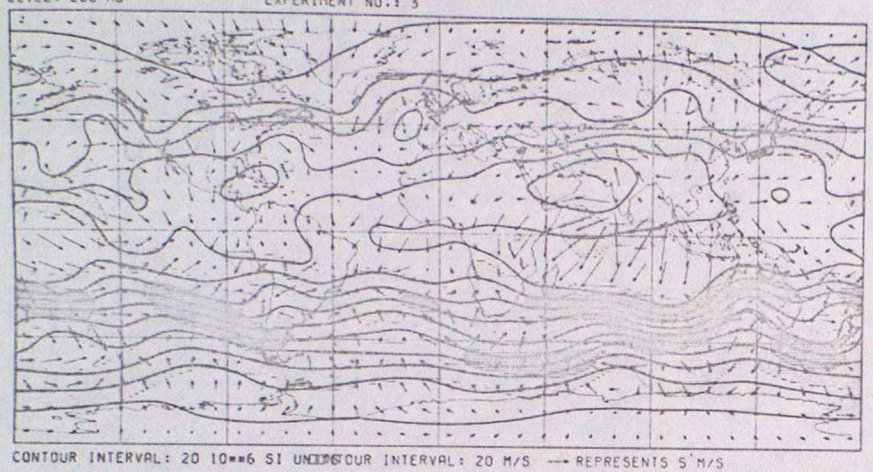

CONTOUR INTERVAL: 20 10**6 SI UNITS CONTOUR INTERVAL: 20 M/S → REPRESENTS 5 M/S

MET OFFICE FGGE IIIA ANALYSIS. SMOOTHED IN SPACE (T18) & TIME (24HRS).
STREAMFUNCTION + DIVERGENT WIND ARROWS + TOTAL ISOTACHS (>20M/S & >40M/S SHADED)
VALID AT 12Z ON 18/6/79 MODEL TIME: DAY 169 HR 12
LEVEL: 200 MB EXPERIMENT NO.: 3

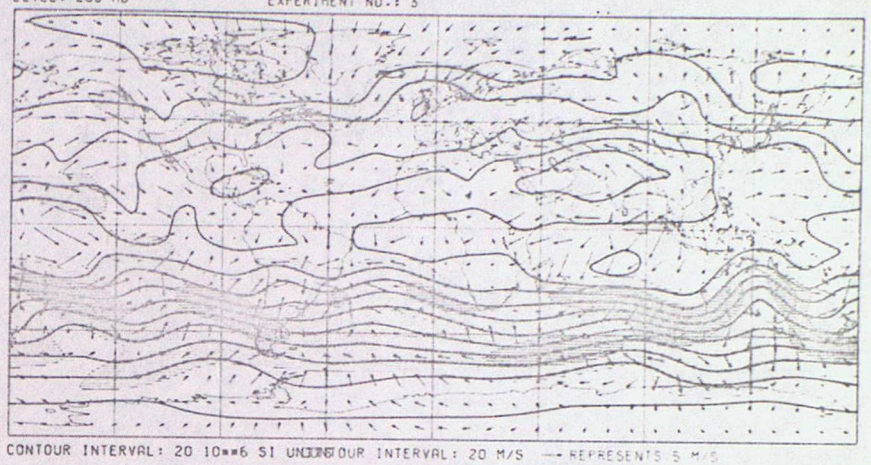

CONTOUR INTERVAL: 20 10**6 SI UNITS CONTOUR INTERVAL: 20 M/S → REPRESENTS 5 M/S

MET OFFICE FGGE IIIA ANALYSIS. SMOOTHED IN SPACE (T18) & TIME (24HRS).
STREAMFUNCTION + DIVERGENT WIND ARROWS + TOTAL ISOTACHS (>20M/S & >40M/S SHADED)
VALID AT 12Z ON 19/6/79 MODEL TIME: DAY 170 HR 12
LEVEL: 200 MB EXPERIMENT NO.: 3

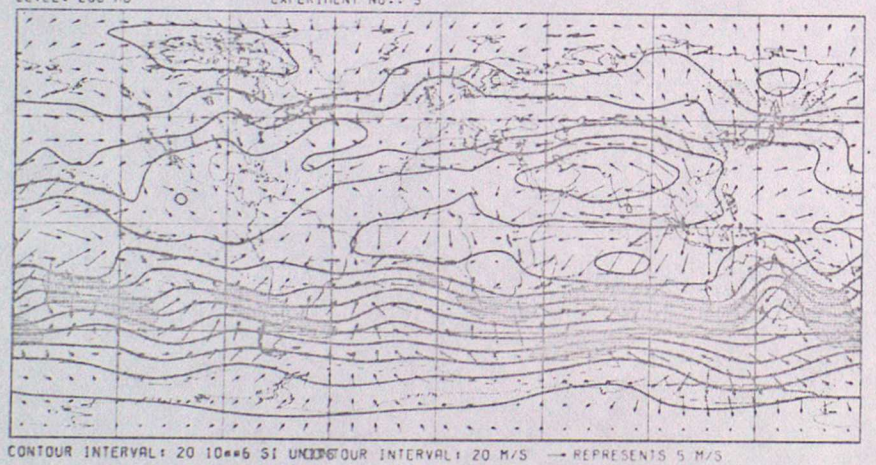

CONTOUR INTERVAL: 20 10**6 SI UNITS CONTOUR INTERVAL: 20 M/S → REPRESENTS 5 M/S

MET OFFICE FGGE IIIA ANALYSIS. SMOOTHED IN SPACE (T18) & TIME (24HRS).
STREAMFUNCTION + DIVERGENT WIND ARROWS + TOTAL ISOTACHS (>20M/S & >40M/S SHADED)
VALID AT 12Z ON 20/6/79 MODEL TIME: DAY 171 HR 12
LEVEL: 200 MB EXPERIMENT NO.: 3

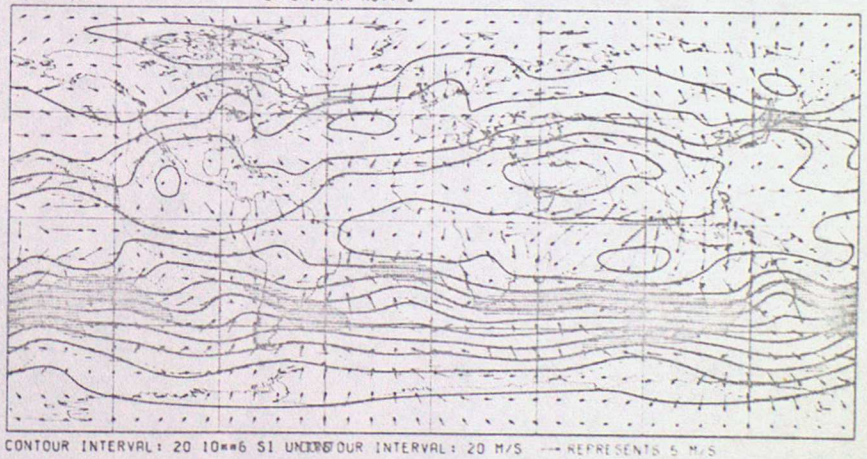

CONTOUR INTERVAL: 20 10**6 SI UNITS CONTOUR INTERVAL: 20 M/S → REPRESENTS 5 M/S

Figure 29

MET OFFICE FGGE IIIA ANALYSIS. SMOOTHED IN SPACE (T18) & TIME (24HRS).
STREAMFUNCTION + DIVERGENT WIND ARROWS + TOTAL ISOTACHS (>20M/S & >40M/S SHADED)
VALID AT 12Z ON 21/6/79 MODEL TIME: DAY 172 HR 12
LEVEL: 200 MB EXPERIMENT NO.: 3

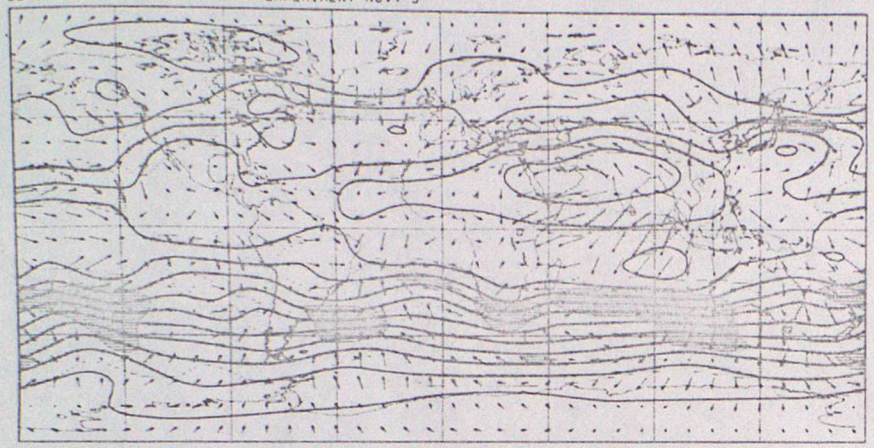

CONTOUR INTERVAL: 20 10**6 SI UNITS CONTOUR INTERVAL: 20 M/S → REPRESENTS 5 M/S

MET OFFICE FGGE IIIA ANALYSIS. SMOOTHED IN SPACE (T18) & TIME (24HRS).
STREAMFUNCTION + DIVERGENT WIND ARROWS + TOTAL ISOTACHS (>20M/S & >40M/S SHADED)
VALID AT 12Z ON 22/6/79 MODEL TIME: DAY 173 HR 12
LEVEL: 200 MB EXPERIMENT NO.: 3

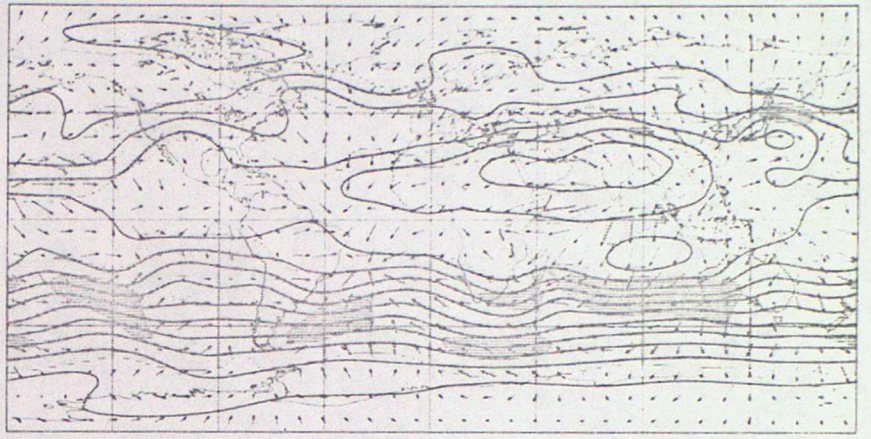

CONTOUR INTERVAL: 20 10**6 SI UNITS CONTOUR INTERVAL: 20 M/S → REPRESENTS 5 M/S

MET OFFICE FGGE IIIA ANALYSIS. SMOOTHED IN SPACE (T18) & TIME (24HRS).
STREAMFUNCTION + DIVERGENT WIND ARROWS + TOTAL ISOTACHS (>20M/S & >40M/S SHADED)
VALID AT 12Z ON 23/6/79 MODEL TIME: DAY 174 HR 12
LEVEL: 200 MB EXPERIMENT NO.: 3

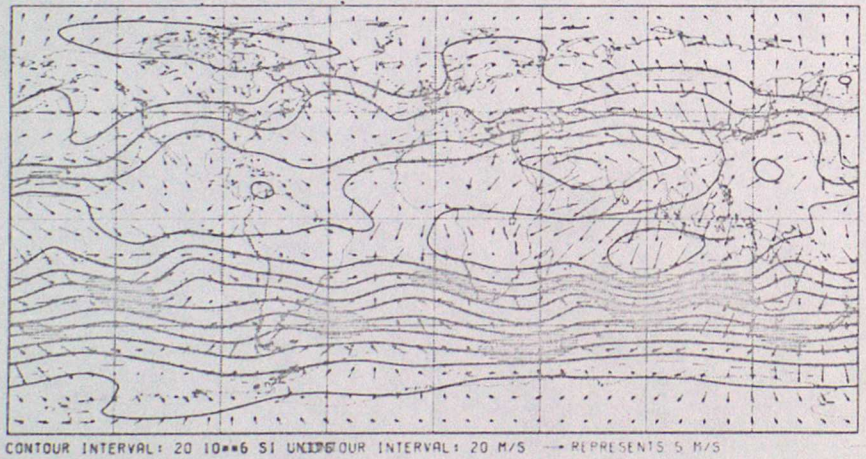

CONTOUR INTERVAL: 20 10**6 SI UNITS CONTOUR INTERVAL: 20 M/S → REPRESENTS 5 M/S

MET OFFICE FGGE IIIA ANALYSIS. SMOOTHED IN SPACE (T18) & TIME (24HRS).
STREAMFUNCTION + DIVERGENT WIND ARROWS + TOTAL ISOTACHS (>20M/S & >40M/S SHADED)
VALID AT 12Z ON 24/6/79 MODEL TIME: DAY 175 HR 12
LEVEL: 200 MB EXPERIMENT NO.: 3

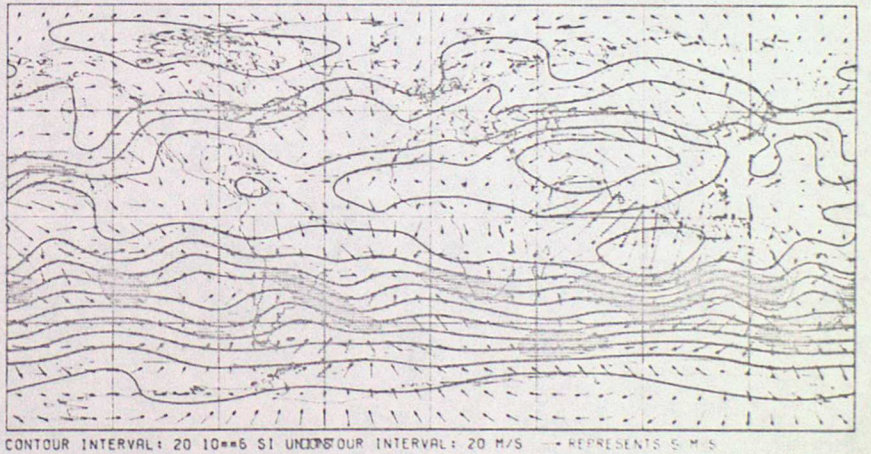

CONTOUR INTERVAL: 20 10**6 SI UNITS CONTOUR INTERVAL: 20 M/S → REPRESENTS 5 M/S

Figure 30

MET OFFICE FGGE IIIA ANALYSIS. SMOOTHED IN SPACE (T18) & TIME (24HRS).
STREAMFUNCTION + DIVERGENT WIND ARROWS + TOTAL ISOTACHS (>20M/S & >40M/S SHADED)
VALID AT 12Z ON 25/6/79 MODEL TIME: DAY 176 HR 12
LEVEL: 200 MB EXPERIMENT NO.: 3

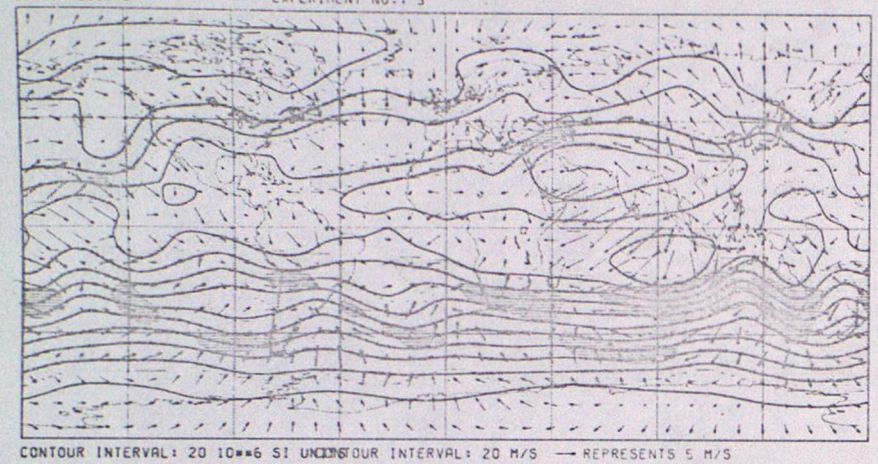

CONTOUR INTERVAL: 20 10**6 SI UNITS CONTOUR INTERVAL: 20 M/S —→ REPRESENTS 5 M/S

MET OFFICE FGGE IIIA ANALYSIS. SMOOTHED IN SPACE (T18) & TIME (24HRS).
STREAMFUNCTION + DIVERGENT WIND ARROWS + TOTAL ISOTACHS (>20M/S & >40M/S SHADED)
VALID AT 12Z ON 26/6/79 MODEL TIME: DAY 177 HR 12
LEVEL: 200 MB EXPERIMENT NO.: 3

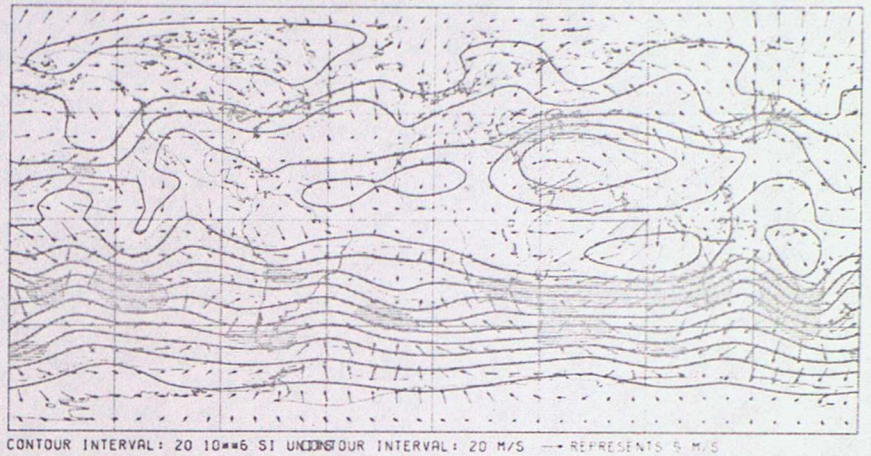

CONTOUR INTERVAL: 20 10**6 SI UNITS CONTOUR INTERVAL: 20 M/S —→ REPRESENTS 5 M/S

MET OFFICE FGGE IIIA ANALYSIS. SMOOTHED IN SPACE (T18) & TIME (24HRS).
STREAMFUNCTION + DIVERGENT WIND ARROWS + TOTAL ISOTACHS (>20M/S & >40M/S SHADED)
VALID AT 12Z ON 27/6/79 MODEL TIME: DAY 178 HR 12
LEVEL: 200 MB EXPERIMENT NO.: 3

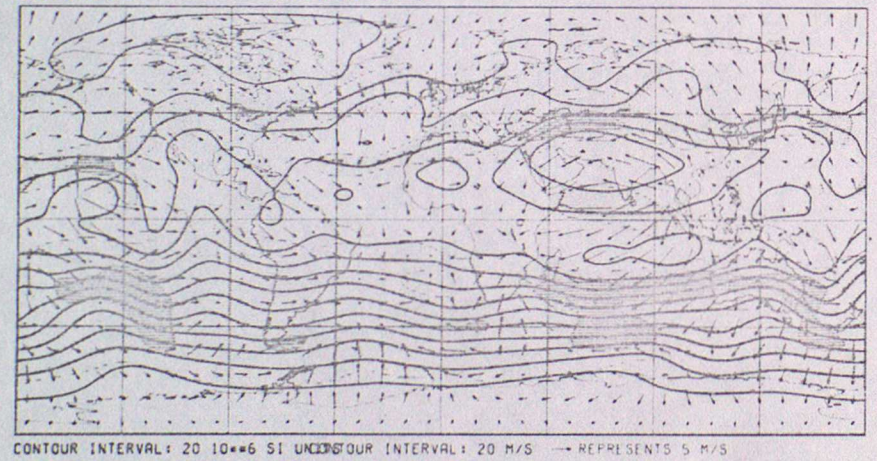

CONTOUR INTERVAL: 20 10**6 SI UNITS CONTOUR INTERVAL: 20 M/S —→ REPRESENTS 5 M/S

MET OFFICE FGGE IIIA ANALYSIS. SMOOTHED IN SPACE (T18) & TIME (24HRS).
STREAMFUNCTION + DIVERGENT WIND ARROWS + TOTAL ISOTACHS (>20M/S & >40M/S SHADED)
VALID AT 12Z ON 28/6/79 MODEL TIME: DAY 179 HR 12
LEVEL: 200 MB EXPERIMENT NO.: 3

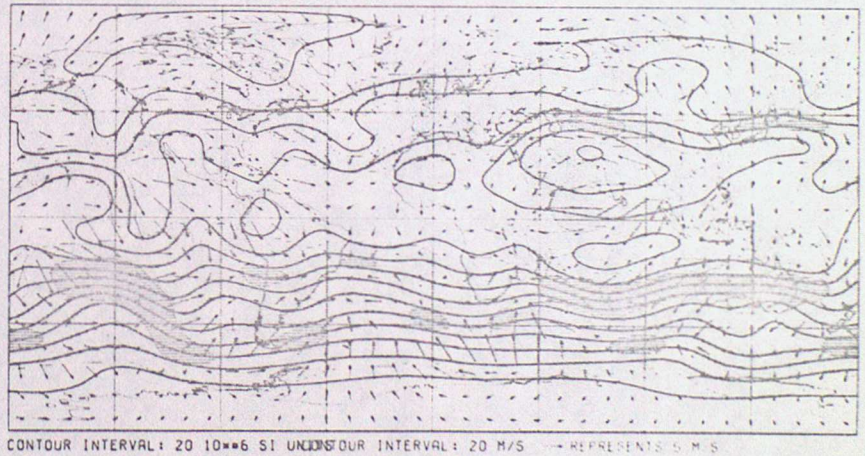

CONTOUR INTERVAL: 20 10**6 SI UNITS CONTOUR INTERVAL: 20 M/S —→ REPRESENTS 5 M/S

Figure 31

a

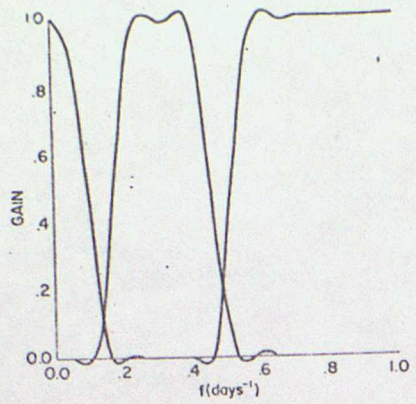

The amplitudes of the filters as a function of frequency.

b Values of the coefficients a_p for the low-pass, medium-pass and high-pass filters discussed in the text.

Coefficients	Filters		
	Low-pass	Medium-pass	High-pass
a_0	0.0974726419	0.2776877534	0.4762599236
a_1	0.0954676702	0.1433496840	−0.3186000638
a_2	0.0896329731	−0.1020097578	0.0197489990
a_3	0.0804876892	−0.1947701551	0.1009810886
a_4	0.0688283154	−0.0923257264	−0.0185972473
a_5	0.0556356004	0.0283041151	−0.0546750050
a_6	0.0419626250	0.0419335015	0.0167834343
a_7	0.0288191067	0.0033466748	0.0333056699
a_8	0.0170670479	0.0041075557	−0.0144542141
a_9	0.0073407153	0.0328072034	−0.0207251125
a_{10}	0.0	0.0304306715	0.0117924147
a_{11}	−0.0048789007	−0.0020017146	0.0125704103
a_{12}	−0.0074769889	−0.0191709641	−0.0089978990
a_{13}	−0.0081766107	−0.0096723016	−0.0071490567
a_{14}	−0.0074864031	−0.0001341773	0.0062672457
a_{15}	−0.0059591606	−0.0030384857	0.0036193743

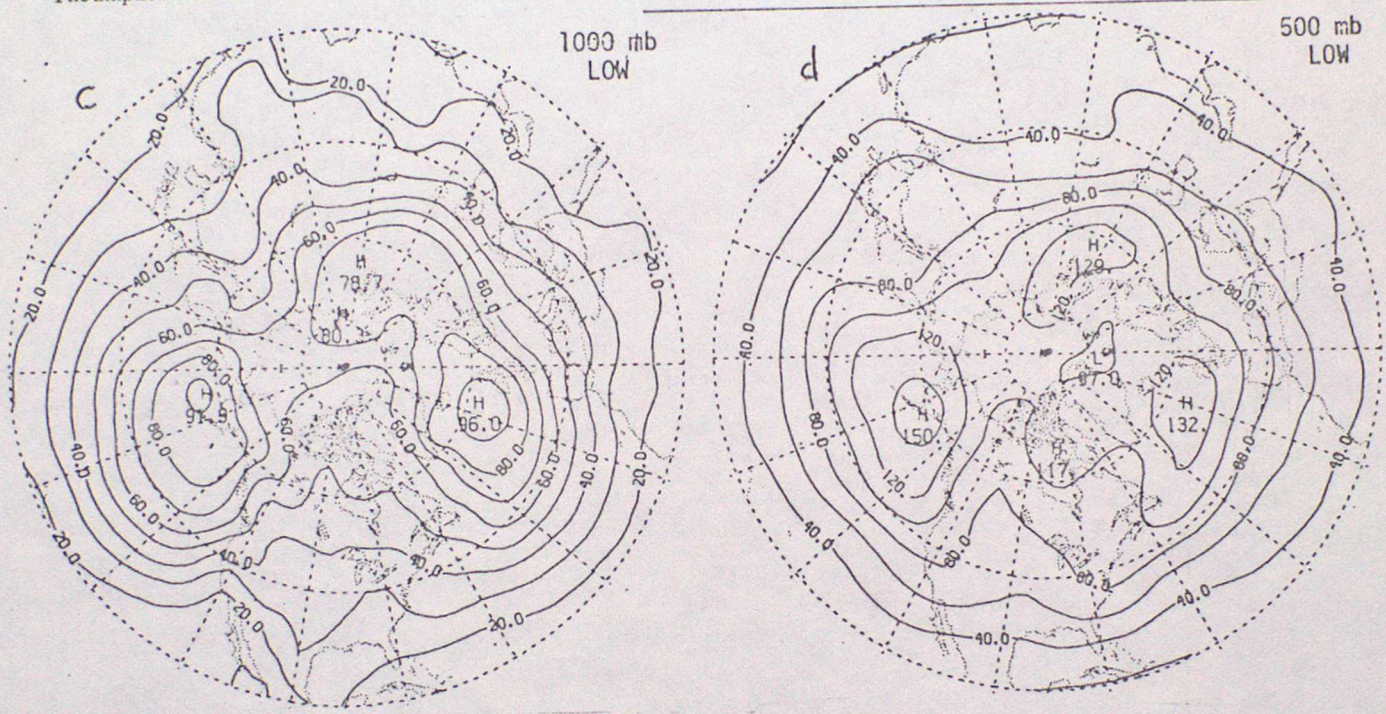

Wintertime standard deviation of geopotential height $(\overline{Z'^2})^{1/2}$. Blackmon low pass filtered. c) 1000 mb, contour interval 10 m; d) 500 mb, contour interval 20 m.

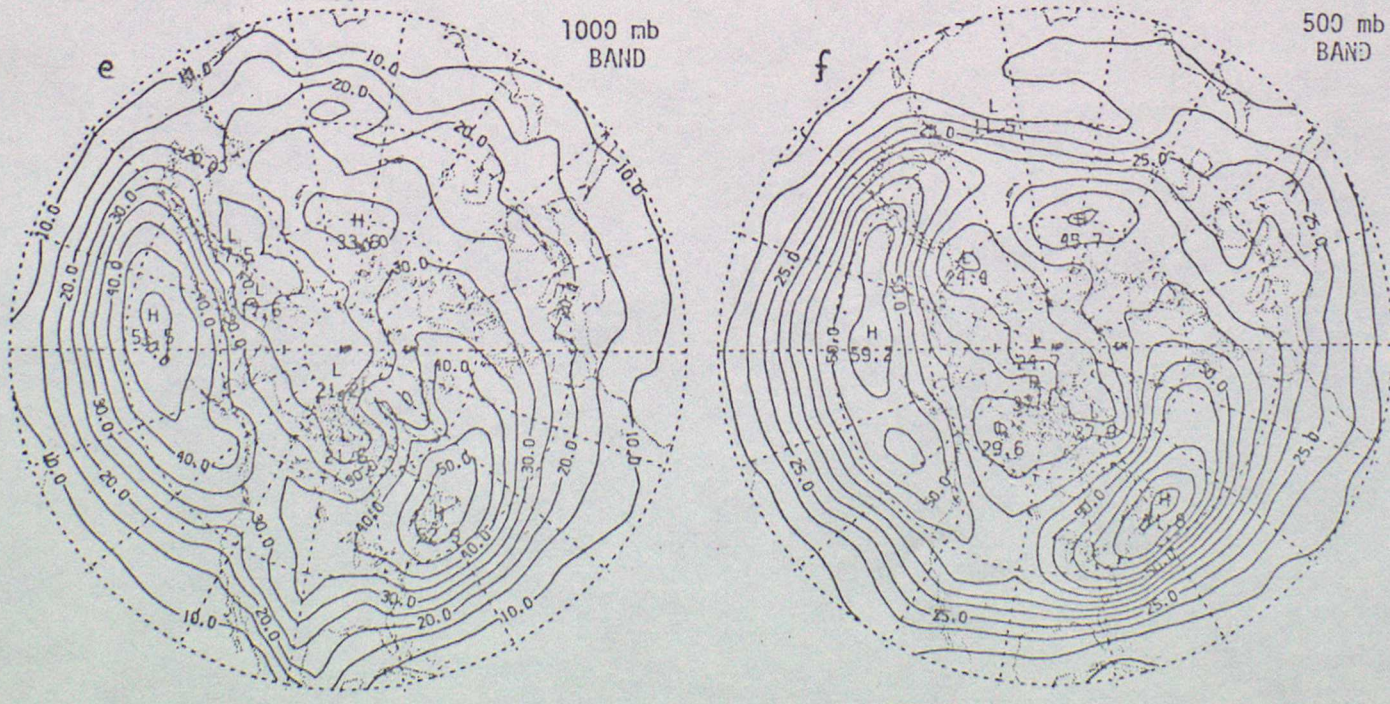

Wintertime standard deviation of geopotential height $(\overline{Z'^2})^{1/2}$. Blackmon band pass filtered. e) 1000 mb, f) 500 mb, contour interval 5 m.

Figure 32

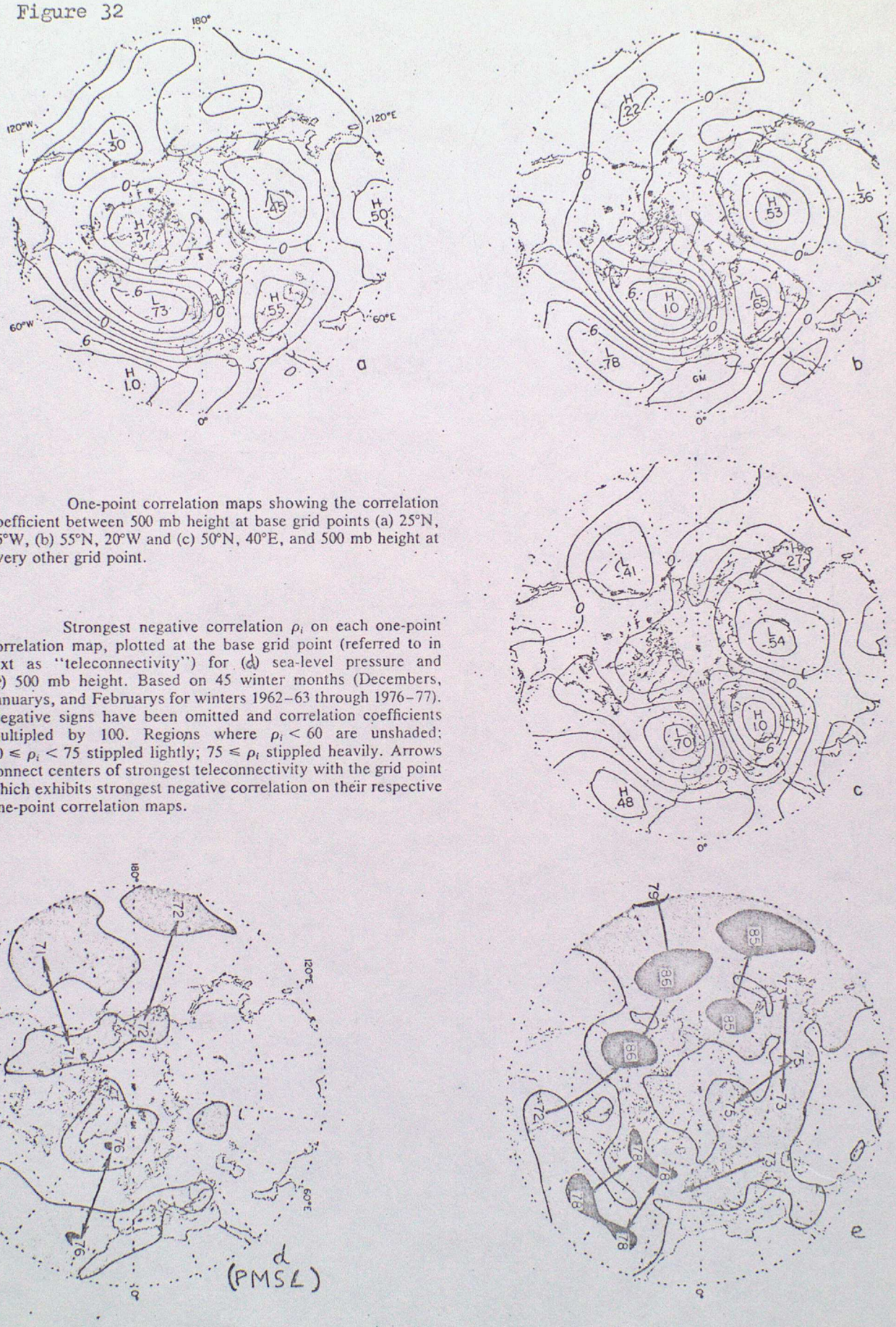

One-point correlation maps showing the correlation coefficient between 500 mb height at base grid points (a) 25°N, 25°W, (b) 55°N, 20°W and (c) 50°N, 40°E, and 500 mb height at every other grid point.

Strongest negative correlation ρ_i on each one-point correlation map, plotted at the base grid point (referred to in text as "teleconnectivity") for (d) sea-level pressure and (e) 500 mb height. Based on 45 winter months (Decembers, Januarys, and Februarys for winters 1962–63 through 1976–77). Negative signs have been omitted and correlation coefficients multipled by 100. Regions where $\rho_i < 60$ are unshaded; $60 \leq \rho_i < 75$ stippled lightly; $75 \leq \rho_i$ stippled heavily. Arrows connect centers of strongest teleconnectivity with the grid point which exhibits strongest negative correlation on their respective one-point correlation maps.

From Wallace, J.M. and Gutzler, D.S., 1981, Mon. Weath. Rev., 109.

Figure 33

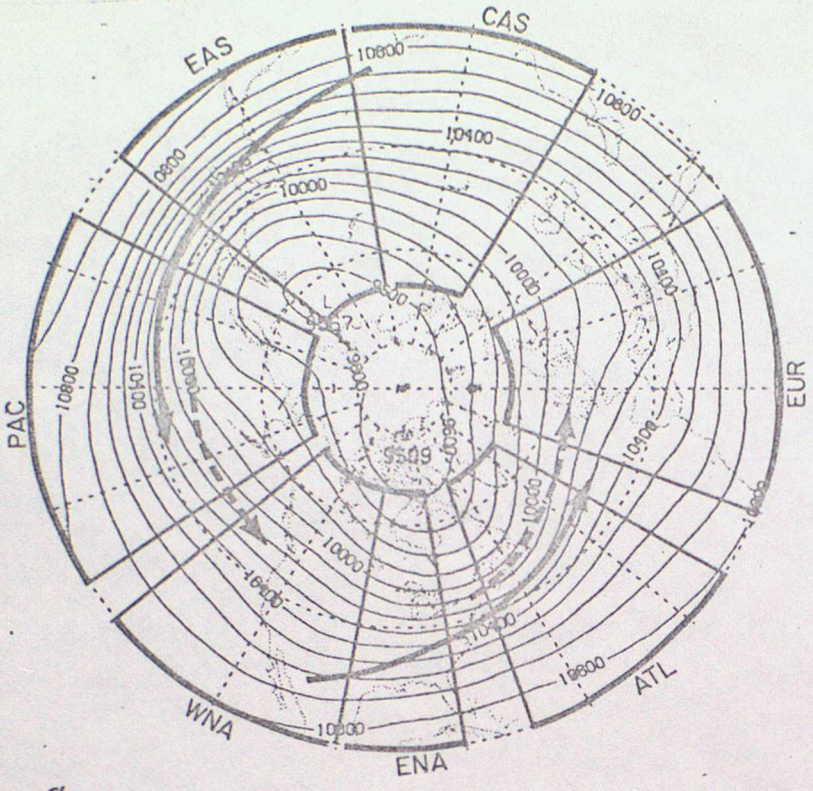

a The distribution of time mean geopotential height at 250 mb, contour interval 100 m. Arrows with solid shafts denote locations of the jet streams. Arrows with dashed shafts correspond to regions with maximum geopotential height variability in the bandpass (2.5–6 days) period range. Also shown are longitudinal sectors for which partial zonal averages of circulation statistics are computed.

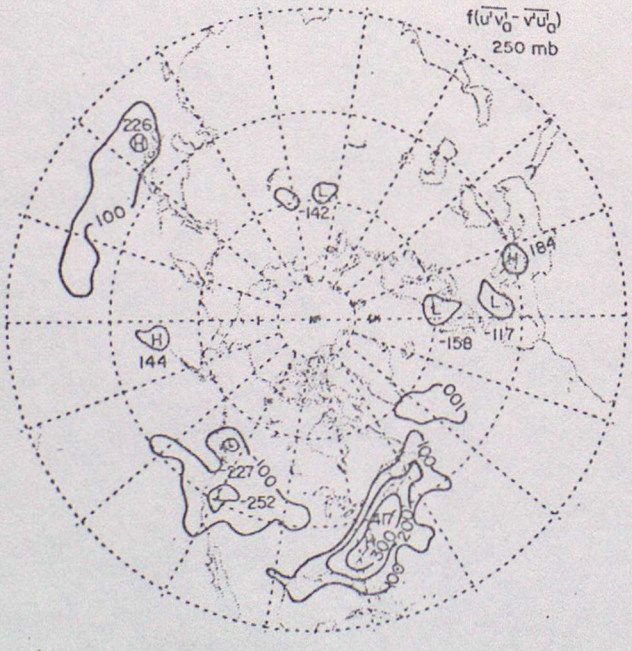

d The distribution of $f(\overline{u'v_a} - \overline{v'u_a})$ at 250 mb. For the sake of clarity, the zero contour is not plotted. Contour interval 1×10^{-3} m^2 s^{-3}.

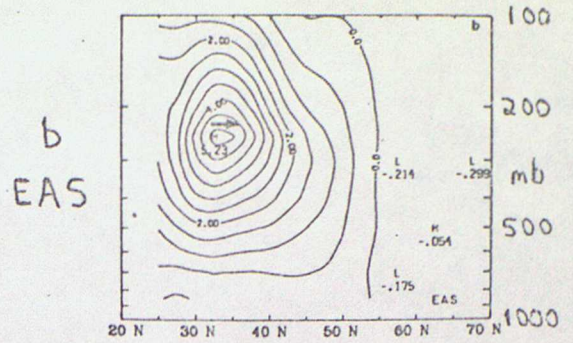

meridional component of the time-mean ageostrophic flow v_a, computed by the indirect method

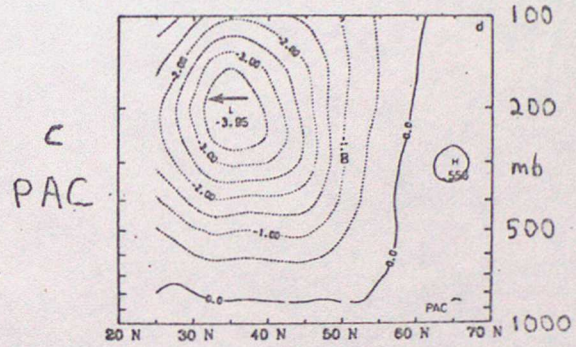

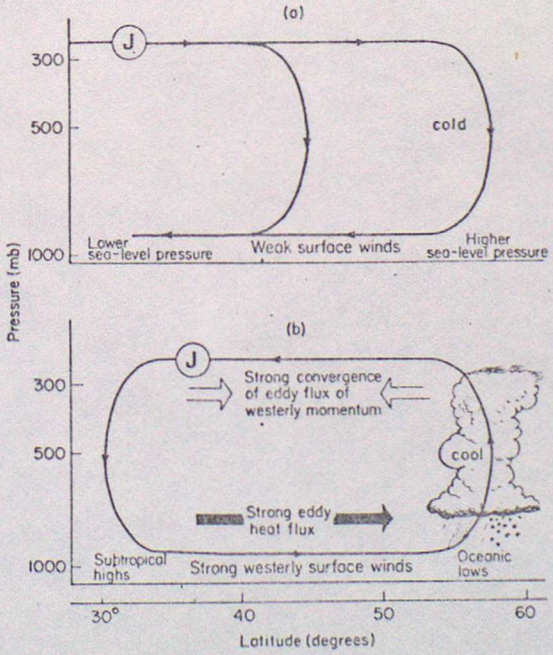

e Schematic illustration showing relationship between the jet streams (denoted by the letter J), the time-mean circulation transverse to the jet streams (continuous thin line with arrows), and the band-pass eddy fluxes of westerly momentum at the jet stream level (heavy white arrows) and heat at the 850 mb level (heavy black arrow), in cross sections (a) upstream and (b) downstream from the jet cores.

ADVANCED LECTURES 1982 - GENERAL CIRCULATION OF THE ATMOSPHERE

LECTURE 8 - General Circulation Models (I)

1. Introduction

The preceding lectures have shown that the general circulation of the earth's atmosphere is extremely complex. In the first four lectures some of the broad features of the circulation were explained using simple, but necessarily qualitative, arguments. In order to provide a quantitative description of meteorological variables and their development, however, considerable effort has been spent over the past three decades in constructing detailed numerical models. Such general circulation models (GCMs) may be used not only as tools for understanding the present climate and changes in response to natural or man-made perturbations, but also for weather forecasting and the design of efficient global observing systems. Any one of these applications could itself be the subject of a series of advanced lectures, but the purpose here is to concentrate on the first. The structure of GCMs and the physical processes they treat will be described briefly, followed by a review of models currently in use and their ability to reproduce the observed circulation. In the final lecture some specific examples of the use of GCMs in understanding the circulation will be shown and current research outlined. It should be appreciated that this is an enormous subject and these two lectures will therefore be very selective.

The first numerical experiment on the general circulation was carried out by Phillips (1956), who used a two-level geostrophic model. The computational domain was a rectangular grid of 17 x 16 points, with cyclic east-west boundary conditions. The external forcing was prescribed as a function of latitude. Despite the simplicity of the model, important features of the observed circulation were reproduced, such as the surface easterlies at low latitudes giving way to westerlies in the middle latitudes. In subsequent studies, the restrictive equations used by Phillips have been replaced by the more general 'primitive' equations. Smagorinsky (1963) integrated a primitive equation model on a hemispheric grid bounded by the equator and 64° latitude. The poleward heat transfer in a 60 day integration was accomplished by a Hadley circulation near the equator and by baroclinic waves of realistic scale at the higher latitudes. Mintz (1965) and Arakawa formulated a global model including a realistic distribution of surface topography and performed the first GCM experiments on orographic forcing.

2. Basic Structure

General circulation models currently in use employ a wide variety of mathematical formulations, resolutions and physical parametrization schemes. The basic equations used are in general fairly similar, however. The general dynamical equations for the motion of a fluid on a rotating sphere are simplified by making use of the fact that the large-scale circulation is close to hydrostatic equilibrium. The motion is then described by the horizontal momentum equation, the equation of continuity and the hydrostatic equation. The assumption of hydrostatic equilibrium means that the vertical motion is calculated diagnostically from the convergence or divergence of the horizontal winds. The full set of "primitive" equations are completed by the thermodynamic equation, the equation of state and an equation for the continuity of water substance.

Some of the mathematical techniques used to integrate these equations in finite difference form have been reviewed in a GARP publication (1976/9). The choice of technique is closely related to the vertical and horizontal grid employed. The equations may be written with either height or pressure as the vertical variable, but in both cases problems arise with the treatment of orography. This is because the

coordinate system intersects the surface in the region of mountains, creating difficulties for the specification of the lower boundary conditions. To overcome this, most models are written in terms of sigma coordinates, in which pressure normalized by its surface value is used, so the coordinates follow the terrain as shown by Figure 8.1. The simplest form of horizontal grid is a regular latitude-longitude array. The simplicity of this system has considerable programming advantages, but the convergence of the lines of longitude towards the poles creates computational problems, because as the physical separation of the grid points decreases the timestep employed must also decrease to ensure numerical stability. The implied timestep near the poles is unacceptably short and instead a single timestep is usually chosen for the whole model to ensure stability up to some critical latitude. Beyond this latitude the unstable modes are removed or damped by a carefully chosen numerical filter. The version of the Met O 20 11-layer model under development on the Cyber computer uses this technique applied to a $2^{\circ} \times 3^{\circ}$ latitude-longitude grid. An alternative approach suggested by Kurihara (1965) is to distribute the points non-uniformly over the sphere, decreasing the number of points around a latitude circle as the pole is approached so that the horizontal resolution remains roughly constant. Such a grid was used in the 5 and 11-layer models when integrated on the IBM 360/195 computer (Corby et al 1977, Saker 1975). The 11-layer model grid is illustrated in Figure 8.2. The irregular grid has advantages in terms of numerical stability, but it is necessary to add extra points in the immediate vicinity of the poles to reduce errors from the finite-difference approximations. For these rows a decrease in the timestep or filtering are therefore required. The irregular nature of the grid also introduces an additional element of complexity to the computer program. Some of the problems which grid-point models experience, whether on regular or irregular grids, may be overcome by using a spectral model (Bourke et al (1977). These models represent the solutions to the primitive equations as expansions in spherical harmonic functions, rather than in grid-point form, although it is still necessary to transform back to real space in order to perform certain physical calculations.

3. Physical parametrizations

The highest horizontal resolution currently employed by GCMs is about 250 km, so that motions of larger scale such as the Hadley and monsoonal circulations are represented explicitly. There are, however, many smaller scale processes, such as convection, which make important contributions to the energy and momentum balance and which must be represented. This means that, in addition to the primitive equations outlined earlier, GCMs must also include subroutines to compute the effects of these sub-gridscale physical processes. It is especially important that these routines enable a proper representation of the location and intensity of the energy sources and sinks. In extended integrations measured in months or years, it is these sources and sinks which determine the character of the circulation. The initial conditions used are thus less important than in numerical weather prediction and it is perfectly feasible to begin from an isothermal atmosphere at rest relative to the surface. In the rest of this section a very brief summary will be given of the processes which are treated. Most involve contributions to the thermodynamic equation, but in some cases the momentum equations and the water continuity equation are also affected.

Large scale condensation

Large scale condensation is deemed to occur when the convergence of water vapour into a grid box leads to supersaturation. In the real atmosphere this corresponds, for example, to the widespread cloud associated with mid-latitude depressions. The latent heat released is used to increment the temperature through

the thermodynamic equation and the excess water is assumed to fall as rain or snow. This may partially evaporate into the lower layers and upon reaching the ground takes part in the surface hydrological cycle.

Convection

Convective processes in the atmosphere take place on a wide variety of scales, from the unsaturated convection above a heated land surface, through cumulus and cumulonimbus clouds, to the organised line squalls and cloud clusters of the tropics. A convection scheme must attempt to model the effect of all of these processes and the associated precipitation, and must complement the treatment of large scale condensation. The simplest approach is the so-called convective adjustment method, in which the temperature profile is adjusted so as to remove lapse rates steeper than a critical value. The Arakawa-Schubert scheme is a much more comprehensive attempt to model the interaction of cumulus and cumulonimbus clouds with their environment. The effect of deep "penetrative" convection through several model levels is especially important in the tropics and is also treated in the scheme developed in Met O 20 by Lyne and Rowntree (1976). In schemes of this type, the latent heat release is used to increase the buoyancy of an ensemble of plumes, representing clouds of different vertical extents. Detrainment typically occurs at a level of neutral buoyancy and the net warming of the column results from the compensating environmental subsidence. The ECMWF workshop report (1978) contains several useful papers on this subject.

Dissipation

The non-linearity of the dynamical equations means that energy is continually being exchanged between different scales of motion. The transfer of energy from the resolvable motion to that occurring on scales smaller than the grid has a dissipative, or smoothing, effect on the circulation. This transfer can therefore be treated as a form of diffusion, by applying a numerical filter to the dynamical variables. It is obviously important that the filter should be conservative and in practice its form is dictated primarily by the need to control the computational noise injected into the model by the finite grid, with the constraint that it should not lead to excessive damping of baroclinic waves.

Boundary Layer

The boundary layer marks the transition region through which the large-scale flow interacts with the surface. It is normally turbulent, so a boundary layer scheme must calculate the sub-gridscale vertical fluxes of momentum, heat and moisture and their effect on the surface and on the structure of the lowest atmospheric levels. The turbulent transport is commonly treated as a diffusive process, but the parametrizations have to take account of the large changes in the fluxes, and hence in the boundary layer structure and depth, in the change from stable to convective conditions. It is common to increase the vertical resolution within the boundary layer, which may either be assumed to occupy a fixed number of levels, or may be allowed to vary in depth in response to the surface forcing. A brief review of methods used to parametrize the boundary layer, with a useful reference list, is by Driedonks and Tennekes (1981) and recent examples of the explicit calculation of boundary layer depth in a GCM have been presented by Suarez et al (1981).

Surface properties

Most of the energy for atmospheric motion is supplied from the surface in the form of the fluxes of heat and moisture. These depend strongly on the nature of the

surface, so it is necessary to employ a realistic distribution of surface type. For example, in the case of the 11-layer model the surface may be land, sea, sea-ice or ice-covered land (Figure 8.2). Surface characteristics such as the roughness and shortwave albedo may be given different values according to the surface type. The sea surface temperatures and the sea-ice distribution are normally prescribed from climatological values, unless a model is to be run interactively with ocean and sea-ice models. The land surface temperature is an important variable to be calculated within the model, however. This depends on the energy balance between the surface radiative, sensible and latent heat fluxes. The hydrological cycle is represented by the use of a soil moisture content, which is increased by precipitation, condensation and snowmelt, decreased by evaporation and limited to a maximum value by runoff. Although the treatment of land surface processes is crude, sensitivity studies have shown that model simulations are sensitive to the methods used, and this is an active research area (Carson 1980).

Radiation and clouds

Radiation schemes are required to compute the longwave cooling and shortwave heating of the atmosphere, in addition to the components of the surface radiation balance. In order to do this they must take account of the distribution of gaseous absorbers, most important of which are water vapour, carbon dioxide and ozone, and the distribution of cloudiness. The longwave spectrum is usually split into a number of spectral bands because of the strong dependence of the absorption on wavelength, and clouds are assumed to absorb and radiate as black bodies. In the shortwave region a single spectral band is normally used and the absorptivity and reflectivity of clouds are taken from observational studies or more detailed modelling. Clouds represent a considerable problem in GCMs because while on the one hand they exert a profound influence on both the longwave and shortwave radiation fields, there is as yet no general theory of cloud formation which can be used to predict cloud height, thickness and coverage over a grid box from the other model variables. The mass flux from a convection scheme may be used to predict the amount of convective cloud (Slingo 1980), but for other cloud types it is necessary to use empirical relationships between cloud amount and humidity and tune the coefficients so that the model generates a reasonable cloud climatology. Current research in cloud prediction is mainly concerned with ensuring that the major features of the observed cloud distribution can be reproduced and that the clouds interact realistically with the rest of the model, especially for clouds associated with the boundary layer, such as cumulus and stratocumulus. Some results of GCM investigations of the role of cloudiness in the general circulation will be discussed in the final lecture.

4. Models in current use

A list of the models currently being employed in general circulation and/or climate simulations and the institutions responsible for them is shown in Table I, adapted from the compilation of Carson (1980). The institutions are listed roughly in the order in which they began developing such models. The table gives the number of vertical levels used and the horizontal resolution for grid-point models, whether on irregular or latitude-longitude grids. For spectral models the number of waves retained is shown in brackets. The references marked with an asterisk are all found in the report of the Study Conference on Climate Models (JOC 1979). There is a certain amount of redundancy between these models. For example, the grid and dynamical formulation of the RAND and GISS models (which later became the OSU and the first GLAS model, respectively) were based on the work by Arakawa at UCLA. The physical parametrizations used in the Australian spectral model are based extensively on the work carried out at GFDL. The Met O 20 11-layer model was developed as a higher resolution version of the 5-layer model with more complex physical parametrizations, which are also being used by the new version of the model on the Cyber computer.

5. Comparison of modelled and observed circulations

A general circulation model should be able to reproduce as many features of the observed circulation as is possible, whatever the intended application. One of the purposes of the FGGE experiment was to provide extensive datasets for such validation. The large circulation changes between summer and winter mean that the ability to simulate both mean January and July conditions is a useful test and many such comparisons will be found in the JOC report (1979). Examples are shown in Figures 8.3 to 8.6 of the pressure at mean sea level (PMSL) and precipitation distributions for January and July, for four of the models listed in Table I. These are the GFDL M30 spectral model, the third-generation NCAR model, the Met O 20 5-layer model and the OSU 2-layer model. In noting differences between these simulations, it will be appreciated that models usually differ in a number of important respects which all make a contribution. The value of a given parametrization or technique in a particular model is normally assessed by experiments in which the differences between versions of the same model are carefully controlled.

Each model has its own characteristic strengths and weaknesses, but some shortcomings are common to a number of models. In both seasons, the lower resolution models tend to produce mean sea level pressures which are too high in the polar regions. Over Antarctica, this may be due partly to the difficulty in reducing the surface pressure to its sea level value because of the high elevation of the surface. In the northern hemisphere winter, there tends to be too strong a westerly flow at around 50°N in the models with increased resolution. All models, except possibly that from NCAR, suffer from depressions which are too deep over the northern hemisphere oceans in winter, with the result that pressures are too low in the Icelandic and Aleutian low pressure areas. In terms of the kinetic energy of the flow, there tends to be too much zonal kinetic energy and too little transient eddy kinetic energy, so that the 500 mb flow is too zonal. In the July simulations the continental heat lows are generally too deep, which may be seen by following the 1005/1004 mb contours. Finally, the low resolution models have pressures which are too low in the equatorial regions.

Systematic differences are more difficult to see between the charts of precipitation because of the different contour intervals used. Nevertheless, areas in which the mean sea level pressure is too low are generally associated with excessive rainfall, such as in the northern hemisphere winter depression tracks and along the eastern seaboards of the northern continents in summer.

The climatologies used in these comparisons are derived from several years of observations and the fields are therefore relatively smooth. On the other hand, the model results usually come from the mean of only 30 days of a single integration. This means that not only are the results less smooth, but they also represent only one realization from the climatology of each model. A more rigorous comparison would involve running a large number of such integrations in order to compare not only the mean but also the variance fields with those observed. In practice, a more realistic way of achieving this objective is to continue the integration through a series of annual cycles, which also provides information on the response to the seasonal changes in forcing. Such experiments were first performed at GFDL, and results from a recent integration with the 5-layer model are shown in Figure 8.7. The inherent model variability in the northern hemisphere in winter is considerable (Figure 8.8), but it compares quite favourably with that observed (Figure 8.9). The assessment of the effect of changes in the formulation of the model can be very difficult in the face of such variability, because it may mask any smaller, but systematic, response taking place.

References

Arakawa A. 1972 Design of the UCLA general circulation model. Numerical simulation of weather and climate Technical Report No. 7, Dept. of Met., UCLA.

Arakawa A. and Lamb V.R. 1977 Computational design of the basic dynamical processes of the UCLA general circulation model. Methods in Computational Physics, 17, 173-265, Academic Press.

Bourke W., McAvaney B. Puri K. and Thurling R. 1977 Global modeling of atmospheric flow by spectral methods. Ibid, 267-324.

Carson D.J. 1980 Current parametrizations of land-surface processes in atmospheric general circulation models. Met O 20 Technical Note II/152.

Carson D.J. and Cunnington W.M. 1979 General circulation experiments with an 11-layer model. GARP WGNE Report No. 19.

Corby G.A., Gilchrist A. and Rowntree P.R. 1977 United Kingdom meteorological office Five-level general circulation model. Methods in computational physics, 17, 67-110.

Driedonks A.G.M. and Tennekes H. 1981 Parametrization of the atmospheric boundary layer in large scale models. Bull. Amer. Met. Soc., 62, 594-598.

ECMWF 1978 ECMWF workshop on the parameterization of cumulus convection, 23-25 October 1978.

Gates W.L. and Schlesinger M.E. 1977 Numerical simulation of the January and July global climate with a two-level atmospheric model. J. Atmos. Sci., 34, 36-76.

GARP 1976/9 Numerical methods used in atmospheric models. GARP publications series No. 17, vols 1 & 2.

Holloway J.L. and Manabe S. 1971 Simulation of climate by a global general circulation model. I. Hydrological cycle and heat balance. Mon. Weath. Rev., 99, 335-370.

JOC 1979 Report of the JOC study conference on climate models: performance, intercomparison and sensitivity studies, Volume I. Garp publications series No. 22.

Kasahara A. and Washington W.M. 1971 General circulation experiments with a six-layer NCAR model, including orography, cloudiness and surface temperature calculations, J. Atmos. Sci., 28, 657-701.

Kurihara Y. 1965 Numerical integration of the primitive equations on a spherical grid. Mon. Weath. Rev., 93, 399-415.

Lyne W.H. and Rowntree P.R. 1976 Development of a convective parametrization using GATE data. Met O 20 Technical Note II/70.

Manabe S. and Terpstra T.B. 1974 The effects of mountains on the general circulation of the atmosphere as identified by numerical experiments. J. Atmos. Sci., 31, 3-42.

Manabe S. Hahn D.G. and Holloway J.L. 1974 The seasonal variation of the tropical circulation as simulated by a global model of the atmosphere. J. Atmos. Sci., 31, 43-83.

Manabe S. and Holloway J.L. 1975 The seasonal variation of the hydrologic cycle as simulated by a global model of the atmosphere. J. Geophys. Res., 80, 1617-1649.

Mintz Y. 1965 Very long term global integration of the primitive equations of atmospheric motion. WMO Technical Note No. 66, pp 141-167.

Miyakoda K. and Sirutis J. 1977 Comparative integrations of global models with various parametrized processes of sub grid-scale vertical transports: Descriptions of the parametrizations. Contrib. Atmos. Phys., 50, 445-487.

Phillips N.A. 1956 The general circulation of the atmosphere: a numerical experiment. Quart. J. R. Met. Soc., 82, 123-164.

Saker N.J. 1975 An 11 layer general circulation model. Met O 20 Technical Note II/30.

Slingo J.M. 1980 A cloud parametrization scheme derived from GATE data for use with a numerical model. Quart. J.R. Met. Soc., 106, 747-770.

Smagorinsky J. 1963 General circulation experiments with the primitive equations. I. The basic experiment. Mon. Weath. Rev., 91, 99-164.

Stone P.H., Chow S. and Quirk W.J. 1977 The July climate and a comparison of the January and July climates simulated by the GISS general circulation model. Mon. Weath. Rev., 105, 170-194.

Suarez M.J., Arakawa A. and Randall D.A. 1981 Simulation of the planetary boundary layer with the UCLA general circulation model. Preprints volume, Fifth conference on numerical weather prediction, American Met. Soc.

	INSTITUTION	LEVELS	RESOLUTION	REFERENCES
GFDL	Geophysical Fluid Dynamics Laboratory, Princeton, New Jersey.	9	250/500 km	Holloway and Manabe (1971) Manabe and Terpstra (1974)
		11	250 km	Manabe et al (1974) Manabe and Holloway (1975)
		18	500 km	Miyakoda and Sirutis (1977)
		9	(15, 21, 30)	Manabe et al (1979)*
UCLA	University of California, Los Angeles	3/6 6/12	$4^\circ \times 5^\circ$	Arakawa (1972) Arakawa and Lamb (1977)
NCAR	National Center for Atmospheric Research, Boulder, Colorado	6	$5^\circ \times 5^\circ$	Kasahara and Washington (1971)
		8	$5^\circ \times 5^\circ$	Washington et al (1979)*
RAND	The RAND Corporation	2	$4^\circ \times 5^\circ$	Gates and Schlesinger (1977)
OSU	Oregon State University	2	$4^\circ \times 5^\circ$	Schlesinger and Gates (1979)*
MO	Meteorological Office (Met O 20)	5	330 km	Gilchrist (1979)*
		11	220 km	Saker (1975) Carson and Cunnington (1979)
GISS	Goddard Institute for Space Studies (Both NASA)	9	$4^\circ \times 5^\circ$	Stone et al (1977)
GLAS	Goddard Laboratory for Atmospheric Sciences	9	$4^\circ \times 5^\circ$	Halem et al (1979)*
CCSAS	Siberian Academy of Sciences	3/5	$5^\circ/10^\circ$	Marchuk et al (1979)*
ANMRC	Australian Numerical Meteorology Research Centre	9	(15)	McAvaney et al (1979)*
AES	Canadian Climate Centre	5	(20)	Boer and McFarlane (1979)*

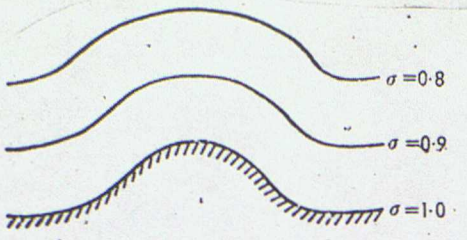

Sigma coordinate system in which $\sigma = p/p_s$ is the vertical coordinate, p_s being the pressure at the Earth's surface. The Earth's surface thus coincides with the coordinate surface $\sigma = 1$ and the other coordinate surfaces follow the terrain

Figure 8.1

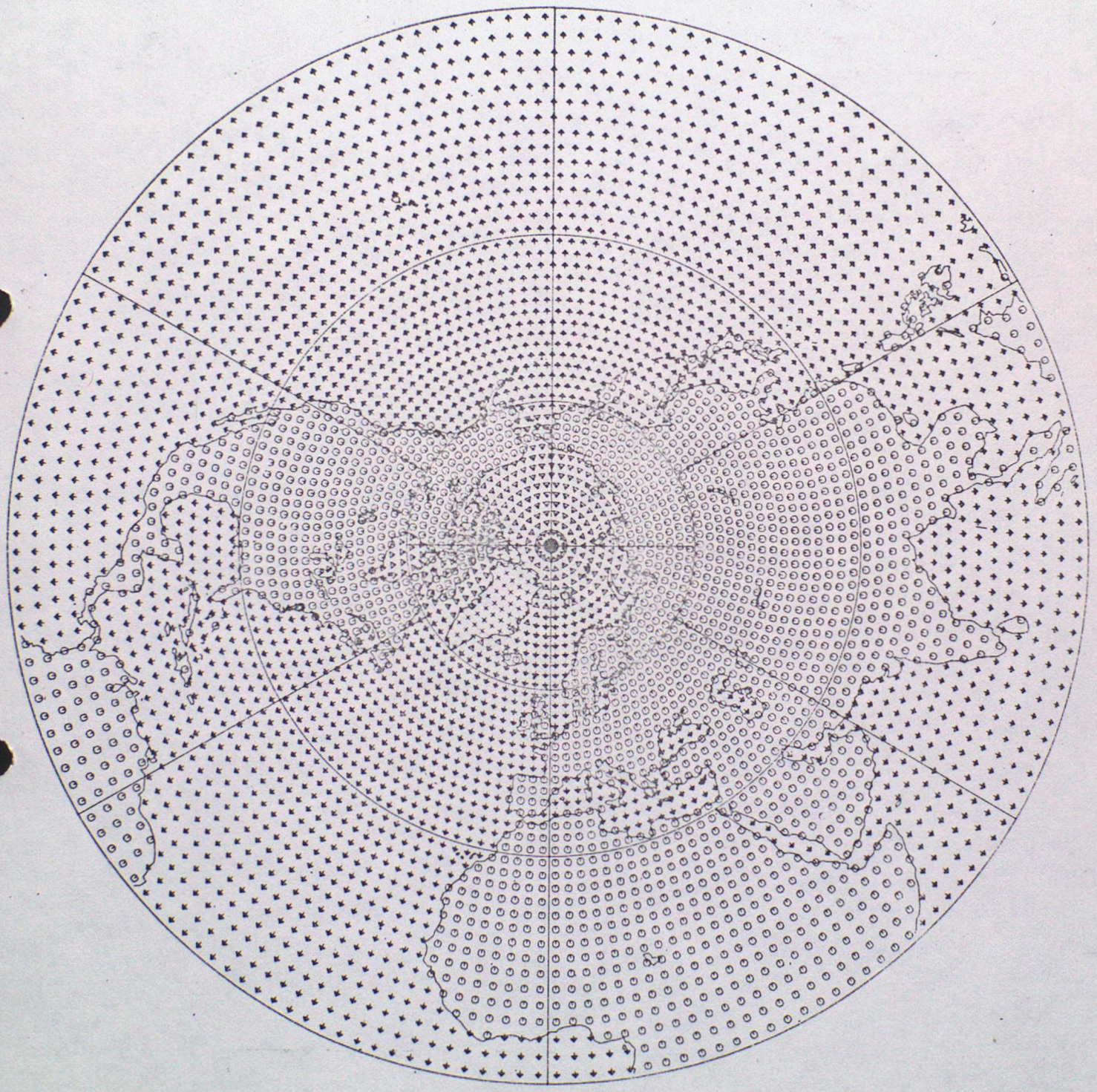

Figure 8.2 Northern hemisphere grid used by the 11-layer model in integrations on the IBM 360/195 computer. The symbols denote sea (⏚), sea-ice (⚠), land (⓪) and land with permanent ice cover (+). The sea-ice distribution is prescribed according to climatological information.

Observed

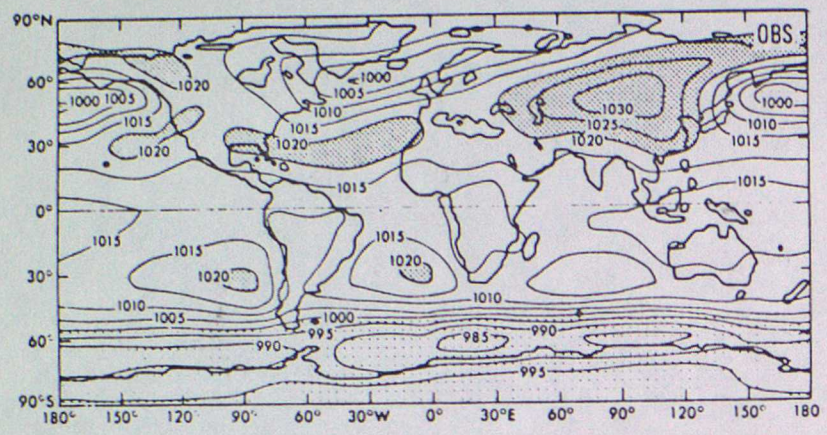

GFDL M30

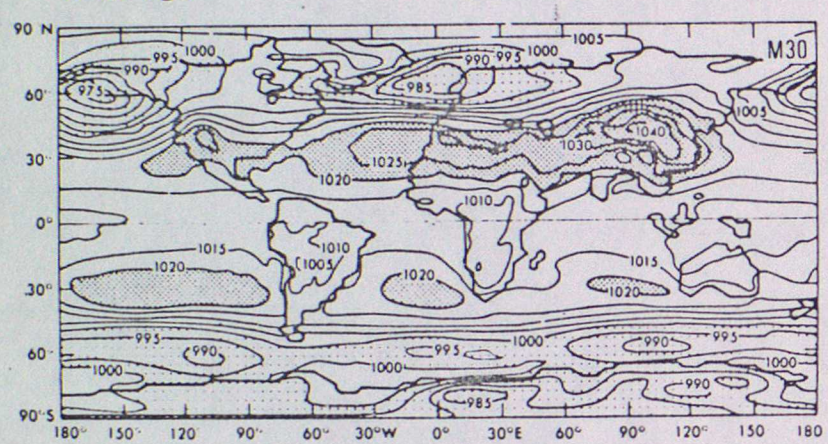

NCAR

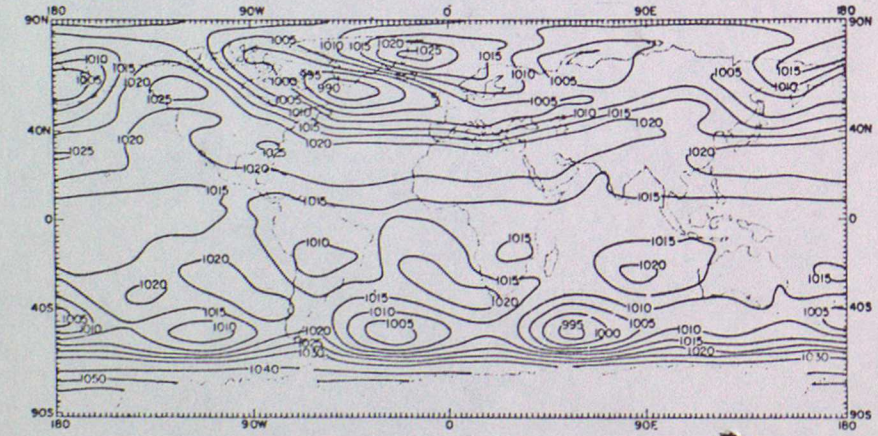

Met. Office 5-layer

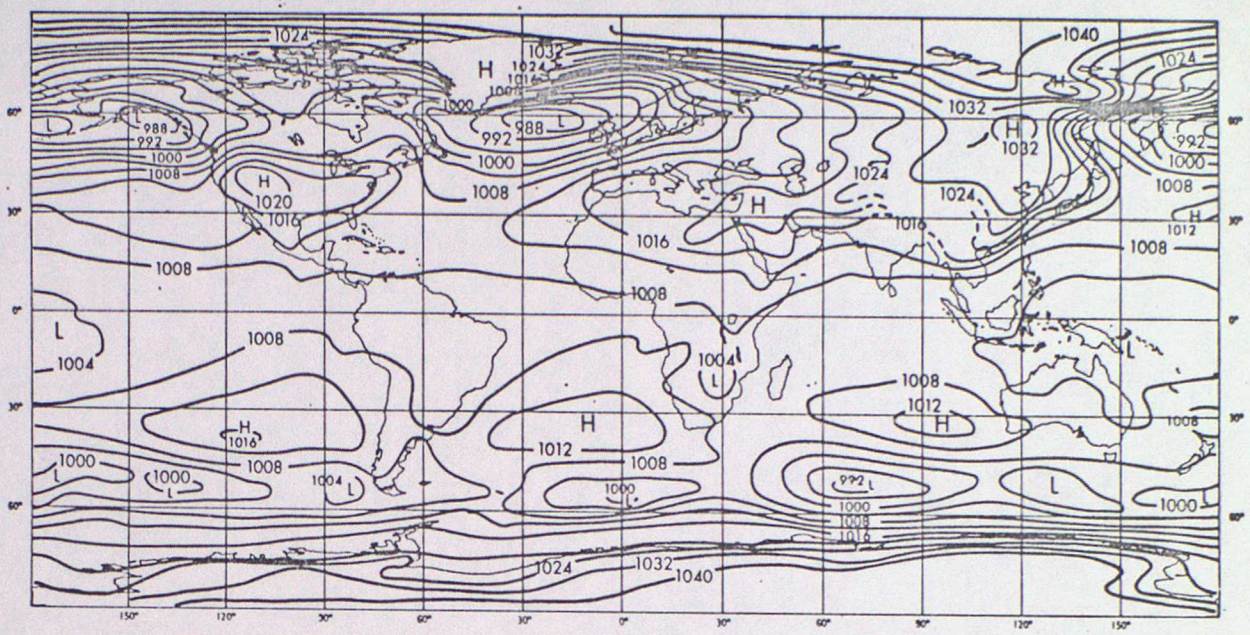

OSU

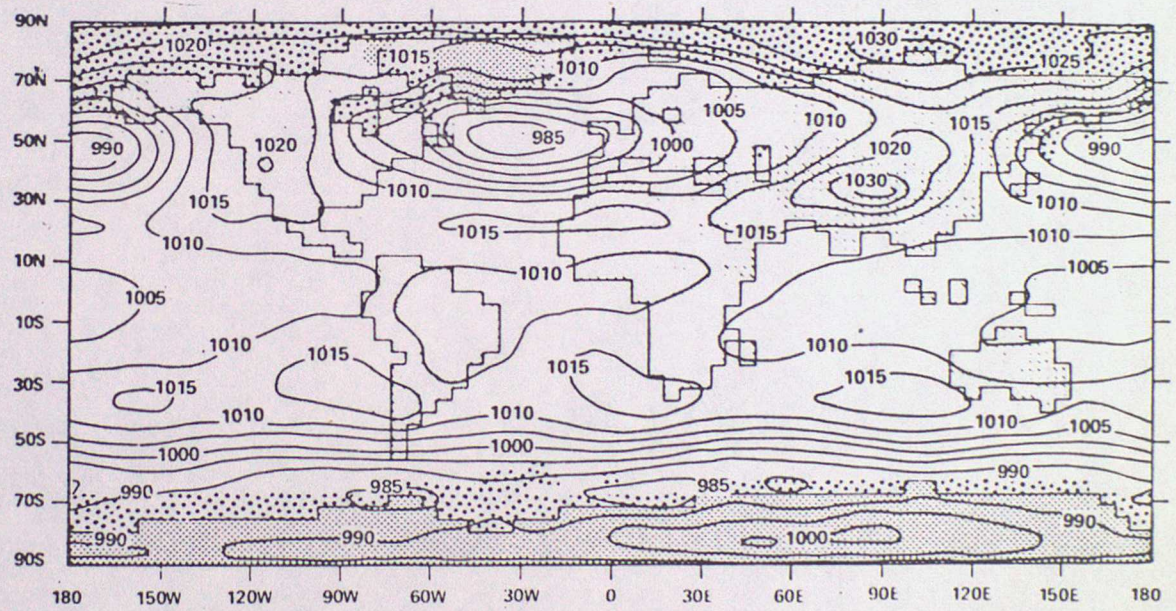

Figure 8.3 Comparison of the observed January PMSL with simulations by the GFDL M30, NCAR, Met. Office 5-layer and OSU models.

Observed

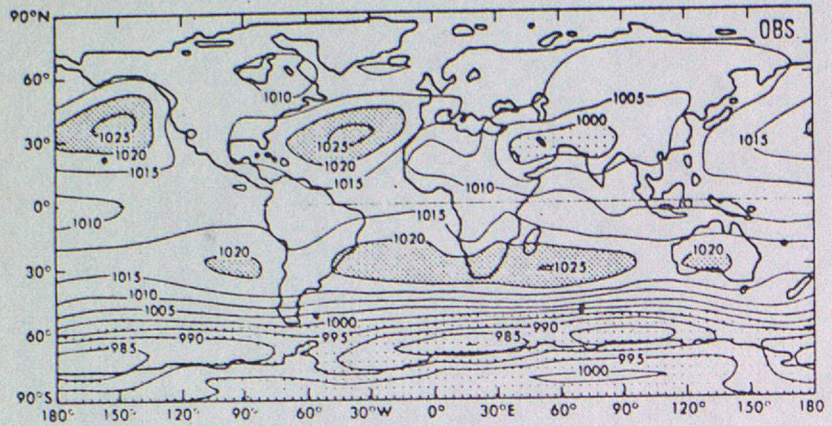

Met. Office 5-layer

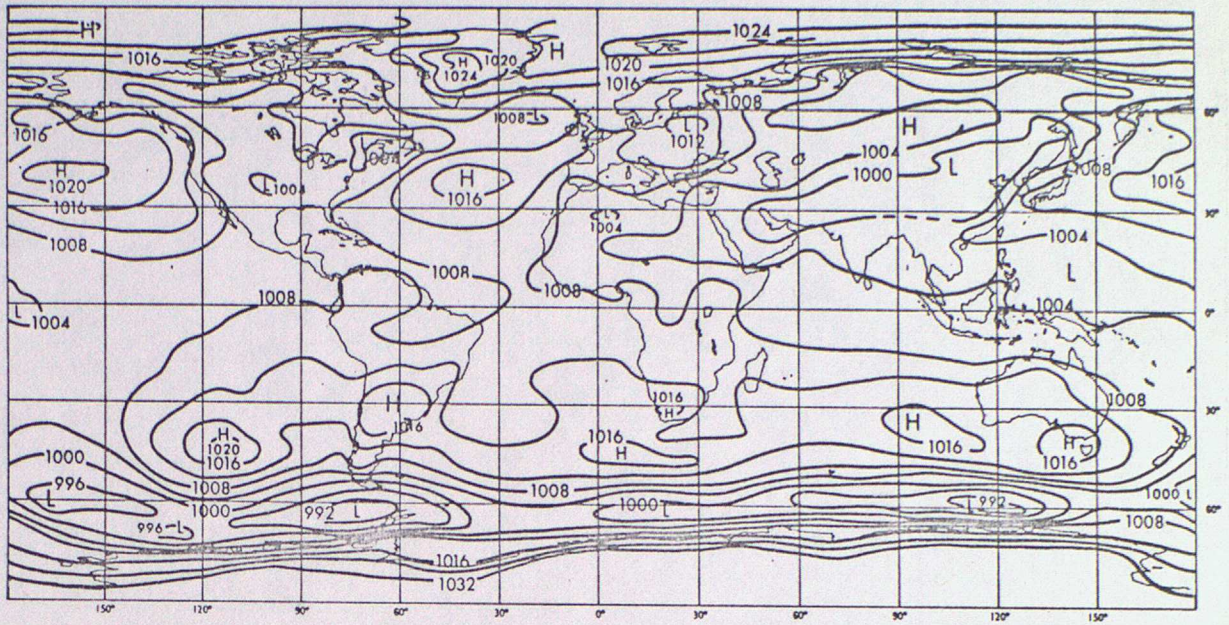

GFDL M30

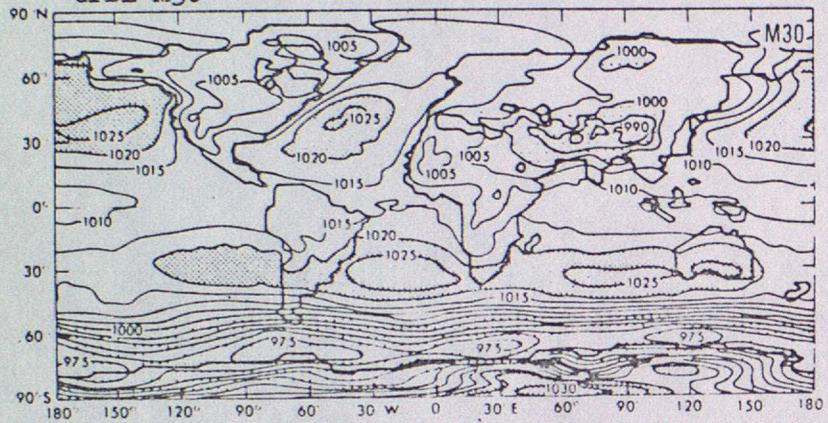

NCAR

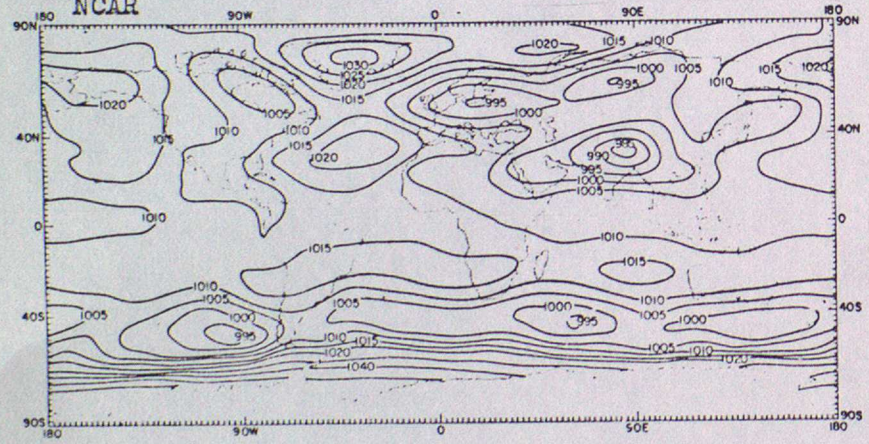

OSU

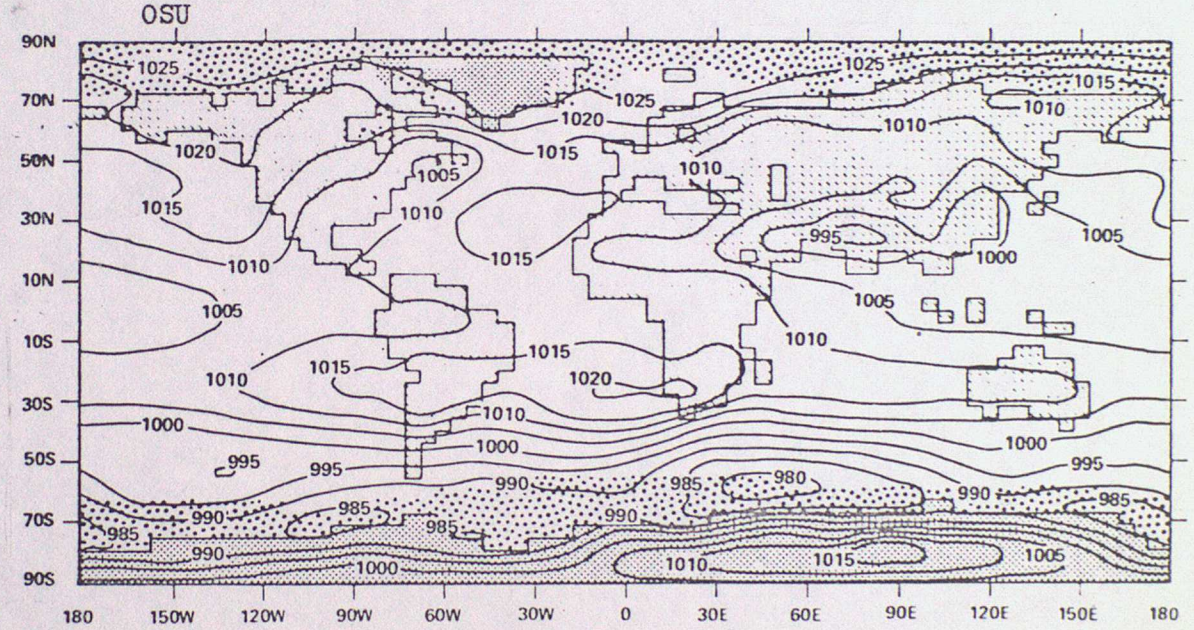

Figure 8.4 As for Figure 8.3 but July PMSL

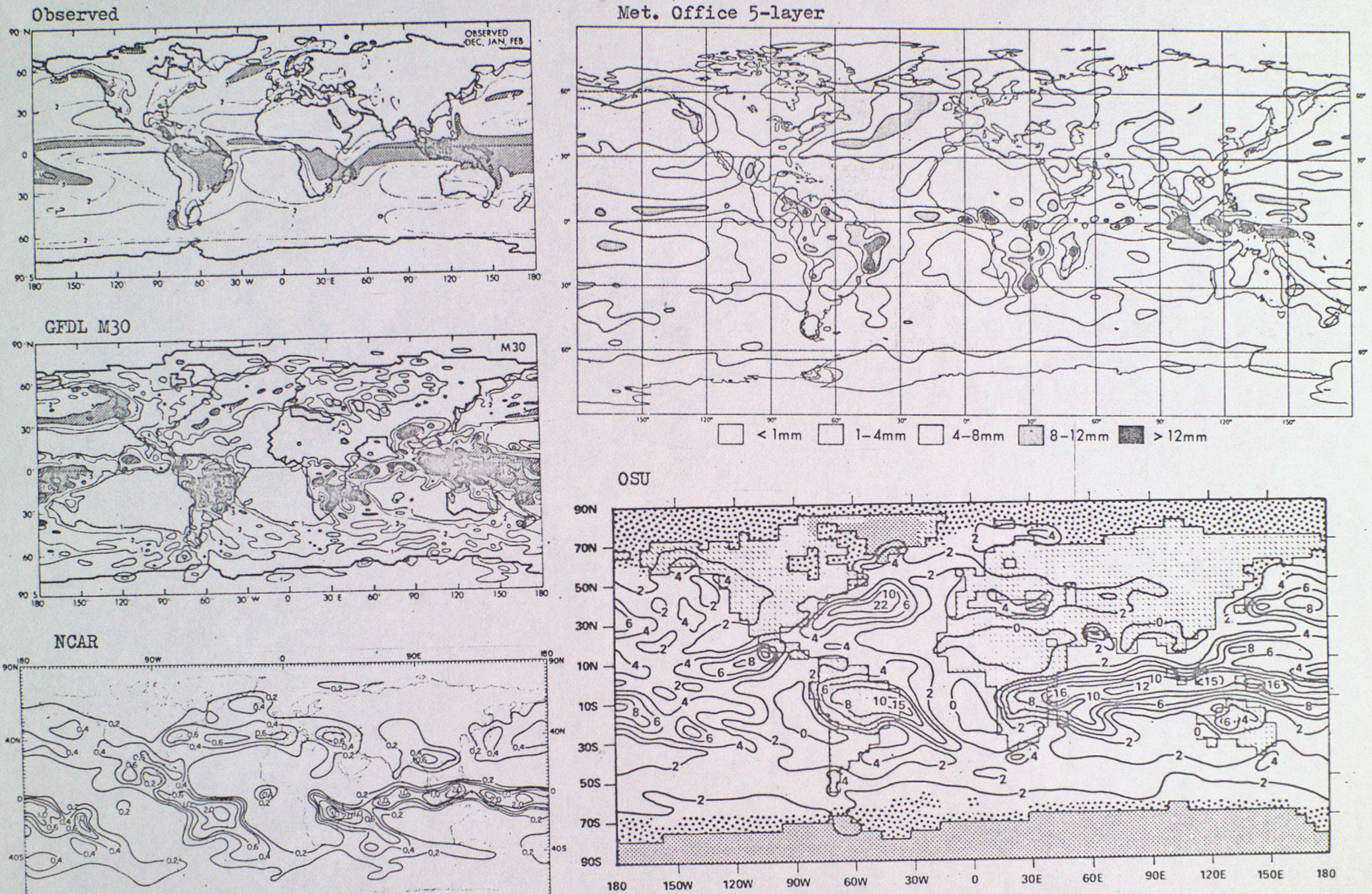

Figure 8.5 As for Figure 8.3 but January precipitation

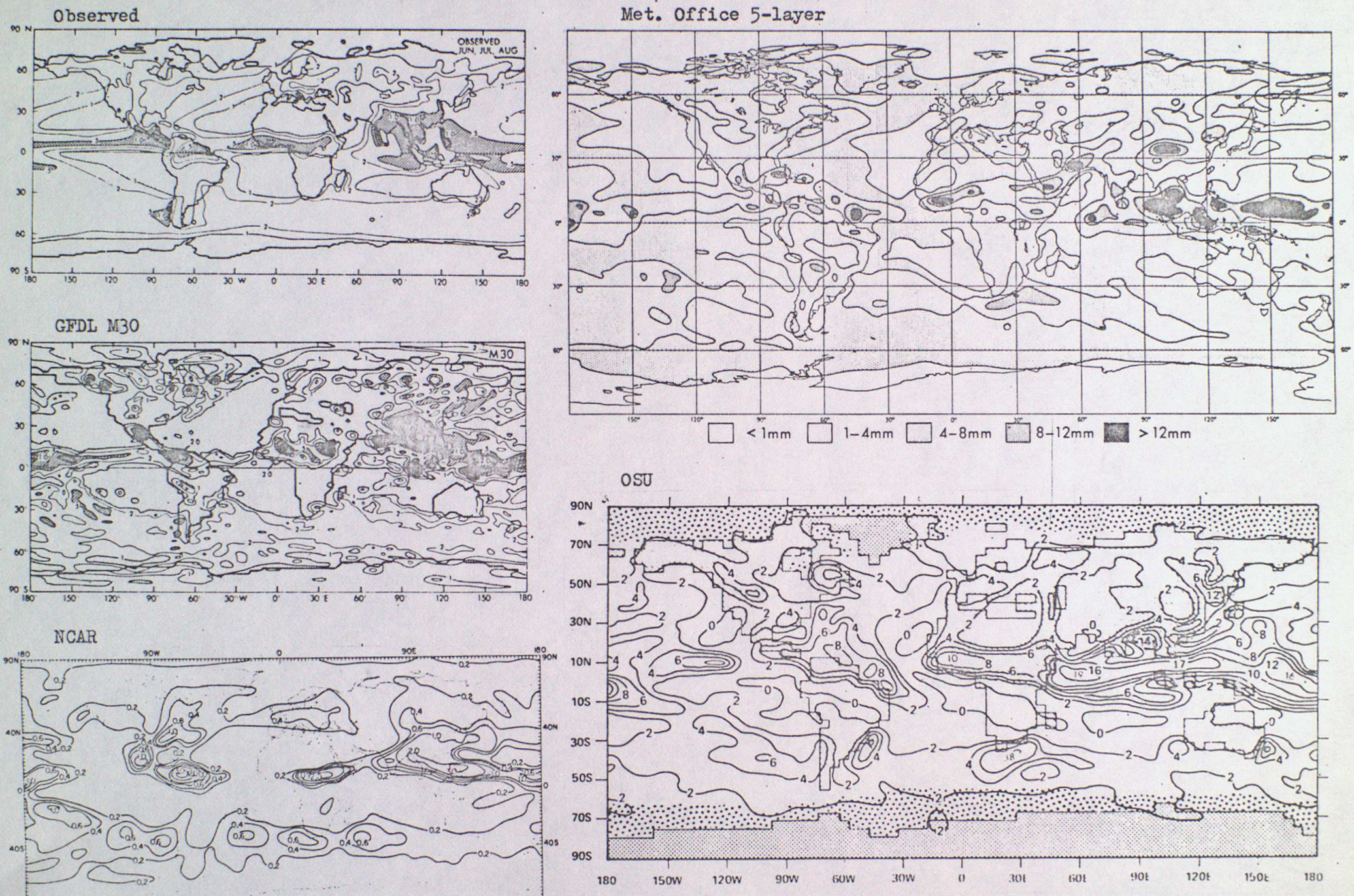

Figure 8.6 As for Figure 8.3 but July precipitation

Figure 8.7 5 LAYER MODEL PRESSURE AT MEAN SEA LEVEL JANUARY

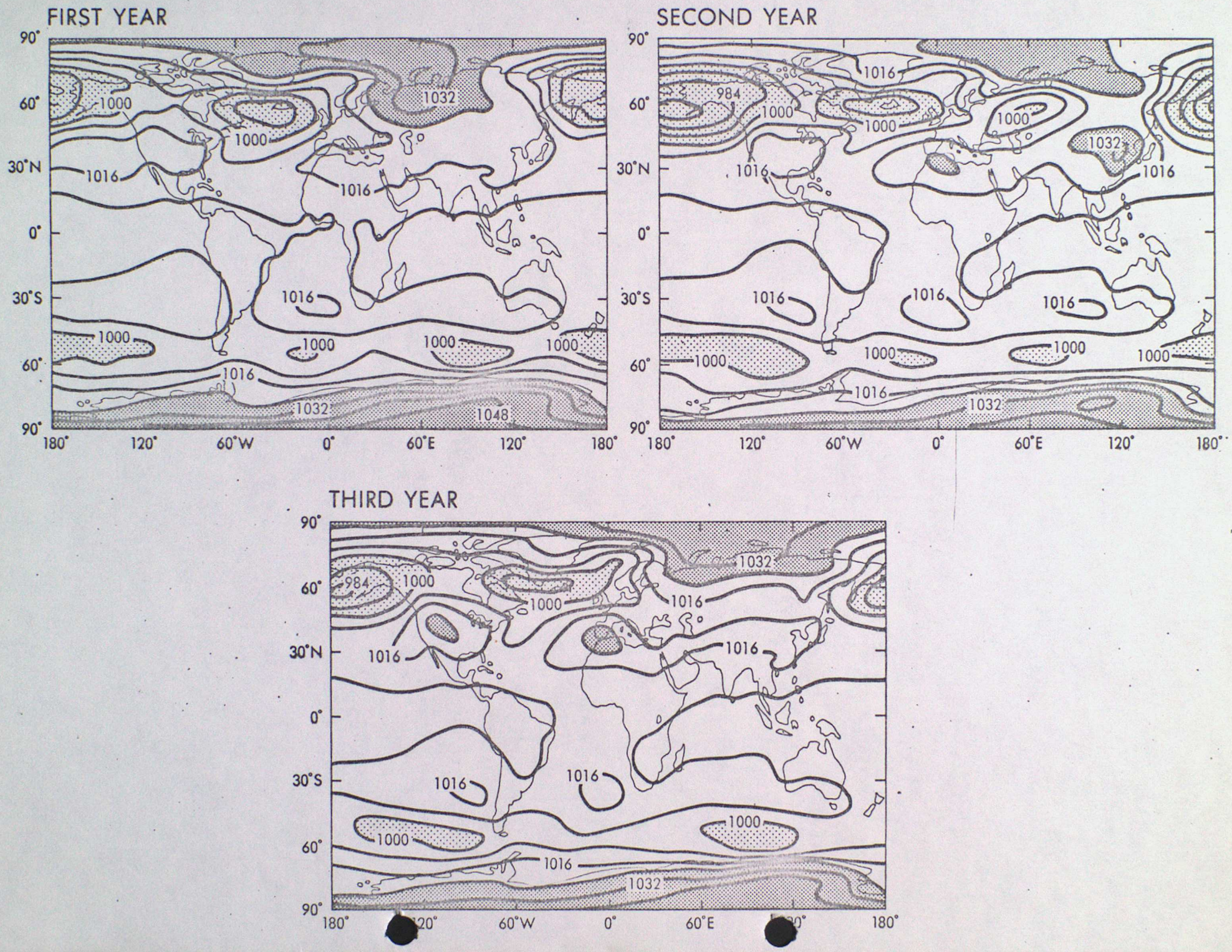

Figure 8.8

STANDARD DEVIATION OF SURFACE PRESSURE FOR WINTER MONTHS (DECEMBER, JANUARY, FEBRUARY) MILLIBARS

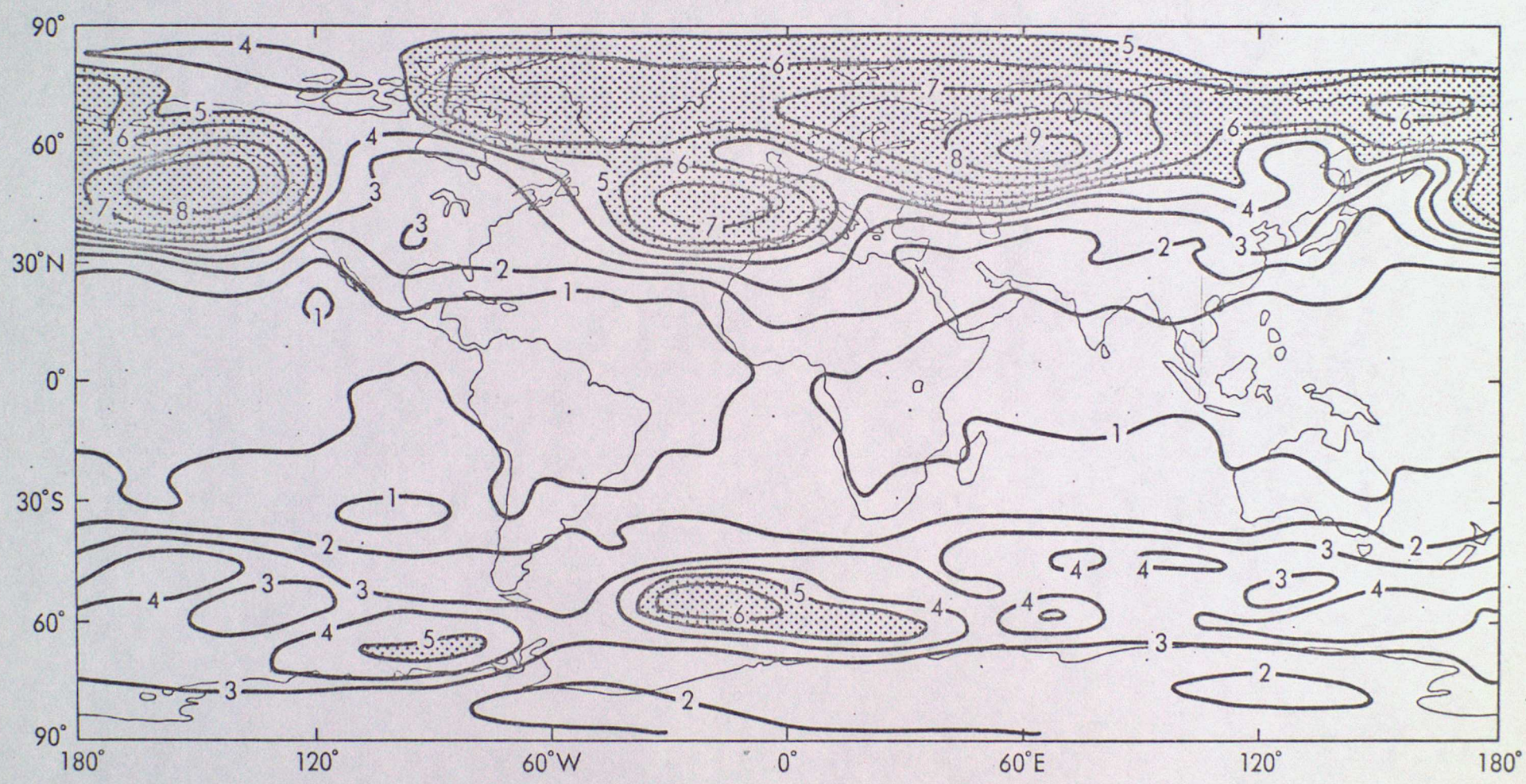

Figure 8.9

JANUARY STANDARD DEVIATION OF PRESSURE AT MEAN SEA LEVEL 1875—1974 (MILLIBARS)

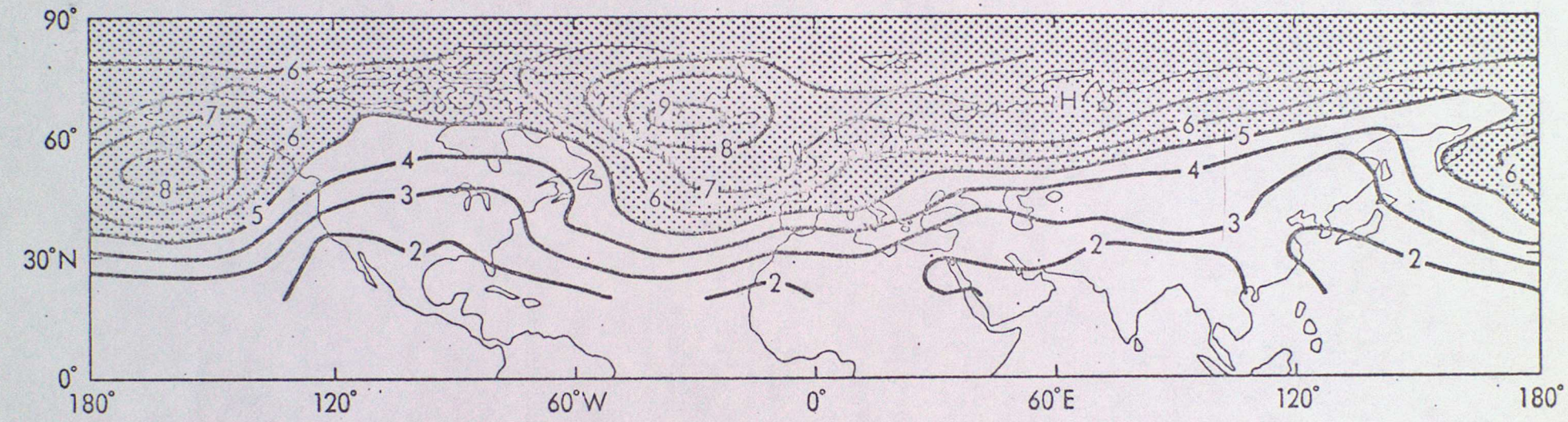

ADVANCED LECTURES 1982 - GENERAL CIRCULATION OF THE ATMOSPHERE

LECTURE 9 - General Circulation Models (II)

1. Introduction

In this final lecture of the series, some examples will be given of the use of GCMs in research on the general circulation. It will be noticed that most of the examples chosen are less concerned with the nature of the circulation itself than with its response and sensitivity to variations in the forcing mechanisms. This reflects the choice of subject outlined in the introduction to the previous lecture and the fact that many of the models discussed there have been developed primarily for use in climate change and sensitivity experiments. Although none of the topics will be developed in detail, they illustrate the wide variety of work carried out and in progress, with special emphasis on research performed in Met O 20.

2. Orographic forcing

The work reported by Mintz (1965) was carried out with a two level, global primitive equation model on a relatively coarse grid of 9° in longitude and 7° in latitude, the resolution being increased near the poles. The integration began with an atmosphere at rest relative to the surface and the external forcing was chosen to represent northern winter conditions. The bottom boundary was initially taken to be flat, but later in the run a realistic distribution of topography was suddenly introduced. The effect is described by Mintz in graphic terms;

"After the experiment with the smooth, mountainless globe, I changed the Φ_s data cards, at a given instant in the middle of a run, and in this way suddenly raised into place the large-scale mountain systems of the earth. As soon as this was done the air began to pour down the mountain sides (as would water down the sides of an island emerging from the sea), producing large gravity waves. After some days these large external gravity waves died out and only the familiar meteorological motions remained, as the synoptic charts will show."

One perhaps surprising result which Mintz found was that, despite the large differences in forcing between the two experiments, the globally averaged kinetic energy of the flow showed no discernable change. Manabe and Terpstra (1974) carried out a much more comprehensive study which illuminates this and other points. They performed integrations for mean January forcing, using a 250 km resolution 9 layer model, both with and without mountains. Although the total eddy kinetic energy did not change significantly, the introduction of mountains transferred energy from the transient (TR) to the stationary component (ST), as shown by the latitudinal distribution of the energy terms (Figure 9.1) and by the ratio of the two components in each integration (Figure 9.2). The importance of the stationary component in the meridional transport of heat, absolute angular momentum and water substance was also increased at the expense of the transient component. By comparing the integrations with observations at different levels, Manabe and Terpstra also showed that the effects of thermal forcing were most obvious in the lower troposphere, while orographic forcing dominated at higher levels, as had been suggested by Bolin (see Lecture 4). This result is demonstrated in Figure 9.3. The troughs in the 1000 mb geopotential height were formed 20°-30° downstream of the major heat sources in the north-western parts of the Atlantic and Pacific oceans. At 500 mb, however, only the integration with mountains included was able to reproduce the observed amplitude and position of the major troughs and ridges. An increased probability of cyclogenesis was shown to exist in the lee of the major mountain ranges, which

were also responsible for a less zonal distribution of precipitation. In many respects, the simulation was less zonal and more realistic when the effect of mountains was included.

3. Effect of sea surface temperature anomalies

Thermal forcing by the oceans is an important factor in determining the distribution of mean sea level pressure, and one would therefore expect that variations or anomalies in sea surface temperature (SST) would be reflected in atmospheric changes. This is a good example of an area where observational and GCM studies have complemented one another, correlations between the observed SST and atmospheric anomalies being used to develop hypotheses which can be tested by GCM integrations. Namias (1959) observed a correlation between mid-latitude SST anomalies and large-scale circulation changes and such associations have also been studied with a view to improving long-range weather forecasts (eg Ratcliffe and Murray 1970). The atmospheric response to mid-latitude SST anomalies is relatively weak, however, and to obtain a signal above the inherent variability the modellers have either composited the results of several experiments (eg Rowntree 1979) or applied a very large anomaly (12 deg C) with the hope that the response to a more reasonable perturbation is similar (eg Chervin et al 1980). In general, a warm SST anomaly leads to a direct thermal circulation with pressure falls and increased vertical motion and precipitation in the vicinity of the anomaly, although these studies show that the response is very dependent on the scale, position and magnitude of the perturbation.

Mid-latitude SST anomalies are less important than those in tropical regions, whose effects may be felt well away from the source. During the severe winter of 1962/3 in north-west Europe, for example, SST anomalies of about +2 deg C were present in an extensive area of the tropical east Atlantic (Figure 9.4), at the same time as large PMSL anomalies were observed in middle latitudes (Figure 9.5). Rowntree (1976) used the SST data in integrations with versions of the 5-layer model and in all cases obtained falls in surface pressure over the anomaly, extending at least to 60°N. In middle latitudes the magnitude of the response was up to about 7 mb and in one experiment the pressure anomaly pattern was similar to that observed, with large pressure rises in the region north of the UK (Figure 9.6).

One of the best known examples of the effect of ocean-atmosphere interaction is the El Niño phenomenon. Sea surface temperatures off the western coast of South America are normally much colder than the zonal mean values, because the south-easterly trade winds drive an Ekman drift of the surface waters away from the coast, leading to upwelling of colder water. In El Niño years, weakening of the trades leads to anomalously warm water off the western coasts of Peru and Chile, as for example in 1972 (Figure 9.7), and a large increase in precipitation. Rowntree (see 1979 and references therein) demonstrated the local increase in precipitation in GCM integrations (Figure 9.8) and confirmed the hypothesis of Bjerknes that the warmer water was also responsible for significant changes in the strength and position of the Aleutian surface low (Figure 9.9).

4. Surface albedo and soil moisture experiments

During the last few years there has been an increased awareness of the importance of land surface processes in the general circulation, and in particular the role of albedo and soil moisture content anomalies. Some of the stimulus came from the persistent drought in the Sahel region of North Africa and Charney's suggestion that this was the result of a complex positive feedback mechanism, whereby lack of rainfall or over-grazing leads to a reduction in vegetation and hence an increase in the surface albedo. The resulting deficit in the radiation balance encourages subsidence in the overlying air, which leads to additional

drying and hence persistence of the arid conditions (Charney 1975). Walker and Rowntree (1977) investigated the importance of soil moisture in a limited area tropical version of the 11-layer model, for a zonally symmetric approximation to North Africa. When soil moisture contents were initialized as zero over the desert region, the aridity persisted throughout the integration. Although disturbances did enter the region, they carried too little moisture to remove the soil moisture anomaly. On the other hand, when the desert was replaced by moist land and the integration repeated, from the same initial conditions, the increased moisture availability led to increased rainfall and the disturbances helped to maintain the moist conditions.

The persistence of such anomalies has recently been studied by Carson and Sangster (1981), in longer integrations with a low resolution version of the 5-layer model. Figure 9.10 shows two 30-day mean charts of the differences in precipitation rate between two experiments in which the soil moisture content was set to either zero or 15 cm initially and thereafter was allowed to interact with the rest of the model. The integrations converge, as expected, but they do so only slowly and even after 110 days there are persistent differences over a large fraction of the land area. The fact that the hydrological cycle takes such a long time to reach equilibrium and the difficulty of providing realistic initial conditions shows that meaningful statistics which truly reflect the climatology of the model can only be obtained after long periods. In practice, this means that the model must be integrated through several years of simulation and the results from the first year or so discarded. This is demonstrated in the analysis of such an integration with the 5-layer model performed by Mitchell (1981). It should also be remembered that in most GCMs the treatment of soil moisture is very crude, and more complex (though not necessarily more realistic) methods have been proposed by Deardorff (1978) and adopted in the NCAR model, and by Lin et al (1978) for inclusion in the GLAS model.

Carson and Sangster also examined the effect of changing the snow-free land albedo from 0.3 to 0.1 (Figure 9.11). A decrease in albedo produces increased shortwave absorption at the surface, which accentuates the land-sea thermal contrast. As a result, surface pressure decreases by up to 8 mb and the rainfall rate increases markedly over the land, with changes in the opposite sense over the oceans. The sensitivity of the modelled circulation to the surface albedo demonstrates the need for a realistic geographical specification of this parameter, which is now being developed.

5. Clouds and radiation

In many experiments with GCMs, the cloud amounts have been specified according to a zonal-mean climatology. This ensures that at least the overall radiative effects of clouds on the general circulation are represented and avoids the many problems associated with trying to predict reasonable cloud distributions from the model variables. In order to relax this constraint and so examine the role of clouds in more detail, however, considerable effort is being spent on cloud prediction schemes. The effect of clouds on the earth's radiation budget is a delicate balance between the so-called 'albedo' and 'greenhouse' effects. The high albedo of clouds means that they reflect more shortwave radiation back to space than surrounding cloud-free areas and hence act so as to cool the system. In the longwave spectral region, however, clouds are optically thick and so replace the upwelling longwave flux by that from the cooler cloud top, so they enhance the greenhouse effect and warm the system. Herman et al (1980) performed sensitivity studies with the GLAS model and concluded that the albedo effect is slightly the greater, so the net effect of clouds is a cooling influence. Using the same model, Shukla and Sud (1981) compared two integrations, the first with model-generated clouds and the second with a fixed geographical distribution obtain from the first integration and having the same zonally-averaged amounts

of cloud. In the second run, the fixed zonally asymmetric radiative heating led to a large increase in the kinetic energy of the stationary eddies, with a smaller reduction in the transient eddy kinetic energy. In an experiment with the GFDL M21 spectral model, Meleshko and Wetherald (1981) obtained complementary results; a July integration with a fixed cloud distribution increased the land-sea contrast and also enhanced the aridity of the desert regions. Wetherald and Manabe (1980) used a sector model and confirmed the compensation between the albedo and greenhouse effects, which reduces the sensitivity of all these models to changes in cloud amount.

Cloud schemes are currently under development in Met O 20, based on the work of Slingo (1980). Integrations have been carried out to assess the realism of the cloud fields and compare with climatological data. Wilderspin (Figure 9.12) has performed both winter and summer integrations with the 11-layer model starting from FGGE data. The cloud distribution is broadly satisfactory and regions such as the ITCZ, the areas of persistent sub-tropical stratocumulus and mid-latitude cyclones may be seen, but there is a tendency for cloud amounts to be too high. The cloud scheme was also incorporated into the 5-layer model and Wilson (1981) has performed a similar analysis in that model. Figure 9.13 shows an example of the model's simulation of the diurnal cycle of surface and near-surface variables for a point in the western Sahara in July. In the early hours before dawn, there is little or no cloud and the longwave cooling leads to relatively low surface temperatures and a shallow boundary layer. The sensible heat flux is directed downwards towards the cool surface and dew is forming (ie evaporation is negative). As soon as the sun rises, the strong shortwave surface warming increases the surface temperature markedly and with a rapid increase in the sensible heat flux the boundary layer deepens considerably. The warming of the lowest atmospheric level (σ = 0.9) leads to a decrease in the relative humidity, inhibiting the formation of stratiform cloud, but the strong convective activity and associated latent heat flux produces a maximum convective cloud cover of over 30% in the early afternoon. Later in the day the surface temperature falls and as the boundary layer collapses the variables return to their nocturnal values. It will be noticed that during this period advective changes are small and the development is dominated by the local effects in the diurnal cycle.

In the first lecture it was pointed out that global observations through a complete annual cycle can be used to derive not only the annual mean poleward atmospheric energy flux but also the flux transported by the oceans. In the final example, Figures 9.14 and 9.15 illustrate how similar calculations can be performed with a GCM (Slingo 1982). The terms were derived from a single year of the 5-layer model multi-annual integration and compare favourably with previous conventional estimates. Unlike the earlier work based on observations, the model results do not suffer from poor spatial resolution in the southern hemisphere, although they do of course depend on the ability of the model to develop a realistic circulation in response to the prescribed sea surface temperatures.

References

Carson, D J and Sangster, A B (1981) The influence of land-surface albedo and soil moisture content on general circulation model simulations. GARP NEP Report No 2, 5.14-5.21.

Charney, J G (1975) Dynamics of deserts and droughts in the Sahel. Quart. J.R. Met. Soc., 101, 193-202.

Chervin, R M, Kutzbach, J E, Houghton, D D and Gallimore, R G (1980) Response of the NCAR General Circulation Model to prescribed changes in ocean surface temperature. Part II: Mid-latitude and sub-tropical changes. J. Atmos. Sci., 37, 308-332.

Deardorff, J W (1978) Efficient prediction of ground surface temperature and moisture, with inclusion of a layer of vegetation. J. Geophys. Res., 83, 1889-1903.

Herman, G F, Wu, M C and Johnson, W T (1980) The effect of clouds on the earth's solar and infra-red radiation budgets. J. Atmos. Sci., 37, 1251-1261.

Lin, J D, Alfano, J and Bock, P (1978) Documentation of a ground hydrology parametrization for use in the GISS atmospheric GCM. NASA Contract Report CR-158766.

Manabe, S and Terpstra, T B (1974) The effects of mountains on the general circulation of the atmosphere as identified by numerical experiments. J. Atmos. Sci., 31, 3-42.

Meleshko, V P and Wetherald, R T (1981) The effect of a geographical cloud distribution on climate: A numerical experiment with an atmospheric general circulation model. J. Geophys. Res., 86, 11995-12014.

Mintz, Y (1965) Very long-term global integration of the primitive equations of atmospheric motion. WMO Tech Note No 66, 141-167.

Mitchell, J F B (1981) The hydrological cycle as simulated by an atmospheric general circulation model. Met O 20 Technical Note II/169.

Namias, J (1959) Recent seasonal interactions between North Pacific waters and the overlying atmospheric circulation. J. Geophys. Res., 64, 631-646.

Ratcliffe, R A S and Murray, R (1970) New lag associations between North Atlantic sea temperature and European pressure applied to long-range weather forecasting. Quart. J.R. Met. Soc., 96, 226-246.

References continued

Rowntree, P R (1976) Response of the atmosphere to a tropical Atlantic ocean temperature anomaly. Quart. J.R. Met. Soc., 102, 607-625.

Rowntree, P R (1979) The effects of changes in ocean temperature on the atmosphere. Dynamics of Atmospheres and Oceans, 3, 373-390.

Shukla, J and Sud, Y (1981) Effect of cloud-radiation feedback on the climate of a General Circulation Model. J. Atmos. Sci., 38, 2337-2353.

Slingo, Julia M (1980) A cloud parametrization scheme derived from GATE data for use with a numerical model. Quart. J.R. Met. Soc., 106, 747-770.

Slingo, Julia M (1982) A study of the earth's radiation budget using a general circulation model. Quart. J.R. Met. Soc., 108, (April issue).

Walker, Julia M and Rowntree, P R (1977) The effect of soil moisture on circulation and rainfall in a tropical model. Quart. J.R. Met. Soc., 103, 29-46.

Wetherald, R T and Manabe, S (1980) Cloud cover and climate sensitivity. J. Atmos. Sci., 37, 1485-1510.

Wilson, C A (1981) Cloud parametrization in the 5-level general circulation model. GARP NEP Report No 2, 5.22-5.26.

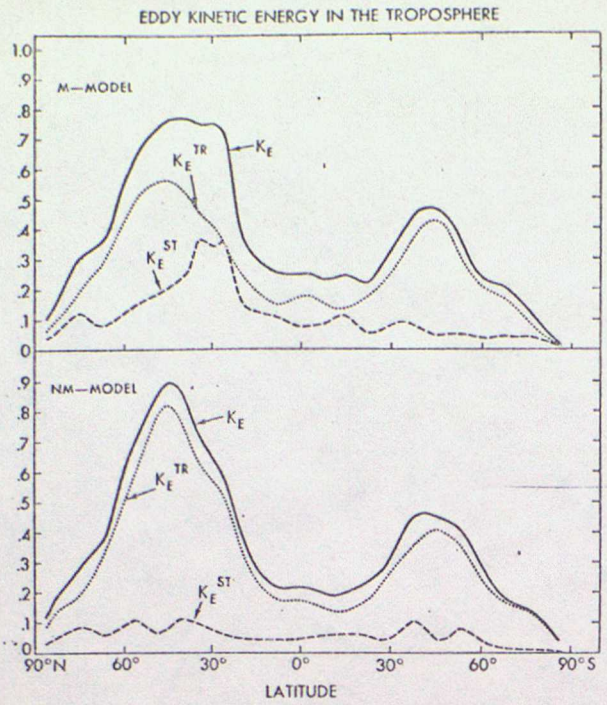

The latitudinal distribution of K_E (solid line), K_E^{ST} (dashed line) and K_E^{TR} (dotted line) integrated over the model troposphere in units of 100 J cm^{-2}. The troposphere is defined as the part of the model atmosphere below 240 mb. Top, the M-model; bottom, the NM-model.

Figure 9.1

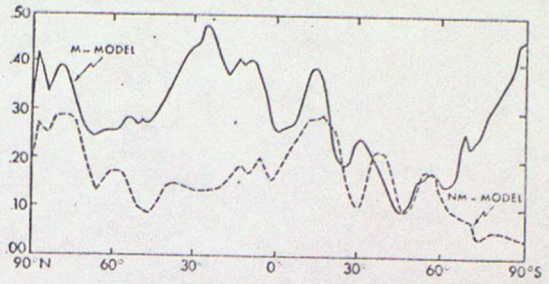

The latitudinal distribution of the ratio of K_E^{ST} to K_E^{TR}: M-model, solid line; NM-model, dashed line. (Here, K_E^{ST} and K_E^{TR} represent the mass integrals over the model tropospheres).

Figure 9.2

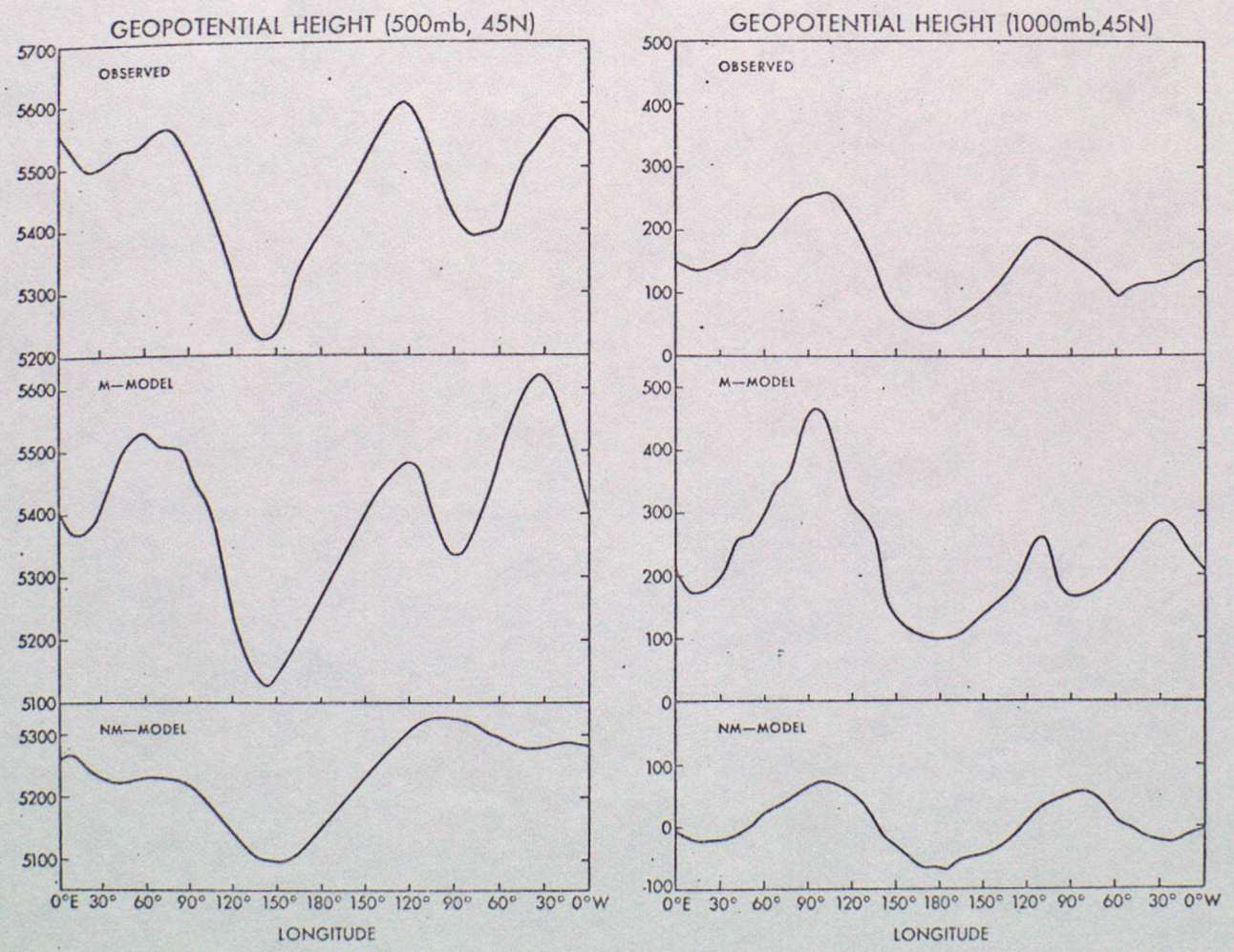

Longitudinal variation of the time-mean geopotential height (geopotential meters) of 500- and 1000-mb levels at 45N: top, observed (Oort and Rasmusson, private communication); middle, the M-model; bottom, the NM-model.

Figure 9.3

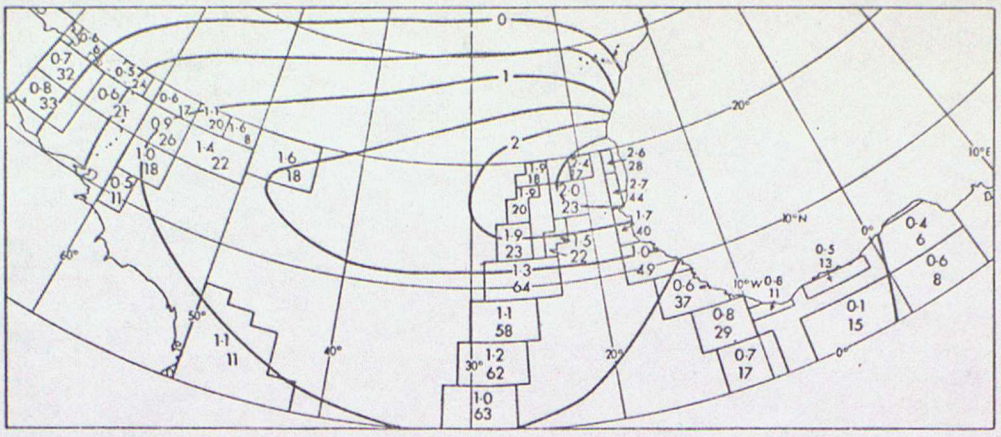

Sea surface temperature anomalies (deg C) for January 1963 (see text). Anomalies averaged for areas shown are plotted with number of observations below. Solid lines show anomaly analysis used in experiments A1, A2, A3.

Figure 9.4

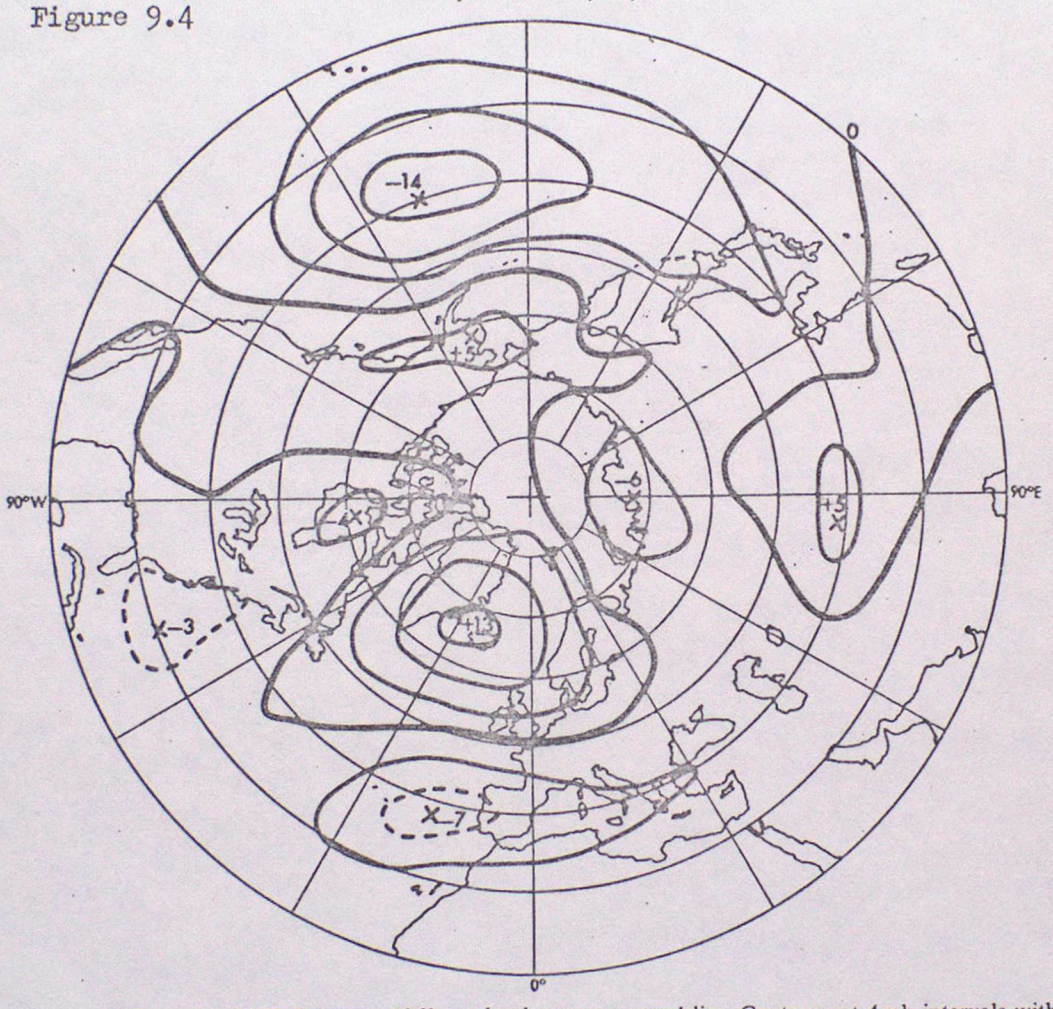

December 1962–February 1963 sea level pressure anomalies. Contours at 4 mb intervals with zero line heavy and some dashed 2 mb interval contours.

Figure 9.5

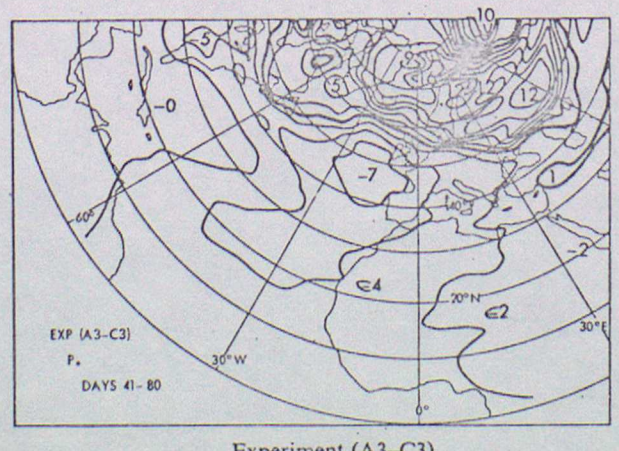

Experiment (A3–C3)

Day 41–80 mean differences in surface pressure obtained with Atlantic warming. Contours at 2 mb intervals with zero line heavy.

Figure 9.6

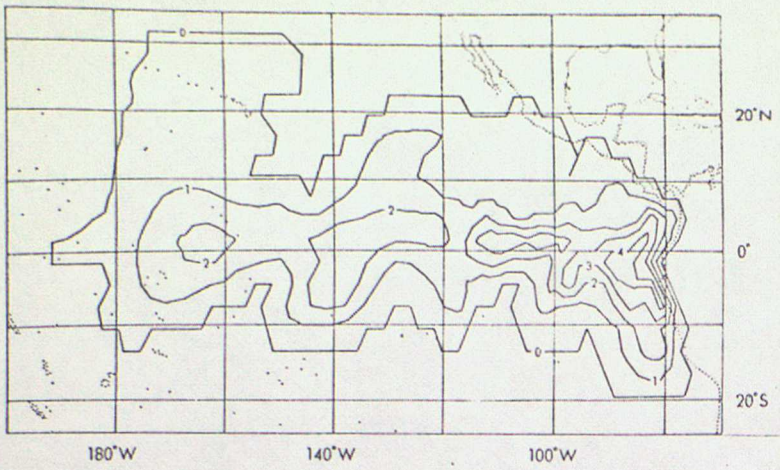

Figure 9.7 East Pacific SST anomaly in July 1972 associated with El Niño phenomenon

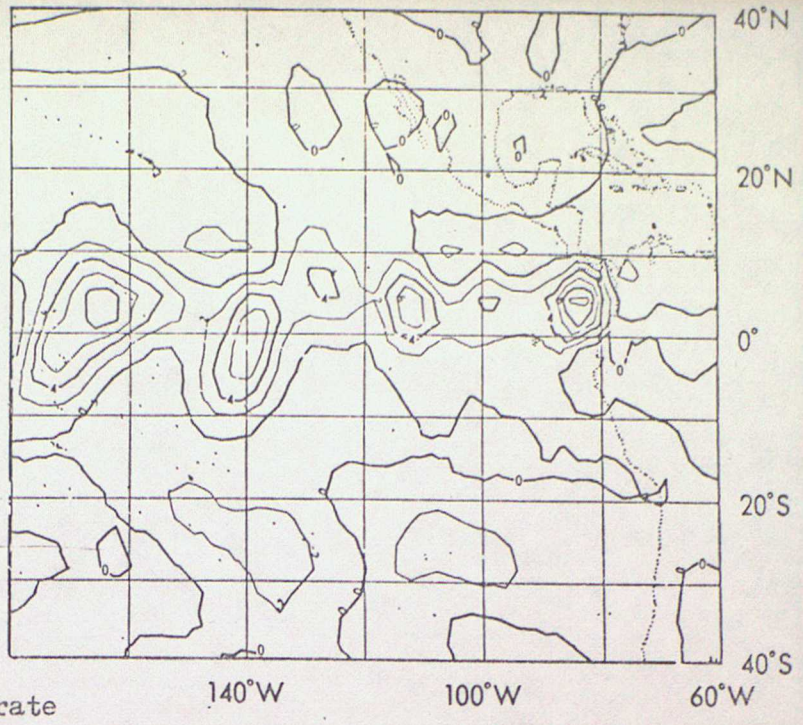

Figure 9.8 Computed change in precipitation rate (mm/day) due to SST anomaly

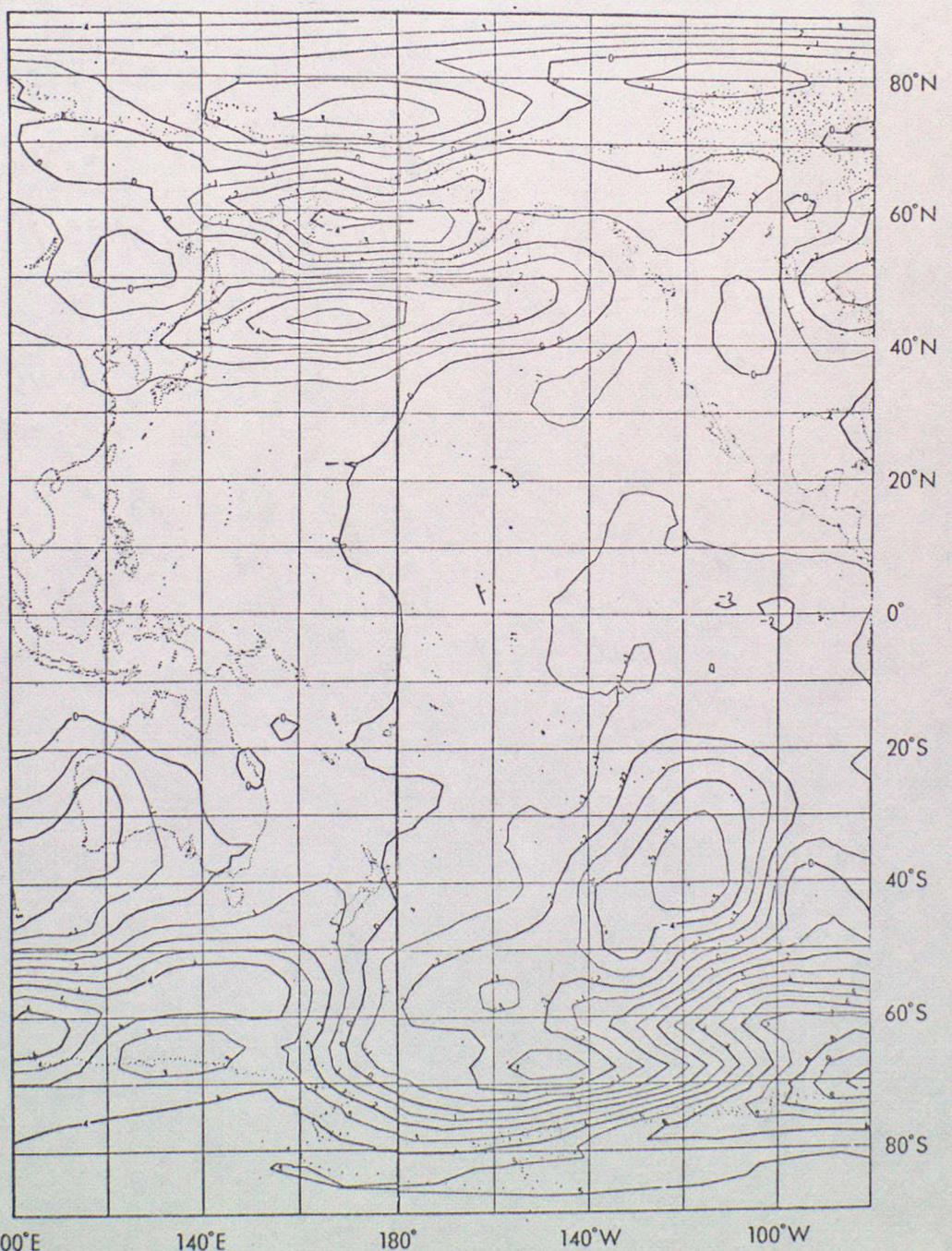

Figure 9.9 Computed change in surface pressure (mb) due to SST anomaly

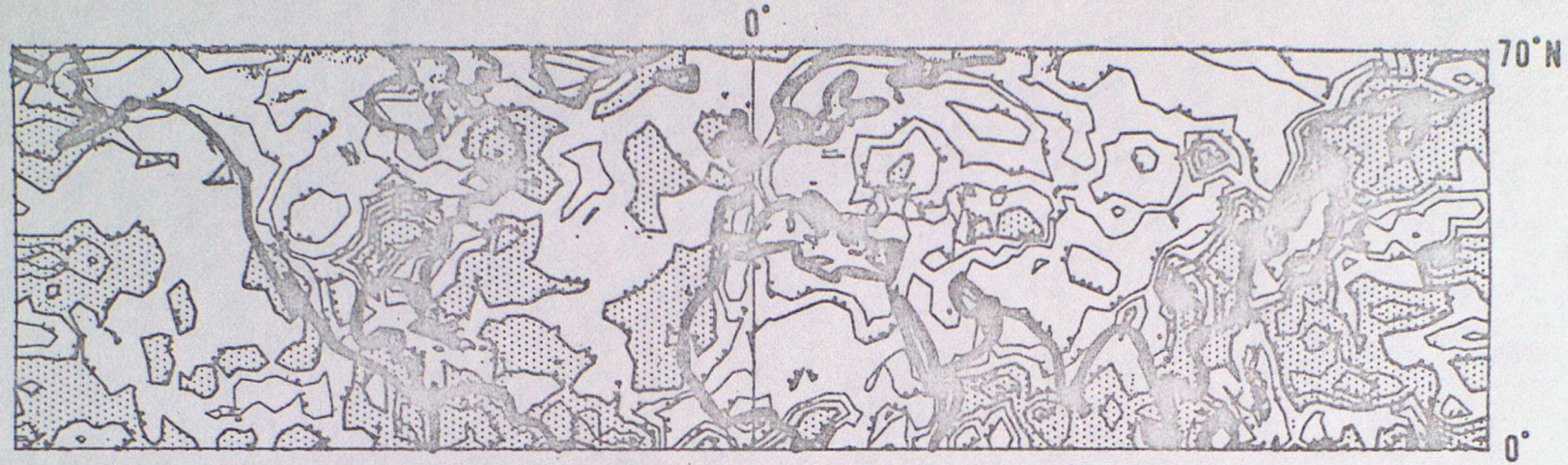

(a) Day 21-50 mean. "Initially wet soil" case – "Initially dry soil" case.

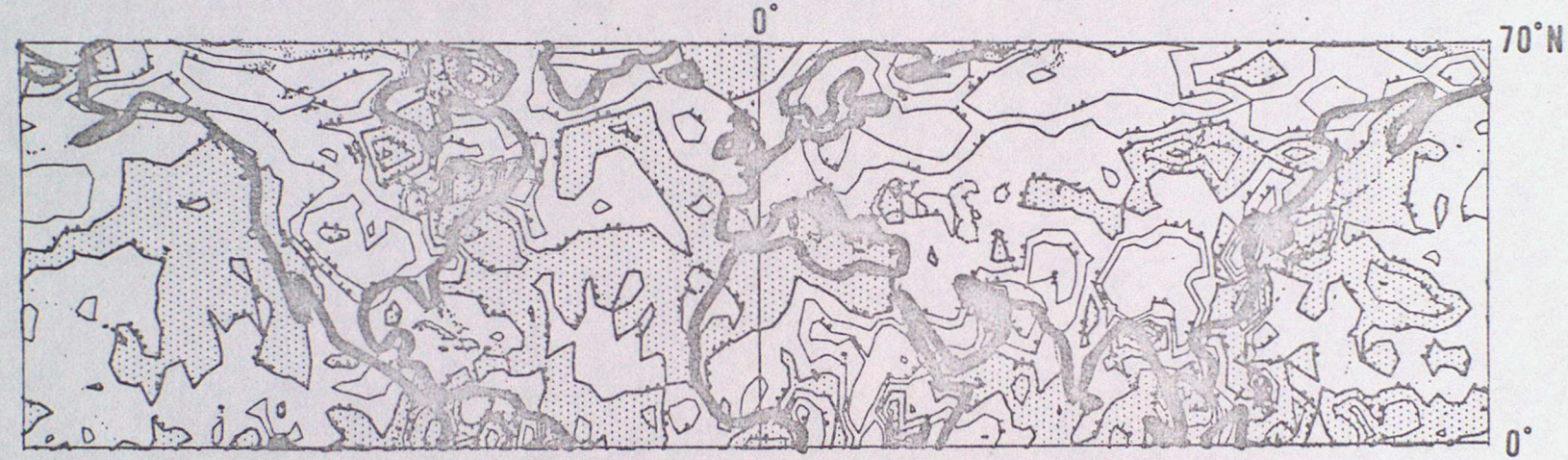

(b) Day 81-110 mean. "Initially wet soil" case – "Initially dry soil" case.

Two 30-day mean differences in the rainfall rates (mm day^{-1}) between two low-resolution 5-layer model integrations which had initial soil moisture contents universally 15 cm and 0 cm, respectively. Both experiments had fixed July radiative conditions, fixed snow-and ice-free land albedo of 0.2 and interactive soil moisture. The rainfall rates are GREATER in the "INITIALLY WET SOIL" case in UNSTIPPLED REGIONS. Contours are 0, 1, 2, 5, 10 mm day^{-1}

Figure 9.10

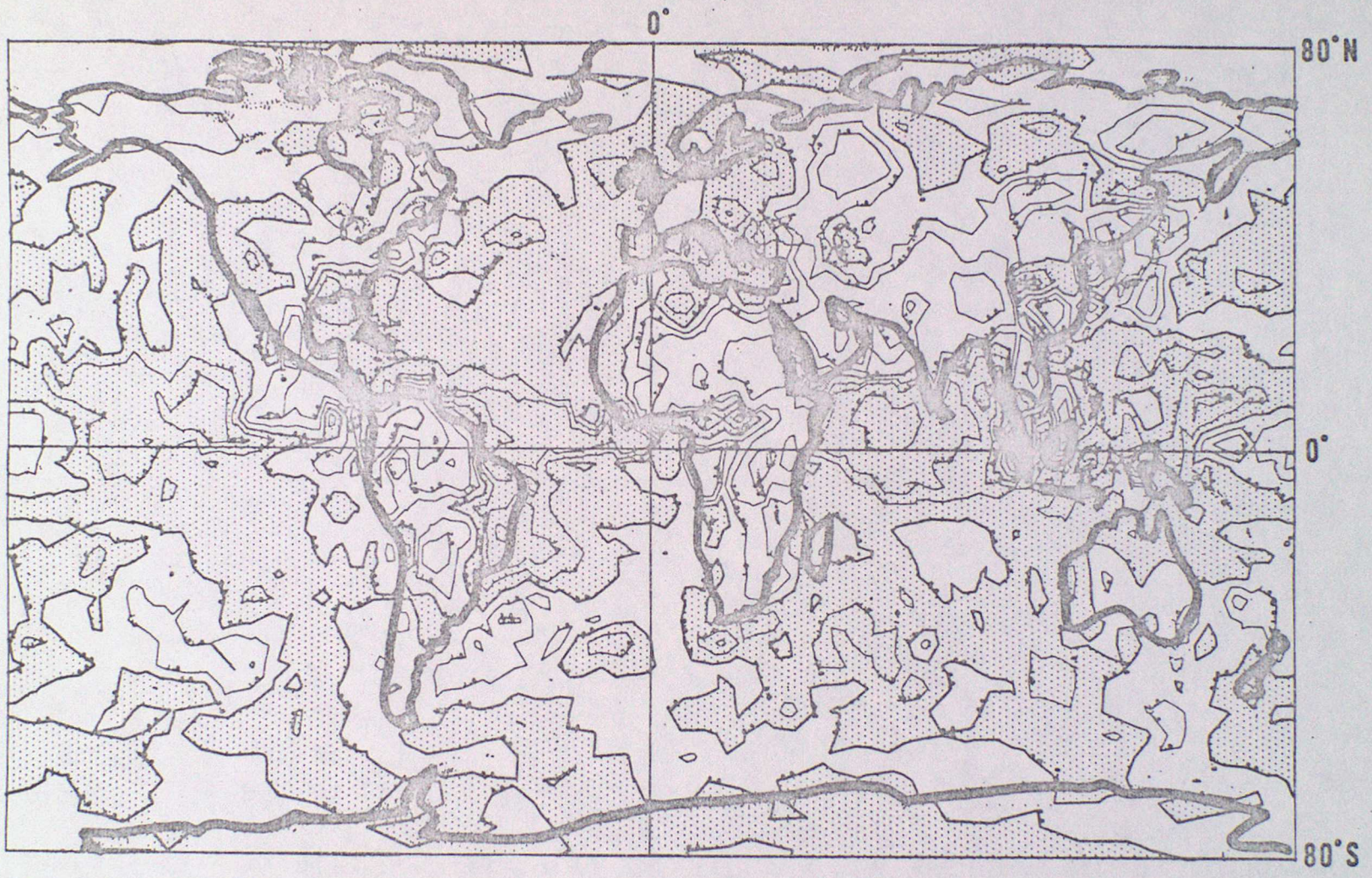

90-day (Days 21–110) mean differences in the rainfall rates (mm day $^{-1}$) between two low-resolution 5-layer model integrations with fixed July radiative conditions and with fixed snow-and ice-free land albedos of 0.1 and 0.3, respectively. Soil moisture content was initialised at 15 cm everywhere and not allowed to fall below 15 cm during the integrations. The rainfall rates are GREATER with the LOWER ALBEDO in the UNSTIPPLED REGIONS. Contours are 0, 1, 2, 5, 10 mm day $^{-1}$

Figure 9.11

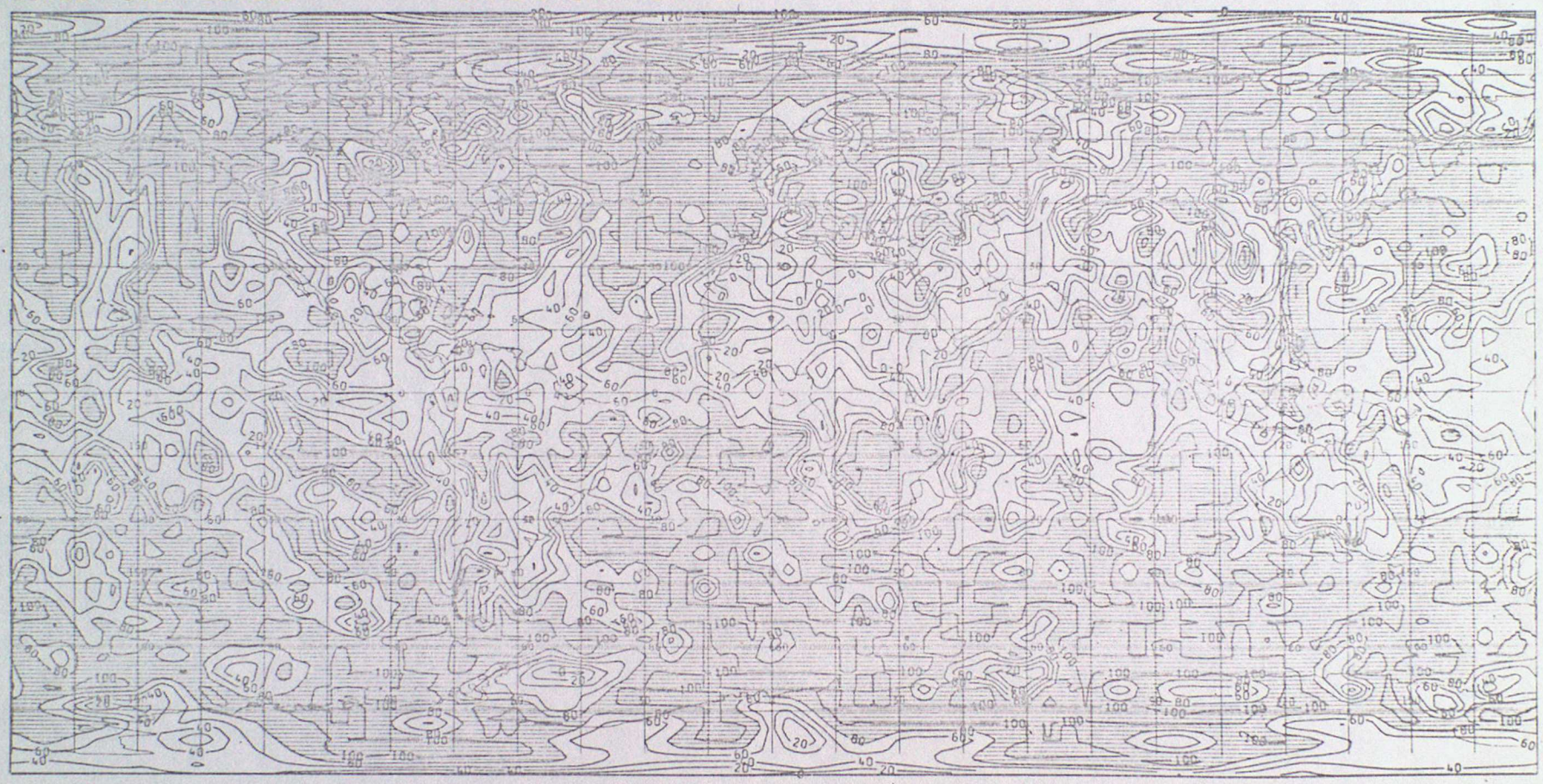

Figure 9.12 Total cloud amount at Day 10 of an 11-layer model integration from January FGGE data.

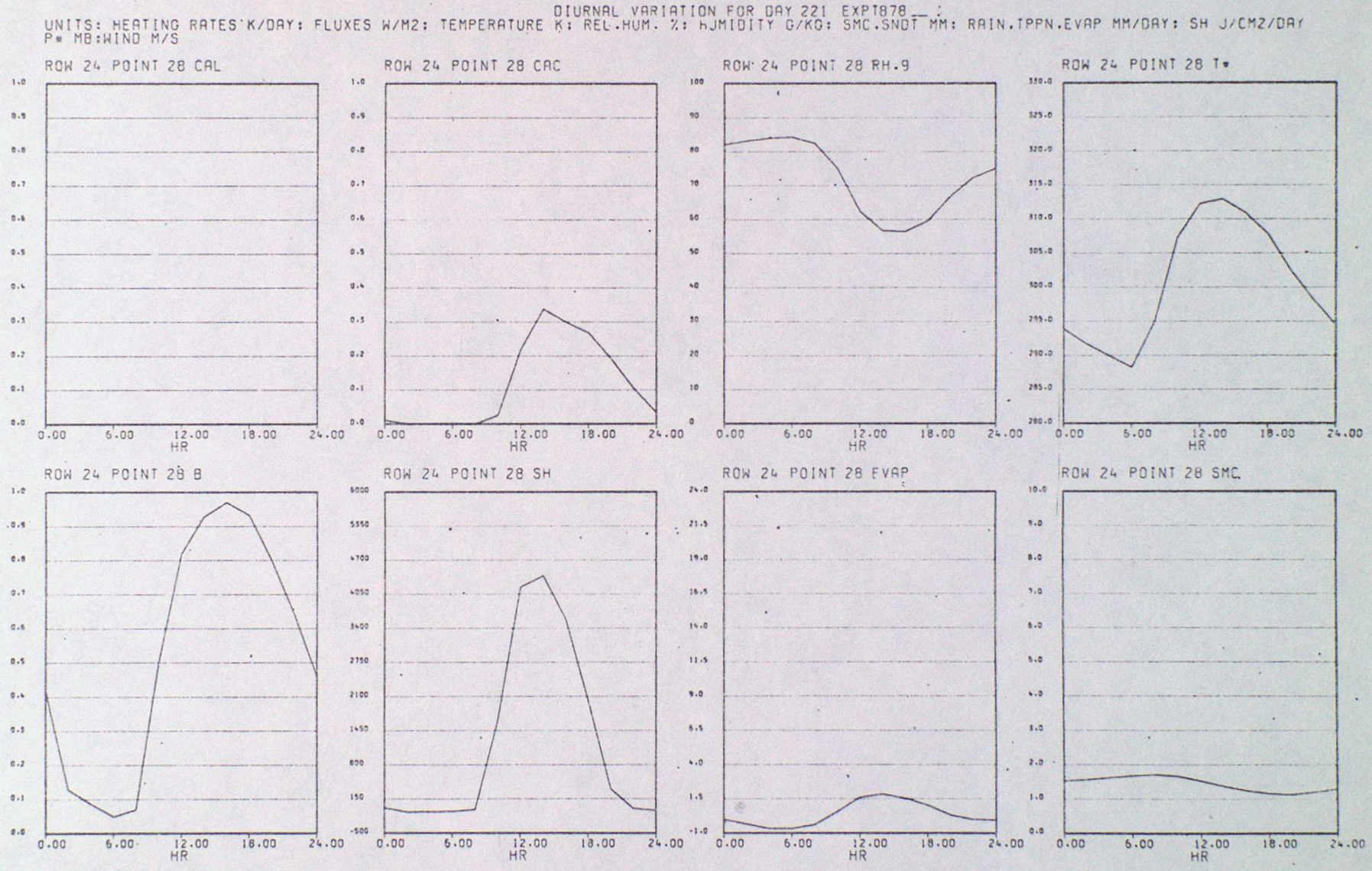

Figure 9.13 Behaviour of various surface and near-surface variables in a 5-layer model integration. The variables are low cloud amount, convective cloud amount, relative humidity at $\sigma = 0.9$, surface temperature, boundary layer depth, surface sensible and latent heat fluxes and soil moisture content.

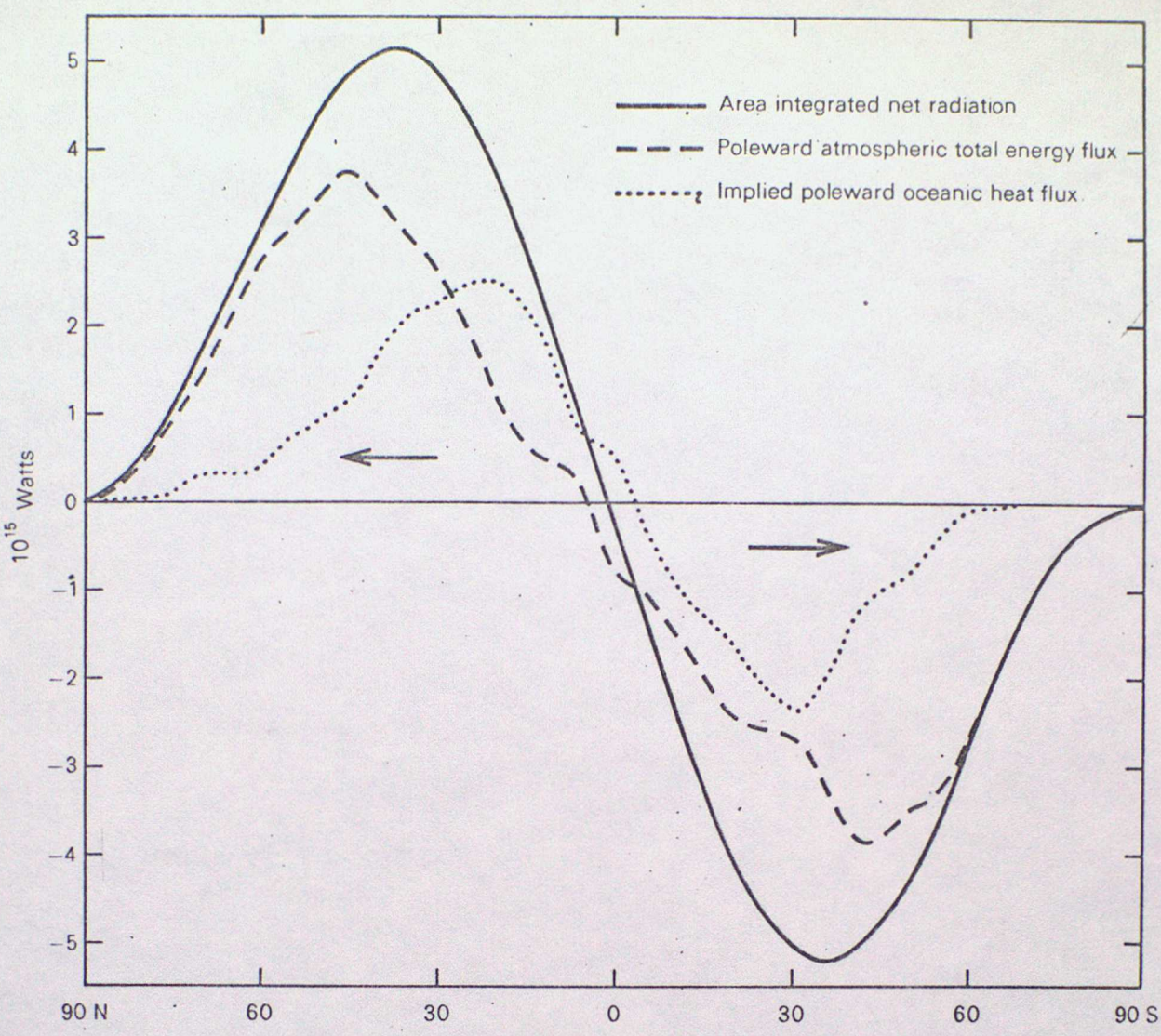

Figure 9.14

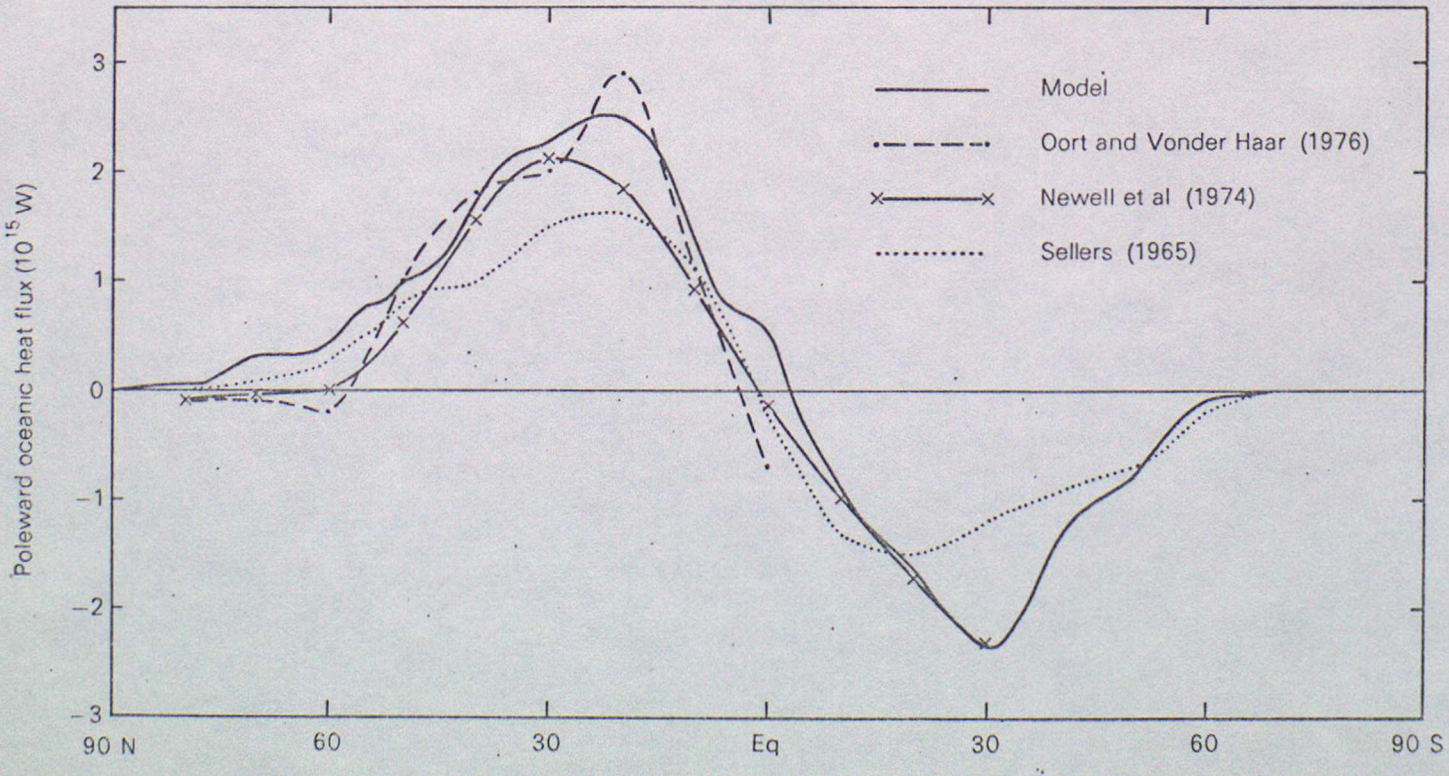

Figure 9.15